DISSIMILATIVE Fe(III) REDUCTION BY *PSEUDOMONAS* SP. 200

Thesis by

Robert G. Arnold

In Partial Fulfillment of the Requirements

for the Degree of

Doctor of Philosophy

California Institute of Technology

Pasadena, California

1987

(Submitted August 15, 1986)

ACKNOWLEDGEMENTS

George Jackson got me involved in this. Before it ended, I received help from many others, some of whom will be friends for life. I cannot even begin to thank Sandy Brooks, Tom DiChristina, Mike Hoffmann, and Katie.

ABSTRACT

The feasibilities of (i) liberating free energy from dissimilative iron reduction and (ii) coupling oxidative phosphorylation to electron transport to Fe(III) are sensitive to the aqueous chemistry of iron. The addition of ligands, such as nitrilotriacetic acid (NTA), to solution significantly impacts both the overall thermodynamics and kinetics of dissimilative iron reduction. The overall free-energy change due to electron transfer from glucose or lactate ion to Fe(III) is negative, but when Fe(III) is presented as an iron oxide there may be insufficient free energy in the transformations to permit coupled ATP generation. A systematic investigation of iron-reduction kinetics as a function of Fe(III) speciation indicated that in Pseudomonas sp. 200 (i) iron-reduction rate was functionally related to the concentrations of individual iron species and (ii) direct contact between Fe(III) and the electron-transport chain (ferrireductase) was required for electron transfer. Iron reduction in the absence of microbial activity was negligible. The addition of equimolar quantities of NTA enormously accelerated the initial rate of microbial iron reduction, and the calculated concentration of $Fe(NTA)(OH)_2^{2-}$ correlated strongly with measured iron-reduction rates.

When Fe(III) was provided as an iron oxide, the overall reduction rate was much slower, though still dependent upon the concentration of NTA added to solution. Primary factors controlling mineral dissolution and Fe(III) reduction were mineral surface area (or concentration of high-energy surface sites), ligand concentration, and cell number. Saturation kinetics were evident, as indicated by the following relationship governing reductive dissolution of hematite:

$$\frac{d[Fe(II)]}{dt} = \frac{V_{max(I)}K_{m(NTA)}V_{max(II)}[NTA]}{K_{m(NTA)} + [NTA]} \cdot \frac{[Fe(III)]}{K_{m(Fe)} + [Fe(III)]}$$

where $V_{max(I)} = 2.8 \times 10^{-5}$ M·hr^{-1}

$V_{max(II)} = 6.3 \times 10^{-4}$ M·hr^{-1}

$K_{m(NTA)} = 1.2 \times 10^{-3}$ M

$K_{m(Fe)} = 1.0 \times 10^{-1}$ M (as Fe)

NTA = nitrilotriacetic acid

[Fe(III)] = volume concentration of hematite (as Fe).

Experiments involving oxide/microorganism separation indicated that cell/mineral contact was essential to reductive dissolution of goethite.

Specific respiratory inhibitors were utilized to identify elements of electron transport chains involved in reduction of molecular oxygen and Fe(III) and to compare transport-chain compositions of cells grown under high- versus limited-O_2 conditions. Pseudomonas sp. 200 expressed both a constitutive (cytochrome *o*) and an inducible (cytochrome *d*) cytochrome oxidase. Induction of the alternate transport pathway resulted from growth at low oxygen tension (<0.01 atm.). Induced cells were capable of O_2 utilization at moderately increased rates. Pseudomonas sp. 200 also expressed a constitutive and an inducible ferrireductase. Growth at low oxygen tension resulted in acceleration of the overall rate of dissimilative iron reduction by a factor of 6 to 8, but iron reduction appeared to be uncoupled from oxidative phosphorylation. Maximum rates of electron

transfer in induced cells were independent of the identity of the electron acceptor indicating a common rate-limiting step. Dissimilative iron reduction occurred via an abbreviated electron transport chain in both the induced and uninduced cases. Electron-transport-chain compositions for the induced and uninduced cases are postulated.

TABLE OF CONTENTS

LIST OF FIGURES

LIST OF TABLES

Chapter 1

INTRODUCTION

1.1 Environmental Motivation

Despite its general abundance within the earth's crust, in aquatic environments iron is generally unavailable to biota, prompting speculation that iron assimilation can limit biological productivity (Jones, 1975; Barber and Ryther, 1969; Glover, 1978; Menzel and Ryther, 1961; Ryther and Guillard, 1959; Anderson and Morel, 1980; 1982). The cause of this apparent contradiction lies with the extreme insolubility of Fe(III) in the neutral and high-pH regimes. The dominant equilibrium species of iron in an aqueous system in the presence of CO_2 are displayed as functions of pH and redox potential in Figure 1.1. Although this phase diagram represents an oversimplification of natural waters, it is apparent that in the presence of molecular oxygen (high redox potential) Fe(III) is the dominant oxidation state of iron. Because the solubility product for amorphous ferric hydroxide is small (estimated at $K_{so} = 10^{-38.7}$, 25°C, I = 3 M $NaClO_4$ (Stumm and Morgan, 1981)) the solubilities of free ferric ion and its hydroxo complexes in water are negligible; the concentration of Fe^{3+} in equilibrium with $Fe(OH)_3$(s,amorph) at pH 7.0 is between 10^{-17} and 10^{-18} M. In a very dense bacterial culture, this amounts to little more than one ion for each million microorganisms. In the absence of ligands other than OH^-, the equilibrium concentrations of Fe^{3+} and its hydroxo complexes are functions of pH alone (at fixed temperature and pressure). Between pH 6.0 and 8.0 the total solubility of Fe(III) is $\leq 5 \times 10^{-9}$ M (Figure 1.2(a)); in the presence of more stable iron oxides such as hematite (α-Fe_2O_3) or goethite (α-FeO(OH)) the equilibrium concentrations are

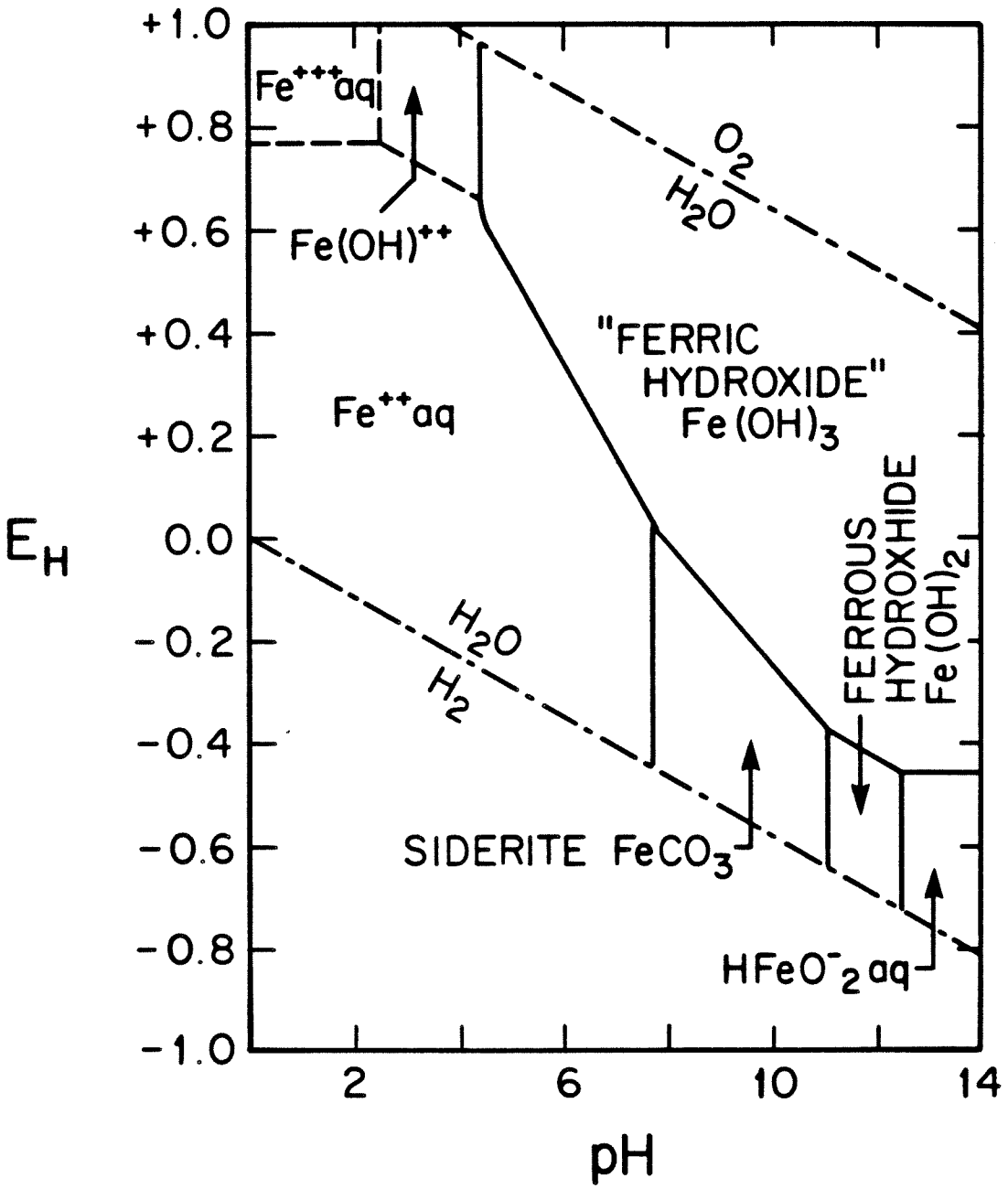

Figure 1.1. Phase diagram showing dominant Fe species as a function of E_H and pH in a system consisting of 10^{-2} M total dissolved carbonate and iron in H_2O. Solid boundaries are positioned at {ion} = 10^{-6} M. Ferric hydroxide is an amorphous, metastable intermediate to more stable iron oxides. (From Garrels and Christ, 1965.)

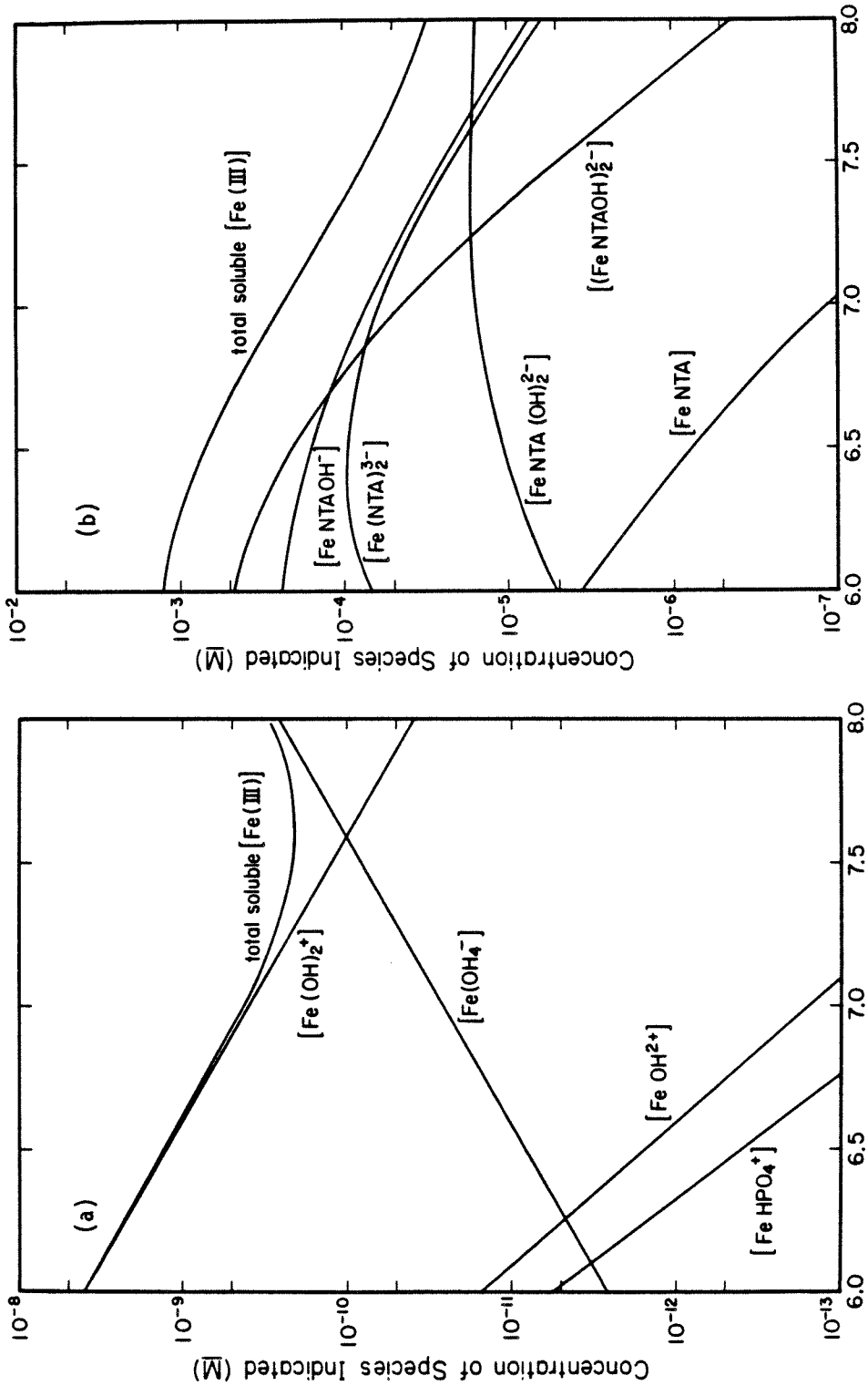

Figure 1.2. The pH-dependent concentrations of soluble Fe(III) species (a) in equilibrium with amorphous ferric hydroxide and (b) in equilibrium with equimolar NTA ($Fe(III)_T$ = 1.86 x 10-3 M; NTA = 1.86 x 10-3 M).

even lower. The effect of complexing agents such as nitrilotriacetic acid (NTA) on the overall solubility of Fe(III) is striking, as indicated in Figure 1.2(b) in which equilibrium concentrations of several Fe(III)-NTA species are plotted as a function of solution pH. Under these conditions (1.86×10^{-3} M $Fe(III)_T$ and equimolar NTA), NTA addition increases the total solubility of Fe(III) by a factor of more than 10^5. The equilibrium concentration of free ferric iron remains unaffected by NTA.

Under reducing conditions (again referring to Figure 1.1) the stable oxidation state for iron is Fe(II), which is moderately soluble within the mid- and low-pH range. On this basis, one might envision a cycle in which Fe(III) precipitates as ferric hydroxide or a more stable iron oxide in the surface waters of a lake or coastal marine environment. These solids would coagulate and settle with organic detritus, eventually reaching reduced bottom waters or sediments. Here, although anaerobic conditions might make Fe(II) thermodynamically stable, reductive dissolution of Fe(III) solids could be slow enough to control the overall rate at which iron becomes biologically available. Davidson et al. (1980) have shown that 70-90% of the iron which entered a productive lake was permanently retained in the sediments.

In a number of environmental studies, it has been shown that the rate of solubilization of iron-bearing minerals, and hence the rate at which iron is rendered biologically available, is determined by microbial activity:

(i) Takai and Kamura (1966) studied reductive processes in rice-paddy soils. They indicated that a primary determinant of electron potential in many soils was the Fe(III) ----> Fe(II) redox couple;

ferric iron was far more abundant than other potential electron acceptors including molecular oxygen, nitrate, and Mn(IV). They observed a clear succession in the utilization of electron acceptors with higher-energy reactions proceeding first (O_2, nitrate, Mn(IV), Fe(III)). Addition of antibiotics to these soils resulted in total loss of Fe(III) reduction, indicating the microbial origin of this activity. The observed dependence of crop yield on redox condition of the paddy field waters during specific growth stages may have been related to iron availability.

(ii) Sorensen (1982) found that iron-reduction activity in anaerobic slurries of marine coastal sediments was eliminated by sediment sterilization. He concluded that reduction of Fe(III) was either directly associated with microbial metabolism or driven indirectly by microorganisms which produce soluble, reducing metabolites. Sulfide was not an effective chemical reductant of Fe(III). Bacterially mediated Fe(III) reduction may be instrumental to sediment mineralization under anaerobic, low-nitrate conditions.

(iii) Jones et al. (1983, 1984) found that the rate of release of Fe(II) from anoxic lake sediments had a temperature optimum at 30°C and was inhibited by $HgCl_2$, reflecting the biological nature of the mineralization process. From these sediments, the authors isolated two microorganisms capable of catalyzing electron transfer to Fe(III) in pure cultures.

(iv) The reduction of ferric iron in sediments from the Potomac River Estuary was found to depend on microbial activity (Lovley and Phillips, 1986). The microbially catalyzed rate of iron reduction increased by a factor of 50 when amorphous ferric hydroxide was

substituted for hematite in enrichment media. Experiments indicated that iron-reducing microorganisms can outcompete methanogenic consortia for sediment organic substrates. It was concluded that under appropriate chemical conditions bacterial iron reduction could provide a significant pathway for mineralization of sedimentary organic material.

1.2 Commerical Motivation

The importance of microorganisms in promoting the leaching of metals is well established. Acidophilic chemolithotrophs Thiobacillus ferrooxidans and Thiobacillus thiooxidans catalyze the oxidation of sulfidic minerals such as pyrite (FeS_2) releasing component metals. Oxidative dissolution has been used for the hydrometallurgical extraction of copper and uranium from low-grade ores; microbial extraction of nickel, lead, and zinc are also feasible due to the non-specific nature of bacterial substrate requirements (Brierley, 1982).

When Fe(III) produced by direct enzymatic transformation drives subsequent oxidation and release of mineral components, the leaching process is classified as indirect. In this manner, T. ferrooxidans can accelerate the oxidative dissolution of FeS_2 by a factor of 10^6 or more. Iron(III), soluble under conditions of extreme acidity, is known to be a major factor in the indirect bacterial leaching of copper and uranium; bacterially generated, soluble Fe(III) chemically oxidizes U(IV) to U(VI) under acid conditions resulting in mineral dissolution. Other indirect leaching processes (both oxidative and reductive) have been proposed. For instance, it has been suggested that Fe(III) reduction can be chemically mediated by microbially produced sulfide (Sorensen,

1982), and soluble, extracellular metabolites are frequently cited as potential intermediates in bacterially driven reductive dissolution of Fe(III) (see below).

Microbial leaching of iron from natural Fe-bearing minerals may provide a commercially attractive alternative to extraction and ore-beneficiation processes currently in use within the steel industry. Since biological extraction could result in a concentrated Fe(II) slurry, there would be attendant savings attributable to reduced transportation costs and mitigated demand for reductants during subsequent steps in the production of elemental iron. Unit processes within a hypothetical iron-extraction scheme are represented in Figure 1.3. The economic viability of such a process depends upon the kinetics of microbially mediated reductive dissolution of Fe(III) oxides or other iron-bearing minerals. Bacterial iron reduction might also be applied commercially for the removal of corrosion products from the surface of ferrous metals.

1.3 The Physiology of Bacterial Respiration

1.3.1 Energy Transduction.

Dissimilative iron reduction, a process in which respiratory electrons enzymatically convert Fe(III) to Fe(II), is distinguished from assimilative reduction in which iron is processed for incorporation into metabolically functional systems (Ehrlich, 1981). Enzymes of the respiratory system, including those responsible for electron transport to Fe(III) are associated with the cytoplasmic membrane. Assimilative iron reduction is catalyzed by iron reductases within the cell

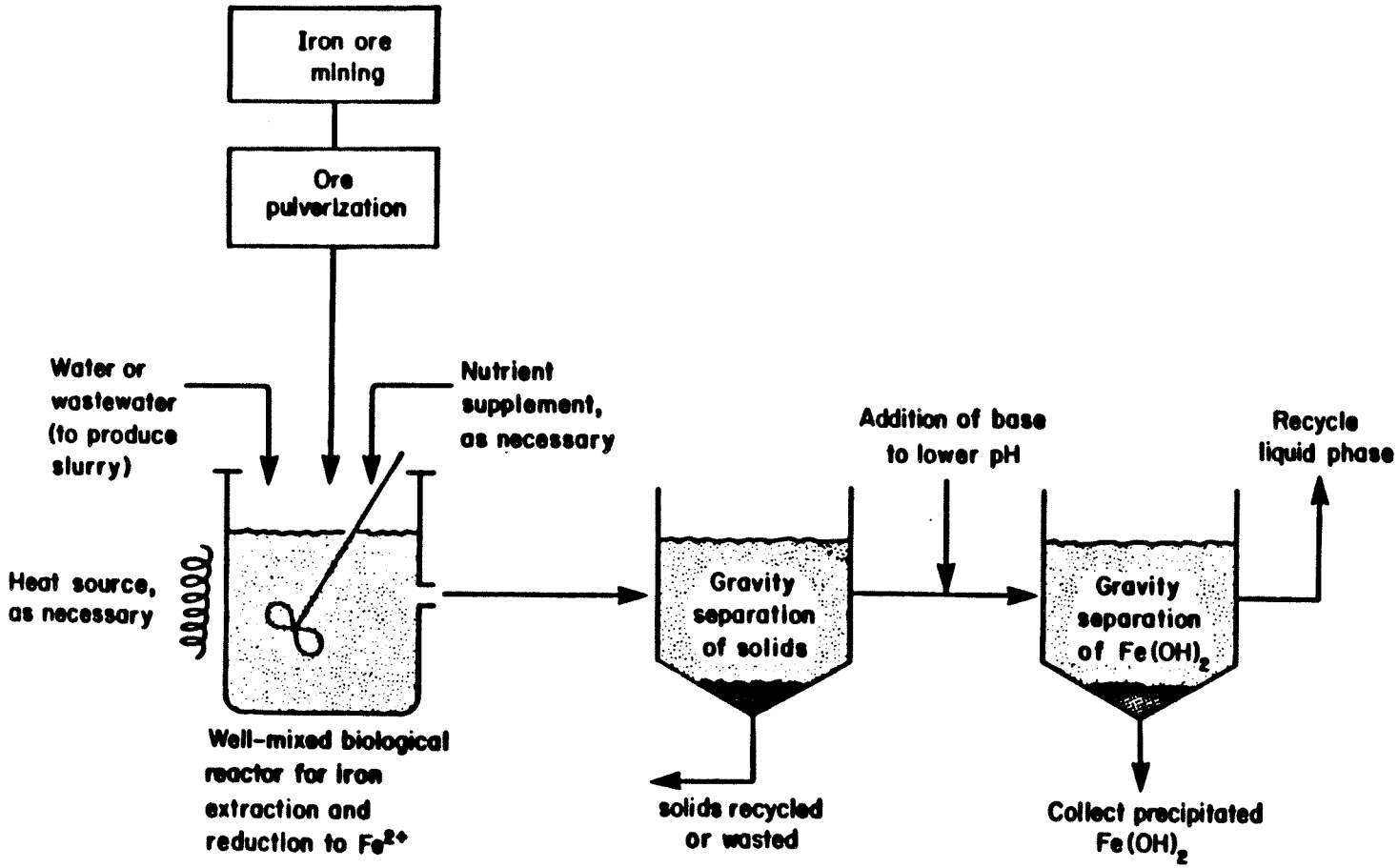

Figure 1.3. Schematic representation of relationships among unit processes for the reductive dissolution of Fe(III)-bearing ores with subsequent recovery of Fe(II).

cytoplasm. The rate of Fe(III) ----> Fe(II) conversion by dissimilative processes is potentially much faster.

A set of typical catabolic reactions, starting with glucose and leading to the production of ATP via oxidative phosphorylation, is schematically represented in Figures 1.4 and 1.5. Cellular respiration is the process by which reducing power, temporarily conserved as reduced nicotinamide adenine dinucleotide (NADH) within the tricarboxylic acid cycle, is converted to useable chemical energy in the form of adenosine-5'-triphosphate (ATP). In addition to NADH, reducing equivalents may be donated to membrane-bound enzymes of the electron transport chain by such reductants as succinate, lactate, and methanol. Membrane-bound respiratory enzymes are alternately reduced and oxidized by the transfer of electrons; transport is terminated with the reduction of a terminal electron acceptor. In mitochondrial and aerobic bacterial respiration, the terminal electron acceptor is invariably molecular oxygen. However, because response to rapidly changing environmental conditions may afford selective advantages among prokaryotes, bacteria frequently possess branched electron transport systems capable of reducing a variety of terminal electron acceptors including O_2, nitrate, nitrite, sulfate and partially oxidized sulfidic forms, and ferric iron (White and Sinclair, 1971). When Fe(III) serves as terminal electron acceptor, the process is known as dissimilative iron reduction.

Enzymes of the respiratory system can be thought of as descending rungs in an energy ladder. Specific redox reactions (single steps on this enzymatic ladder) are sufficiently exergonic to drive the coupled translocation of protons from the cytoplasm (across the cytoplasmic membrane) into the cell surroundings or periplasmic space (Lehninger,

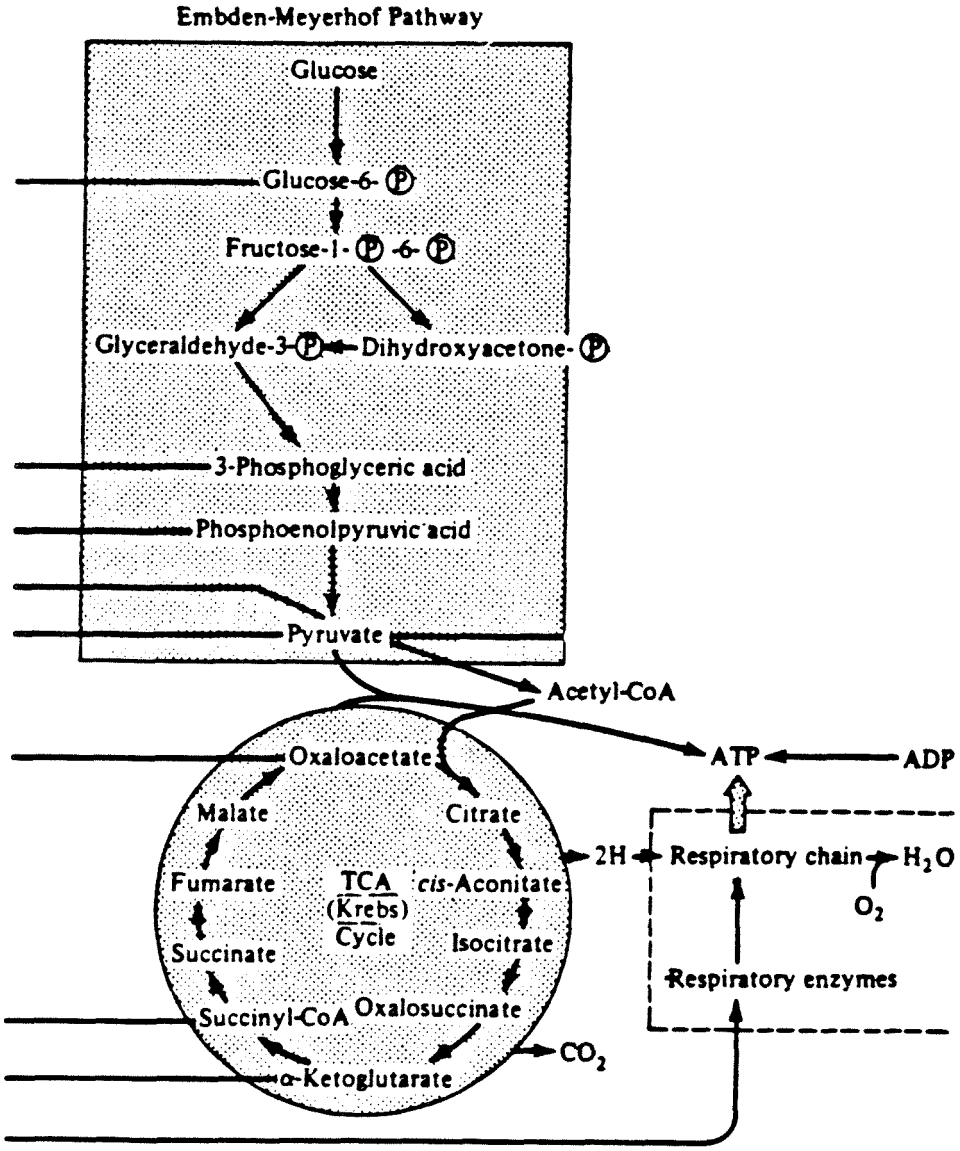

Figure 1.4. Catabolism of glucose with ATP generation via oxidative phosphorylation; steps include those of the glycolytic pathway, citric-acid cycle, and electron-transport chain. Processes are representative since catabolism of alternative substrates and/or alternative metabolic pathways are frequently encountered. (From Bailey and Ollis, 1977.)

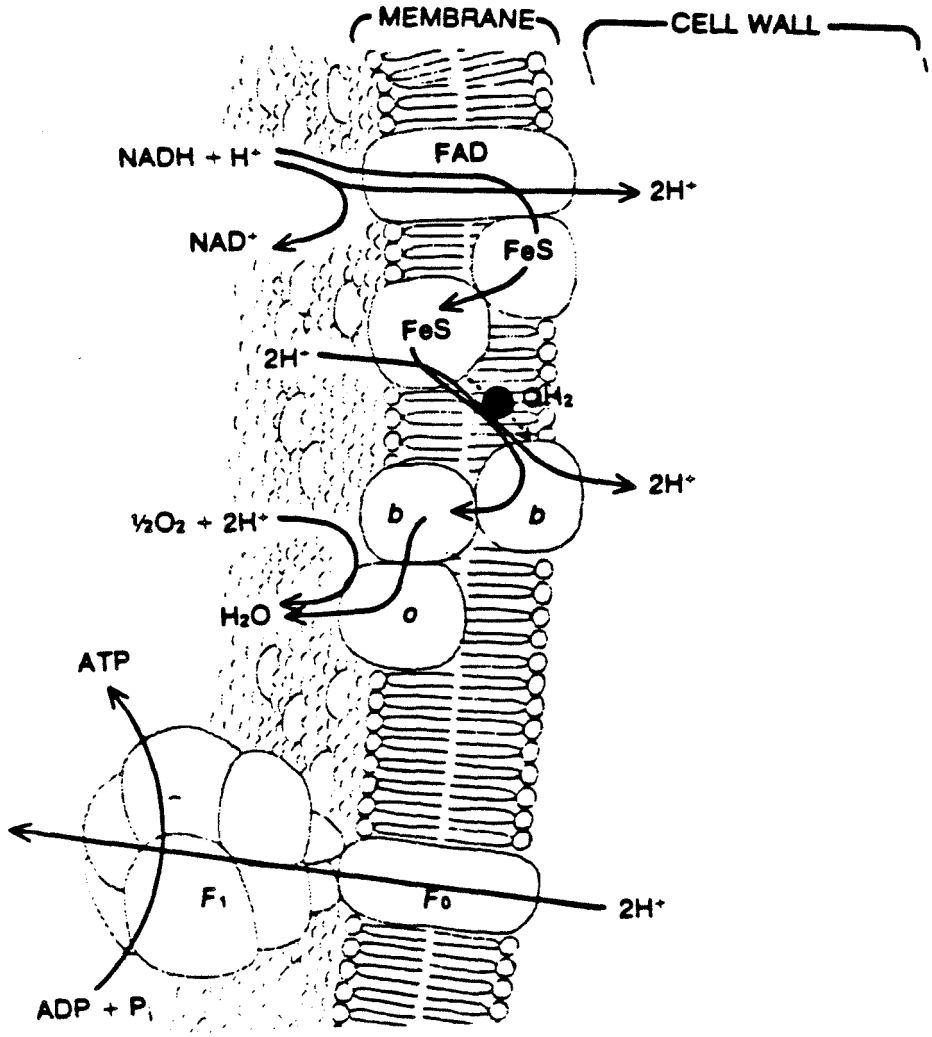

Figure 1.5. Function and (typical) composition of E. coli aerobic electron-transport chain. Electron transport is linked to ADP phosphorylation by proton translocation and establishment of transmembrane proton-motive force. (From Hinkle and McCarty, 1978.)

1973). Among actively respiring cells, the process occurs with sufficient frequency to support a transmembrane proton-motive force directed towards the cytoplasm. This force is comprised to a variable degree of two components: (i) the proton gradient, and (ii) electrical potential:

$$\Delta p = \Delta\psi - Z\,\Delta pH$$

where Δp is the proton motive force (mV);

ψ is the electrical potential ($\Delta\psi$ is formed because proton translocation removes positive charges from the cytoplasm and accumulates them in the cell surroundings); and

$Z = 2.3\ RT/F$. (R is the gas constant; T the absolute temperature; and F the Faraday constant. $Z \cong 60$ mV at 25°C) (Konings and Veldkamp, 1983).

Potential energy stored as proton-motive force is subsequently used to generate ATP. Protons are retranslocated from the cell surroundings or periplasmic space to the cytoplasm via membrane-bound ATPase (Figure 1.5); retranslocation is enzymatically coupled to the phosphorylation of adenosine diphosphate (ADP) (Hinkle and McCarty, 1978). Energy liberated from the subsequent hydrolysis of ATP drives most energy-demanding metabolic processes.

This overall mechanism for coupling electron transport to phosphorylation of ADP, known as the chemiosmotic hypothesis, has gained general acceptance since its formulation by Mitchell (1961). Several

important predictions of Mitchell's theory are supported by experimentation: (i) it is possible to drive ATP synthesis independent of electron transport by imposing a proton-motive force across an intact bacterial (cytoplasmic) or mitochondrial inner membrane; (ii) it has never been convincingly shown that energy transduction can be successfully carried out by other than a topologically closed membrane; (iii) respiration rate can be slowed by back pressure in the form of excessive Δp when dissipation of proton-motive force is blocked; and (iv) compounds which render the cytoplasmic membrane permeable to ions, particularly H^+ or OH^-, act as uncoupling agents, encouraging electron transport without oxidative phosphorylation by dissipating Δp (Jones, 1983).

1.3.2 Cellular Ultrastructure.

The majority of the experimental program described herein consists of an investigation of dissimilative iron reduction by a single gram-negative bacterial species. In order to appreciate the topological problems which such a bacterium must overcome in order to catalyze this process, a few structural aspects of cell physiology warrant review.

Van Iterson (1984a,b) summarized recent inquiry into the nature of the bacterial cell envelope. In gram-negative bacteria, the cytoplasmic membrane is surrounded by an aqueous periplasmic space, approximately 10 nm in thickness including the peptidoglycan layer or true cell wall (see Figure 1.6). An outer membrane is connected to the peptidoglycan layer by lipoprotein molecules and to the cytoplasmic membrane at adhesion zones of unknown character. Cell countenance and antigenic specificity are provided by lipopolysaccharide molecules extending several nanometers into the cell surroundings (Lin et al., 1984). Comprehensive

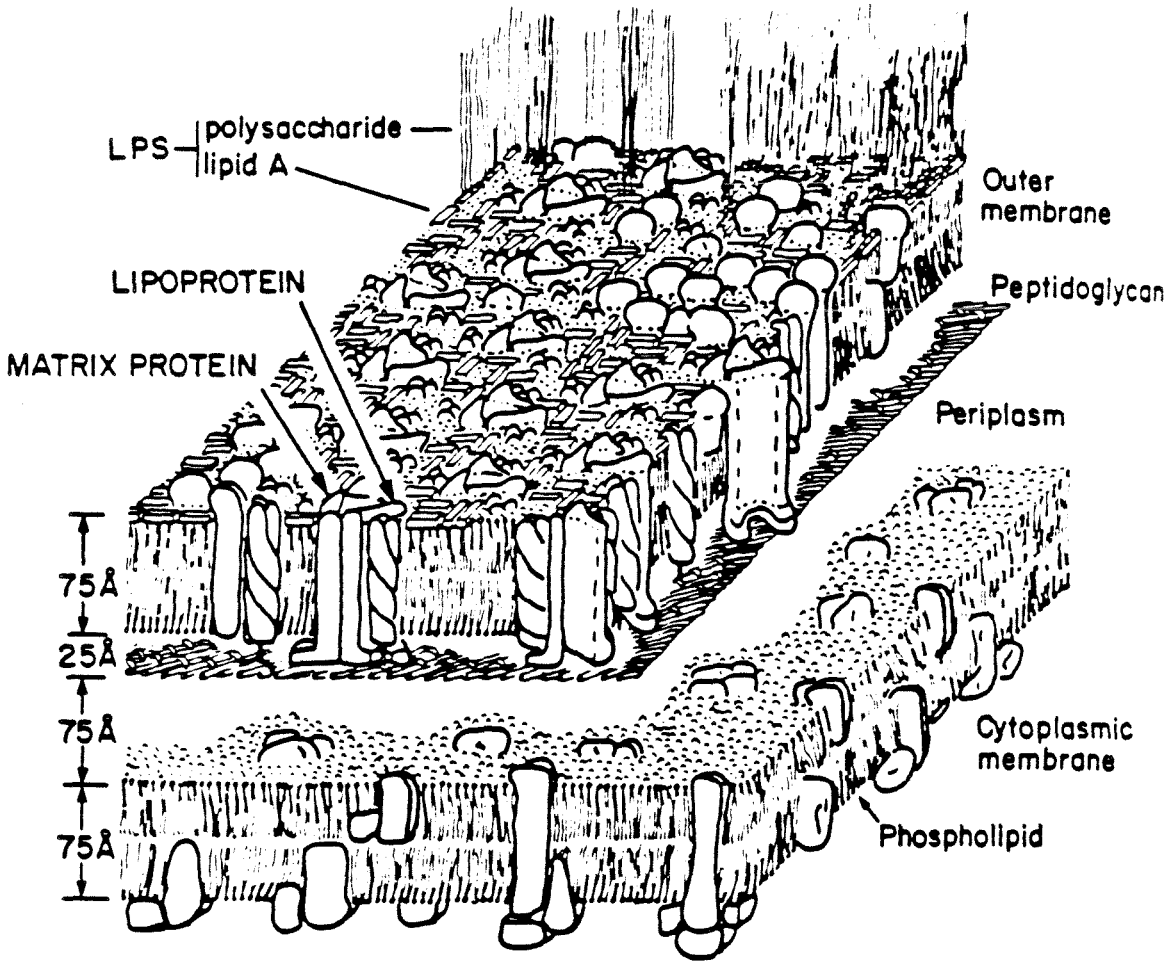

Figure 1.6. Schematic representation of the cell envelope of gram-negative bacteria. (From Lin et al., 1984.)

reviews of cell structural aspects are available in Wright and Tipper (1979), Rogers et al. (1980),and DiRienzo et al. (1978).

Both the outer and cytoplasmic membranes of gram-negative bacteria are fluid structures comprised largely of lipids, proteins, and (outer membrane only) carbohydrates. Roughly half the protein component of the outer membrane is comprised of a regularly distributed, transmembrane protein known as porin, originally labelled matrix protein by Inouye (1974). Using electron microscopy, porin was observed to form a regular, hexagonal array over much of the outer membrane (Steven et al., 1977). Porin molecules are thought to surround passive diffusion pores which span the outer membrane and serve as hydrophilic channels 1 or 2 nm in diameter. Three such pores visible at the cell exterior are thought to merge to a single, larger opening on the cytoplasmic side (Engel et al., 1985). Pore sizes are such that diffusive transport of polysaccharide m.w. $\leq$ 700 is possible (Nakae and Nikaido, 1975).

1.3.3 Transport-Chain Composition.

Bacterial respiration is based upon the types of redox carriers that are found in mitochondria. These include flavoproteins and iron-sulfur proteins (which comprise the dehydrogenases), quinones, cytochromes, and cytochrome oxidases. However, the scale of variation encountered in bacterial transport-chain composition makes generalization difficult and enumeration tedious.

1.3.3.1 Dehydrogenases.

Bacterial dehydrogenases catalyze the oxidation of a variety of substrates including, in addition to those already mentioned,

glycerol-3-phosphate, NADPH, formate, lactate, malate, and others. Flavoproteins are apoproteins of varied molecular weight and amino acid composition equipped with a tightly-bound prosthetic group -- either flavin mononucleotide (FMN) or flavin adenine nucleotide (FAD) (Jones, 1983). Flavins bind a maximum of two hydrogen atoms. In their oxidized form, they are yellow ($\lambda_{max} \cong 450$ nm), and essentially colorless upon reduction. FMN operates at a lower redox potential than FAD due to the method of attachment to the apoprotein (FAD is covalently bound while FMN is usually ionically bound).

Iron-sulfur proteins contain either 2, 4, or 8 proximately located iron atoms and an equal number of atoms of labile sulfur (released as H_2S under acid conditions). The [8Fe-8S] proteins consist of two [4Fe-4S] centers. Upon reduction, the [2Fe-2S] and [4Fe-4S] proteins accept a single electron; [8Fe-8S] proteins can accept two electrons. FMN and four Fe-S centers have been identified in the NADH dehydrogenases of Escherichia coli and Paracoccus dentrificans. FAD and three Fe-S centers are located in the succinate dehydrogenase of Escherichia coli. Most, but not all, of the bacterial respiratory-chain dehydrogenases are tightly embedded in the cytoplasmic membrane (Jones, 1983).

1.3.3.2 Quinones.

Lipid-soluble quinones of the ubiquinone type (Figure 1.7) normally accept reducing equivalents from the respiratory-chain dehydrogenases of gram-negative bacteria (Gel'man et al., 1975). Vitamin-K quinones of the menaquinone type have been isolated from E. coli although normally menaquinones are present in gram-positive bacteria. Quinones are firmly

(a)

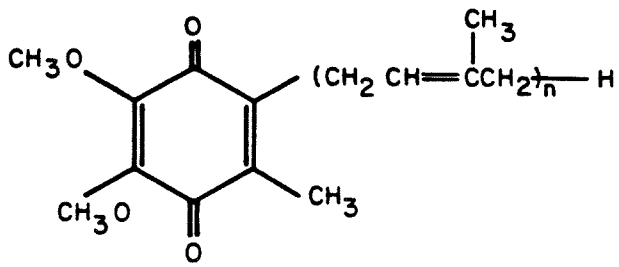

(b)

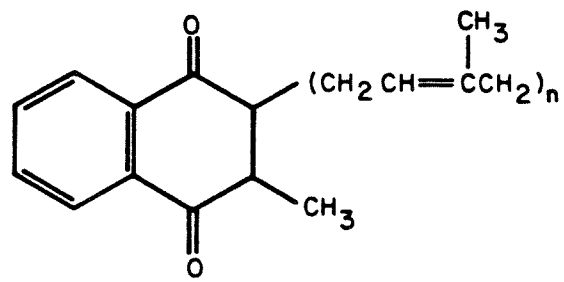

Figure 1.7. Bacterial quinones.

(a) Ubiquinones (coenzymes Q): occur in the majority of gram-negative aerobes; n indicates the number of mono-unsaturated isoprenoid units in the terpenoid side chain. Differences in properties are attributable to side-chain length. In naturally occurring members, n = 6 to 10.

(b) Menaquinones (vitamins K_2): isolated from gram-positive bacteria, anaerobic and facultative nonphotosynthetic gram-negative bacteria, and photosynthetic bacteria. In most microorganisms, n = 7, 8, or 9.

(Merck Index, 1976)

bound within bacterial membranes, which on reduction accept 2H to form quinols. They occupy a central position in the overall electron-transport chain, transferring reducing equivalents from dehydrogenases to the terminal cytochrome system. Bacterial quinones are present in considerable molar excess (5 to 25 times) compared to membrane concentrations of specific cytochromes. A similar ratio has been observed in mitochondria. It has been hypothesized that mitochondrial ubiquinone provides a pool of reducing equivalents from various flavoprotein dehydrogenases from which electrons are transferred to the cytochrome chain. Variety and relative complexity associated with bacterial electron transport do not appear to have altered this role.

1.3.3.3 Cytochromes and Cytochrome Oxidases.

There are four known cytochrome types (a, b, c, and d) (Lemberg and Barrett, 1973). Each consists of a heme prosthetic group bound to an apoprotein. The heme is an iron(II) porphyrin which in its oxidized (ferric) form can accept a single electron (Fe(III) + e <====> Fe(II)). The four classes of cytochromes are distinguished on the basis of minor variations in the prosthetic groups: Cytochrome c is a mesoheme; cytochrome b, a protoheme; cytochrome a, a heme; and cytochrome d, a ferrochlorin (Figure 1.8). Differences in properties of the cytochromes within a single major type arise from the character of apoproteins to which these four heme types are added. Variation exists in the identity or nature of substituted groups at the heme periphery and in the method of binding between heme and apoprotein. Only cytochrome c contains heme which is covalently bound to apoprotein. Although most b-type cytochromes, a-type cytochromes, and cytochrome oxidases (see below) are

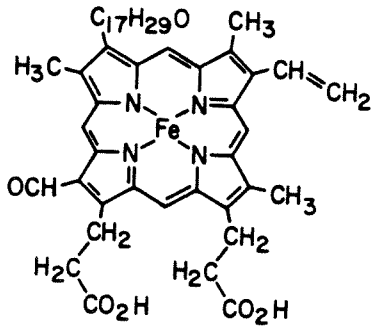

(a) Heme a

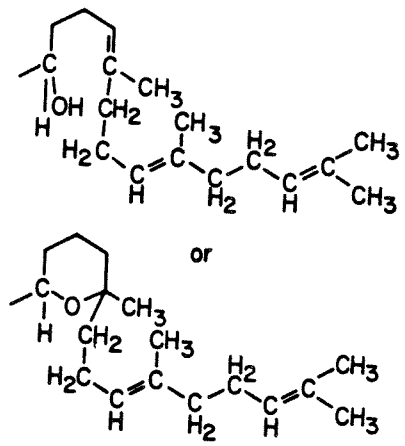

(b) Protoheme (cytoheme b)

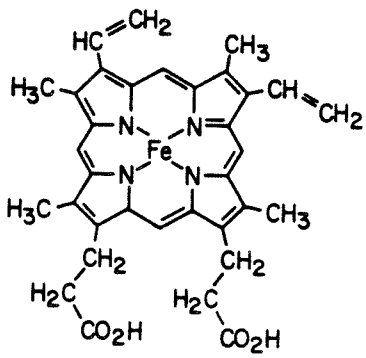

(d) Cytoheme d

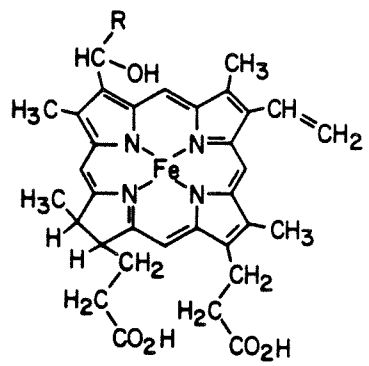

(c) Heme c

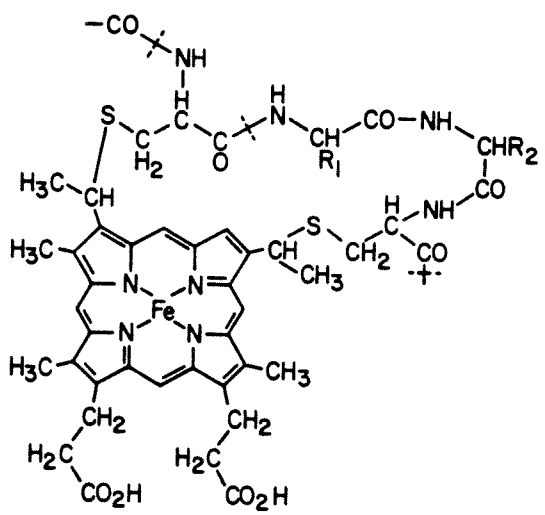

Figure 1.8. Classification and structure of bacterial cytochromes. (From Lemberg and Barrett, 1973.)

tightly held, integral membrane proteins, many c-type cytochromes are hydrophilic and peripherally attached to the cytoplasmic membrane (periplasmic side) or are present in the periplasm (Gel'man et al., 1975). Reducing equivalents generally enter the bacterial cytochrome chain via b-type cytochromes (Jones, 1983; Gel'man et al., 1975; Jones and Poole, 1985). Cytochromes are frequently organized into polyenzyme complexes. They are detected by analysis of their absorption spectra (α, β -bands at 500-650 nm, γ-band at 400-500 nm). Cytochromes account for no more than 5-10% of the total membrane protein (by weight) (Gel'man et al., 1975).

Heme iron forms a stable octehedral coordination complex with six ligands. Four of the six coordination sites are filled by nitrogen atoms of the porphyrin (one from each component pyrrole ring, see Figure 1.8); the remainder are filled by atoms from neighboring amino acid residues. When one of these latter two positions can bind molecular oxygen, autoxidation of reduced heme is usually rapid, and the cytochrome can act as a terminal oxidase (Jones, 1983). However, cytochromes which bind carbon monoxide may be regarded as only potential terminal oxidases until such activity is confirmed by kinetic analysis (Jones and Poole, 1983). Such a function has been confirmed for cytochromes aa_3, o, d and a_1. These commonly contain four one-electron redox centers which are combinations of different hemes or of heme and copper centers. The structure permits catalysis of the 4-electron reduction of molecular oxygen to H_2O. (For a recent analysis of structural aspects of cytochrome c oxidase metal centers see Gelles et al., 1983).

Among the bacterial cytochrome oxidases, type aa_3 most closely resembles the mitochondrial oxidase (though still much simpler in terms of subunit composition) (Poole, 1983). Cytochrome aa_3 is commonly detected among all known physiological groups of aerobic bacteria, usually in the presence of other cytochrome oxidases. (See discussion of electron transport chain branching, below.) As implied by its name, the enzyme contains two hemes, one of which (a_3) binds in the ferrous state (sixth axial position) to O_2, CO, and other ligands, and in the ferric state to CN^-. The spectral properties of reduced cytochrome aa_3 include visible absorption bands at 600-605 and 440-445 nm. The presumed role of copper in promoting electron transport to O_2 via this enzyme is supported by experiments in which membranes of various bacteria grown under copper-limiting conditions exhibited lowered oxidase content and activity. Upon reconstitution into phospholipid vesicles, cytochrome oxidase aa_3 serves as a proton-translocation site. The enzyme's large size permits it to extend across the cytoplasmic membrane.

Cytochrome a_1 is the least understood of the cytochrome oxidases. Heme a_1 binds to oxygen and carbon monoxide in the ferrous form and to cyanide in the ferric form. Its presence has been detected in a variety of bacterial genera. The enzyme's spectral character is poorly defined: its α-band (peak absorption between 585-595 nm) is weak, and its Soret band is diffuse and easily confused with cytochrome d. In this range, other bacterial components such as free protoheme and cytochrome c peroxidase could interfere with its identification. Carbon monoxide causes a blue shift in the Soret band to 424-427 nm but has little effect in the α-region. Cytochrome a_1 is frequently co-synthesized with

other cytochrome oxidases. Meyer and Jones (1973) suggested that three cytochrome oxidases (a_1, d, and o) are frequently encountered among heterotrophic, gram-negative bacteria which adapt well to unstable environmental conditions. The presence of multiple cytochrome-oxidases is most common following O_2-limited, sulfate-limited, or cyanide-supplemented growth.

Cytochrome o, a b-type cytochrome though originally designated "o" for oxidase, is the most widely distributed of the known bacterial cytochrome oxidases. Although it may serve as the sole oxidase, cytochrome o more frequently comprises one limb of a branched electron transport system. Its synthesis, sometimes regarded as constitutive, is less sensitive to growth conditions than is that of other cytochrome oxidases. The most distinct spectral indicator of o-type cytochromes is in the Soret region. Peak absorbance for the CO-liganded form is from 410-421 nm. The α-peak of reduced-minus-oxidized spectra lies in the 555-565 nm range but is frequently difficult to distinguish (Poole, 1983). In its oxidized form, the cytochrome o binds CN^- making electron transport sensitive to cyanide inhibition. K_m values (substrate concentration at which enzyme is half-bound) for O_2 binding to cytochrome o generally lie between 1.8 and 6.5 μM, although a much lower value has been derived for E. coli. In the redox scheme proposed by Webster (1979), two cytochrome o molecules bind O_2 reducing it to H_2O_2, which is stoichiometrically produced in the overall NADH-cytochrome o oxidase reaction.

Cytochrome d is commonly found among gram-negative heterotrophs in co-existence with other cytochrome oxidases (particularly o and a_1, see above). It is induced by low-O_2 conditions, entry into late-exponential

or stationary growth on non-fermentable substrates, and growth on non-fermentable carbon in the presence of CN^-. Oxidized cytochrome oxidase d is characterized by a spectral peak in the range 647-652 nm; upon reduction, peak absorption is near 632 nm. Carbon monoxide binding shifts the latter band to $\sim$ 637 nm. Its Soret band is weak (Poole, 1983). The oxidase is tightly held in the cytoplasmic membrane and is frequently isolated as an enzyme complex with b-type cytochromes. Oxidases of the d type are relatively CN^- resistant due to poor binding qualities of CN^-. There is evidence that cytochrome d binds and reduces nitrogen-containing compounds, suggesting that the enzyme has a role in anaerobic respiration. Experimentally derived K_m values tend to be lower (0.018-0.35 μM) than those assigned to the other oxidases implying that cytochrome oxidase d may provide competitive advantages under low-O_2 conditions. There is disagreement regarding the ability of the E. coli cytochrome b ----> d pathway to act as a proton translocation site (Poole, 1983). It has been suggested that respiratory systems terminating in cytochrome d evolved to protect O_2-labile enzymes by "wasting" O_2 (respiration without coupled proton translocation). The molecule's ability to trap O_2 at low concentrations, afforded by low K_m values, is consistent with such a hypothesis. Properties of the bacterial cytochrome oxidases are summarized in Table 1.1.

1.3.3.4 Variation in Transport-Chain Composition.

Substantial inter-species variation has been found in electron transport chain composition. In a few bacterial species (Paracoccus dentrificans, Alcaligenes eutrophus), the complement of electron carriers has proven similar to that of mitochrondia (Jones, 1983)

Table 1.1. Relevant Properties of Known Bacterial Cytochrome Oxidases.

Oxidase	Type of redox center	Absorption maxima (reduced form; α- and γ-bands) nm	Occurrence	Proton translocation capacity	K_m (molecular oxygen)
aa_3	a; a_3; 2Cu	600-605; 440-445	widespread	yes	4-7 μM (probably high)
a_1	a-type heme	585-596; ≅ 440	widespread; esp. gram-negative heterotrophs	unknown	0.33 μM (single species - Acetobacter sp.)
o	protoheme	555-565; ≅ 430	widespread; most common of the cytochrome oxidases	unknown	1.8-6.5 μM (usual range) 0.1-0.3 μM (E. coli)
d	chlorin heme	≅ 630; weak	common among gram-negative heterotrophs	probably none	0.018-0.35 μM (lower than values corresponding to other oxidases)

Note: K_m is the Michaelis half-saturation concentration or concentration at which half of the enzyme active sites are bound to substrate. It is also the reciprocal of the stability constant for enzyme substrate and active site binding.

prompting speculation that the present-day organelle originated as a bacterial endosymbiont within a primitive host. (Others maintain that mitochondria arose from specialized (mososmal) bacterial membranes (Poole, 1983).) Three kinds of variation have been noted among bacterial redox carriers: (i) substitution of one component for another with similar redox properties (e.g., menaquinone for ubiquinone); (ii) substitutions involving components with significantly different properties; (iii) addition or loss of a limited number of transport-chain elements.

Electron transport chains can terminate with reduction of a variety of electron acceptors due to the existence of branches and specialized electron carriers such as nitrate and iron reductases (White and Sinclair, 1971). More frequently branches are based on the existence of multiple cytochrome oxidases within a single species. Such a network may be no more complex than the transfer of electrons from a single cytochrome carrier to two oxidases (see Figure 1.9 for examples). Branches may be inducible in the absence of more energetically favorable electron-transport alternatives. For instance, a high-O_2-affinity, d-type cytochrome oxidase appears to be induced in response to low-oxygen conditions in Proteus vulgarus (Moyed and O'Kane, 1956; Castor and Chance, 1959), Klebsiella aerogenes (Castor and Chance, 1959; Harrison, 1972; Moss, 1956), E. coli (Castor and Chance, 1959; Haddock et al., 1976; Pudek and Bragg, 1974), Pseudomonas putida (Sweet and Peterson, 1978), and others. When higher concentrations of dissolved oxygen are available, a lower-affinity oxidase, cytochrome oxidase o, is generally encountered. Low-O_2 conditions are frequently cited as a source of nitrate-reductase induction, but low cellular energy levels or

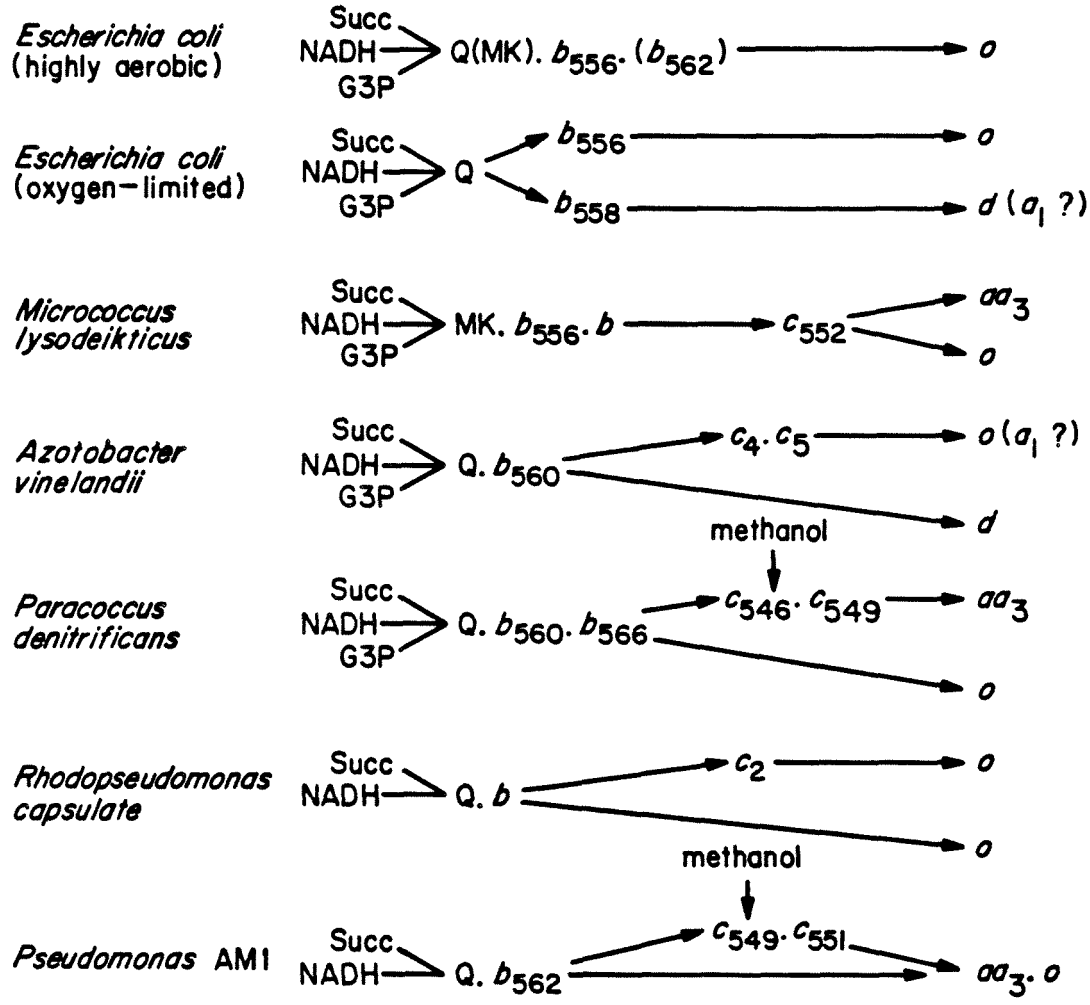

Figure 1.9. Known pathways of aerobic respiration in chemoheterotrophic and facultatively phototrophic bacteria. Single, italicized letters represent cytochrome types; characteristic maxima in difference spectra are provided as subscripts when available. (Jones, 1983)

even the reduced nature of the redox carriers themselves (in the absence of a suitable terminal electron acceptor) could be the direct cause of system expression since these conditions are difficult to separate. Relative O_2 affinities of the cytochrome oxidases are of the order d>aa_3 or o. See Table 1.1 (Poole, 1983).

Variation in transport-chain composition has also been encountered in response to depletion of a nutrient which is essential for redox carrier synthesis. Perhaps the simplest such example involves bacterial growth in low-iron media, which produces correspondingly low concentrations of iron-sulfur proteins and cytochromes. Sulfate-limitation decreases membrane concentrations of iron-sulfur proteins but seems to stimulate cytochrome synthesis. Bacterial growth on a rapidly metabolizable carbon source such as glucose can lead to a general decrease in concentrations of bacterial respiratory chain components without altering the qualitative nature of the electron-transport chain (Jones, 1983). In general, redox carrier composition appears to respond to external stimuli in ways which tend to minimize biosynthesis of unnecessary components and/or electron-transport system branches.

1.3.4 Control of Electron Transport.

Under most circumstances, kinetic control of electron transport is exerted at the level of the primary dehydrogenase, as opposed to the quinone-cytochrome system (Harrison, 1976). As one might expect from an enzymatically catalyzed reaction, dehydrogenase activity is affected by the rate at which reductant is generated within the cell (and hence steady-state concentration of reductant), dehydrogenase concentration,

substrate-dehydrogenase affinity, and allosteric modulation by such endogenous metabolites as NAD^+ and AMP. Cytochrome-oxidase activity becomes rate-controlling in the presence of limiting concentrations of molecular oxygen or such competitive inhibitors as CN^-, N_3^-, or CO. Comparison with aerobic respiration rates indicates that when electron transport is to Fe(III), respiratory control usually lies with iron reductase activity. However, prior to this work there has been no systematic investigation of dissimilative iron reduction kinetics.

As indicated previously, respiratory control is exerted on a much broader (and slower) level via biosynthesis of specific cellular components in response to environmental conditions or perhaps intracellular energy status. Examples of such control which have been mentioned include adjustment of electron carrier concentration and composition (i.e., development of alternative cytochrome oxidases or electron transfer branches which terminate in electron acceptors other than molecular oxygen). All such broad-scale adjustments affect the electron-transport and energy-generation capacities of the cell, though relatively slowly. Molecular details governing such control measures are largely unknown.

1.3.5 Stoichiometry of Oxidative Phosphorylation.

In light of the variation (both inter-species and temporal) which characterizes collective bacterial electron transport systems, it is not surprising that considerable disparity exists in the efficiency with which bacterial cells convert energy from substrate oxidations into useable cellular energy. There are two factors in the overall conversion efficiency: (i) the $H^+/2e^-$ ratio (alternatively the H^+/O

ratio, etc.) is a direct measure of the number of proton translocation sites in the electron transport chain, and (ii) the ATP/H^+ ratio reflects the stoichiometry of ATP generation during proton retranslocation via the membrane-bound ATPase. The product of these ratios ($ATP/2e^-$ or ATP/O) is a measure of cellular efficiency in generating ATP from the transfer of electrons from substrate to oxygen.

As one might expect from the foregoing discussion, the $H^+/2e^-$ ratio is dependent upon the identities of the substrate (when multiple dehydrogenases are present), intermediate electron carriers, and terminal electron acceptor (or even cytochrome oxidase). There is considerably more energy potentially available from electron transport to molecular oxygen (Chapter 2) than to alternate electron acceptors. Although mechanistic details are scarce, proton translocation, and hence energy transduction, is thought to be dependent on the spatial arrangement of electron carriers into transmembrane loops such that protons are accepted at the cytoplasmic side and released into the cell surroundings or periplasm during the course of electron transport (Haddock and Jones, 1977; Harold, 1978). An example of such a (proposed) translocation loop is provided as Figure 1.10. The number of proton translocation sites clearly depends upon transport chain composition. Finally, although cytochrome oxidase aa_3 provides a proton translocation site, the proton-pumping capabilities of other cytochrome oxidases has not been unequivocally established.

The number and location of proton-translocating sites within the respiratory chains of whole-cell preparations is determined by isolating specific portions of the electron transport chain. This is accomplished chemically via judicious choice of reductant and oxidant based upon redox

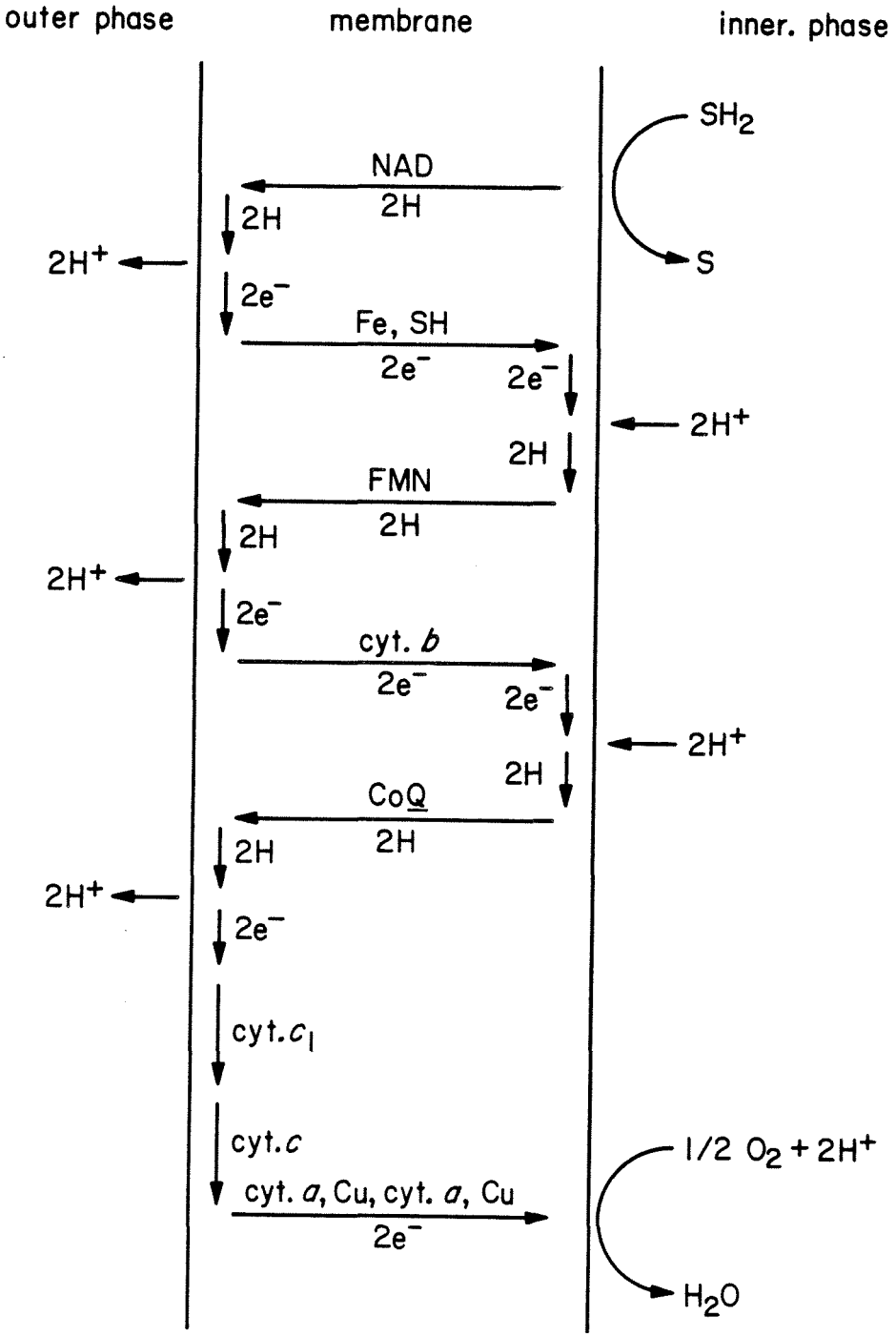

Figure 1.10. Schematic diagram illustrating Mitchell's concept of folding or looping of respiratory pathways. Loops were proposed as a means for coupling proton translocation to electron transport in mitochondria. (Mitchell, 1966)

potential or by addition of transport inhibitors of known activity (capable of blocking electron transport in specific regions or branches of the chain). Pulses of oxidant are then injected into starved whole-cell suspensions in the presence of excess reductant, and the $H^+/2e^-$ quotient is measured on the basis of initial rates of H^+ ejection and oxidant utilization. Results of such experiments conducted using E. coli, A. eutrophus, Pseudomonas dentrificans, Pseudomonas AM1, and Micrococcus methylotrophus have revealed the existence of up to 4 proton translocation sites: At the level of the energy-dependent dehydrogenase (site Ø) proton retranslocation and/or ATP hydrolysis is coupled to the reduction of $NADP^+$ via the equation:

$$NADP^+ + H^+ + NADH \longrightarrow NADPH + NAD^+ + H^+$$

The reaction illustrates the (generally) reversible nature of bacterial electron transport. Proton translocation is also possible at the NADH dehydrogenase (site 1) and within the quinone-cytochrome system (sites 2 and 3) (Jones, 1983). Energy-transduction sites have been found to be inducible or inoperative during specific modes of electron transport. Whole-cell H^+/O quotients of approximately 4 (e.g., E. coli, Klebsella pneumoniae, Bacillus megaterium), 6 (Micrococcus lysodeikticus, P. AM1, M. methylotrophus) and 8 (P. dentrificans, A. eutrophus, Thiobacillus thermophilus, Pseudomonas ovalis) have been observed for the O_2 oxidation of endogenous substrates under conditions which maximize the stoichiometry of proton translocation (Jones, 1983). From such experiments, it is evident that proton translocation efficiency is

dependent on transport-chain composition in addition to the identities of endogenous substrate and terminal electron acceptor.

Measurement of ATP/O ratios among whole cells via O_2-pulse techniques has largely been frustrated by difficulties attendant to analysis of gross intracellular ATP production. Consequently, measurements have more commonly been carried out in suspensions of inside-out vesicles. Since such preparations rarely produce completely sealed vesicles, estimates of overall energy transduction efficiencies have proven generally low.

Measurements of ATP/H^+ ratios are beset by a similar set of difficulties. That is, direct measurements of simultaneous rates of intracellular ATP synthesis and H^+ uptake can be confused by simultaneous ATP hydrolysis or H^+ uptake via other membrane-bound transport systems. When such measurements are made using inside-out vesicles, membrane integrity has again produced unreasonably low quotients. An alternate means for indirectly measuring the ATP/H^+ ratio is based on the thermodynamics of ADP phosphorylation coupled to proton retranslocation. By assuming that equilibrium exists between the transmembrane proton-motive force and ATP synthesis, it is possible to write:

$$H^+/ATP = \Delta G_p/\Delta p \cdot F, \text{ where}$$

ΔG_p is the free energy required for ATP synthesis under intracellular conditions, in kcal/mole,

Δp is the proton-motive force across the cytoplasmic membrane in mV, and F is the Faraday constant.

ΔG_p is also defined by:

$$\Delta G'_p = -\Delta G^{o'} + RT \ln \frac{[ATP]}{[ADP][P_i]}, \text{ where}$$

$\Delta G^{o'}$ is the standard free energy of ATP hydrolysis ($kcal \cdot mole^{-1}$) at pH 7 and brackets denote (intracellular) concentrations in molar units. Thus, if Δp and ΔG_p can be estimated via independent means, it should be possible to calculate the ATP/H^+ quotient. Kashket (1982) applied such a method to the estimation of H^+/ATP stoichiometry in growing and non-growing, respiring E. coli cells. Here, Δp was estimated by measuring the intracellular (energy-dependent) accumulation of lactose in a lac-operon-constitutive, β-galactosidase-negative mutant. Values for $\Delta G'_p$ were estimated from measurement of intracellular concentrations of ATP, ADP and inorganic phosphate (physiological pH ≅ 7.0). The H^+/ATP ratio calculated in this manner was 3, although parallel calculations based on alternative methods for estimating Δp yielded variable results. Previously reported estimates include 2 or 3 for H^+/ATP in mitochondria and 3 for chloroplasts (Fillingame, 1980), 3 for resting cells of Paracoccus dentrificans (McCarthy et al., 1981), and up to 8 for the alkalophile Bacillus alkalophilus (Guffanti et al., 1981). Direct measurements of H^+ influx and ATP synthesis in Streptococcus lactis yielded a ratio of 2.

1.4 Dissimilative Iron Reduction - Previous Studies

Halvorson and Starkey (1927) discovered that pure cultures of *E. coli* and *Clostridium sporogenes* could reduce ferric iron anaerobically. The same phenomenon was observed when bacteria were provided in a mixed soil inoculum. Twenty years later Roberts (1947) observed changes in the fermentation products of *Bacillus polymyxa* grown anaerobically in the presence and absence of ferric iron. Extensive reduction of iron provided as ferric hydroxide again indicated that Fe(III) was apparently able to serve as terminal electron acceptor in the absence of molecular oxygen.

Subsequent investigation (Bromfield, 1954a) indicated that *Bacillus circulans* and to a lesser extent *Escherichia freundii*, *Aerobacter aerogenes*, and *B. megaterium* could also reduce Fe(III) when presented as ferric hydroxide. The degree of iron reduction was dependent on medium composition and pH, and only *B. circulans* reduced iron present in a natural soil. In cultures of *B. circulans*, it was shown that ferrous iron production was inversely related to the degree of aeration, defined as culture surface area divided by depth (inch units). Bromfield (1954b) subsequently indicated that organic acids or other agents which complex Fe(III) were essential to bacterial iron-reduction activity. At final concentrations of 0.17% w/v, neither azide nor cyanide inhibited iron reduction in cultures of *B. circulans*.

Troshanov (1968, 1969) isolated manganese- and iron-reducing microorganisms from the sediments of ore-containing lakes of the Karelian peninsula in the U.S.S.R. Isolates were required to solubilize ground ferro-manganese ores. He found that all bacterial strains which reduced Fe(III) reduced MnO_2 as well (although the reverse was not

true). Species identified as iron reducers included B. circulans, Pseudomonas liquefaciens, B. mesentericus, Clostridium polymyxa, Aerobacter aerogenes, and Micrococcus radiatus. Among these, B. circulans showed the greatest activity and widest distribution. Microaerophiles dominated the list of bacteria exhibiting iron-reduction capabilities. In subsequent kinetic studies, it was determined that freshly precipitated ferric hydroxide was reduced much more readily than was Fe(III) from iron ore and that nitrate inhibited Fe(III), but not Mn(IV), reduction. Troshanov noted that the age (and hence degree of crystallinity) was a partial determinant of bacterial iron-reduction rate when iron was provided as ferric hydroxide. However, the relative rates of iron reduction among capable bacteria were essentially the same for all Fe(III) sources. Troshanov anticipated that the reduction of colloidal iron oxides must be preceded by a dissolution step; in experiments in which Fe(III) was complexed with citrate, activities of several microorganisms increased sharply, but Fe(III) reduction by B. circulans was impaired.

Inhibition of dissimilative iron reduction by NO_3^- has been explained largely via the efforts of Ottow and co-workers. To determine whether or not Fe(III) serves as terminal electron acceptor for respiration in a manner similar to nitrate, Ottow (1968) measured the effect of 0.2% KNO_3 on iron reduction by a variety of capable species: When an organism was endowed with nitrate reductase, Fe(III) reduction was suppressed; in the absence of nitrate reductase activity, however, iron reduction was essentially unimpaired. Mutants of Aerobacter aerogenes blocked in nitrate reductase were inhibited in iron reduction capacity (though this activity was not entirely eliminated) indicating

that Fe(III) serves as an alternative electron acceptor for nitrate reductase in that species. Residual iron reduction activity was not inhibited by nitrate addition. The non-specific substrate requirements of the nitrate-sensitive reductase had been observed previously by Pichinoty (1963) and Hackenthal et al. (1964) who determined that chlorate and perchlorate, respectively, could serve as oxidants for that system. Similarly, nit$^-$ mutants were generated in B. polymyxa, S. morcescens, Pseudomonas aeruginosa, B. circulans, and B. cereus (Ottow, 1970). Implications for iron-reduction capacity were similar to the effects of nitrate reductase mutation in A. aerogenes: elimination of NO_3^--reduction activity led to a partial loss of iron-reduction capacity. Residual iron-reductase activity was unaffected by nitrate addition suggesting that at least two different enzymatic mechanisms are involved in Fe(III) reduction.

Ottow and Glathe (1971) isolated 71 strains of facultative anaerobic bacteria from gleyed subsoils which were capable of reducing iron oxide in pure cultures. Although species represented a variety of genera, all but three were also capable of reducing nitrate to nitrite. Conditions for nitrate reductase induction in these microorganisms were identical to those of the iron reductase.

The lack of iron-reduction activity which is commonly observed in the presence of NO_3^- is apparently due to competitive inhibition. From an energetic standpoint, electron transport to NO_3^- is considerably more favorable than dissimilative iron reduction (see Chapter 2). Strains of Clostridium butyricum and Clostridium saccharobutyricum isolated from gleyed subsoils (wild-type, nit$^-$) exhibited iron reduction activity which was unaffected by nitrate addition but substantially suppressed by

the presence of MnO_2 powder, another electron acceptor which is energetically favored in comparison to iron (Hammann and Ottow, 1974).

Mechanistic aspects of iron reduction by capable bacteria remain somewhat dubious, although the enzymatic basis of the Fe(III) ----> Fe(II) conversion is reasonably certain. The process may be direct (Fe(III) serves as terminal electron acceptor for bacterial respiration) or indirect (ferric iron is chemically reduced by soluble bacterial metabolites). The mechanism of iron reduction by acidophiles Thiobacillus thiooxidans, T. ferrooxidans, and Sulfolobus acidocaldarius, all of which are able to reduce ferric iron when growing on elemental sulfur, is particularly uncertain. The biological basis of this conversion is evident from the abiotic stability of elemental sulfur and Fe(III) under acid conditions. Brock and Gustafson (1976) found that both species catalyzed iron reduction under aerobic conditions using elemental sulfur as substrate. (At sufficiently low pH, the rate of autoxidation of Fe(II) is negligible (Sung and Morgan, 1980)). However, because observed Fe(III) reduction could have been indirect, resulting from aerobic respiration with subsequent chemical reduction of Fe(III) by metabolic intermediates, Kino and Usami (1982) reproduced these experiments, growing T. thiooxidans on elemental sulfur under a nitrogen atmosphere. Neither growth nor ferric iron reduction was detected, suggesting an indirect mechanism for iron reduction by this species.

Recent experiments by Sugio et al. (1985) indicate that T. ferrooxidans can utilize ferric iron as electron acceptor for respiration. Under anaerobic conditions, the ferrous-iron product is

stable, but in the presence of molecular oxygen the cell's iron oxidase rapidly reoxidizes Fe^{2+}.

These findings (iron reduction by acidophiles) probably do not reflect the mechanism of iron reduction in the majority of capable bacteria. Lascelles and Burke (1978) found that membrane preparations of Staphylococcus aureus were capable of catalyzing the transfer of electrons from several substrates including NADH and glycerol-6-phosphate to ferric iron. Their experiments clearly established the enzymatic, respiration-dependent nature of dissimilative iron reduction in this species. Other investigators have consistently concluded that Fe(III) serves as an alternate electron acceptor, equivalent to nitrate, in a variety of microorganisms (see above).

When electron transport results in reduction of solid-phase Fe(III), the logistics of dissimilative iron reduction present additional problems. Cell-envelope structure of (particularly) gram-negative bacteria seems to rule out direct contact between insoluble Fe(III) and respiratory enzymes which are localized within the cytoplasmic membrane. Munch and Ottow (1982) found that separation of solid-phase iron oxide from iron-reducing bacteria (both nit^+ and nit^- wild types) resulted in nearly complete suppression of iron-reduction activity, indicating that neither low E_h nor development of soluble, reducing intermediates was responsible for Fe(III) reduction. Direct cell-iron oxide contact was assumed to be requisite to iron reduction. However, such a scheme seems to require transfer of reducing equivalents across the periplasmic space (gram-negative case only) or the cell wall of gram-positive bacteria. Although no experimental evidence exists in this area, Munch and Ottow (1983) suggested that a soluble electron carrier, capable of diffusing

across this space, could function in this manner. Since c-type cytochromes are often peripherally attached to the periplasmic side of the cytoplasmic membrane or free in the periplasm, they seem likely candidates for such a role.

Finally a mechanistic explanation is lacking for the observed preference of iron-reducing bacteria for more thermodynamically favorable electron acceptors. Munch, Hillebrand, and Ottow (1978) observed that non-crystalline iron oxides are reduced in preference to crystalline forms (which were not reduced until all active, non-crystalline iron oxides had been utilized). In mixtures of crystalline Fe(III)-oxides, those of greater free energy (least stability) were reduced preferentially (order of reduction lepidocrocite > hematite > goethite; Munch and Ottow, 1982). DeCastro and Ehrlich (1970) had previously made a similar observation: Bacillus 29, isolated from ferromanganese nodule, and a derivative strain, Bacillus 29A, enzymatically reduced Fe(III) in a variety of iron oxides. Both limonite and goethite were reduced much faster than hematite, perhaps reflecting stability relationships. Neither strain was capable of reducing nitrate. Addition of phenosafranin substantially enhanced observed rates of reductive dissolution of iron oxides, perhaps by acting as avenues for electron transfer between iron oxides and microbial enzyme systems. Chelation of ferrous iron by the dye was not observed.

1.5 Fe(III) Reduction by Pseudomonas sp. 200.

Pseudomonas sp. 200, isolated and taxonomically characterized by Obuekwe (1980), is among the most efficient iron-reducers yet encountered. Though it is difficult to compare literature values due to differences in cell densities or other fermentation conditions, iron-reduction rates reported for this microorganism by Obuekwe et al. (1981) and Obuekwe and Westlake (1982a) are striking. The relationship between NO_3^- utilization and Fe(III) reduction in Pseudomonas sp. 200 has been studied in some detail (Obuekwe et al., 1981; Obuekwe and Westlake, 1982b) leading to the conclusion that iron reduction is inhibited by the development of NO_2^- in solution, as opposed to competitive inhibition of Fe(III) reduction by nitrate (the supposed inhibitory mechanism of NO_3^- in other microorganisms).

The Pseudomonas sp. 200 ferri-reductase was found to be partially inducible. Its development was considerably greater in rich than in a defined medium, and when cells were grown in a defined medium without iron, ferri-reductase activity was essentially missing (Obuekwe and Westlake, 1982a). The cytochrome complement of Pseudomonas sp. 200 was found to consist, as a minimum, of cytochrome c_{552} and several other b- or c-type cytochromes. Iron-reduction capacity was directly related to intensity of the cytochrome absorption maxima.

The impact of carbon monoxide on dissimilative iron reduction was severe when cells were grown on rich media or on a defined medium plus iron. However, residual ferri-reductase activity among cells grown on iron-deficient media was essentially unaffected by CO (Obuekwe and Westlake, 1982a). Sodium amytal, 2-n-heptyl-4-hydroxyquinoline-N-oxide (HOQNO) and sodium cyanide (but not sodium oxalate) proved inhibitory,

to varying degrees, to electron transport to Fe(III) (Obuekwe, 1980). The electron transport chain configuration supported by Obuekwe's difference spectra and inhibition experiments is illustrated in Figure 1.11.

1.6 Summary of Research Objectives

It is now possible to identify the major questions or areas of inquiry which motivate our study:

1. Can the energetics of dissimilative iron reduction tell us anything about the susceptibility of specific minerals to bacterially mediated reductive dissolution? What are the probable effects of ligand addition and chemical speciation on process energetics and feasibility; under what chemical conditions can bacteria generate useful cellular energy via electron transport to Fe(III) (i.e., when is oxidative phosphorylation possible)?

2. Is it possible to find a valid basis for comparison of iron-reduction catalysis by a variety of capable bacterial species? Are there other growth or metabolic factors which should be considered in selecting microorganisms or specific enzymatic systems for development of a commercially attractive, iron-leaching system?

3. Can thermodynamic relationships be relied upon to predict the speciation of ferric- and ferrous-forms in iron-reduction media? To what extent does the overall solubility of Fe(III) affect the facility with which iron serves as terminal electron acceptor for bacterial respiration; are the concentrations of individual species important determinants of the overall rate of dissimilative iron reduction?

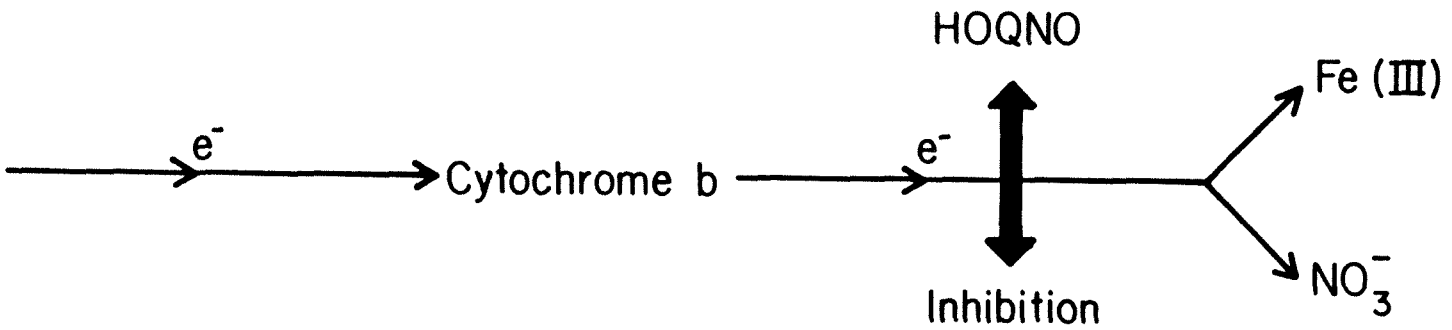

Figure 1.11. Electron-transport chain configuration of Pseudomonas sp. 200 as developed by experiments involving reduced-minus-oxidized difference spectra and chemical inhibition of electron transport. (Obuekwe and Westlake, 1981.)

4. What are the relationships between enzymes of aerobic electron transport and those of dissimilative iron reduction? Does the physical nature of the electron transport system reflect specific growth conditions, and can rate-limiting steps be identified within the electron-transport chain? Can practical, experimental methods be applied to explore relationships between dissimilative iron reduction and oxidative phosphorylation (i.e., does electron transport to Fe(III) drive ADP phosphorylation)?

5. Can spectral characteristics of whole-cell or membrane preparations be utilized to determine cell cytochrome content and the degree to which respiratory enzymes are localized within the cytoplasmic membrane? To what degree do these results reflect conditions of cell growth and medium composition?

6. What factors determine the rate of reductive dissolution of Fe(III)-bearing solids when respiratory electrons are transferred to iron oxides? Is direct cell contact between cells and iron oxide particles requisite to reductive dissolution, or is the process indirectly catalyzed via bacterial production of soluble, reducing intermediates? What is the mechanism by which ligand addition accelerates reductive dissolution of iron oxides, and to what extent can thermodynamic relationships be used to anticipate process kinetics?

These areas are approached sequentially in Chapters 2 through 6. By Chapter 7 it will be possible to return to specific questions and assess the degree to which theoretical and experimental investigations have produced answers.

1.7 REFERENCES

Anderson, M. A. and Morel, F. M. M. Uptake of Fe(II) by a diatom in oxic culture medium. Mar. Biol. Lett. 1: 263-268 (1980).

Anderson, M. A. and Morel, F. M. M. The influence of aqueous iron chemistry on the uptake of iron by the coastal diatom Thalassiosira weissfloggi. Limnol. Oceanog. 27: 789-813 (1982).

Bailey, J. E. and Ollis, D. F. Biochemical Engineering Fundamentals. McGraw-Hill, New York (1977).

Barber, R. T. and Ryther, J. H. Organic chelators: factors affecting primary production in the Cromwell Current upwelling. J. Exp. Mar. Biol. Ecol. 3: 191-199 (1969).

Brierley, C. L. Microbiological mining. Scient. Amer. 247(2): 44-53 (1982).

Brock, T. D. and Gustafson, J. Ferric iron reduction by sulfur- and iron-oxidizing bacteria. Appl. Environ. Microbiol. 32: 567-571 (1976).

Bromfield, S. M. The reduction of iron oxide by bacteria. J. Soil Sci. 5: 129-139 (1954a).

Bromfield, S. M. Reduction of ferric compounds by soil bacteria. J. Gen. Microbiol. 11: 1-6 (1954b).

Castor, L. N. and Chance, B. Photochemical determinations of the oxidases of bacteria. J. Biol. Chem. 234: 1587-1592 (1959).

Davidson, W.; Heaney, S. I.; Talling, J. F. and Rigg, E. Seasonal transformations and movements of iron in a productive English lake with deep-water anoxia. Schweiz. Z. Hydrol. 42: 196-224 (1980).

DeCastro, A. F. and Ehrlich, H. L. Reduction of iron oxide minerals by a marine Bacillus. Antonie van Leeuwenhoek 36: 317-327 (1970).

DiRienzo, J. M.; Nakamura, K. and Inouye, M. The outer membrane proteins of gram-negative bacteria: biosynthesis, assembly and functions. Ann. Rev. Biochem. 47: 481-532 (1978).

Ehrlich, H. L. Geomicrobiology. pp. 187-192. Marcel Dekker, New York (1981).

Engel, A.; Massalski, A.; Schindler, H.; Dorset, D. L. and Rosenbusch, J. P. Porin channel triplets merge into single outlets in Escherichia coli outer membranes. Na. 317: 643-645 (1985).

Fillingame, R. H. The proton-translocating pumps of oxidative phosphorylation. Annu. Rev. Biochem. 49: 1079-1113 (1980).

Garrels, R. M. and Christ, C. L. Solutions, Minerals, and Equilibria. Harper and Row, New York (1965).

Gelles, J.; Blair, D. F.; Martin, C. T.; Wang, H. and Chan, S. I. Structural studies on the metal centers of cytochrome c oxidase, pp. 259-277. In: Frontiers in Biochemical and Biophysical Studies of Proteins and Membranes. Eds. T. Liu, S. Sakakibara, A. N. Schechter, K. Yagi, H. Yajima and K. T. Yasunobu. Elsevier, New York (1983).

Gel'man, N. S.; Lukoyanova, M. A. and Ostrovskii, D. N. Biomembranes, Vol. 6. pp. 129-215. Plenum, New York (1975).

Glover, H. E. Iron in marine coastal waters; seasonal variation and its apparent correlation with dinoflaggelate bloom. Limnol. Oceanog. 23: 534-537 (1966).

Guffanti, A. A.; Bornstein, R. F. and Krulwich, T. A. Oxidative phosphorylation by membrane vesicles from Bacillus alcalophilus. Biochim. Biophys. Acta 635: 619-630 (1981).

Hackenthal, E.; Mannheim, W.; Hackenthal, R. and Beeker, R. Die Reduktion von Perchlorat durch Bakterien I. Untersuchungen an intakten Zellen. Biochem. Pharmacol. 13: 195-206 (1964).

Haddock, B. A.; Downie, J. A. and Garland, P. B. Kinetic characterization of the membrane-bound cytochromes of Escherichia coli grown under a variety of conditions by using a stopped-flow dual-wavelength spectrophotometer. Biochem. J. 154: 285-294 (1976).

Haddock, B. A. and Jones. C. W. Bacterial respiration. Bacteriol. Rev. 41: 47-99 (1977).

Halvorson, H. O. and Starkey, R. L. Studies on the transformations of iron in nature, Part II. Concerning the importance of microorganisms in the solution and reduction of iron. Soil Sci. 24: 381-390 (1947).

Hammann, R. and Ottow, J. C. G. Reductive dissolution of Fe_2O_3 by saccharolytic Clostridia and Bacillus polymyxa under anaerobic conditions. Z. Pflanzenernaehr Bodenkd. 137: 108-115 (1974).

Harold, F. M. Vectorial metabolism. In: The Bacteria, Vol. VI, eds. L. N. Ornston and J. R. Sokatch; editor-in-chief I. C. Gunsalus, Academic Press, New York (1978).

Harrison, D. E. F. A study of the effect of growth conditions on chemostat-grown Klebsiella aerogenes and kinetic changes of a 500-nm absorption band. Biochim. Biophys. Acta 275: 83-92 (1972).

Harrison, D. E. F. The regulation of respiration rate in growing bacteria. In: Adv. Microb. Physiol., Vol. 14, eds. A. H. Rose and D. W. Tempest (1976).

Hinkle, P. C. and McCarty, R. E. How cells make ATP. Scient. Amer. 228(3): 104-122 (1978).

Inouye, M. A three-dimensional molecular assembly model of a lipoprotein from the Escherichia coli outer membrane. Proc. Natl. Acad. Sci. USA 71: 2396-2400 (1974).

Jones, C. W. Bacterial Respiration and Photosynthesis, Aspects of Microbiology, 5. American Society for Microbiology, Washington, D.C. (1983).

Jones, C. W. and Poole, R. K. The analysis of cytochromes. In: Methods in Microbiology, Vol. 18, Chapter 10. Academic Press, New York (1985).

Jones, J. G. Some observations on the occurrence of the iron bacterium Leptothrix ochracea in fresh water, including reference to large experimental enclosures. J. Appl. Bact. 39: 63-72 (1975).

Jones, J. G.; Gardener, S. and Simon, B. M. Bacterial reduction of ferric iron in a stratified lake. J. Gen. Microbiol. 129: 131-139 (1983).

Jones, J. G.; Gardener, S. and Simon, B. M. Reduction of ferric iron by heterotrophic bacteria in lake sediments. J. Gen. Microbiol. 130: 45-51 (1984).

Kashket, E. R. Stoichiometry of the H^+-ATPase of growing and resting, aerobic Escherichia coli. Biochem. 21: 5534-5538 (1982).

Kino, K. and Usami, S. Biological reduction of ferric iron by iron- and sulfur-oxidizing bacteria. Agric. Biol. Chem. 46: 803-805 (1982).

Konings, W. N. and Veldkamp, H. Energy transduction and solute transport mechanisms in relation to environments occupied by microorganisms. In: Microbes in their Natural Environments. Eds. J. H. Slater, R. Whittenbury and J. W. T. Wimpenny. Cambridge Univ. Press, Cambridge (1983).

Lascelles, J. and Burke, K. A. Reduction of ferric iron by lactate and DL-glycerol-3-phosphate in membrane preparations from Staphylococcus aureus and interaction with nitrate reductase system. J. Bacteriol. 134: 585-589 (1978).

Lehninger, A. H. Bioenergetics, pp. 75-95. Benjamin/Cummings, Menlo Park, CA (1973).

Lemberg, R. and Barrett, J. Cytochromes. Academic Press, New York (1973).

Lin, E. C. C.; Goldstein, R. and Syvanen, M. Bacteria, Plasmids and Phages. Harvard University Press, Cambridge, MA (1984).

Lovley, D. R. and Phillips, E. J. P. Organic matter mineralization with reduction of ferric iron in anaerobic sediments. Appl. Environ. Microbiol. 51: 683-689 (1986).

McCarthy, J. E. G.; Ferguson, S. J. and Kell, D. B. Estimation with an ion-selective electrode of the membrane potential in cells of Parococcus dentrificans from the uptake of the butyltriphenylphosphonium cation during aerobic and anaerobic respiration. Biochem. J. 196: 311-321 (1981).

Menzel, D. W. and Ryther, J. H. Nutrients limiting the production of phytoplankton in the Sargasso Sea, with special reference to iron. Deep Sea Re. 7: 276-281 (1961).

Meyer, D. J. and Jones, C. W. Int. J. Syst. Bacteriol. 23: 459-467 (1973).

Mitchell, P. Coupling of phosphorylation to electron and hydrogen transfer by a chemi-osmotic type of mechanism. Na. 191: 144-148 (1961).

Mitchell, P. Chemiosmotic coupling in oxidative and photosynthetic phosphorylation. Biol. Rev. 41: 445-502 (1966).

Moss, F. Adaptation of the cytochromes of Aerobacter aerogenes in response to environmental oxygen tension. Aust. J. Exp. Biol. Med. Sci. 34: 395-406.

Moyed, H. S. and O'Kane, D. J. Enzymes and coenzymes of the pyruvate oxidase of Proteus. J. Biol. Chem. 218: 831-840 (1956).

Munch, J. C.; Hillebrand, T. and Ottow, J. C. G. Transformations in the Fe_o/Fe_d ratio of pedogenic iron oxides affected by iron-reducing bacteria. Can. J. Soil. Sci. 58: 475-486 (1978).

Munch, J. C. and Ottow, J. C. G. Effect of cell contact and iron(III)-oxide on bacterial iron reduction. Z. Pflanzenernaehr Bodenk. 145: 66-77 (1982).

Munch, J. C. and Ottow, J. C. G. Reductive transformation mechanism for ferric oxides in hydromorphic soils. Environmental Geochemistry Ecol. Bull. (Stockholm) 35: 383-394 (1983).

Nakae, T. and Nikaido, H. Outer membrane as a diffusion barrier in Salmonella typhimurium. Penetration of oligo- and polysaccharides into isolated outer membrane vesicles and cells with degraded peptidoglycan layer. J. Biol. Chem. 250: 7359-7365 (1975).

Obuekwe, C. O. Microbial corrosion of crude oil pipeline. Ph.D. dissertation. Univ. of Alberta, Edmonton, Alberta (1980).

Obuekwe, C. O.; Westlake, D. W. S. and Cook, F. D. Effect of nitrate on reduction of ferric iron by a bacterium isolated from crude oil. Can. J. Microbiol. 27: 692-697 (1981).

Obuekwe, C. O. and Westlake, D. W. S. Effects of medium composition on cell pigmentation, cytochrome content, and ferric iron reduction in a Pseudomonas sp. isolated from crude oil. Can. J. Microbiol. 28: 989-992 (1982a).

Obuekwe, C. O. and Westlake, D. W. S. Effect of reducible compounds (potential electron acceptors) on reduction of ferric iron by Pseudomonas species. Microbios Lett. 19: 57-62 (1982b).

Ottow, J. C. G. Evaluation of iron-reducing bacteria in soil and the physiological mechanism of iron reduction in Aerobacter aerogenes. Z. Allg. Mikrobiol. 8: 441-443 (1968).

Ottow, J. C. G. Selection, characterization, and iron-reducing capacity of nitrate reductaseless (nit^-) mutants of iron-reducing bacteria. Z. Allg. Mikrobiol. 10: 55-62 (1970).

Ottow, J. C. G. and Glathe, H. Isolation and identification of iron-reducing bacteria from gley soils. Soil Biol. Biochem. 3: 43-55 (1971).

Pichinoty, F. Recherches sur la nitrate reductase d'Aerobacter aerogenes. Ann. Inst. Pasteur 104: 394-418 (1963).

Poole, R. K. Bacterial cytochrome oxidases, a structurally and functionally diverse group of electron-transfer proteins. Biochim. Biophys. Acta 726: 205-243 (1983).

Pudek, M. R. and Bragg, P. D. Inhibition by cyanide of the respiratory chain oxidases of Escherichia coli. Arch. Biochem. Biophys. 164: 682-693 (1974).

Roberts, J. L. Reduction of ferric hydroxide by strains of Bacillus polymyxa. Soil Sci. 63: 135-144 (1947).

Rogers, H. J.; Perkins, H. R. and Ward, J. B. Microbial Cell Walls and Membranes. Chapman and Hall, London (1980).

Ryther, J. H. and Guillard, R. L. Enrichment experiments as a means of studying nutrients limiting to phytoplankton populations. Deep Sea Re. 6: 65-69 (1959).

Sørensen, J. Reduction of ferric iron in anaerobic, marine sediment and interaction with reduction of nitrate and sulfate. Appl. Environ. Microbiol. 43: 319-324 (1982).

Steven, A. C.; Ten Heggeler, B.; Mueller, R.; Kistler, J. and Rosenbusch, J. P. Ultrastructure of a periodic protein layer in the outer membrane of Escherichia coli. J. Cell Biol. 72: 292-301 (1977).

Stumm, W. and Morgan, J. J. Aquatic Chemistry. Wiley, New York (1981).

Sugio, T.; Domatsu, C.; Munakata, O.; Tano, T. and Imai, K. Role of a ferric iron-reducing system in sulfur oxidation of Thiobacillus ferrooxidans. Appl. Environ. Microbiol. 49: 1401-1406 (1985).

Sung, W. and Morgan, J. J. Kinetics and product of ferrous iron oxygenation in aqueous systems. Environ. Sci. Technol. 14: 561-568 (1980).

Sweet, W. J. and Peterson, J. A. Changes in cytochrome content and electron transport patterns in Pseudomonas putida as a function of growth phase. J. Bacteriol. 133: 217-224 (1978).

Takai, Y. and Kamura, T. The mechanism of reduction in waterlogged paddy soil. Folia Microbiol. 11: 304-313 (1966).

Troshanov, E. P. Iron- and manganese-reducing microorganisms of ore-containing lakes of the Karelian isthmus. Mikrobiol. 37: 786-791 (1968).

Troshanov, E. P. Conditions affecting the reduction of iron and manganese by bacteria in the ore-bearing lakes of the Karelian isthmus. Mikrobiol. 38: 528-535 (1969).

Van Iterson, W. Outer Structures of Bacteria. Van Nostrand Reinhold, New York (1984a).

Van Iterson, W. Inner Structures of Bacteria. Van Nostrand Reinhold, New York (1984b).

Webster, D. A. The formation of hydrogen peroxide during the oxidation of reduced nicotinamide adenine dinucleotide by cytochrome o from Vitreoscilla. J. Biol. Chem. 250: 4955-4958 (1975).

White, D. C. and Sinclair, P. R. Branched electron-transport systems in bacteria. Adv. Microbiol. Physiol. 5: 173-211 (1971).

Windholz, M. (editor) The Merck Index, 9th ed. Merck; Rahway, NJ (1976).

Wright, A. and Tipper, D. J. The outer membrane of gram-negative bacteria. In: The Bacteria, Vol. VII: Mechanisms and Adaptation. eds. J. R. Sokatch and L. N. Ornston; editor-in-chief I. C. Gunsalus. Academic Press, New York (1979).

Chapter 2

THE THERMODYNAMICS OF DISSIMILATIVE IRON REDUCTION

2.1 Introduction.

Thermodynamic calculations were carried out to:

(i) compare free energies available from oxidation of glucose, lactate ion, or NADH by a variety of electron acceptors including molecular oxygen, nitrate ion, and several chemical forms of Fe(III) and

(ii) assess the feasibility of coupling oxidative phosphorylation to dissimilative iron reduction via a chemiosmotic mechanism.

Energetic arguments were developed in the following way: (1) half-reactions representing the redox process of interest were postulated and combined to form the overall reactions of interest; (2) corresponding thermodynamic data were collected and standard electron potentials or free-energy changes calculated on that basis; (3) free-energy calculations were extended to non-standard, physiological or environmentally relevant conditions; and (4) computed free-energy changes were compared with each other and with estimated energy requirements for ADP phosphorylation. The overall procedure is illustrated in the following series of examples.

2.2 Heterotrophic bacteria.

2.2.1 Overall process energetics.

The oxidation of glucose to carbon dioxide by molecular oxygen is used to illustrate calculation of free-energy changes associated with

substrate utilization by heterotrophs under aerobic conditions. The following half-reactions pertain:

$$1/24\ C_6H_{12}O_6 + 1/4\ H_2O = 1/4\ CO_2(g) + H^+ + e^- \qquad p\varepsilon^\circ(w) = 7.20 \quad (2.1)$$

$$1/4\ O_2(g) + H^+ + e^- = 1/2\ H_2O \qquad p\varepsilon^\circ(w) = 13.75 \quad (2.2)$$

Overall:

$$1/4\ O_2(g) + 1/24\ C_6H_{12}O_6 = 1/4\ H_2O + 1/4\ CO_2(g) \qquad \Delta p\varepsilon^\circ(w) = 20.95 \quad (2.3)$$

In the expression $p\varepsilon^\circ(w)$, the superscript indicates standard conditions; (w) indicates that the "standard" hydrogen-ion activity has been modified to 10^{-7} M in order to yield standard potentials which are reasonably representative of physiological conditions or those of natural waters (Stumm & Morgan, 1981).

The change in electron potential associated with equation (2.3) can be converted to Gibbs free energy (per mole of electrons transferred) using:

$$\frac{\Delta G^\circ(w)}{n} = -2.3\ RT\ \Delta p\varepsilon^\circ(w)$$

where T is the absolute temperature under standard conditions (298°K), and R is the gas constant in appropriate units (1.987 cal/mol, °K).

Thus, $\frac{\Delta G°(w)}{n}$ = -28.5 kcal/mole of electrons transferred. The actual (intracellular) concentrations of reactants and products are: $\{C_6H_{12}O_6\}$ = 0.2% w/v ≅ 0.1 M; $\{O_2(g)\}$ = 0.1 atm. (about 50% of saturation with air); and $\{CO_2(g)\}$ = 0.001 atm. Then:

$$\Delta p = \Delta p\varepsilon°(w) - \log \frac{\{CO_2\}^{1/4}}{\{C_6H_{12}O_6\}^{1/24}\{O_2\}^{1/4}} = 21.41$$

and $\frac{\Delta G}{n}$ = -2.3 RT$\Delta p\varepsilon$ = -29.16 kcal/mole of e^- transferred. It is evident that free-energy changes associated with glucose oxidation are independent of pH and depend only weakly on the concentration of glucose. In suspensions of discrete bacterial cells, limitation of cellular respiration rate by diffusion of molecular oxygen from the bulk fluid is considered to be very unlikely, even at low-oxygen concentrations (Harrison, 1976); O_2 concentration at the cytoplasmic side of the plasma membrane should be approximately equal to that of the bulk solution.

Oxidation of glucose by ferric hydroxide was examined in a similar way using the additional half-reaction:

$$Fe(OH)_3(s,amorph) + 3H^+ + e^- = Fe^{2+} + 3H_2O;\ p\varepsilon°(w) = -5.0 \qquad (2.4)$$

(Stumm and Morgan, 1981)

Combining equations 2.1 and 2.4:

$$Fe(OH)_3(s,amorph) + 1/24\ C_6H_{12}O_6 + 2H^+ = 11/4\ H_2O + Fe^{2+}$$

$$+ 1/4\ CO_2(g) \qquad (2.5)$$

$$\Delta p\varepsilon^\circ(w) = 2.2;\ \frac{\Delta G^\circ(w)}{n} = -3.0 \text{ kcal/mole } e^- \text{ transferred}$$

If, under non-standard conditions, $\{CO_2(g)\} = 0.001$ atm., $\{Fe^{2+}\} = 10^{-3}$ M, $\{C_6H_{12}O_6\} = 0.1$ M, and pH = 7.0, then

$$\Delta p\varepsilon(w) = \Delta p\varepsilon^\circ(w) - \log \frac{\{CO_2(g)\}^{1/4}\{Fe^{2+}\}\{10^{-7}\}^2}{\{C_6H_{12}O_6\}^{1/24}\{H^+\}^2} = 5.9,$$

and $\frac{\Delta G}{n}$ = -8.0 kcal/mole of e^- transferred.

From the latter relationships, it is evident that a 1-unit drop in pH (to pH 6) results in a significant increase in free-energy liberated:

$$\frac{\Delta G}{n}\ (pH\ 6) = -10.8 \text{ kcal/mole of } e^- \text{ transferred.}$$

A note regarding process topology is also appropriate. If $Fe(OH)_3$(s,amorph) is to serve as electron acceptor for respiration, the bacterial ferrireductase must be oriented toward the periplasmic space (gram-negative bacteria) or cell surroundings. This orientation is also required when Fe(III) is provided in soluble form since the charged nature of most soluble iron species precludes its passage across the cytoplasmic membrane via passive diffusion, and arguments based on energetics may be used to rule out any other type of transport.

Consequently, the relevant concentration of Fe^{2+} for the purpose of free-energy computations is that of the periplasmic space or cell surroundings.

Similar calculations were performed for other redox processes which are potentially important to aerobic or anaerobic respiration. These involved various combinations of glucose, succinate, and lactate (organic substrates) and electron acceptors $O_2(g)$, NO_3^-, SO_4^{2-}, and Fe(III) as ferric hydroxide. Relevant thermodynamic data are provided in Table 2.1. Free-energy calculations were extended to non-standard conditions using a general formula based on overall process stoichiometry:

$$\frac{\Delta G}{n} = \frac{\Delta G^\circ}{n} + 2.3\ RT\{\sum_i m_i \log[\text{product}]_i - \sum_j n_j \log[\text{reactant}]_j\} \qquad (2.6)$$

where m_i is the stoichiometric coefficient of product species i,

n_j is the stoichiometric coefficient of reactant species j,

and other variables and constants are defined above.

Computational procedures and a sample calculation involving lactate oxidation are summarized in Table 2.2. Reactant and product concentrations considered typical of environmental and/or physiological conditions are provided in Table 2.3. Computational results are summarized in Figure 2.1.

Results are interpreted as follows: Oxidations involving molecular oxygen or NO_3^- as electron acceptors are considerably more exergonic than their counterparts in which SO_4^{2-} or Fe(III) serves as electron acceptor. As an energy source, glucose is only slightly more attractive than lactate or succinate (based on energy liberated per mole of

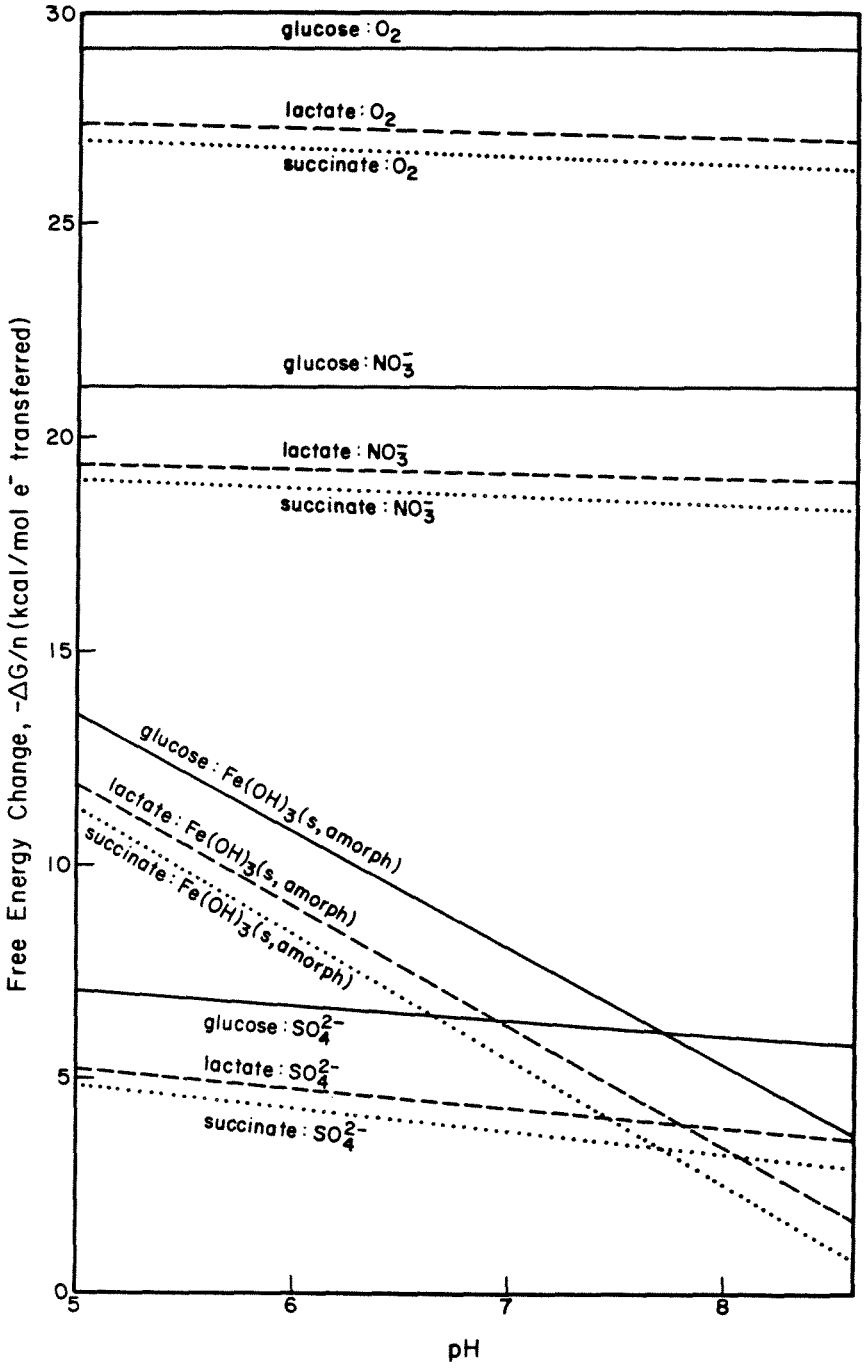

Figure 2.1. Overall thermodynamics of redox reactions involving organic substrates and a variety of oxidants found in natural waters. Reactions were chosen to illustrate the relative energetics of electron transport to a variety of chemical oxidants.

Table 2.1. Half-reactions and Thermodynamic Data Relevant to Selected Bacterial Respiratory Processes.

	Half reactions (as reductions)	$p\varepsilon°(w)$	Source
	Glucose:		
(i)	$\frac{1}{4}\ CO_2(g) + H^+ + e^- = \frac{1}{24}\ C_6H_{12}O_6 + \frac{1}{4}\ H_2O$	-7.20	Morel, 1983
	Succinate:		
(ii)	$\frac{2}{7}\ CO_2(g) + \frac{6}{7}\ H^+ + e^- = \frac{1}{14}\ (CH_2COO^-)_2 + \frac{2}{7}\ H_2O$	-5.23	Morel, 1983
	Lactate:		
(iii)	$\frac{1}{4}\ CO_2(g) + \frac{11}{12}\ H^+ + e^- = \frac{1}{12}\ CH_3CHOHCOO^- + \frac{1}{4}\ H_2O$	-5.74	Morel, 1983
	Oxidants:		
(iv)	$\frac{1}{4}\ O_2(g) + H^+ + e^- = \frac{1}{2}\ H_2O$	13.75	Morel, 1983
(v)	$\frac{1}{8}\ SO_4^{2-} + \frac{5}{4}\ H^+ + e^- = \frac{1}{8}\ H_2S(g) + \frac{1}{2}\ H_2O$	-3.50	Stumm & Morgan, 1981
(vi)	$\frac{1}{2}\ NO_3^- + H^+ + e^- = \frac{1}{2}\ NO_2^- + \frac{1}{2}\ H_2O$	7.15	Stumm & Morgan, 1981
(vii)	$Fe(OH)_3(s,amorph) + 3H^+ + e^- = Fe^{2+} + 3H_2O$	-5.0	Stumm & Morgan, 1981
(viii)	$Fe^{3+} + e^- = Fe^{2+}$	13.0	Stumm & Morgan, 1981

Table 2.2. Summary of Method for Computation of Free-energy Changes Associated with Electron-transfer Reactions; Illustration Involving Lactate Oxidation by $Fe(OH)_3(s)$.

Step 1: Select appropriate half-reactions comprising the overall electron transfer reaction of interest and corresponding thermodynamic data.

(i) $\frac{1}{12}\ CH_3CHOHCOO^- + \frac{1}{4}\ H_2O =$

$\frac{1}{4}\ CO_2(g) + \frac{11}{12}\ H^+ + e^-$ $\quad p\varepsilon^\circ(w) = 5.74$

(ii) $Fe(OH)_3(s,amorph) + 3H^+ + e^- =$

$Fe^{2+} + 3H_2O$ $\quad p\varepsilon^\circ(w) = -5.0$

Step 2: Combine half-reactions into overall reaction of interest; add electron activities as an indication of overall process energetics.

$\frac{1}{12}\ CH_3CHOHCOO^- + Fe(OH)_3(s,amorph) + \frac{25}{12}\ H^+ =$

$\frac{1}{4}\ CO_2(g) + Fe^{2+} + \frac{11}{4}\ H_2O$ $\quad p\varepsilon^\circ(w) = 0.74$

Step 3: Convert to non-standard $\Delta p\varepsilon$ using the general formula:

$$\Delta p\varepsilon = \Delta p\varepsilon^\circ(w) + \sum_j n_j \log [\text{reactants}]_j - \sum_i m_i \log [\text{products}]_i - 7\ h^+$$

where m_j is the stoichiometric coefficient of product species i, n_j is the stoichiometric coefficient of reactant species j, and h^+ is the stoichiometric coefficient of hydrogen-ion concentration (positive for product, negative for reactants).

Assumed concentrations:

$[CH_3CHOHCOO^-] = 0.1\ \underline{M}$

$[Fe^{2+}] = 10^{-3}\ \underline{M}$ $\qquad [CO_2(g)] = 10^{-3}$ atm.

$$\Delta p\varepsilon = 0.74 + \log \frac{[CH_3CHOHCOO^-]^{1/12}[H^+]^{25/12}}{[Fe^{2+}][CO_2(g)]^{1/4}[10^{-7}]^{25/12}}$$

@ pH 7, $\Delta p\varepsilon = 4.58$

Table 2.2. (continued)

Step 4: Convert $\Delta p\varepsilon$ to free-energy change per mole of electrons transferred using

$$\frac{\Delta G}{n} = -2.3\ RT\Delta p\varepsilon$$

where $\frac{\Delta G}{n}$ is the free energy of electron transfer in kcal/mol e^- transferred,

R is the gas constant, 1.987 cal/mol°K

T is the absolute temperature, 298°K.

$$\frac{\Delta G}{n}\ (\text{pH } 7) = -1.362\ (4.58)$$

$$= 6.2\ \text{kcal/mol } e^- \text{ transferred}$$

Table 2.3. Non-standard Conditions Considered Typical for Overall, Energy-yielding Reactions Important within the Context of Bacterial Respiration. Free-energy Calculations Summarized in Figure 2.1 are based on these Figures.

Overall Reaction	Assumed Physiological or Environmental Activities of Reactants and Products
$\frac{1}{24}$ glucose + $\frac{1}{4}$ $O_2(g)$ = $\frac{1}{4}$ H_2O + $\frac{1}{4}$ $CO_2(g)$	[glucose] = 0.1 M; $[O_2(g)]$ = 0.1 atm.; $[CO_2(g)] = 10^{-3}$ atm.
$\frac{1}{24}$ glucose + $\frac{1}{2}$ NO_3^- = $\frac{1}{4}$ $CO_2(g)$ + $\frac{1}{2}$ NO_2^- + $\frac{1}{4}$ H_2O	[glucose] = 0.1 M; $[NO_3^-] = 10^{-2}$ M; $[NO_2^-] = 10^{-3}$ M; $[CO_2(g)] = 10^{-3}$ atm.
$\frac{1}{24}$ glucose + $\frac{1}{8}$ SO_4^{2-} + $\frac{1}{4}$ H^+ = $\frac{1}{4}$ $CO_2(g)$ + $\frac{1}{8}$ $H_2S(g)$ + $\frac{1}{4}$ H_2O	[glucose] = 0.1 M; $[SO_4^{2-}] = 10^{-2}$ M; $[CO_2(g)] = 10^{-3}$ atm.; $[H_2S(g)] = 10^{-4}$ M
$\frac{1}{24}$ glucose + $Fe(OH)_3$(s,amorph) + $2H^+$ = $\frac{1}{4}$ $CO_2(g)$ + Fe^{2+} + $\frac{11}{4}$ H_2O	[glucose] = 0.1 M; $[Fe^{2+}] = 10^{-3}$ M; $[CO_2(g)] = 10^{-3}$ atm.
$\frac{1}{12}$(lactate)$^-$ + $\frac{1}{4}$ $O_2(g)$ + $\frac{1}{12}$ H^+ = $\frac{1}{4}$ $CO_2(g)$ + $\frac{1}{4}$ H_2O	[lactate$^-$] = 0.1 M; $[O_2(g)]$ = 0.1 atm.; $[CO_2] = 10^{-3}$ atm.
$\frac{1}{12}$(lactate)$^-$ + $\frac{1}{2}$ NO_3^- + $\frac{1}{12}$ H^+ = $\frac{1}{4}$ $CO_2(g)$ + $\frac{1}{4}$ H_2O + $\frac{1}{2}$ NO_2^-	[lactate$^-$] = 0.1 M; $[O_2(g)]$ = 0.1 atm.; $[NO_3^-] = 10^{-2}$ M; $[NO_2^-] = 10^{-3}$ M; $[CO_2(g)] = 10^{-3}$ atm.

Table 2.3. (continued)

Overall Reaction	Assumed Physiological or Environmental Activities of Reactants and Products
$\frac{1}{12}(\text{lactate})^- + \frac{1}{8}\,SO_4^{2-} + \frac{1}{3}\,H^+ = \frac{1}{4}\,CO_2(g) + \frac{1}{8}\,H_2S(g) + \frac{1}{4}\,H_2O$	$[\text{lactate}^-] = 0.1$ M; $[SO_4^{2-}] = 10^{-2}$ M; $[CO_2(g)] = 10^{-3}$ atm.; $[H_2S(g)] = 10^{-4}$ M
$\frac{1}{12}(\text{lactate})^- + Fe(OH)_3(s,\text{amorph}) + \frac{25}{12}\,H^+ = \frac{1}{4}\,CO_2(g) + Fe^{2+} + \frac{11}{4}\,H_2O$	$[\text{lactate}^-] = 0.1$ M; $[Fe^{2+}] = 10^{-3}$ M; $[CO_2(g)] = 10^{-3}$ atm.
$\frac{1}{14}(\text{succinate})^{2-} + \frac{1}{4}\,O_2 + \frac{1}{7}\,H^+ = \frac{2}{7}\,CO_2(g) + \frac{3}{14}\,H_2O$	$[\text{succinate}^{2-}] = 0.1$ M; $[O_2(g)] = 0.1$ atm.; $[CO_2(g)] = 10^{-3}$ atm.
$\frac{1}{14}(\text{succinate})^{2-} + \frac{1}{8}\,SO_4^{2-} + \frac{11}{28}\,H^+ = \frac{2}{7}\,CO_2(g) + \frac{1}{8}\,H_2S(g) + \frac{3}{14}\,H_2O$	$[\text{succinate}^{2-}] = 0.1$ M; $[SO_4^{2-}] = 10^{-2}$ M; $[CO_2(g)] = 10^{-3}$ atm.; $[H_2S(g)] = 10^{-4}$ M
$\frac{1}{14}(\text{succinate})^{2-} + Fe(OH)_3(s,\text{amorph}) + \frac{15}{7}\,H^+ = \frac{2}{7}\,CO_2(g) + Fe^{2+} + \frac{19}{7}\,H_2O$	$[\text{succinate}^{2-}] = 0.1$ M; $[CO_2(g)] = 10^{-3}$ atm.; $[Fe^{2+}] = 10^{-3}$ M
$\frac{1}{14}(\text{succinate})^{2-} + \frac{1}{2}\,NO_3^- + \frac{1}{7}\,H^+ = \frac{2}{7}\,CO_2(g) + \frac{1}{2}\,NO_2^- + \frac{3}{14}\,H_2O$	$[\text{succinate}^{2-}] = 0.1$ M; $[NO_3^-] = 10^{-2}$ M; $[NO_2^-] = 10^{-3}$ M; $[CO_2(g)] = 10^{-3}$ M

electrons lost). However, this difference comprises a reasonable percentage of the overall energy available when electron transfer is to either sulfate or ferric hydroxide. The effect of lowering pH is particularly favorable when $Fe(OH)_3$(s,amorph) is the electron acceptor implying that pH may play an important role in promoting or discouraging dissimilative iron reduction in natural waters. For the moment, it is simply pointed out that when respiration terminates with an insoluble or charged electron acceptor, computations representing energetics of respiration under non-standard conditions would appropriately employ concentrations of species expected within the periplasmic space or cell surroundings. Thus, it may be appropriate to utilize different hydrogen-ion concentrations within the oxidation and reduction half reactions (see below). Here it is assumed that pH is uniform across the cytoplasmic membrane, an assumption which is almost certainly in error (Chapter 1). Changes in energetic computations attributable to a transmembrane proton gradient are explored subsequently.

2.2.2 Ligand effects.

The effects of ligand addition on the thermodynamics of Fe(III) reduction were investigated using NTA as a model complexing agent. Equilibrium data for iron-NTA complexes are provided in Table 2.4, and computational results are summarized in Figure 2.2. A sample calculation involving NTA complexation is provided for illustration in Table 2.5. In general, ligands which form stronger complexes with ferrous than ferric iron will enhance free energies liberated via iron reduction (Basolo and Pearson, 1967). In the case of NTA, increments to process energetics (Figure 2.2) are modest but may be significant in

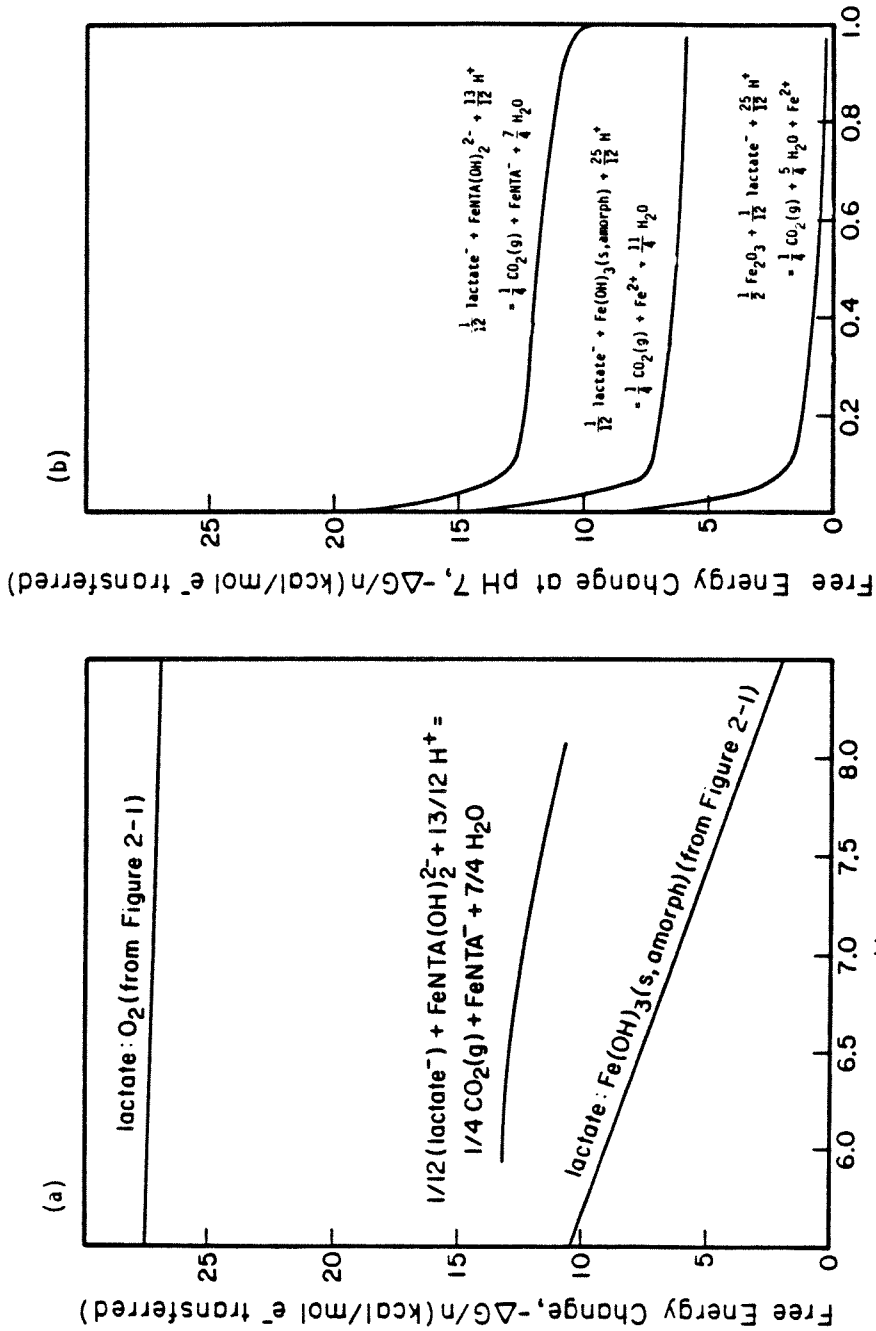

Figure 2.2. Changes in the thermodynamics of dissimilative iron reduction attributable to addition of equimolar NTA (Fe_T = 1.86 x 10^{-3} M; NTA = 1.86 x 10^{-3}) to solution.
(a) Comparison with overall energetics of lactate oxidation without an organic ligand, and
(b) energetics as a function of fractional extent of Fe(III) ——> Fe(II) conversion.
Equilibrium concentrations used in free-energy calculations were determined using MINEQL (see Chapter 3).

Table 2.4. Equilibrium Data for Complexation of Fe(III) and Fe(II) by NTA[1,2]

	Equilibria	log K
(i)	$Fe^{3+} + NTA^{3-} = FeNTA(aq)$	17.95
(ii)	$Fe^{3+} + 2NTA^{3-} = Fe(NTA)_2^{3-}$	26.30
(iii)	$Fe^{3+} + OH^- + NTA^{3-} = FeNTAOH^-$	27.55
(iv)	$Fe^{3+} + 2OH^- + NTA^{3-} = FeNTA(OH)_2^{2-}$	33.45
(v)	$2Fe^{3+} + 2OH^- + 2NTA^{3-} = (FeNTAOH)_2^{2-}$	44.80
(vi)	$Fe^{2+} + NTA^{3-} = FeNTA^-$	10.17
(vii)	$Fe^{2+} + OH^- + NTA^{3-} = FeNTAOH^{2-}$	13.20
(viii)	$Fe^{2+} + H^+ + NTA^{3-} = FeHNTA(aq)$	12.40
(ix)	$Fe^{2+} + 2NTA^{3-} = Fe(NTA)_2^{4-}$	13.60

Notes:

(1) Thermodynamic data are primarily from Martel and Smith (3 vols) corrected to 31°C using the integrated Arrhenius equation. Constants shown were corrected to zero ionic strength using the Davies equation.

(2) NTA^{3-} represents deprotonated nitrilotriacetic acid.

Table 2.5. Calculations of Overall Free-Energy Changes in Electron Transport.

Generalized Steps	Parallel Calculation (example)	
1. Select reactants and products -- reducing agent (substrate) and electron acceptor (oxidizing agent).	lactate $\longrightarrow$ $CO_2(g)$; $FeNTA(OH)_2^{2-} \longrightarrow FeNTA^-$	
2. Select redox half-reactions and equilibria relating half-reaction species to Step 1 reactants and products.	$\frac{1}{12}(lactate^-) + \frac{1}{4} H_2O = \frac{1}{2} CO_2(g) + \frac{11}{12} H^+ + e$	$\Delta G° = 0.91 \frac{kcal}{mole\ e}$
	$Fe^{3+} + e = Fe^{2+}$	$\Delta G° = -17.68 \frac{kcal}{mole\ e}$
	$Fe^{2+} + NTA^{3-} = FeNTA^-$	$\Delta G° = -13.83 \frac{kcal}{reaction}$
	$FeNTA(OH)_2^{2-} = Fe^{3+} + NTA^{3-} + 2OH^-$	$\Delta G° = 45.42 \frac{kcal}{reaction}$
	$2H^+ + 2OH^- = 2H_2O$	$\Delta G° = -38.08 \frac{kcal}{reaction}$
		(1), (2)
3. Combine Step 2 half-reactions and equilibria into overall reaction; combine free energies as appropriate.	$\frac{1}{12}(lactate^-) + FeNTA(OH)_2^{2-} + \frac{13}{12} H^+$ $= \frac{1}{4} CO_2(g) + FeNTA^- + \frac{7}{4} H_2O$	$\Delta G° = -23.36 \frac{kcal}{mole\ e}$
4. Convert standard free energy change to free energy changes under anticipated environmental conditions (non-unit chemical activity and temp. $\neq$ 25°C). (3)	$\Delta G = \Delta G° + 2.3\ RT \log \frac{\{CO_2(g)\}^{1/4}\{FeNTA^-\}}{\{lactate^-\}^{1/12}\{FeNTA(OH)_2^{2-}\}\{H^+\}^{13/12}}$	
	$\Delta G = 24.15 + 1.51\ pH + 1.39 \log \frac{\{FeNTA^-\}}{\{FeNTA(OH)_2\}^{2-}}$	

(1) Sources of thermodynamic data:

Morel (1983)
Stumm and Morgan (1981)
Martell and Smith (1977)

(2) Required conversions for thermodynamic data:

$\Delta G^\circ = -2.3\ RT \log K$

$\Delta G^\circ/n = -2.3\ RT\ p\varepsilon^\circ$ (n is the number of electrons transferred per reaction)

(3) Estimated reactant/product concentration reflect levels anticipated in fermentations of interest. See text (Chpt. 3) for description of fermentation conditions. Assumed activities follow:

$T = 31°C$

$pH = 6.0$ to 8.0

$\{CO_2(g)\} = 10^{-3}$ atm

$\{lactate^-\} = 1.6 \times 10^{-2}$ M

$\{FeNTA^-\}$ (from MINEQL results with ~10% Fe(III) ⟶ Fe(II) conversion)

$\{FeNTA(OH)_2^{2-}\}$ (from MINEQL results with ~10% Fe(III) ⟶ Fe(II) conversion)

relation to overall free-energy changes associated with dissimilative iron reduction. It is clear that NTA addition cannot elevate process energetics to levels predicted for aerobic respiration.

These results suggest methods by which the thermodynamics of dissimilative iron reduction might be improved. A ligand such as phenanthroline, which binds Fe(II) specifically, would add significantly to the overall energy of iron reduction. Phenanthroline is itself a potent inhibitor of aerobic electron transport (Heinen, 1971), though perhaps not of dissimilative iron-reduction.

2.2.3 Reductive dissolution of iron oxides.

To assess the feasibility of bacterially catalyzed reductive dissolution of iron oxides the thermodynamics of electron transport to Fe(III) in hematite and goethite were investigated. Again, in general, forms of Fe(III) which are more chemically stable than $Fe(OH)_3$(s,amorph) affect the thermodynamics of dissimilative iron reduction adversely (relative to Figure 2.1 and 2.2 results). The computational procedure is illustrated below using electron transfer from glucose to $-Fe_2O_3$ as a model transaction. Additional equilibria and thermodynamic data for these calculations are provided as Table 2.6. For other necessary relationships, refer to Table 2.1. For computational purposes, the reductive dissolution of hematite is postulated to involve a dissolution and a reduction step. Equation (i), Table 2.6 represents the assumed dissolution step; the dissolution equation can be combined with the half-reaction for Fe^{3+} ----> Fe^{2+} (Table 2.1) to yield the half-reaction of interest. Combining equations as appropriate, the overall reaction for reductive dissolution becomes:

Table 2.6. Additional Thermodynamic Relationships and Data Necessary for Free Energy Computations Involving Reductive Dissolution of Hematite and Goethite.

	Equilibria	log K	Source
(i)	α-Fe_2O_3 (hematite) + $3H_2O$ = $2Fe^{3+}$ + $6OH^-$	-85.4	Garrels and Christ, 1965
(ii)	FeOOH (goethite) + H_2O = Fe^{3+} + $3OH^-$	-42.6	Garrels and Christ, 1965
(iii)	H^+ + OH^- = H_2O	14.0	Stumm and Morgan, 1981

$$1/2\ \alpha\text{-}Fe_2O_3 + 1/24\ \text{glucose} + 2H^+ = Fe^{2+} + 1/4\ CO_2(g) + 5/4\ H_2O.$$

Reaction stoichiometry is expressed in terms of a one-electron transfer from glucose to Fe(III).

For computational convenience, process energetics are broken down by:

$$\left\{\begin{array}{l}\text{Overall } \Delta G \\ \text{of reductive} \\ \text{dissolution}\end{array}\right\} = \left\{\begin{array}{l}\Delta G, \\ \text{dissolution}\end{array}\right\} + \left\{\begin{array}{l}\Delta G, \text{ redox} \\ Fe^{3+} \text{ ---> } Fe^{2+}\end{array}\right\}$$

Since only the overall energetics, independent of reaction pathway, are of interest, this breakdown is arbitrary. Furthermore, it is computationally convenient to assume that free ferric iron is in equilibrium with hematite. This is tantamount to assuming that a fast chemical dissolution step precedes a slow, bacterially catalyzed redox step in which Fe(III) ----> Fe(II). Again, since <u>overall</u> process energetics are independent of the steady-state Fe^{3+} concentration, the validity of this assumption is inconsequential for these purposes. The actual mechanism for reductive dissolution of hematite could involve direct electron transport from the bacterial ferrireductase or intermediate metabolite to the iron-oxide metal center, obviating the need for prior mineral dissolution.

From equation (i), Table 2.6:

$[Fe^{3+}] = 10^{-0.7}[H^+]^3$ (equilibrium concentration in the presence of hematite). Since there is no free-energy change for a reaction at equilibrium, overall process energetics can be analyzed using the following reaction:

$$1/24\ C_6H_{12}O_6 + 1/4\ H_2O + Fe^{3+} = 1/4\ CO_2(g) + H^+ + Fe^{2+};$$

$$\Delta p\varepsilon^\circ(w) = 20.2.$$

For this reaction:

$$\Delta G^\circ(w) = -2.3\ RT\ \Delta p\varepsilon^\circ(w) = -27.55\ \text{kcal/mole } e^- \text{ transferred.}$$

Under non-standard conditions, however ($[Fe^{2+}] = 10^{-3}$ M; pH, variable; $\{Fe^{3+}\} = 10^{-0.7}\ \{H^+\}^3$; $\{C_6H_{12}O_6\} = 0.1$ M; $\{CO_2(g)\} = 10^{-3}$ atm.)

$$\Delta G = \Delta G^\circ(w) + 2.3\ RT \log \frac{\{CO_2(g)\}^{1/4}\{H^+\}\{Fe^{2+}\}}{\{C_6H_{12}O_6\}^{1/24}\{Fe^{3+}\}\{10^{-7}\}}$$

$$\text{or } \Delta G = -22.12 + 2.72\ pH \qquad \text{(kcal/mole } e^- \text{ transferred).}$$

This expression (plotted in Figure 2.3) represents the overall, pH-dependent energetics of reductive dissolution of hematite. The function representing reductive dissolution of goethite was developed via similar means. From Figure 2.3 and the computational procedure, it is apparent that the energetics of iron-oxide dissolution are sensitive to pH and reasonably sensitive to the choice (though not the concentration) of organic substrate. There is little difference between computational results for goethite and hematite dissolution. Furthermore, at neutral pH, it is unlikely that reductive dissolution of goethite or hematite can be coupled to oxidative phosphorylation (see below). Significant improvement in overall process thermodynamics is

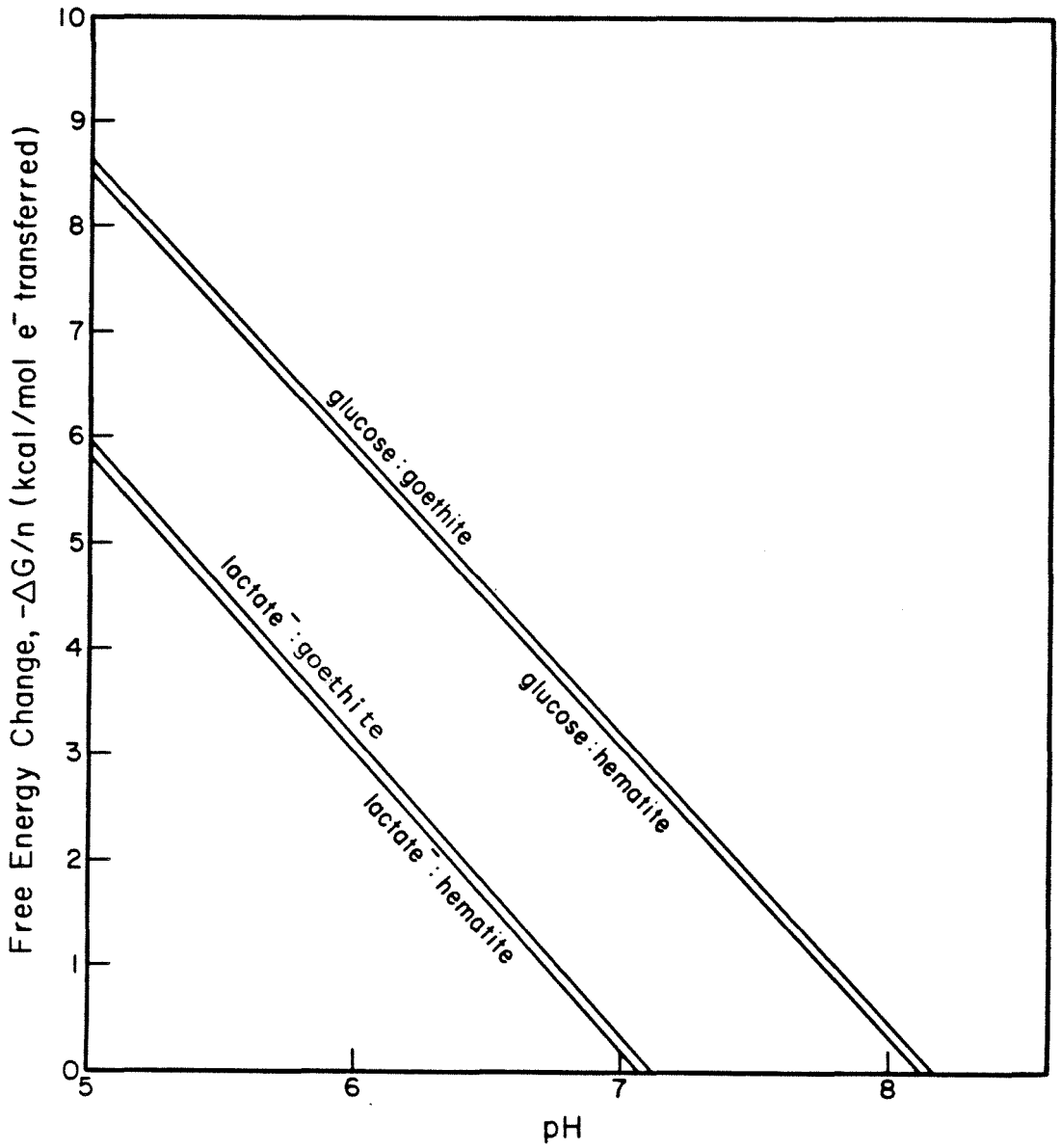

Figure 2.3. Energetics of redox reactions resulting in reductive dissolution of hematite and goethite. Reductant is either 0.1 M glucose or 0.1 M lactate ion. Assumed concentrations of Fe^{2+} and $C\bar{O}_2(g)$ are 10^{-3} M and 10^{-3} atm., respectively.

predicted for the low-pH range.

The existing thermodynamic data base will not support calculation of Fe(III) (equilibrium) speciation when NTA is added to an iron-oxide suspension. Consequently, free-energy calculations, which depend upon the relative concentrations of Fe(III) and Fe(II) forms, have not been carried out. There is speculation, however, that acceleration of metal-oxide dissolution, observed upon ligand addition, is attributable to stretching of Me-O bonds at the mineral surface (Sidhu et al., 1981). As such, one might expect NTA addition to raise the free energy of surface-coordinated Fe(III) in hematite and goethite. Results of reductive dissolution experiments (Chapter 4) involving goethite indicate that NTA addition shifts the chemical equilibrium of the Fe(III)/Fe(II) redox pair towards Fe(II). Ligand addition permits essentially stoichiometric reductive dissolution of goethite (neutral pH, lactate medium). As indicated by Figure 2.3, there is essentially no free energy associated with this transformation in the absence of NTA addition.

2.2.4 Feasibility of oxidative phosphorylation.

Thermodynamic arguments may also be applied to test the feasibility of coupling oxidative phosphorylation to dissimilative iron reduction. Since NADH is primary electron donor for respiration (see Chapter 1), this metabolite is chosen as reductant in the following illustrative computation involving electron transport to Fe(III) as $Fe(OH)_3$(s,amorph). An additional half-reaction is necessary:

$$1/2\ NADH = 1/2\ NAD^+ + 1/2\ H^+ + e^-; \qquad p\varepsilon^\circ(w) = 5.4 \text{ (Morel, 1983).}$$

Coupling with equation (vii), Table 2.1 yields:

$$1/2\ NADH + Fe(OH)_3(s,amorph) + 5/2\ H^+ = 1/2\ NAD^+ + Fe^{2+} + 3H_2O;$$

$$\Delta p\varepsilon^\circ(w) = 0.4.$$

Under non-standard conditions,

$$\Delta p\varepsilon = 0.4 + \log \left\{ \left(\frac{[H^+]}{10^{-7}} \right)^{5/2} \left(\frac{[NADH]}{[NAD^+]} \right)^{1/2} \left(\frac{1}{[Fe^{2+}]} \right) \right\}$$

and if $[NADH]/[NAD^+] = 10$ and $[Fe^{2+}] = 10^{-3}$ M, then

$$\Delta p\,\varepsilon = 21.4 - 2.5\ pH \qquad (2.7)$$

However, as indicated above, process topology makes equation (2.7) inappropriate for calculation of free-energy change. As currently understood, bacterial respiration supports a proton gradient across the cytoplasmic membrane. Transmembrane pH differences of several units have been observed (Konings and Veldkamp, 1983). Since topological considerations dictate that NADH dehydrogenase acts at the cytoplasmic side of the plasma membrane while Fe(III) is reduced in the periplasmic space or cell surroundings, it is clear that half-reaction standard potentials must be modified individually to account for non-standard proton concentrations before they are combined to calculate an overall energy change. For instance, assuming that the cell cytoplasm is at neutral pH and the periplasmic space is two pH units lower, then free energy change should be calculated using:

$$1/2\ NADH = 1/2\ NAD^+ + 1/2\ H^+ + e^-;\quad p\varepsilon^\circ(w) = 5.4$$

(or, assuming $\frac{[NADH]}{[NAD^+]} = 10$ and pH = 7, $p\varepsilon = 5.9$) and

$$Fe(OH)_3(s,amorph) + 3H^+ + e^- = Fe^{2+} + 3H_2O;\ p\varepsilon^\circ(w) = -5.0$$

(or $p\varepsilon = 1.0$, assuming $[Fe^{2+}] = 10^{-3}$ M and pH = 6). Under these circumstances, the overall reaction potential change is $\Delta p\varepsilon = 6.9$ and $\frac{\Delta G}{n} = -9.38$ kcal/mol e^- transferred. Notice that this compares favorably with the -5.3 kcal/mol e^- transferred, calculated using equation (2.7) (without considering the transmembrane proton gradient).

Again according to Mitchell's theory, the phosphorylation of cellular ADP is coupled to the retranslocation of protons from the periplasmic space or cell surroundings into the cytoplasm. Calculation of energy requirements for oxidative phosphorylation rest upon the following assumptions:

(i) ATP production is governed by,

$$H^+ + ADP^{3-} + HPO_4^{2-} = ATP^{4-} + H_2O;\ \Delta G^\circ(w) = 7.4\ kcal/mol \qquad (2.8)$$

(Jones, 1983)

However, the pH dependence of process energetics is complicated by the acid-base properties of HPO_4^{2-} in the neutral pH range ($H_2PO_4^- = HPO_4^{2-} + H^+$; pK = 7.2, I = 0; Morel, 1983). Thermodynamic computations based on equation (2.8) and summarized in Figure 2.4 reflect the dependence of HPO_4^{2-} concentration on the assumed concentration of total inorganic

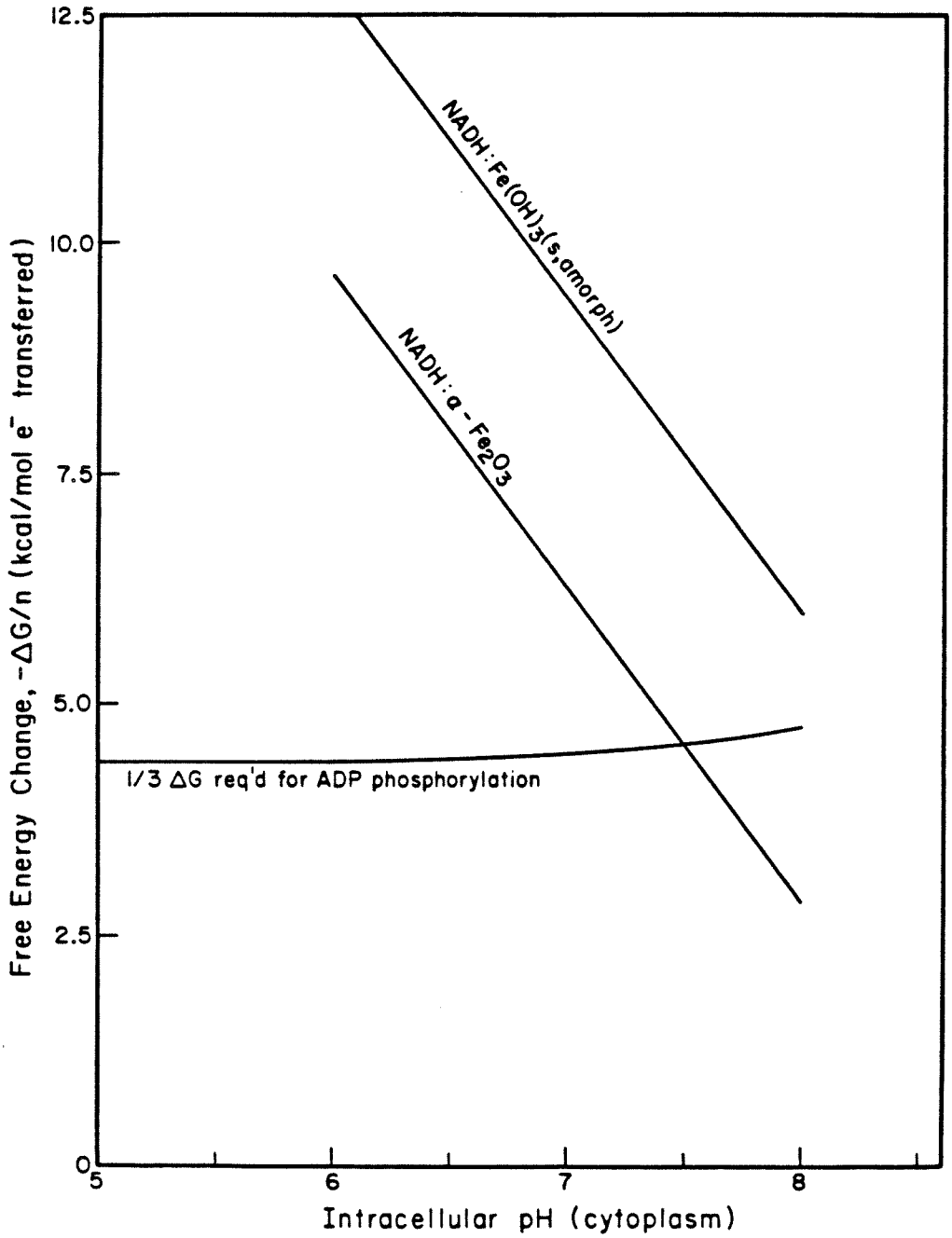

Figure 2.4. Free-energy changes of electron transport from NADH to ferric hydroxide and hematite in relation to free-energy requirements of ADP phosphorylation. Assumed concentrations: $[Fe^{2+}] = 10^{-3}$ M; $[NADH]/[NAD^{+}] = 10$; total inorganic phosphate = 10^{-3} M. Intracellular pH was assumed to be 1 pH unit lower than that of the cell surroundings.

phosphate (10^{-3} M) and solution pH. The assumed intracellular ratio of ATP/ADP was 10.

(ii) The minimum respiratory H^+/e^- ratio (protons translocated per electron transferred) for support of oxidative phosphorylation is one.

(iii) Phosphorylation of a mole of ADP is coupled to retranslocation of 3 moles of protons (Kashket, 1982). That is, $ATP/2e^- \geq 2/3$.

Under these circumstances, energetic requirements for coupled ADP phosphorylation dictate that:

$$3\{\Delta G \text{ (electron transport)}\} \geq \Delta G \text{ (phosphorylation)}.$$

The comparison is made for processes of interest in Figure 2.4. Results indicate that the energy of ATP generation is virtually independent of pH in the neutral-pH range due to the compensating effects of changes in hydrogen ion and HPO_4^{2-} concentrations in that region. A more rapid increase in the free energy required is expected at pH > 8 since most inorganic phosphate is already HPO_4^- at that point. Free-energy curves in Figure 2.4 are based on an assumed transmembrane proton gradient of 1 pH unit (low pH outside). It is evident that when the periplasmic space is at neutral pH, oxidative phosphorylation based on electron transport to hematite is not thermodynamically feasible; ATP generation driven by electron transport to amorphous ferric hydroxide would demand reasonably high efficiency. Low pH dramatically improves the thermodynamics of reductive dissolution of Fe(III)-bearing minerals.

2.3 Lithotrophic Bacteria.

The role of chemolithotrophic bacteria Thiobacillus thiooxidans, T. ferrooxidans, and Sulfolobus acidocaldarius in catalysis of dissimilative iron reduction is not entirely established. Uncertainty centers on their ability to utilize Fe(III) directly as terminal electron acceptor for respiration, and the ability of T. thiooxidans to respire anaerobically is doubtful (Brock and Gustafson, 1976; Kino and Usami, 1982) (see Chapter 1). In direct contrast, T. ferrooxidans reduces Fe(III) anaerobically using elemental sulfur as energy source (Sugio et al., 1985). In the presence of molecular oxygen, Fe(II) produced via dissimilative iron reduction is immediately reoxidized by the cell's Fe(II) oxidase. Because this enzyme is cyanide sensitive, reoxidation by O_2 is inhibited in the presence of 5 mM CN^-. The T. ferrooxidans ferrireductase is rapidly destroyed by treatment with heat or phenol. Sulfolobus acidocaldarius is capable of promoting Fe(III) reduction using elemental sulfur or glutamate as energy source.

The energetics of electron transfer from elemental sulfur to ferric iron or molecular oxygen are explored below. Only one additional half-reaction is required:

$$1/6\ SO_4^{2-} + 4/3\ H^+ + e^- = 1/6\ S(s) + 2/3\ H_2O;\quad p\varepsilon^\circ(w) = -3.30$$

(Stumm and Morgan, 1981)

This is coupled with equation (iv), Table 2.1 to yield:

$$1/6\ S(s) + 1/6\ H_2O + 1/4\ O_2(g) = 1/6\ SO_4^{2-} + 1/3\ H^+;$$

$$\Delta p\varepsilon^\circ(w) = 17.05;$$

and $\frac{\Delta G°(w)}{n}$ = -23.2 kcal/mole e^- transferred.

Similarly, combination with equation (viii), Table 2.1 yields:

$$1/6\ S(s) + 2/3\ H_2O + Fe^{3+} = 1/6\ SO_4^{2-} + 4/3\ H^+ + Fe^{2+};$$

$$\Delta p\varepsilon°(w) = 16.30;\ \frac{\Delta G°(w)}{n} = -22.2 \text{ kcal/mole } e^- \text{ transferred.}$$

T. ferrooxidans, T. thiooxidans, and S. acidocaldarius grow under extreme pH conditions; growth of T. thiooxidans has been reported at pH values as low as 0.5 (Breed et al., 1957), and the species is thought to be inactive at pH 6. It is evident from the previous formulae that free energy liberated via these reactions is pH-sensitive. Calculations summarized in Figure 2.5 are based upon the following assumed chemical concentrations: $\{O_2(g)\}$ = 0.1 atm., $\{SO_4^{2-}\}$ = 0.1 M; $\{Fe^{2+}\}$ = 0.1 M; $\{Fe^{3+}\}$ = 0.1 M; pH, variable. Solid-phase sulfur is assumed to transfer electrons directly to the bacterial electron-transport chain at the outside of the cytoplasmic membrane.

Results indicate that while electron transfer to molecular oxygen is energetically favored throughout the pH range of interest, there is sufficient potential energy in dissimilative iron reduction to drive oxidative phosphorylation down to pH 1 and below. The lack of iron-oxide stability in the low-pH range and resultant high equilibrium concentration of Fe^{3+} are responsible for the favorable energetic results.

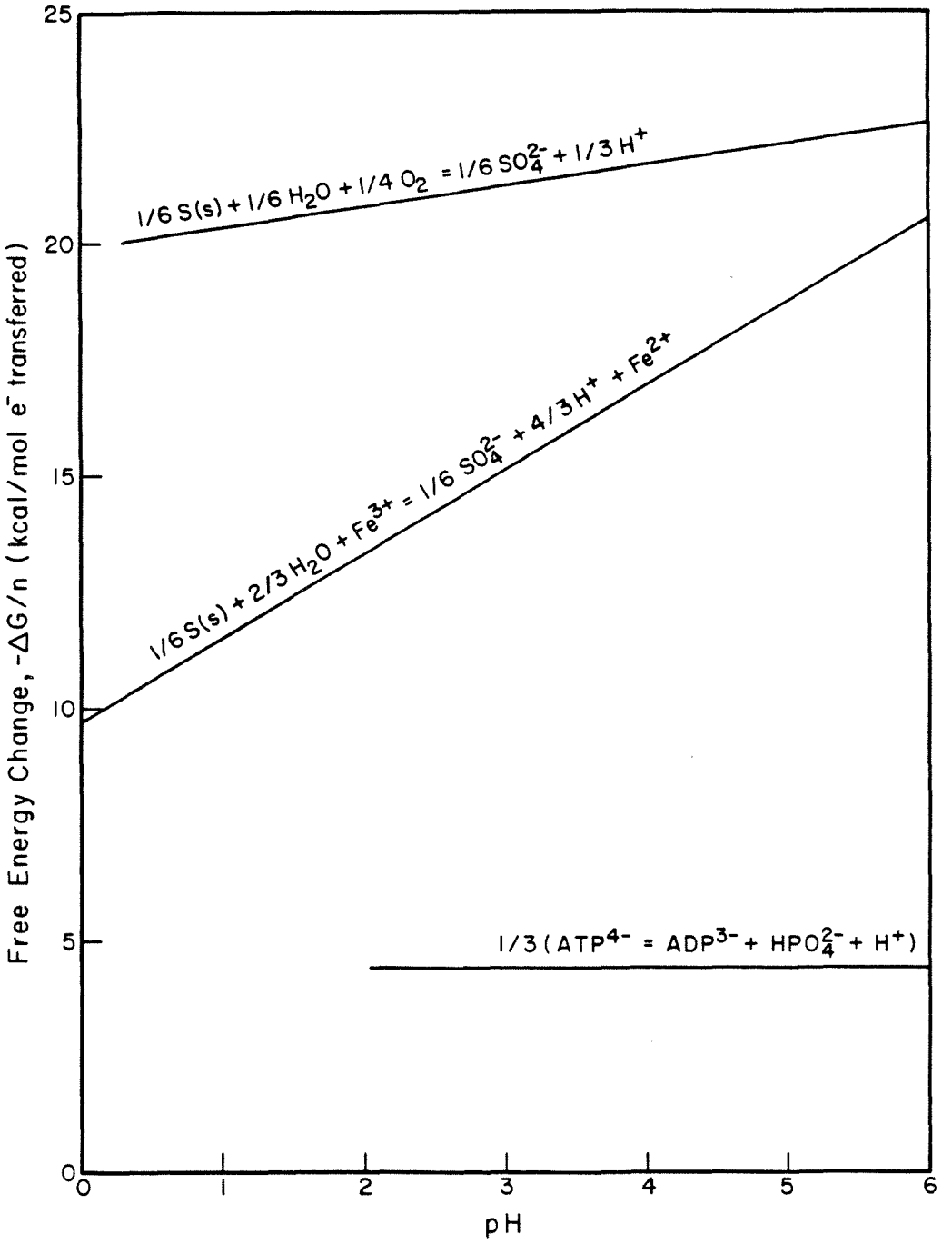

Figure 2.5. Comparison of energy required for ADP phosphorylation with energy liberated via electron transfer from elemental sulfur to O_2 or Fe^{3+}. Reactions are assumed to represent overall electron transport in acidophiles such as T. thiooxidans growing on elemental sulfur.

Chemolithotrophs, unlike the heterotrophic bacteria examined above, do not utilize NADH as a primary electron donor for respiration (Jones, 1983). Reducing equivalents enter the electron transport chain at the same chemical potential as the substrate (e.g., elemental sulfur). Consequently, energy constraints associated with oxidative phosphorylation can be compared directly with the energy of electron transport from exogenous substrate to terminal electron acceptor (Figure 2.5).

2.4 Summary and Conclusions

1. Under representative environmental conditions, thermodynamic considerations justify the use of Fe(III) as primary oxidant for bacterial respiration. Under most conditions investigated, free-energy changes associated with redox reactions involving reduced organic or inorganic substrates and Fe(III) are sufficiently exergonic to drive oxidative phosphorylation. However, when Fe(III) is provided as hematite or goethite and no ligand (e.g., NTA) is provided, free-energy changes associated with reductive dissolution are smaller than the energy requirements of ADP phosphorylation.

2. Low pH favors the energetics of redox reactions involving reduced organic substrates and Fe(III) as oxidant. Additional energy associated with reductive dissolution of goethite or hematite at relatively high proton concentrations may be sufficient to drive ATP synthesis.

3. Choice of reductant (lactate vs. glucose) is of secondary importance within the overall energetics of dissimilative iron reduction. The relatively modest increase in free-energy change which

is associated with glucose oxidation can, under some conditions, be critical to overall process energetics.

4. Ligand addition can critically affect the free energies of Fe(III) reduction. In general, ligands which bind Fe(III) more tightly than Fe(II) diminish the free energy available from dissimilative iron reduction. On the other hand, process energetics benefit from the presence of ligands such as 1-10 orthophenanthroline, which bind Fe(II) specifically. NTA addition modestly enhances the energy potentially available from iron reduction.

5. Aside from very rapid changes during the initial stage of the Fe(III) ----> Fe(II) conversion (before an appreciable concentration of product builds up) extent of reaction is relatively unimportant as a determinant of energy changes associated with dissimilative iron reduction.

6. From the standpoint of process energetics, molecular oxygen and nitrate ion are superior to Fe(III) as oxidants. Although NTA addition benefits the energetics of dissimilative iron reduction, energy changes do not approach those associated with aerobic respiration.

7. There is little difference in the thermodynamics of reductive dissolution of hematite and goethite.

2.5 References

American Society for Microbiology. Bergey's Manual of Determinative Bacteriology, 7th edition. Ed., R. S. Breed. Williams and Wilkins, Baltimore (1957).

Basolo, F. and Pearson, R. G. Mechanisms of Inorganic Reactions. Wiley, New York (1967).

Brock, T. D. and Gustafson, J. Ferric iron reduction by sulfur- and iron-oxidizing bacteria. Appl. Environ. Microbiol. 32: 567-571 (1976).

Garrels, R. M. and Christ, C. L. Solutions, Minerals, and Equilibria. Harper and Row, New York (1965).

Harrison, D. E. F. The regulation of respiratory rate in growing bacteria. In: Adv. Microb. Physiol., Vol. 14, eds. A. H. Rose and D. W. Tempest (1976).

Heinen, W. Inhibitors of electron transport and oxidative phosphorylation. pp. 383-393. In: Methods in Microbiology, Vol. 6A, eds. J. R. Norris and D. W. Ribbons. Academic Press, New York (1971).

Jones, C. W. Bacterial Respiration and Photosynthesis, Aspects of Microbiology, 5. American Society for Microbiology, Washington, D.C. (1983).

Kashket, E. R. Stoichiometry of the H^+-ATPase of growing and resting, aerobic Escherichia coli. Biochem. 21: 5534-5538 (1982).

Kino, K. and Usami, S. Biological reduction of ferric iron by iron- and sulfur-oxidizing bacteria. Agric. Biol. Chem. 46: 803-805 (1982).

Konings, W. N. and Veldkamp, H. Energy transduction and solute transport mechanisms in relation to environments occupied by microorganisms. In: Microbes in their Natural Environments. Eds. J. H. Slater, R. Whittenbury and J. W. T. Wimpenny. Cambridge Univ. Press, Cambridge (1983).

Martell, A. E. and Smith, R. M. Critical Stability Constants, Vol. 1: Amino Acids. Plenum, New York (1974).

Martell, A. E. and Smith, R. M. Critical Stability Constants, Vol. 3: Other Organic Ligands. Plenum, New York (1977).

Morel, F. M. M. Principles of Aquatic Chemistry. Wiley, New York (1983).

Sidhu, P. S.; Gilkes, R. J.; Cornell, R. M.; Posner, A. M. and Quirk, J. P. Dissolution of iron oxides and oxyhydroxides in hydrochloric and perchloric acids. Clays Clay Miner. 29: 269-276 (1981).

Smith, R. M. and Martell, A. E. Critical Stability Constants, Vol. 4: Inorganic Complexes. Plenum, New York (1976).

Stumm, W. and Morgan, J. J. Aquatic Chemistry. Wiley, New York (1981).

Sugio, T.; Domatsu, C.; Munakata, O.; Tano, T. and Imai, K. Role of a ferric iron-reducing system in sulfur oxidation of Thiobacillus ferrooxidans. Appl. Environ. Microbiol. 49: 1401-1406 (1985).

CHAPTER 3

KINETICS AND MECHANISM OF DISSIMILATIVE Fe(III) REDUCTION BY *PSEUDOMONAS* SP. 200

by

Robert G. Arnold, Terese M. Olson and Michael R. Hoffmann

Submitted to: Biotechnology & Bioengineering

July 1985

The kinetics and mechanism of Fe(III) reduction to Fe(II) were studied in pure, batch cultures of Pseudomonas sp. 200. The rate of iron reduction has been mechanistically related to aqueous-phase iron speciation. In the absence of microbial activity, the iron-reduction rate was negligible. Initial rates of microbial iron reduction were accelerated more than twenty-fold by the addition of equi-molar quantities of nitrilotriacetic acid (NTA) to media initially containing 1.86×10^{-3} M of total Fe(III). Numerical techniques were utilized to quantify relationships between the observed rate of Fe(II) production and the calculated (equilibrium) aqueous-phase speciation. These results indicate that soluble ferric-iron species are not equivalent in terms of their susceptibility to bacterial (dissimilative) iron reduction. The concentration of $Fe(NTA)(OH)_2^{2-}$ correlated strongly with observed iron-reduction rates. Ferrous iron species appeared to inhibit the reduction process.

INTRODUCTION

Microbial reduction of Fe(III) is ecologically important in such complex environments as waterlogged soils[1], marine sediments[2], rice paddies[3], and eutrophic lakes[4]. In the absence of molecular oxygen, a number of bacteria utilize Fe(III) as terminal electron acceptor in electron transport. Figure 1 illustrates the probable vectorial nature and stoichiometry of dissimilative iron reduction[5-6].

Obuekwe[7-10] systematically examined the metabolic capabilities of Pseudomonas sp. 200 and measured dissimilative iron reduction rates that were at least an order of magnitude greater than those previously reported for Thiobacillus thiooxidans[11-12], Bacillus polymyxa and Clostridium butyricum[13], and a variety of soil bacteria[14-15].

Several investigators have noted the dependence of bacterial iron-reduction rate on the chemical form of Fe(III) in the medium (e.g., Fe_2O_3, am-$Fe(OH)_3$, α-FeOOH, γ-FeOOH, Fe-(citrate), etc.). Jones et al.[4] reported that chemoorganotrophs (Vibrio sp.) and chemolithotrophs present in the sediments of an eutrophic lake reduced am-$Fe(OH)_3$ more readily than other Fe(III) oxides and oxyhydroxides. The addition of citrate, a tridentate ligand, to the medium resulted in a 3-fold increase in the observed rate. Munch and Ottow[13,16] reported that C. butyricum and B. polymyxa preferentially reduced x-ray amorphous Fe(III) solids when mixed with crystalline iron oxides.

Munch and Ottow[13] also found that physical contact between the aforementioned microorganisms and the iron solids was necessary for iron reduction. They observed no iron-reducing activity when C. butyricum and B. polymyxa were separated from the mineral phase by a dialysis membrane. In contrast, Jones et al.[4] concluded that more than 30

percent of the iron-reduction activity of their lake sediments was associated with unidentified (biologically produced) diffusible components.

In this paper, the thermodynamics and kinetics of iron reduction by Pseudomonas sp. 200 are explored. Equilibrium chemical speciation is calculated using a computer-based model. With these results, physical and mathematical models are proposed to explain observed variation in iron-reduction rate in terms of equilibrium concentrations of individual iron species.

MATERIALS AND METHODS

Kinetic studies were conducted in a 2-liter Biostat M batch reactor (Braun Instrument Co.). Temperature ($\pm 0.2^{o}C$) and pH (± 0.05) were controlled automatically. Solution pH was maintained at preset levels using a pH-stat. Dissolved oxygen concentration was measured continuously and manipulated by adjusting inlet gas composition, flow rate, and mixing rate.

In a typical experiment, the reactor was filled to 1.5 liters with lactate medium (Table 1) and autoclaved at $121^{o}C$ for 30-60 minutes. Iron for satisfaction of microbial nutritional requirements was added from a filter-sterilized $FeCl_3$ stock solution. Aerobic growth was initiated by adding 1.5 mls from a dense overnight culture (identical medium) of Pseudomonas sp. 200. See Table 2 for species characteristics. Gas flow (Q_{AIR} = 0.5 ℓ/min) and mechanical agitation (250 rpm) provided mixing energy throughout the fermentation. Temperature was maintained at $31^{o}C$. Microbial growth was monitored by periodic measurement of absorbance at λ = 600 nm. During the final

stage of the aerobic growth period, agitation and air-flow rates were reduced to maintain oxygen tensions $\leq$ 0.01 atm.

At an absorbance of 1.00 (λ = 600 nm), the culture was purged of O_2 with high-purity, O_2-free nitrogen gas. Nitrilotriacetic acid (Pfaltz and Bauer, Inc.) was added (to appropriate levels) as H_3(NTA) crystals, followed by $FeCl_3$ addition to 1.86×10^{-3} M Fe(III). Ferrous iron measurements were initiated immediately following $FeCl_3$ addition and continued at roughly 1-minute intervals throughout the remainder of the experiment.

The effects of iron speciation on reduction rate were investigated by systematically varying the solution pH and NTA concentration. Final NTA concentrations ranged from zero to equi-molar NTA (equal to total iron, 1.86×10^{-3} M). At each NTA/total iron ratio, experiments were run at pH 6.5, 7.0, and 7.5. Equilibrium concentrations of iron-NTA species were calculated throughout the iron-reduction period using the computer code MINEQL[17]. Redox equilibria were omitted from such computations; a series of computations representing points in time along the Fe(III) ——> Fe(II) conversion process was performed for each initial medium composition. Thermodynamic data utilized in these calculations are summarized in Table 3. Association constants for ferric- and ferrous-lactate complexes were developed from the linear free-energy relationship[18] shown in Figure 2. Preliminary calculations confirmed that, with the exception of orthophosphate, the mineral composition of the medium did not materially affect iron speciation. Hence, biological uptake of only PO_4^{3-} was considered in formulating

thermodynamic calculations. Similarly, because lactate does not form strong complexes with iron species, changes in lactate concentration could be neglected.

Analytical Procedures

Optical density (a measure of cell density) was determined with a Beckman model DU7 spectrophotometer at λ = 600 nm using a 1-cm cuvette.

Rapid autoxidation of Fe(II) was observed by Kurimura et al.[19] in the presence of chelating agents such as NTA. (The 2nd-order rate constant for $FeNTA^-$ oxidation is 80 M^{-1} sec^{-1}.) To prevent Fe(II) oxidation from masking the microbial reduction rate, 1 ml of anaerobic fermentation medium was rapidly added (within 1 or 2 seconds of sample withdrawal) to a quenching medium consisting of 0.5% w/v 1,10-phenanthroline (sufficient volume to provide excess phenanthroline) and 2 mls of ammonium acetate buffer[20]. Samples were diluted to 10 mls with distilled water prior to absorbance measurements. For measurement of <u>total</u> iron, 2 mls of hydroxylamine solution[20] were substituted for 2 mls of dilution water. After color development, samples were centrifuged at 3000xg for 30 minutes in a model RC-3B Sorvall centrifuge. Centrate color intensity was assayed spectrophotometrically at λ = 510 nm. ε_{510} for the Fe(II)-$(phenanthroline)_3$ complex is 1.11 x 10^4 $(\underline{M}\text{-cm})^{-1}$. Orthophosphate was determined by the method of Eisenreich et al.[21].

Oxygen utilization data were obtained by interrupting the culture's oxygen supply and monitoring the rate of decline in medium dissolved oxygen concentration.

RESULTS

Experimental data representing Fe(II) concentration as a function of time are summarized in Figures 3a-d. Concentration vs. time profiles clearly show that the kinetics of Fe(III) reduction by Pseudomonas sp. 200 are sensitive to the speciation of iron. Each graph contains data gathered at a single NTA level. Individual curves correspond to experiments run at pH 6.5, 7.0 and 7.5. Duplicate experiments are included as dotted lines. Comparison of Figures 3a and 3d (the zero and equi-molar levels, respectively) reveals that ligand addition resulted in a 20-fold increase in the initial iron-reduction rate; intermediate NTA levels produced less pronounced accelerations. Changes in reduction rate attributable to pH variation were modest. Abiotic and dark controls (Figs. 3c and 3b, respectively) indicate that (i) chemical reduction of Fe(III) in the absence of microbial activity is negligible and (ii) observed reduction rates in the presence of bacteria are not light-dependent.

In Figures 4a-d the observed rates of iron reduction are plotted against the remaining concentration of total Fe(III). Saturation kinetics are evident in the zero-NTA experiments (Fig. 4a). In this case, zero-order kinetics were observed at high Fe(III) concentrations and first-order kinetics at lower Fe(III) levels. Although these effects were not apparent at the two intermediate NTA concentrations, saturation kinetics were again observed at high total Fe(III) concentrations when sufficient NTA was added.

In the presence of high NTA concentrations, a decrease in pH to 6.5 reduced the initial rate of iron reduction (Fig. 4d) despite a significant increase in total Fe(III) solubility (see below). This

result, which was confirmed via duplicate experiment, suggests that individual Fe(III) species, as opposed to total soluble Fe(III), determine reaction rate.

Equilibrium concentrations of major Fe-NTA species, calculated for conditions anticipated at the start of the iron-reduction period, are summarized in Figure 5. The three-dimensional histograms represent concentrations or initial iron-reduction rates at each combination of experimental pH and NTA level.

ANALYSIS AND DISCUSSION

Thermodynamics

The following assumptions were made in order to define thermodynamic conditions under which Fe(III) can serve as terminal electron acceptor for bacterial respiration:

1. The overall redox conversion (i.e., lactate oxidation/Fe(III) reduction) must be exergonic under chemical conditions present in the growth medium.
2. A 2-electron transfer from NADH to Fe(III) must liberate sufficient free energy to drive ADP phosphorylation.

Stoichiometries reflected in the latter constraint are derived from mechanistic considerations[6,22] illustrated in Figure 1. Although lactate is an acceptable donor for electron transport in E. coli[23-24], NADH (nicotinamide adenine dinucleotide, reduced form) is considered the more probable reductant for electron transport. If the species subsists anaerobically via substrate-level posphorylation, using iron reduction as only a sink for cellular reductants, then the latter constraint should be relaxed.

Free-energy computations are summarized in Table 4. Cases investigated differ only in the selection of the terminal electron acceptor. Computational results, illustrated in Figure 6 as pH-dependent free-energy profiles, form the basis for the following conclusions:

1. In all cases investigated, the conditions postulated as necessary for the generation of biochemical energy via electron transport appear to be satisfied in the neutral pH range.
2. There is appreciably more energy available from aerobic metabolism than from either of the anaerobic cases investigated.
3. Addition of NTA to the growth medium moderately increases the energy available from redox reactions involving lactate and ferric iron. In general, ligands which increase the stability of reaction products relative to reactants will increase the reaction-dependent free-energy change[25].

Linear Models

A stepwise linear regression model was employed to establish correlations between observed iron-reduction rates and equilibrium concentrations of major iron species (see Table 3). Such correlations are suggested by Figure 5, which illustrates the effect of varying total NTA and hydrogen-ion concentrations on the equilibria of potentially important iron-NTA species.

In the presence of colloidal iron hydroxide, the concentration of free Fe^{3+} is solely a function of pH. Therefore, other inorganic iron species of potential importance such as $FeOH^{2+}$, $Fe(OH)_2^+$, and $Fe(OH)_4^-$

are also functions of pH alone in the presence of the solid, $Fe(OH)_3$. The lack of a straightforward pH dependence among initial reduction rate data suggests that none of those species are important determinants of iron-reduction kinetics. Furthermore, reduction rate correlates poorly with total soluble Fe(III) concentration, indicating that contributions of species to overall iron-reduction kinetics should be considered individually.

Figure 5 suggests that initial reduction rate correlates best with the concentration of $FeNTA(OH)_2^{2-}$. The observation is supported by regression results, summarized in Table 5. In the absence of NTA, the iron(III) reduction rate depends primarily on the concentration of $Fe(OH)_3(s)$, the predominant ferric iron species.

Several independent variables appear in regression equations with negative coefficients. Such results suggest that competition exists among chemical species for reduction sites. Species which bind to active sites but cannot act as electron acceptors (or react slowly) can be identified in this way (negative regression coefficient). However, regression coefficients yield no further physical intuition in competitive cases.

Calculated R^2 values (the fraction of squared variation about the mean value which is explained by the regression equation; see footnote, Table 5) are in general fairly modest. This could result from inherent variation in the experimental procedure (see Figs. 3b, d for examples of duplicate experiments) or from the inappropriate nature of <u>any</u> linear model when used to rationalize what is essentially a non-linear phenomenon.

Non-linear (Michaelis-type) Models

At least three mechanistic interpretations are possible for the observed acceleration of iron-reduction rate due to NTA addition:

1. There is a single type of enzymatic site at which respiratory chain electrons are transferred to both amorphous ferric hydroxide and Fe(III)-NTA complexes. All sites are equivalent. A higher enzyme turnover rate or greater affinity of enzyme active site for complexed Fe(III) is responsible for the increase in Fe(III) ——> Fe(II) conversion rate.
2. There are at least two types of reaction sites; a high-rate (or at least numerically superior) site is sterically inaccessible to colloids but available to some or all Fe(III)-NTA complexes.
3. The Fe(III) reduction rate is limited by solid dissolution, dissociation of Fe(III) complexes, or diffusion to reactive sites.

The first of these possibilities seems improbable. When Fe(III) is presented as colloidal ferric hydroxide, saturation is observed at rates at least twenty times lower than measured rates in the presence of complexed, soluble Fe(III). Because saturation kinetics are observed in both cases, it is unlikely that all enzymatic sites enjoy equal access to the colloid, and a slightly more complex model is warranted.

Proposed non-linear (two-site) kinetic relationships are summarized in Table 6a. In model 1, the two types of enzymatic sites differ in terms of both substrate specificity and turnover rate. In model 2, non-equivalence of sites arises from steric considerations. Both are Michaelis-Menten-type relationships, modified to permit multiple substrate/competitor interactions at the binding sites of membrane-bound

iron-reduction enzymes. Species selection for the non-linear models was based on correlations identified via linear regression analysis.

Model parameters were either extracted graphically (Figs. 4a-d) or estimated using a non-linear least-squares algorithm[26]. In the latter approach, a subset of model parameters (those which can be independently estimated) can be fixed, while remaining constants are fit using the least-squares minimization technique. Results are summarized in Table 6b. In each case, the numerical equivalent of an R^2 statistic was calculated as both an indicator of goodness-of-fit and method for comparing non-linear and regression models. Naturally the analogy should not be extended too far due to statistical dissimilarities in cases tested.

NTA-free experiments were used to estimate the maximum conversion velocity (V_{m1}) and Michaelis constant or half-saturation constant (K_M) for the reduction of amorphous ferric hydroxide (see Figure 4a). Model assumptions dictate that, for the single-substrate case, the enzyme-substrate affinity constant is the reciprocal of the half-saturation concentration, or in our notation $K_1 = K_M^{-1}$. The high-NTA cases support a similar set of graphical estimates for maximum conversion velocity and Michaelis constant for soluble substrate $(Fe(NTA)(OH)_2^{2-}$, see Figure 4d). At constant temperature, pressure, and ionic strength, these parameters represent intrinsic constants; their physical significance is independent of model selection.

Model 1 (two enzymatic sites, <u>functional</u> non-equivalence) yields a reasonable fit ($R^2 > 0.91$) using a set of constants which agree well with graphical estimates. However, model 2 (two sites, <u>steric</u> non-equivalence) provides an equally plausible explanation for rate

data. Numerical results for model 2 suggest that $V_{M(2)} >> V_{M(II)}$ (again, see Table 6a for explanation of symbols), or, equivalently, that only a small percentage of active sites are capable of direct contact with colloidal $Fe(OH)_3(s)$. Furthermore, if $V_{M(II)}$ is on the order of V_{M1} (as suggested by tabulated results), then the enzyme turnover rate (k_{cat}) may be substrate-independent. That is, the overall rate constants for $Fe(OH)_3(s)$ reduction (and dissolution) and $Fe(NTA)(OH)_2^{2-}$ reduction may be about equal. This result was unexpected in light of the apparent dependence of reduction rate on solid-phase speciation.

The non-linear relationships offer a rational modeling approach which accounts for the apparent effects of competitive species. Residual error lies in some combination of (i) inter-experimental variation which is unaccounted for in any model, (ii) non-equilibrium solution chemistry, (iii) inappropriate model structure, and (iv) error in rate measurement or random variation. It is emphasized that although growth conditions were manipulated to produce a consistent biomass at the start of the iron-reduction period, the only real-time measurement of biological activity in these experiments was optical density. A more direct comparison of inter-experimental biological conditions would help resolve sources of residual uncertainty.

Other Explanations

Figure 7 indicates that there is good qualitative agreement between measured rates of iron reduction and model 2 predictions. It is apparent, however, that residual error contains a systematic element -- model predictions are consistently lower than experimental values at the

start of the iron-reduction period and generally higher at the end. The probable explanation lies in the electron-transport data of Figure 8. Oxygen-utilization data resulted from continuous measurement of oxygen concentration in cultures of Pseudomonas sp. 200 (A_{600} = 1.00). Figure 8 suggests that in such cultures the maximum rate of electron transport does not depend on the identity of the terminal electron acceptor. It follows that kinetic control is not exerted at the level of the terminal oxidase at high rates of electron transport. Jones[6] indicated that under aerobic conditions bacterial electron transport is normally controlled at the dehydrogenase level or by the proton motive force, which must be continuously dissipated if proton translocation is to continue. In each of our models, kinetic parameters are estimated for only terminal oxidase activity; if iron reduction rates are in fact truncated by upstream kinetic limitations, our estimate of V_{max} would be low. The high reduction rates predicted at low Fe(III) concentrations compensate for the low initial values (to minimize of overall sum-of-squares for error).

In each model described above, it is assumed that chemical equilibrium is satisfied on each side of the Fe(III) ——> Fe(II) conversion throughout the iron-reduction period. That is, it is assumed that characteristic times for relevant, non-redox chemical transformations such as complexation (ligand-substitution) (ns to ms) and acid-base reactions (ps to μs)[18] are shorter than the characteristic time (min) of Fe(III) ——> Fe(II) reduction. Issues bearing on the credibility of this critical assumption are individually addressed below:

1. In the absence of NTA, the observed rate of Fe(III) reduction may be limited by the kinetics of $Fe(OH)_3(s)$ dissolution. It is possible to envision a two-step iron-reduction mechanism in which solid dissolution precedes enzymatic reduction of free ferric ion or its hydroxo complexes. If dissolution is slow compared to the reduction step, then steady-state levels of soluble Fe(III) species will be depressed below their equilibrium levels. Furthermore, in NTA-free experiments the observed iron-reduction rate would be proportional to the $Fe(OH)_3(s)$ concentration; saturation kinetics, observed at high total Fe(III) concentration, precludes mechanisms in which solid dissolution is the rate-limiting step.

Theis and Singer[27] measured the evolution of Fe(II) in sterile, aqueous suspensions of $Fe(OH)_3$(s,amorph) and tannic acid. Results indicated that the pH-dependent iron-reduction rate was limited by solid-phase dissolution. (Reduction of soluble Fe(III) by tannic acid was comparatively fast.) In the neutral pH range, less than 10% of the 8.0×10^{-5} M ferric iron initially present was reduced in a 24-hour period. The slow chemical dissolution rate observed by Theis and Singer[27] suggests that Pseudomonas sp. 200 plays a direct role in the dissolution/reduction process. It is likely that contact between microbe and solid-phase substrate is required to reach observed reduction rates. Ligand addition and pH reduction are known to promote solid-phase dissolution kinetics, as opposed to simply increasing the stability or depressing the concentration of free ferric ion. Biological surfaces appear

to have similar capabilities; bulk-solution equilibria are probably not upset by abiotic solid-phase dissolution limits.

2. The relatively rapid iron-reduction rates observed in the presence of NTA may be limited by the rate of solid dissolution. Equilibrium calculations indicate that ferric hydroxide comprises more than 50 percent of the total iron concentration at the beginning of all iron-reduction experiments. Consequently, $Fe(OH)_3(s)$ dissolution is inevitably required for the maintenance of high-rate iron reduction. Were the overall rate limited by dissolution, saturation kinetics (which reappear in the equi-molar NTA experiments) should not be observed. Furthermore, the weak dependence of reduction rate on bulk solution pH (Figure 3) conflicts intuitively with a dissolution-limited rate model. A shift in the rate-limiting step to $Fe(OH)_3(s)$ dissolution during the latter phase of iron-reduction experiments remains a possibility, however. Experimental results summarized in Figure 9 indicate that chemical dissolution of $Fe(OH)_3(s)$ in the presence of excess NTA proceeds at a rate comparable to that of iron-reduction in the fastest biological experiments; reduction rates in the latter stages of the high-NTA experiments may in fact be dissolution-controlled. Such kinetic limits would distort the results of equilibrium models, leading to predicted rates which exceed measured values at the end of experiments and correspondingly low initial predictions. Thus, dissolution kinetics offer an alternative explanation for the inexact agreement between observed and predicted

iron-reduction rates. If, as discussed above, maximum iron-reduction rates are determined by dehydrogenase activity or dissipation of proton motive force, solid-dissolution limitations may still arise during the final stages of iron-reduction experiments.

3. In the high-rate cases with NTA present in solution, Fe^{3+} or one of the monomeric hydroxo complexes of Fe(III) may be the reactive species, with reductive rate limited by dissociation of Fe(III)-NTA complexes. At pH 7, the relative dissociation reaction must involve either $Fe(NTA)OH^-$ or $Fe(NTA)(OH)_2^{2-}$. Our analysis of possible limitations imposed by chemical dissociation of $Fe(NTA)OH^-$ is summarized in Table 7. At the start of equimolar (NTA/total Fe) iron-reduction experiments, the estimated maximum rate of complex dissociation is 1.9×10^{-4} $\underline{M}$ hr^{-1}. Because observed reduction rates are about 100 times faster, we conclude that a chemical complex dissociation step does not precede iron reduction. Direct reduction of Fe(III)-NTA complexes is implied.

4. Molecular diffusion of Fe(III)-NTA complexes across the hydrodynamic boundary layer surrounding biological surfaces may limit the rate of biologically mediated iron reduction. The feasibility of such a transport limit is examined mathematically in Table 8. The simplified continuity equation for one-dimensional diffusion in cylindrical coordinates was integrated twice using the bulk concentration and transport of soluble Fe(III) species to the biological surface (observed reaction rate) as boundary conditions. The solution indicates

that at the highest observed reduction rates the spatial distribution of Fe(III) species is nearly uniform throughout the boundary layer. Furthermore, the residence time for reactive species in the boundary layer is short compared to the time scale for Fe(III) disappearance. Thus mass transport neither limits the overall rate of reaction nor causes major departures from bulk-phase equilibria within the hydrodynamic boundary layer.

CONCLUSIONS

1. The rate of microbial iron reduction is a function of both biology and aqueous-phase chemistry. The dependence of rate on iron speciation has been established. Stepwise linear regression analyses suggest that $Fe(NTA)(OH)_2^{2-}$ and $Fe(OH)_3(s)$ are the most important reacting species. Free ferrous iron and $Fe_3(PO_4)_2(s)$ were identified as probable inhibitors. The fastest observed reduction rates may be limited by dehydrogenase activity in Pseudomonas sp. 200 and not by the activity of the terminal oxidase.
2. Even though iron(III) reduction is apparently linked to bacterial electron transport, coupled oxidative phosphorylation is questionable for the following reasons:
   (i) The process must be very efficient. Comparison of free-energy changes for electron transport from NADH to $Fe(OH)_3(s)$ (neutral pH) and phosphorylation of ADP shows that an overall process efficiency approaching 85 percent is necessary for coupled ATP generation. When electron

transport is to molecular oxygen, efficiencies are typically less than 75 percent.

(ii) In oxidative phosphorylation, ATP generation is coupled to ATPase-mediated, transmembrane transport of protons in the direction of a sizeable proton motive force. The probable process topology is illustrated in Figure 1 (electron transport from NADH in the cytoplasm to Fe(III) in the periplasmic space or cell surroundings). When either $Fe(OH)_3(s)$ or $Fe(NTA)(OH)_2^{2-}$ serves as an electron acceptor, the reduction half-reactions (see Table 4) appear to diminish the outward-positive proton gradient by consuming protons outside the cytoplasmic membrane; it is possible that electron transport to Fe(III) cannot sustain a proton motive force or support oxidative phosphorylation. That is, dissimilative iron reduction may provide no more than a sink for cellular reducing power while the bacterium subsists on substrate-level phosphorylation. The topological problem would seemingly disappear if Fe(III) were internalized before reduction. However, transport of colloidal $Fe(OH)_3(s)$ across cell membranes would present formidable obstacles, and expectations regarding the direction of trans-membrane electrical potential (outward-positive) discourage interpretations which depend on transport of anions such as $Fe(NTA)(OH)_2^{2-}$.

3. Non-linear data-fitting exercises suggest that all enzymatic sites are functionally equivalent but that most sites are

sterically limited to chemical interaction with only soluble iron species (Model 2). Fitted parameters support such an interpretation, and this is the simplest hypothesis which is consistent with reduction-rate data.

4. In the absence of NTA, contact between $Fe(OH)_3(s)$ and either the biological surface or a chemical intermediate of biological origin is required to achieve the experimentally observed reduction rates. In such cases, iron reduction may be limited by the rate at which electrons can be transported to enzymatic sites in contact with colloidal ferric hydroxide.
5. Calculated Fe(III)-ligand dissociation rates are considerably slower than observed reduction rates. This suggests that ferric-iron solutes interact directly with biological reductants (i.e., reduced enzyme or biologically produced chemical intermediates).
6. Observed iron-reduction rates are not limited by mass transport across the hydrodynamic boundary layer. Diffusion across such a quiescent layer occurs on a shorter time scale than the observed reduction.

ACKNOWLEDGEMENT

The authors gratefully acknowledge Dr. D. W. S. Westlake of the Department of Microbiology, University of Alberta, Canada, for generously providing the microorganism used in this study, Pseudomonas sp. 200.

This work was supported by United States Department of Energy Contract No. DE-AS03-83ER13125 administered within the Division of Advanced Energy Projects, Office of Basic Energy Sciences. We appreciate the support and encouragement of Drs. Ryszard Gajewski and Duane L. Barney.

Thanks to Ms. Sandy Brooks and Ms. Nancy Tomer for clerical and drafting assistance in preparation of our manuscript.

References

1. J. C. Munch and J. C. G. Ottow, Z. Pflanzenernähr. Düng. Bodenkd., 140, 549 (1977).

2. J. Sørensen, Appl. Environ. Microbiol., 43, 319 (1982).

3. Y. Takai and T. Kamura, Folia Microbiol., 11, 304 (1966).

4. J. G. Jones, S. Gardener, and B. M. Simon, J. Gen. Microbiol., 129, 131 (1983).

5. F. M. Harold, In: The Bacteria, Vol. VI: Bacterial Diversity, eds. L. N. Ornston and J. R. Sokatch (Academic, New York, 1978), pp. 463-522.

6. C. W. Jones, Bacterial Respiration and Photosynthesis (American Society for Microbiology, Washington, D.C., 1983), pp. 38-63.

7. C. O. Obuekwe, Ph.D. dissertation, University of Alberta, Edmonton, Alberta, 1980.

8. C. O. Obuekwe, D. W. S. Westlake, and F. D. Cook, Can. J. Microbiol., 27, 692 (1981).

9. C. O. Obuekwe and D. W. S. Westlake, Can. J. Microbiol., 28, 989 (1982).

10. C. O. Obuekwe and D. W. S. Westlake, Microbios Lett., 19, 57 (1982).

11. T. D. Brock and J. Gustafson, Appl. Environ. Microbiol., 32, 567 (1976).

12. K. Kino and S. Usami, Ag. Biol. Chem., 46, 803 (1982).

13. J. C. Munch and J. C. G. Ottow, In: Environmental Biogeochemistry, R. Hallberg (ed.), Ecol. Bull. (Stockholm) 35, 383 (1983).

14. E. P. Troshanov, Mikrobiol., 37, 934 (1968).

15. E. P. Troshanov, Mikrobiol., 38, 634 (1969).

16. J. C. Munch and J. C. G. Ottow, Z. Pflanzenernähr. Düng. Bodenkd., 145, 66 (1982).

17. J. C. Westhall, J. L. Zachary, and F. M. M. Morel, Technical Note No. 18, Ralph M. Parsons Laboratory for Water Resources and Environmental Engineering, Massachusetts Institute of Technology (1976).

18. M. R. Hoffmann, Environ. Sci. Technol., 15, 1345 (1981).

19. Y. Kurimura, R. Ochiai, and N. Matsuura, Bull. Chem. Soc. Japan, 41, 2234 (1968).

20. American Public Health Association, American Water Works Association, Water Pollution Control Federation, Standard Methods for the Examination of Water and Wastewater, 15th edition (APHA, Washington, D.C., 1981), pp. 201-205.

21. S. J. Eisenreich, R. T. Bannerman and D. E. Armstrong, Environ. Lett., 9, 43 (1975).

22. P. C. Hinkle and R. E. McCarty, Sci. Am., 228, No. 3, 104 (1978).

23. B. A. Haddock and C. W. Jones, Bact. Rev., 41, 47 (1977).

24. A. H. Stouthamer, In: The Bacteria, Vol. VI: Bacterial Diversity, eds. L. N. Ornston and J. R. Sokatch (Academic, New York, 1978), pp. 389-462.

25. F. Basolo and R. G. Pearson, Mechanisms of Inorganic Reactions, 2nd ed. (Wiley-Interscience, New York, 1967), pp. 145-158.

26. D. W. Marquardt, Soc. Ind. Appl. Math. J., 11, 431 (1963).

27. T. L. Theis and P. L. Singer, In: Trace Metals and Metal-Organic Interactions in Natural Waters, ed. P. L. Singer (Ann Arbor, Michigan, 1973), pp. 303-320.

28. A. E. Martell and R. M. Smith, Critical Stability Constants, Vol. 1: Amino Acids (Plenum, New York, 1974).

29. A. E. Martell and R. M. Smith, Critical Stability Constants, Vol. 3: Other Organic Ligands (Plenum, New York, 1977).

30. R. M. Smith and A. E. Martell, Critical Stability Constants, Vol. 4: Inorganic Complexes (Plenum, New York, 1976).

31. W. Stumm and J. J. Morgan, Aquatic Chemistry, 2nd ed. (Wiley-Interscience, New York, 1981), pp. 418-463.

32. F. M. M. Morel, Principles of Aquatic Chemistry (Wiley-Interscience, New York, 1983), pp. 311-338.

33. R. M. Fuoss and C. A. Kraus, J. Am. Chem. Soc., 55, 1019 (1933).

34. R. M. Fuoss, J. Am. Chem. Soc., 80, 5059 (1958).

Figure 1. Postulated physiology of dissimilative iron reduction coupled to oxidative phosphorylation. The energy required for ATP production is given by:

$$\Delta G = \Delta G^{o} + 2.3\ RT \log \frac{\{ATP\}}{\{ADP\}\{P_i\}} \qquad (\Delta G \text{ in kcal/mole of ATP produced})$$

Assuming: $\Delta G^{o} = 7.3$ kcal/mole,

intracellular $\{ATP\}/\{ADP\} \cong 10$,

and $\{P_i\} \cong 10^{-3}$ M,

$\Delta G \cong 12.8$ kcal/mole. From the overall reaction stoichiometry (transport of $2e^-$ forces $2H^+$ into the periplasmic space at each proton translocation site; ATPase-mediated return of $2H^+$ to the cytoplasm is coupled to phosphorylation of each ADP), it is evident that transfer of electrons from NADH to Fe(III) must liberate at least 6.4 kcal per mole of Fe(II) produced if the process is to drive ATP production.

Figure 2. A linear free-energy relationship involving association constants between various cations and glycolate or lactate. All thermodynamic data are from Martell and Smith[28-30]. Values shown were corrected to zero ionic strength using the Davies equation. The excellent correlation between these values suggests that stability constants for lactate and either Fe^{2+} or Fe^{3+} can be reliably estimated from the regression line and available glycolate thermodynamic data.

Regression line: $\log K_a^{gly-} = 0.788 \log K_a^{lac-} + 0.507$

From Martell and Smith:

Fe^{2+} + glycolate$^-$ <====> $Fe(gly)^+$ $\log K_a = 1.94$ I = 0.0

Fe^{3+} + glycolate$^-$ <====> $Fe(gly)^{2+}$ $\log K_a = 3.82$ I = 0.0

Implied equilibria:

Fe^{2+} + lactate$^-$ <====> $Fe(lac)^+$ $\log K_a = 1.82$ I = 0.0

Fe^{3+} + lactate$^-$ <====> $Fe(lac)^{2+}$ $\log K_a = 4.20$ I = 0.0

Figure 3. Fe(II) concentration as a function of time following the addition of high-level (1.86×10^{-3} M) ferric iron to batch cultures of Pseudomonas sp. 200. Experiments were run at all combinations of three pH levels (6.5, 7.0, 7.5) and four total NTA concentrations (molar NTA/total Fe = 0.0, 0.1, 0.5, 1.0). Cell dry weight at the start of the iron-reduction period was approximately 0.55 g/ℓ. Optical density (A_{600}, 1-cm pathlength cuvette) was 1.00.

Figure 4. Rate of iron reduction as a function of Fe(III) remaining (by difference; Fe(III) = Fe_{TOTAL} - Fe(II)). Rates are slopes taken from Fe(II) vs. time curves (Figure 3).

Figure 5. Histograms illustrating correlations between iron-reduction rate and predicted (bulk-phase) equilibrium concentrations of iron species. Histogram elements represent experimental combinations of pH and total NTA concentration. Relative

reaction rate or species concentration is shown on the vertical axis. In each case, the value of the highest (shaded) bar is provided.

Figure 6. Gibbs free energy changes associated with electron transport from lactate (6a) and NADH (6b) to alternative electron acceptors. Points represent results of individual calculations.

Figure 7. Comparison of predicted and measured iron-reduction rates. Predicted values are results of Model 2 application (two-site, steric non-equivalence, see Table 6). At each experimental pH, there are plots of measured and predicted iron-reduction rate corresponding to all four total NTA levels (see experimental methods section).

Figure 8. Rate of electron transport to molecular oxygen or Fe(III) in cultures of Pseudomonas sp. 200, A_{600} = 1.00 (cell dry weight = 0.55 g/ℓ).

Figure 9. Dissolution of freshly precipitated ferric hydroxide in response to (i) sudden drop in pH and (ii) addition of nitrilotriacetic acid.

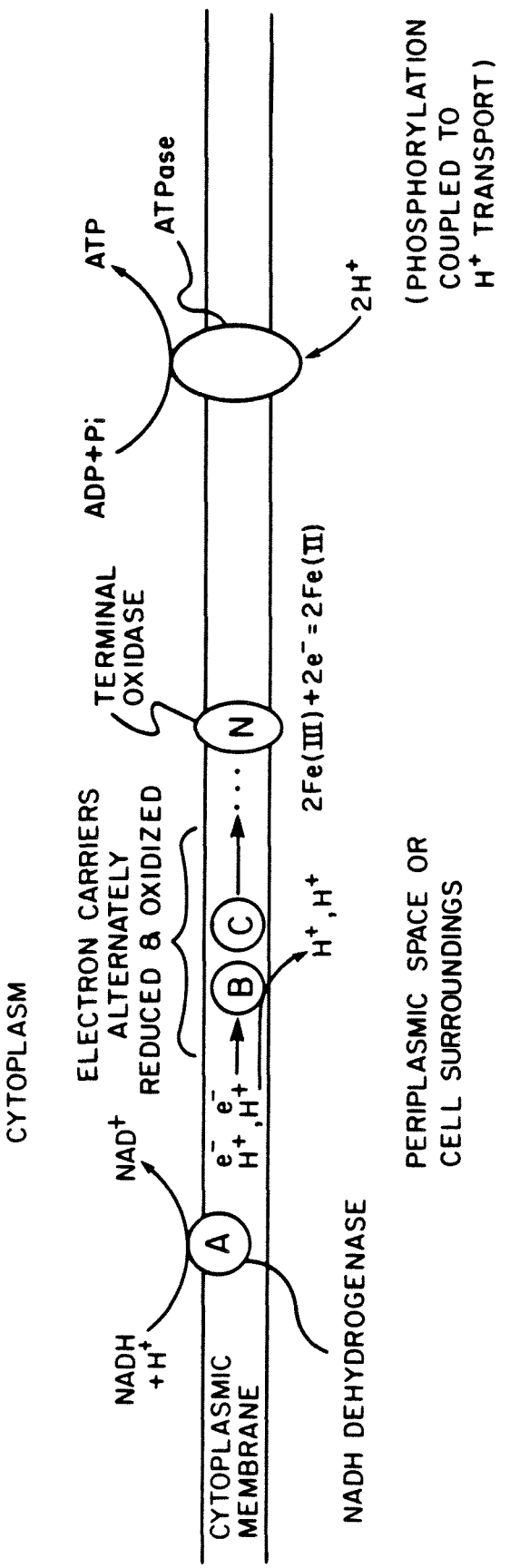
CYTOPLASM
NAD+
NADH
+H+
A
e- e-
H+,H+
B
C
N
ELECTRON CARRIERS
ALTERNATELY
REDUCED & OXIDIZED
TERMINAL
OXIDASE
ADP+Pi
ATP
ATPase
2H+
(PHOSPHORYLATION
COUPLED TO
H+ TRANSPORT)
CYTOPLASMIC
MEMBRANE
NADH DEHYDROGENASE
H+,H+
2Fe(III)+2e-=2Fe(II)
PERIPLASMIC SPACE OR
CELL SURROUNDINGS

Figure 1

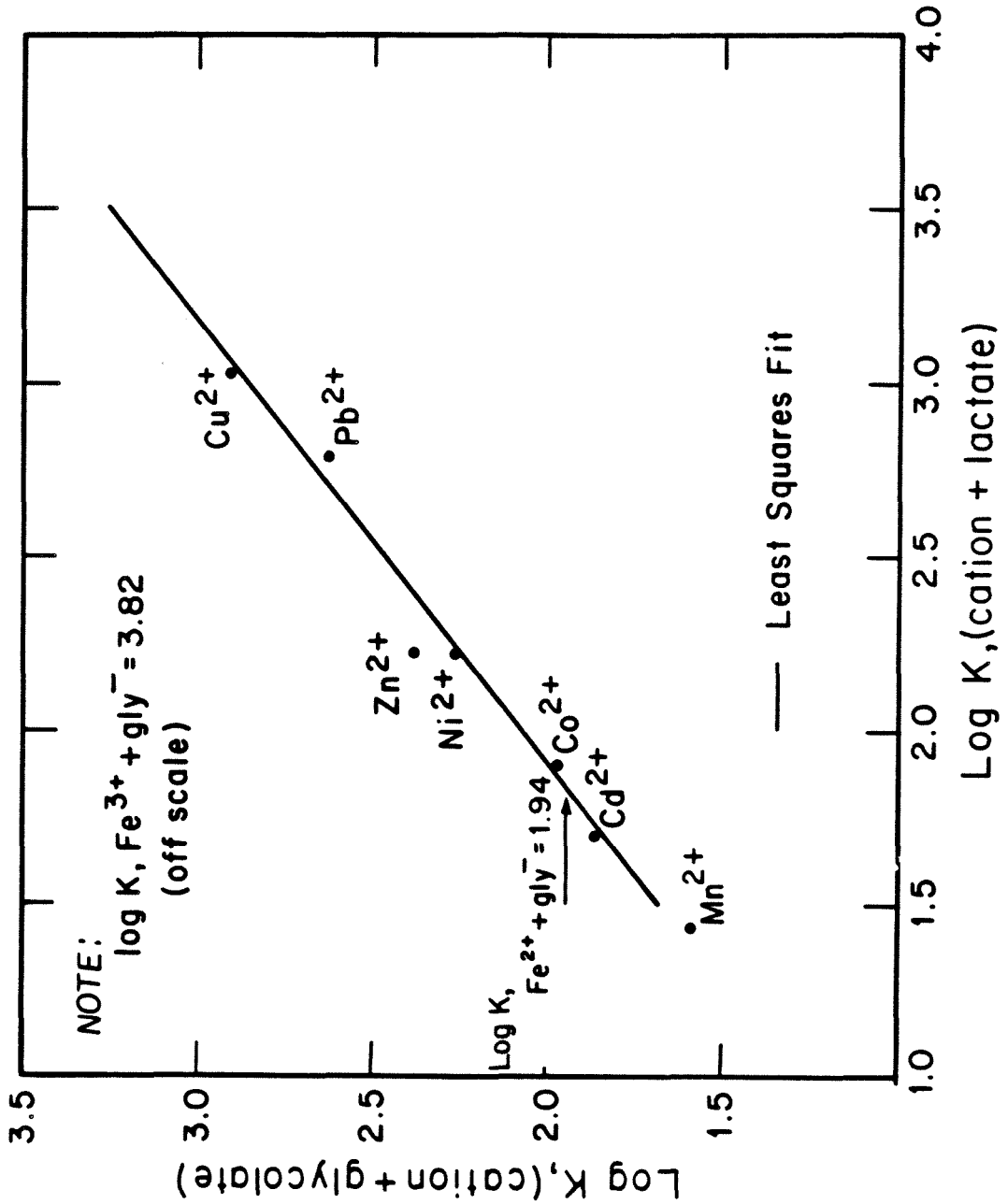
NOTE:
log K, Fe^{3+} + gly^- = 3.82
(off scale)
Cu^{2+}
Pb^{2+}
Zn^{2+}
Ni^{2+}
Co^{2+}
Cd^{2+}
Mn^{2+}
Log K, Fe^{2+} + gly^- = 1.94
Least Squares Fit
Log K, (cation + glycolate)
Log K, (cation + lactate)
3.5
3.0
2.5
2.0
1.5
1.0
4.0

Figure 2

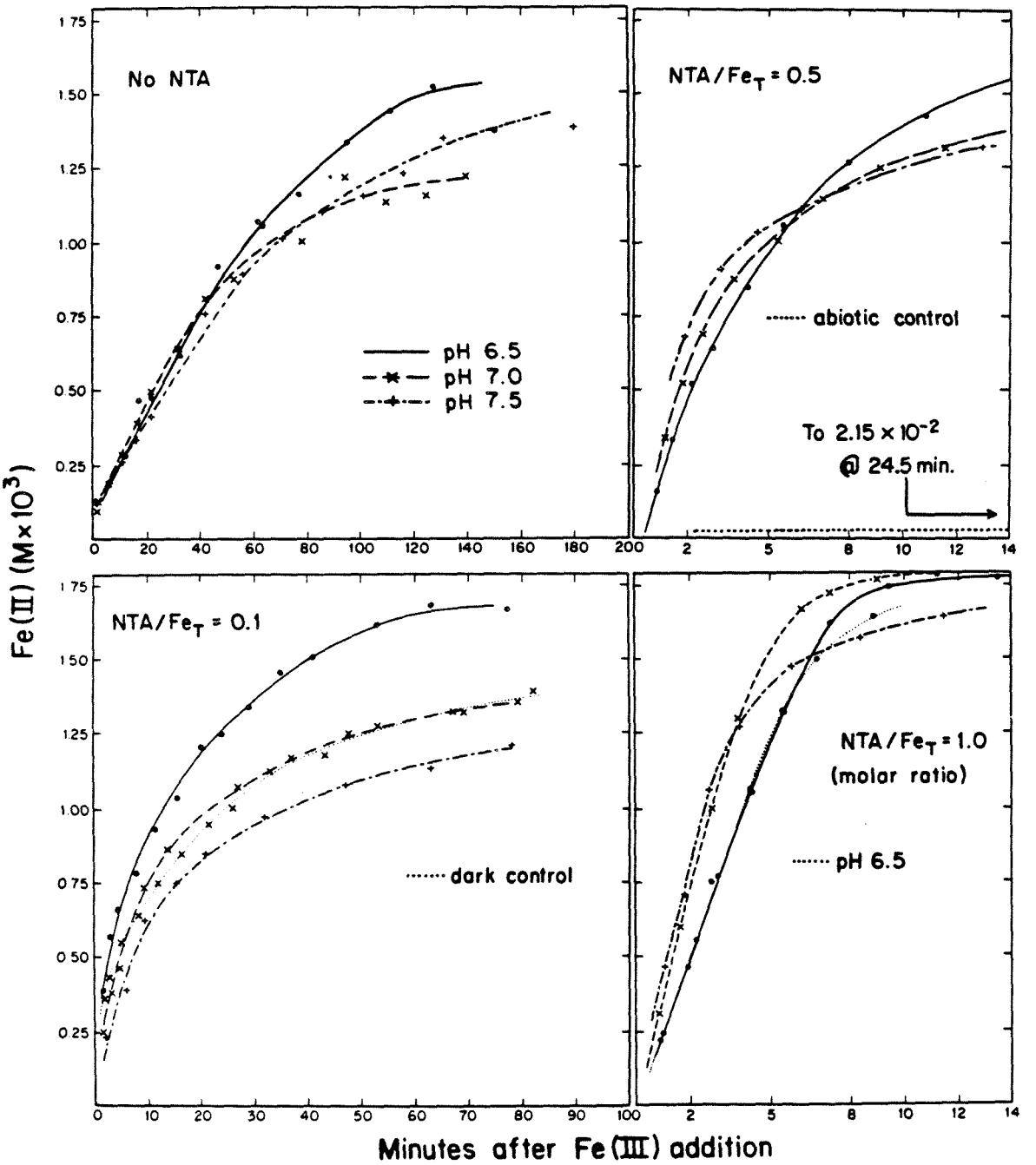
No NTA
pH 6.5
pH 7.0
pH 7.5
NTA/Fe$_T$ = 0.5
abiotic control
To 2.15 x 10^{-2}
@ 24.5 min.
NTA/Fe$_T$ = 0.1
dark control
NTA/Fe$_T$ = 1.0
(molar ratio)
pH 6.5
Fe(II) (M x 10^3)
Minutes after Fe(III) addition

Figure 3

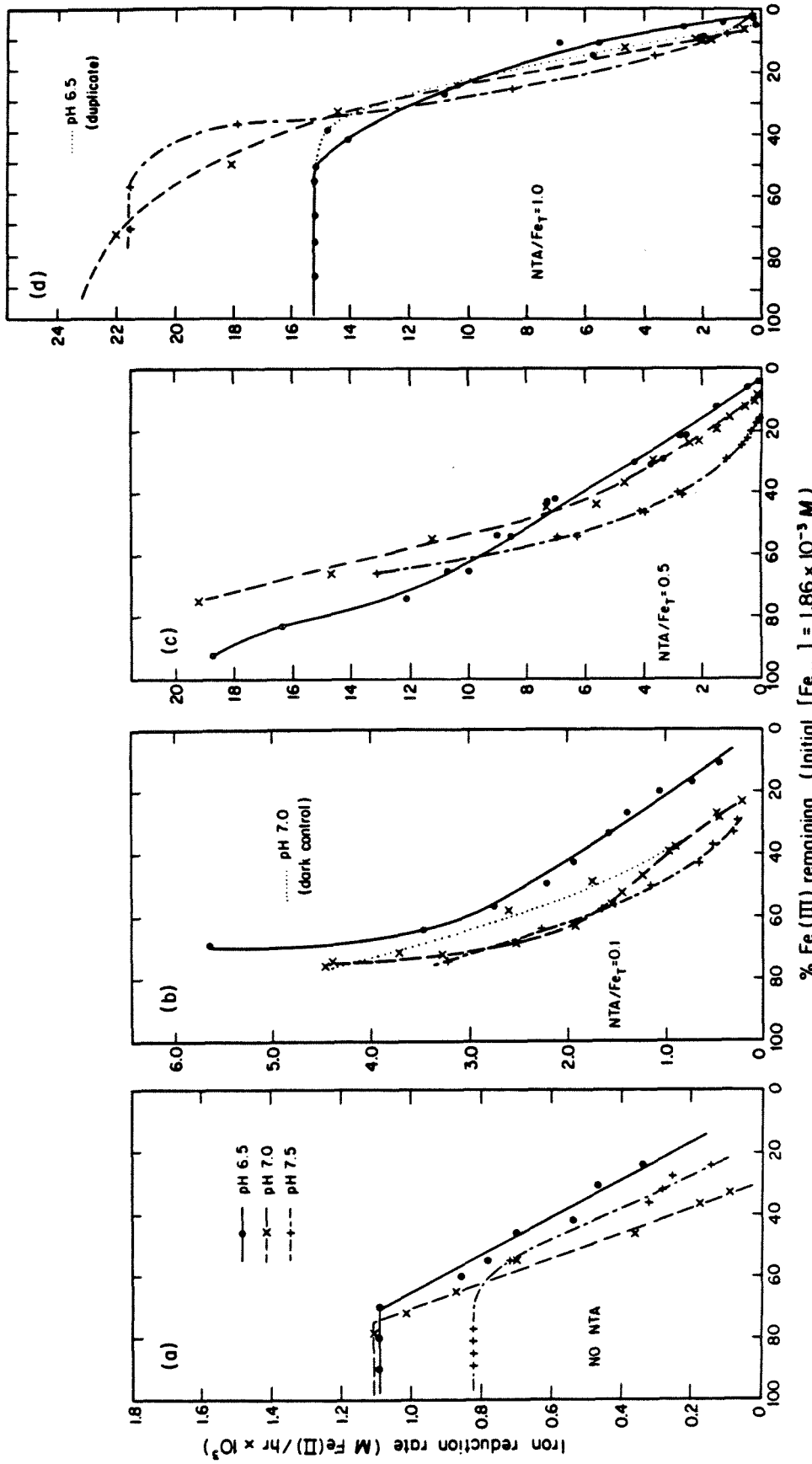
iron reduction rate (M Fe(II)/hr x 10³)
% Fe (III) remaining (Initial [Fe_TOT] = 1.86 x 10⁻³ M)
(a)
NO NTA
pH 6.5
pH 7.0
pH 7.5
(b)
NTA/Fe_T=0.1
pH 7.0
(dark control)
(c)
NTA/Fe_T=0.5
(d)
NTA/Fe_T=1.0
pH 6.5
(duplicate)

Figure 4

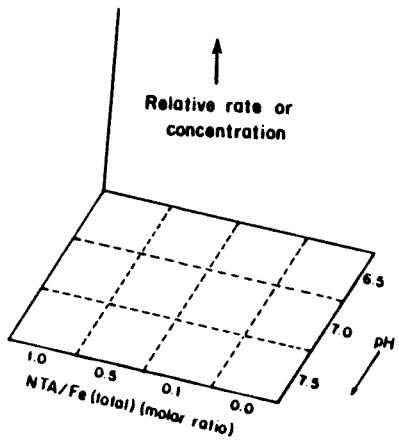

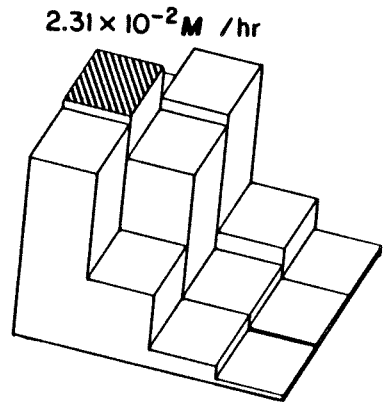

(a) Fe (III) Reduction Rate

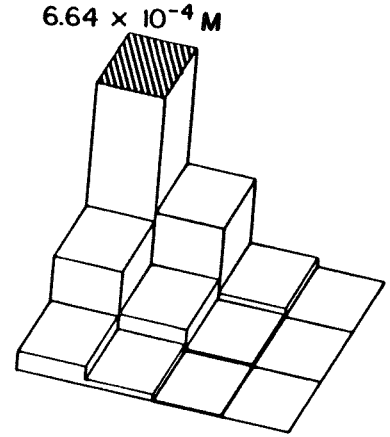

(b) Total Soluble Fe (III)

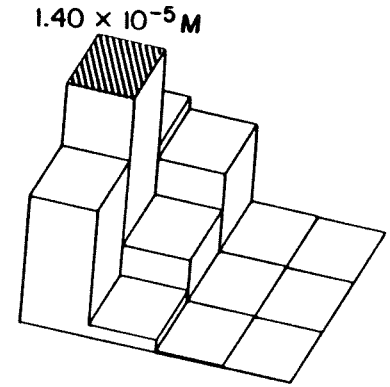

(c) $FeNTA(OH)_2^{2-}$

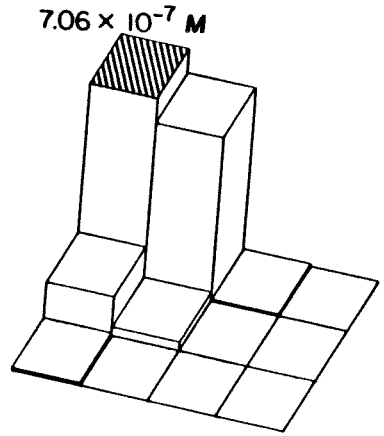

(d) FeNTA

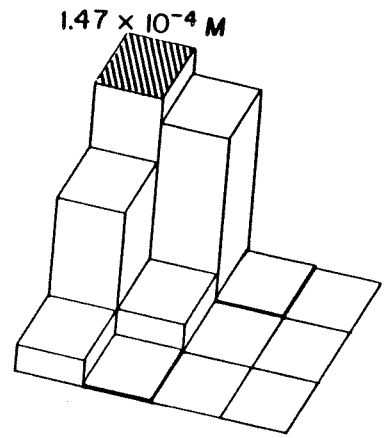

(e) $FeNTAOH^-$

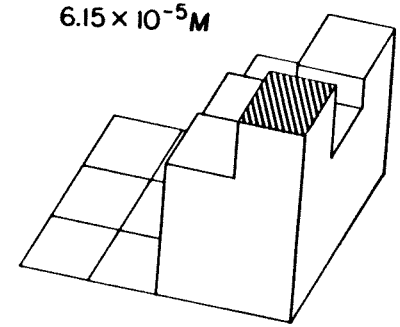

(f) $Fe_3(PO_4)_2$ (s)

Figure 5

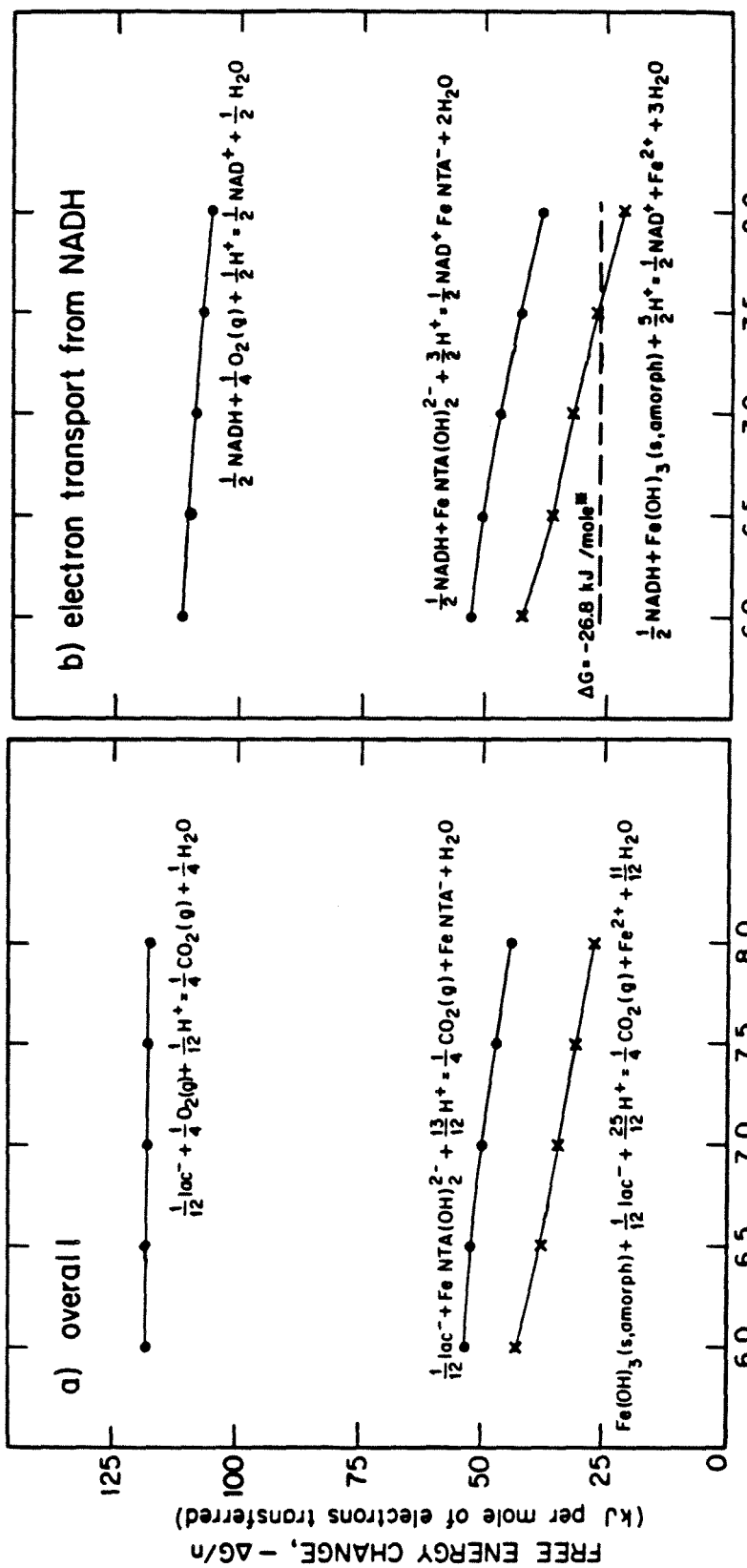
a) overall
b) electron transport from NADH
FREE ENERGY CHANGE, −ΔG/n
(kJ per mole of electrons transferred)
pH
pH
125
100
75
50
25
0
6.0
6.5
7.0
7.5
8.0
$\frac{1}{12}lac^- + \frac{1}{4}O_2(g) + \frac{1}{12}H^+ = \frac{1}{4}CO_2(g) + \frac{1}{4}H_2O$
$\frac{1}{12}lac^- + Fe\,NTA(OH)_2^{2-} + \frac{13}{12}H^+ = \frac{1}{4}CO_2(g) + Fe\,NTA^- + H_2O$
$Fe(OH)_3(s,amorph) + \frac{1}{12}lac^- + \frac{25}{12}H^+ = \frac{1}{4}CO_2(g) + Fe^{2+} + \frac{11}{12}H_2O$
$\frac{1}{2}NADH + \frac{1}{4}O_2(g) + \frac{1}{2}H^+ = \frac{1}{2}NAD^+ + \frac{1}{2}H_2O$
$\frac{1}{2}NADH + Fe\,NTA(OH)_2^{2-} + \frac{3}{2}H^+ = \frac{1}{2}NAD^+ Fe\,NTA^- + 2H_2O$
$\Delta G = -26.8$ kJ /mole
$\frac{1}{2}NADH + Fe(OH)_3(s,amorph) + \frac{3}{2}H^+ = \frac{1}{2}NAD^+ + Fe^{2+} + 3H_2O$

Figure 6

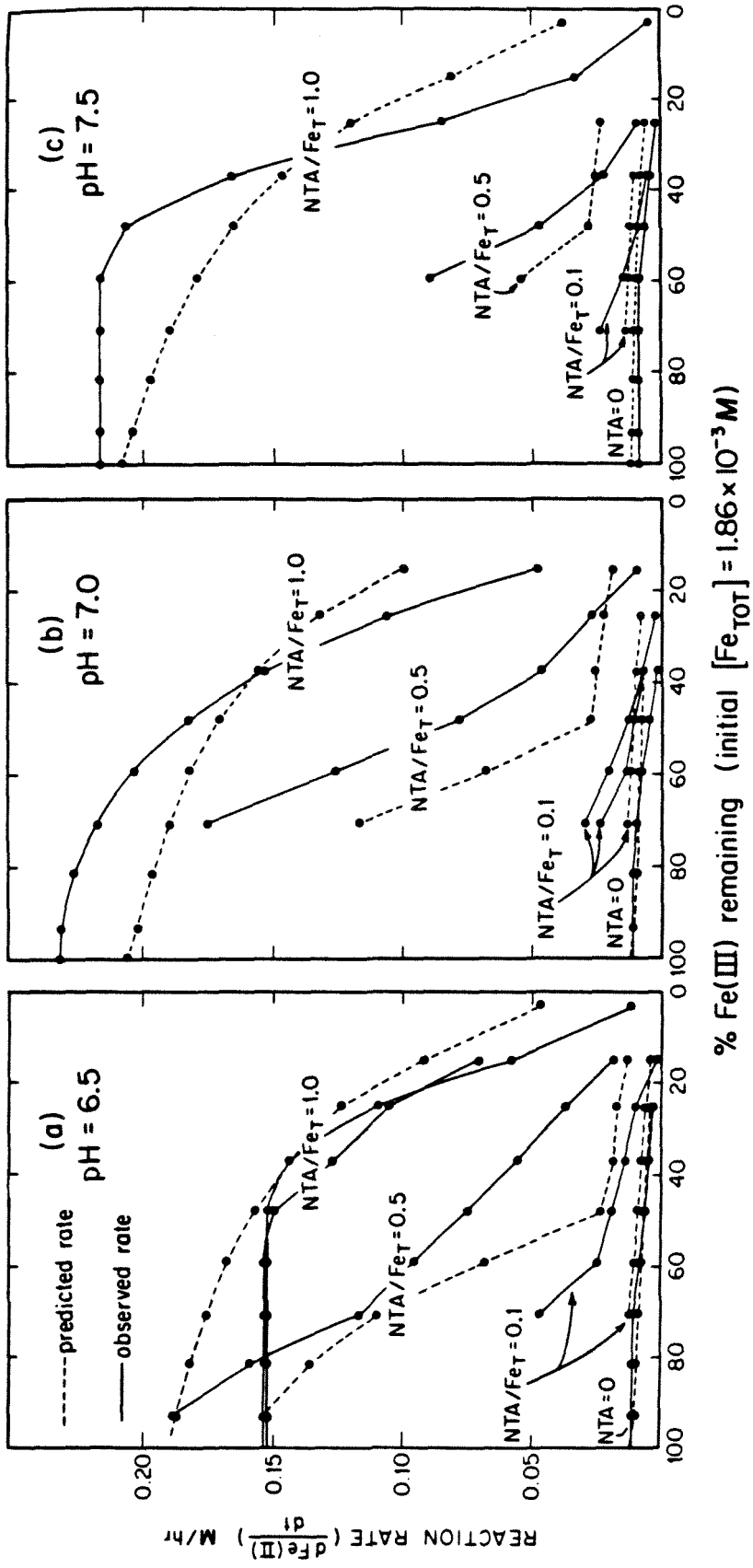
(a)
pH = 6.5
(b)
pH = 7.0
(c)
pH = 7.5
predicted rate
observed rate
NTA/Fe$_T$=1.0
NTA/Fe$_T$=0.5
NTA/Fe$_T$=0.1
NTA=0
REACTION RATE $(\frac{d\,Fe(II)}{dt})$ M/hr
0.20
0.15
0.10
0.05
0
20
40
60
80
100
% Fe(III) remaining (initial $[Fe_{TOT}] = 1.86 \times 10^{-3} M$)

Figure 7

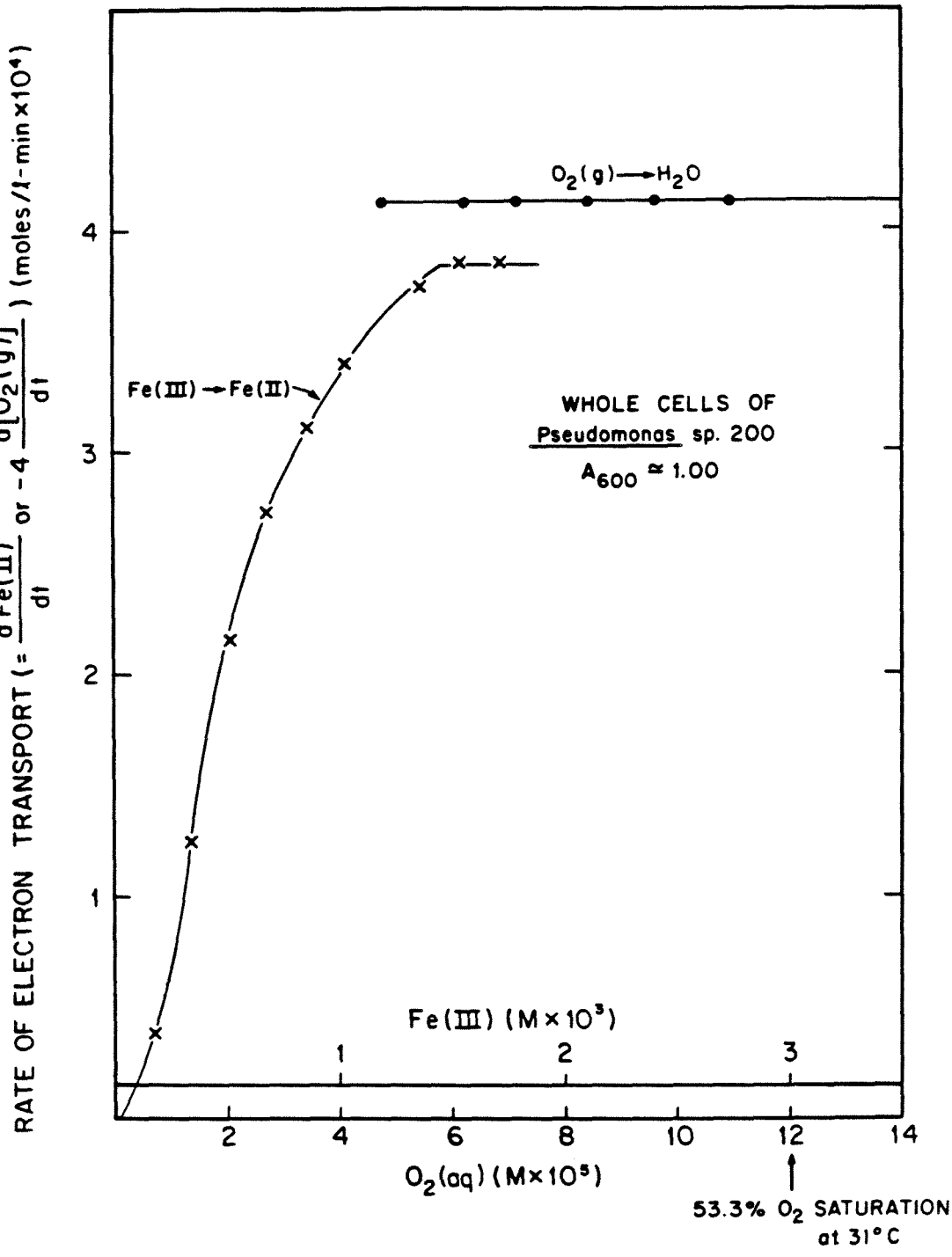
RATE OF ELECTRON TRANSPORT (= dFe(II)/dt or -4 d[O2(g)]/dt) (moles/l-min x10⁴)
O2(g)→H2O
Fe(III)→Fe(II)
WHOLE CELLS OF
Pseudomonas sp. 200
A600 ≃ 1.00
Fe(III) (M x 10³)
O2(aq) (M x 10⁵)
53.3% O2 SATURATION
at 31°C

Figure 8

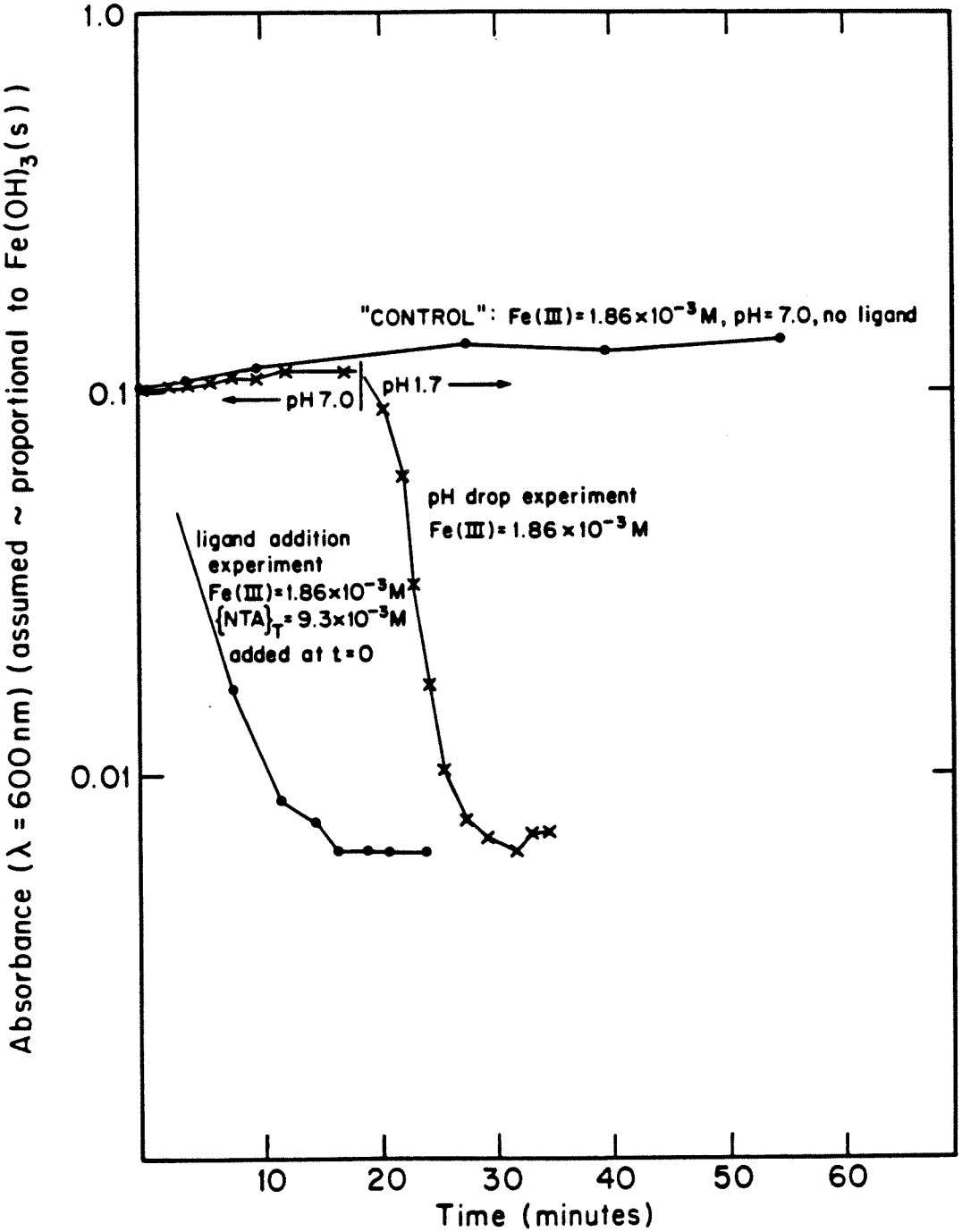
1.0
0.1
0.01
Absorbance (λ = 600 nm) (assumed ~ proportional to Fe(OH)3(s))
"CONTROL": Fe(III) = 1.86×10⁻³M, pH = 7.0, no ligand
pH 7.0
pH 1.7
pH drop experiment
Fe(III) = 1.86×10⁻³M
ligand addition
experiment
Fe(III) = 1.86×10⁻³M
{NTA}T = 9.3×10⁻³M
added at t = 0
10
20
30
40
50
60
Time (minutes)

Figure 9

Table 1. Medium for Growth and Iron Reduction by Pseudomonas sp. 200[7]

K_2HPO_4	0.5 g
Na_2SO_4	2.0 g
NH_4Cl	1.0 g
$CaCl_2$	0.15 g
$MgSO_4 \cdot 7H_2O$	0.1 g
$FeCl_3$	4.0 mg (as Fe) (filter sterilized and added after autoclaving other medium contents)
Yeast extract	0.5 g
Sodium lactate	3 mls from 60% syrup
H_2O	to 1 ℓ total volume

Note: Major organic components of yeast extract include amino acids and B-complex vitamins (Difco Laboratories, personal communication). Major inorganic constituents include iron, potassium, sodium, and chloride ion. Inorganics represent only a small percentage of overall growth medium concentrations. Independent calculations (not reviewed here) indicate that organic components do not appreciably alter iron speciation.

Table 2. Relevant Characteristics of Pseudomonas sp. 200[7]

Physical

- Gram-negative rod
- Motile, possessing 2-4 polar flagella

Metabolic

- Aerobic, catalase/oxidase positive
- Capable of NO_3^- ——> NO_2^- reduction, denitrification
- Reduces SO_3^{2-} ——> S^{2-} using lactate or a variety of amino acids as carbon/energy source
- Nutritionally versatile - grew well on most amino acids, organic acids, sugars, and a few aromatics as sole carbon/energy source
- Growth from 4^oC to 41^oC, optimum $25-30^oC$

Table 3. Selected Equilibria Used in MINEQL Calculation of Iron Speciation[1],[4]

Soluble Complexes	log K[2]
$Fe^{3+} + SO_4^{2-} = FeSO_4^+$	4.20
$Fe^{3+} + 2SO_4^{2-} = Fe(SO_4)_2^-$	5.60
$Fe^{3+} + Cl^- = FeCl^{2+}$	1.40
$Fe^{3+} + 2Cl^- = FeCl_2^+$	2.10
$Fe^{3+} + 3Cl^- = FeCl_3(aq)$	1.30
$Fe^{3+} + H^+ + PO_4^{3-} = FeHPO_4^+$	20.70
$Fe^{3+} + NTA^{3-} = FeNTA(aq)$	17.95
$Fe^{3+} + 2NTA^{3-} = Fe(NTA)^{3-}$	26.30
$Fe^{3+} - H^+ + NTA^{3-} = FeNTAOH^-$	13.55
$Fe^{3+} - 2H^+ + NTA^{3-} = FeNTA(OH)_2^{2-}$	5.45
$Fe^{3+} - H^+ = FeOH^{2+}$	- 2.03
$Fe^{3+} - 2H^+ = Fe(OH)_2^+$	- 5.40
$Fe^{3+} - 3H^+ = Fe(OH)_3(aq)$	-20.10
$Fe^{3+} - 4H^+ = Fe(OH)_4^-$	-20.80
$2Fe^{3+} - 2H^+ = (FeOH)_2^{4+}$	- 2.30
$Fe^{3+} + lac^- = Felac^{2+}$ (3)	4.20
$2Fe^{3+} - 2H^+ + 2NTA = (FeNTAOH)_2^{2-}$	30.80
$Fe^{2+} + SO_4^{2-} = FeSO_4(aq)$	2.30
$Fe^{2+} + Cl^- = FeCl^+$	0.90
$Fe^{2+} + NH_3 = FeNH_3^{2+}$	1.30
$Fe^{2+} + 2NH_3 = Fe(NH_3)_2^{2+}$	2.10
$Fe^{2+} + 4NH_3 = Fe(NH_3)_4^{2+}$	3.60
$Fe^{2+} + NTA^{3-} = FeNTA^-$	10.17

$Fe^{2+} - H^+ + NTA = FeNTAOH^{2-}$	- 0.80
$Fe^{2+} + H^+ + NTA = FeHNTA(aq)$	12.40
$Fe^{2+} + 2NTA^{3-} = Fe(NTA)_2^{4-}$	13.60
$Fe^{2+} - H^+ = FeOH^+$	- 9.30
$Fe^{2+} + lac^- = Felac^+$ (4)	1.82
$H^+ + NTA^{3-} = HNTA^{2-}$	10.21
$2H^+ + NTA^{3-} = H_2NTA^-$	13.15
$3H^+ + NTA^{3-} = H_3NTA(aq)$	14.80
$H^+ + lac^- = Hlac(aq)$ (3)	3.86

Solubility Products	log K_{so} (2)
$Fe^{3+} + PO_4^{3-} = FePO_4(s)$	25.80
$Fe^{3+} - 3H^+ = Fe(OH)_3(s,amorph)$	- 3.00
$3Fe^{2+} + 2PO_4^{3-} = Fe_3(PO_4)_2(s)$	33.30
$Fe^{2+} - 2H^+ = Fe(OH)_2(s)$	-12.10

(1) Thermodynamic data are primarily from Martell and Smith[28-30] corrected to 31°C using integrated Arrhenius equation.

(2) Constants shown are at zero ionic strength. Corrections for ionic strength (Davies equation) are a part of the MINEQL computational procedure.

(3) NTA^{3-} represents deprotonated nitrilotriacetic acid; lac^- is lactate ion.

(4) The MINEQL algorithm permits calculation of equilibrium concentrations of individual chemical species in aqueous media via an iterative procedure. Necessary input data and information include the identity and total amounts of solution components (e.g., PO_4^{3-}, SO_4^{2-}, Na^+, etc.), initial estimates of species concentrations and ionic strength, and changes to the default thermodynamic data deck. Special computational features permit the user to fix solution pH, enter additional variables and equilibria not present among the default data, and exclude specific solids which may be kinetically inaccessible during the time frame of interest.

Table 4. Calculation of Overall Free-Energy Changes in Electron Transport.

Relevant half-reactions, equilibria, and thermodynamic data (1), (2):

$\frac{1}{12}(\text{lactate}^-) + \frac{1}{4}H_2O = \frac{1}{4}CO_2(g) + \frac{11}{12}H^+ + e$ $\quad \Delta G^\circ = 3.81 \frac{kJ}{\text{mole e}}$

$Fe^{3+} + e = Fe^{2+}$ $\quad \Delta G^\circ = -73.94 \frac{kJ}{\text{mole e}}$

$\frac{1}{4}O_2(g) + H^+ + e = \frac{1}{2}H_2O$ $\quad \Delta G^\circ = -118.19 \frac{kJ}{\text{mole e}}$

$\frac{1}{2}NAD^+ + \frac{1}{2}H^+ + e = \frac{1}{2}NADH$ $\quad \Delta G^\circ = 10.81 \frac{kJ}{\text{mole e}}$

$Fe(OH)_3(s,\text{amorph}) + 3H^+ + e = Fe^{2+} + 3H_2O$ $\quad \Delta G^\circ = -91.13 \frac{kJ}{\text{mole e}}$

$Fe^{2+} + NTA^{3-} = Fe(NTA)^-$ $\quad \Delta G^\circ = -57.84 \frac{kJ}{\text{mole}}$

$Fe(NTA)(OH)_2^{2-} = Fe^{3+} + NTA^{3-} + 2OH^-$ $\quad \Delta G^\circ = 189.94 \frac{kJ}{\text{mole}}$

$H^+ + OH^- = H_2O$ $\quad \Delta G^\circ = -79.62 \frac{kJ}{\text{mole}}$

Overall redox expression (for example)

$$\frac{1}{12}(\text{lactate}^-) + Fe(NTA)(OH)_2^{2-} + \frac{13}{12}H^+ = \frac{1}{4}CO_2(g) + Fe(NTA)^- + \frac{7}{4}H_2O \qquad \Delta G^\circ = \frac{-92.27\ kJ}{\text{mole e transferred}}$$

Free-energy under non-standard conditions (free energies in kJ/mole):

$$\Delta G = \Delta G^\circ + 9.62\ RT \log \frac{\{CO_2(g)\}^{1/4}\{Fe(NTA)^-\}}{\{\text{lactate}^-\}^{1/12}\{Fe(NTA)(OH)_2^{2-}\}\{H^+\}^{13/12}} \qquad (3)$$

(1) Sources of thermodynamic data[28-32]

Table 4 (continued)

(2) Required conversions (free energy in kJ/mole):

$\Delta G^\circ = -9.62\ RT \log K$ (= -5.70 log K @ 25°C)

$\frac{\Delta G^\circ}{n} = -9.62\ RT\ p\varepsilon^\circ$ (n is the number of electrons transferred per reaction, ΔG in kJ/mole)

(3) Free-energy computations (Figure 6) reflect estimated reactant/product concentrations anticipated in fermentations of interest. See text (Methods) for description of fermentation conditions. Assumed activities follow:

$T = 31°C$

$pH = 6.0$ to 8.0

$\{CO_2(g)\} = 10^{-3}$ atm.

$\{lactate^-\} = 1.6 \times 10^{-2}$ M

$\{Fe(NTA)^-\} = 1.9 \times 10^{-4} - 1.6 \times 10^{-4}$ M (from MINEQL results with ∿ 10% Fe(III) ——> Fe(II) conversion)
(pH dependent)

$\{Fe(NTA)(OH)_2^{2-}\} = 4.8 \times 10^{-6} - 1.3 \times 10^{-5}$ M (from MINEQL results with ∿ 10% Fe(III) ——> Fe(II) conversion)
(pH dependent)

Table 5. Summary of Linear Regression Analyses. Iron-Reduction Rate as a Function of Predicted (equilibrium) Species Concentrations. Summary of Stepwise-Regression Results.

Cases (data) Used in Model Evaluation (2)	Regression Results (stepwise) (3)	R^2 (4)
Model A: ("non-competition model")	Rate = $f[Fe(OH)_3(s), FeNTA(OH)_2^{2-}, FeNTAOH^-, FeNTA, Fe(NTA)_2^{2-}]$	
[NTA] = 0	Rate = 3.3×10^4 $Fe(OH)_3(s) - 4.0$	0.75
[NTA] = all levels	Rate = 8.9×10^7 $FeNTA(OH)_2^{2-} + 1.5 \times 10^2$	0.82
	Rate = 1.0×10^8 $FeNTA(OH)_2^{2-} - 3.4 \times 10^6$ $Fe(NTA)_2^{3-} + 1.5 \times 10^2$	0.84
	Rate = 1.1×10^8 $FeNTA(OH)_2^{2-} - 1.8 \times 10^7$ $Fe(NTA)_2^{3-}$ $+ 7.5 \times 10^6$ $FeNTAOH^- + 1.0 \times 10^2$	0.90
Model B: ("competition model")	Rate = $f[Fe(OH)_3(s), FeNTA(OH)_2^{2-}, FeNTA, FeNTA^-, Fe_3(PO_4)_2(s)]$	
[NTA] = 0	Rate = -1.1×10^5 $Fe_3(PO_4)_2(s) + 0.6 \times 10^2$	0.80
[NTA] = all levels	Rate = 8.9×10^7 $FeNTA(OH)_2^{2-} + 1.5 \times 10^2$	0.82
	Rate = 7.4×10^7 $FeNTA(OH)_2^{2-} - 8.3 + 10^5$ $Fe_3(PO_4)_2(s) + 2.8 \times 10^2$	0.87
	Rate = 7.7×10^7 $FeNTA(OH)_2^{2-} - 6.2 \times 10^5$ $Fe_3(PO_4)_2(s)$ $+ 8.2 \times 10^4$ $FeNTA^- + 2.1 \times 10^2$	0.88

Note (1) The stepwise regression algorithm used is available within the Statistical Package for the Social Sciences (version $SPSS^X$). $P_{in} = 0.05$, $P_{out} = 0.10$.

Note (2) A portion of the analyses was conducted using only equilibrium predictions and rate data gathered in the absence of NTA additions. Such limitations are noted in this column.

Table 5 (continued)

Note (3) Results are provided for each step in the regression procedure. Iron reduction rate is in units of mg/ℓ-hr. Chemical concentrations are in moles per liter.

Note (4) The squared Pearson correlation coefficient measures the proportion of variance in measurements of the independent variable which can be explained in terms of variation in the independent variable(s). In mathematical terms,

$$R^2 = 1 - \frac{\sum_i (\hat{y}_i - y)^2}{\sum_i (y_i - \bar{y})^2} \quad \text{where,}$$

y_i is the measured value of the independent variable

$\hat{y}_i$ is the predicted value (model prediction)

$\bar{y}$ is the mean value of the independent variable

Note (5) Table of Simple Correlation Coefficients Among Dependent (Rate) and Independent Variables (Major Fe(III) Species from Equilibrium Calculations).

	Rate	$Fe(OH)_3(s)$	Fe(NTA)	$Fe(NTA)_2^{3-}$	$Fe(NTA)OH^-$	$Fe(NTA)(OH)_2^{2-}$	$Fe(NTA)_2(OH)_2^{2-}$
Rate	1.00	--	--	--	--	--	--
$Fe(OH)_3(s)$	0.21	1.00	--	--	--	--	--
Fe(NTA)	0.49	-0.01	1.00	--	--	--	--
$Fe(NTA)_2^{3-}$	0.62	0.17	0.89	1.00	--	--	--
$Fe(NTA)OH^-$	0.63	0.05	0.97	0.95	1.00	--	--
$Fe(NTA)(OH)_2^{2-}$	0.91	0.26	0.54	0.76	0.70	1.00	--
$Fe_2(NTA)_2(OH)_2^{2-}$	0.46	0.07	0.96	0.95	0.95	0.57	1.00

Table 6(a). Summary of Non-Linear Models Tested for Conformance with Observed Kinetic Data.

Model 1: Two active sites; functional non-equivalence

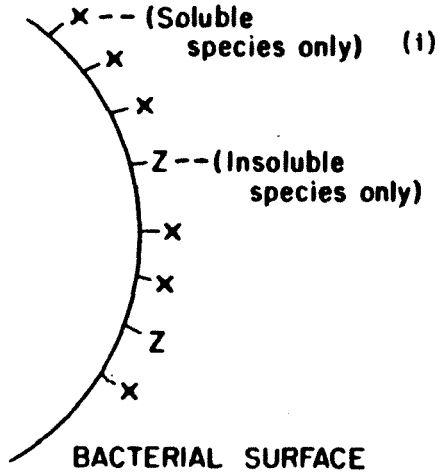

(i) Soluble Fe species bind at different sites than do insoluble species. (Rule applies to both substrates and competitors.)

$$\frac{d\ Fe(II)}{dt} = \frac{K_1 V_{m1} S_1}{1 + K_1 S_1 + K_{c1} S_{c1}} + \frac{K_2 V_{m2} S_2}{1 + K_2 S_2 + K_{c2} S_{c2}}$$

K_i = association constant between S_i and enzyme active site.

V_{mi} = max. rate of reduction of substrate S_i

$S_1 = Fe(OH)_3(s)$

$S_2 = Fe(NTA)(OH)_2^{2-}$

$S_{c1} = Fe_3(PO_4)_2(s)$

$S_{c2} = Fe^{2+}$

(all in concentration units)

Model 2: Two active sites; steric non-equivalence

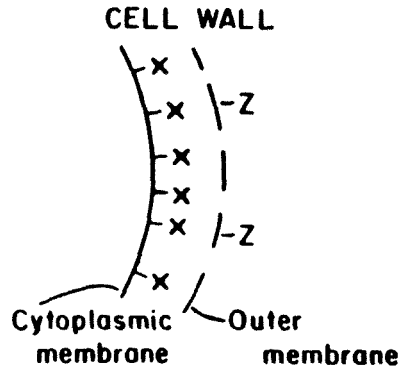

(i) Outer membrane is permeable to soluble species.

(ii) Active sites -x and -z differ only by position (and thus substrate accessibility)

$$\frac{d\ Fe(II)}{dt} = \frac{K_2 V_{m(?)} S_2}{1 + K_2 S_2 + K_{c2} S_{c2}} + \frac{K_1 V_{m1} S_1 + K_2 V_{m(II)} S_2}{1 + K_1 S_1 + K_2 S_2 + K_{c1} S_{c1} + K_{c2} S_{c2}}$$

$V_{m(II)}$ = max. rate of conversion of $FeNTA(OH)_2^{2-}$ to Fe(II) at -z sites.

Table 6(a) (continued)

Notes:

(1) Association constants are defined as follows:

$$K_i = \frac{[x\text{-}s_i]}{[x][s_i]}, \text{ where}$$

$[x]$ is the volume concentration of free active sites,

$[s_i]$ is the concentration of species i, and

$[x\text{-}s_i]$ is the volume concentration of active sites with sorbed s_i.

(2) $V_{mi} = k_i[X_T]$, where

k_i is the rate constant for enzymatic conversion of Fe(III) to Fe(II) (or k_{cat}), and

$[X_T]$ is the total volume concentration of enzymatically active sites

Thus, V_{mi} is the maximum rate of enzymatic conversion of substrate s_i to product, which occurs when solution chemistry/rxn kinetics dictate that essentially all catalytic sites are occupied by s_i.

(3) Sample derivation of kinetic expression.
Given:

(i) $[s_i\text{-}x] = K_i[x][s_i]$ $\qquad i = 1, 2, C1, C2$

(ii) $[x] = [X_T] - \sum_i [s_i\text{-}x]$

(iii) $\frac{d\ Fe(II)}{dt} = k_1[s_i\text{-}x] + k_2[s_2\text{-}x]$

(a) Use expression (i) to eliminate $[s_i\text{-}x]$ from expressions (ii) and (iii);

(b) Use modified expression (ii) to solve for $[x]$ in terms of K_i and $[s_i]$;

(c) Substitute $[x]$ in the (modified) expression (iii).

(d) Rearrangement yields Model kinetics.

Table 6(b). Summary of Efforts to Numerically Fit Constants in Kinetic Models Described Above (2).

Parameter	Graphical Techniques(1)	Model No. 1	Model No. 2
V_{m1}	1.0×10^{-3} M/hr	1.3×10^{-3} M/hr	1.3×10^{-3} M/hr
V_{m2}	2.3×10^{-2} M/hr	2.3×10^{-3} M/hr	N/A
$V_{m(2)}$	N/A	N/A	2.4×10^{-3} M/hr
$V_{m(II)}$	N/A	N/A	9.0×10^{-4} M/hr
K_1 (M^{-1})	1290	5372	3000
K_2 (M^{-1})	3.0×10^{5}	3.2×10^{5}	3.0×10^{5}
K_{c1} (M^{-1})	N/A	3391	976
K_{c2} (M^{-1})	N/A	3.2×10^{4}	1.0×10^{4}
R^2 (unitless)	not calculated	0.916	0.913

Notes:

(1) Estimated using graphs provided in Figures 4(a) and 4(d). V_{m1} is the maximum iron-reduction rate in Figure 4(a); V_{m2} is the maximum rate in Figure 4(d). K_1 and K_2 are reciprocals of tne half-velocity concentration in Figures 4(a) and 4(d), respectively. Graphical estimates are averages of results of the several experiments summarized in the figures.

(2) Except for graphical estimates, the non-linear curve-fitting technique of Marquardt[26] was used to estimate parameters in the models indicated based on a least squares criterion.

(3) $R^2 = 1 - (\sum_i (\hat{y}_i - y_i)^2 / \sum_i (\bar{y} - y_i)^2)$ where

y_i is the i^{th} rate measurement

$\hat{y}_i$ is the i^{th} predicted iron-reduction rate (calculated via model application using fitted parameters)

$\bar{y}$ is the mean value of measured rates.

Table 7. Estimation of an Upper Kinetic Limit to Fe(III)-NTA Complex Dissociation.

1. Fe(III) reduction model when complex dissociation is rate limiting:

$$Fe(H_2O)_4(NTA)OH^- \xrightarrow{k_b} Fe(OH)_2^+ + H(NTA)^{2-}$$

$$Fe^{3+} \xrightarrow{fast} Fe^{2+}$$

$$\frac{d\,Fe(II)}{dt} = k_b\, Fe(H_2O)_4(NTA)OH^-$$

2. Complexation model (Basolo & Pearson, 1967)

$$HNTA^{2-} + Fe(H_2O)_4(OH)_2^+ \overset{K_o}{\rightleftharpoons} \underset{\text{(ion pair)}}{Fe(H_2O)_4(OH)_2^+}, \quad HNTA^{2-} \overset{k_a}{\underset{k_b}{\rightleftharpoons}} Fe(H_2O)_4(NTA)OH^- + H_2O$$

$$K_{eq} = K_o\left(\frac{k_a}{k_b}\right) = 10^{8.3}$$

3. Postulate: $k_a \leq k_{ex}$ (water exchange rate for $Fe(H_2O)_4(OH)_2^+$)

$k_{ex} = 3.4 \times 10^4\ M^{-1}\ sec^{-1}$ (Basolo & Pearson, 1967)

4. From Fuoss and Kraus (1933) and Fuoss (1958):

$$K_o = \frac{4\pi Na^3}{3000} \exp\left(\frac{U_a}{kT}\right)$$

$$U_a = \frac{Z_1 Z_2 e^2}{Da(1+\beta a\sqrt{\mu})}$$

$$\beta = (8\pi Ne^2/1000DkT)^{\frac{1}{2}}$$

$\longrightarrow K_o = 4.2\ \underline{M}^{-1}$

where N = Avogadro's number

a = distance of closest approach between ion-pair centers (in centimeters, assumed equal to 9.0×10^{-8} cm)

$\frac{U_a}{kT}$ = the ratio of coulombic to thermal energies among molecules comprising the ion pair

e = 4.803×10^{-10} $cm^{3/2}\ g^{1/2}\ s^{-1}$ (the charge on a proton)

D = 76.0 (the dielectric constant for H_2O at 31°C; CRC Handbook of Chemistry and Physics, 1975-76)

k = 1.3805×10^{-16} erg/degree K, molecule (Boltzmann's constant)

T = 304 K

μ = ionic strength (assumed equal to 0.2 $\underline{M}$)

Z_i = charge on the ith ion in the ion pair

5. Therefore $k_b \leq 7.2 \times 10^{-4}\ sec^{-1}$, and assuming $[Fe(NTA)OH^-]$ equals $7.27 \times 10^{-5}\ \underline{M}$ (MINEQL result), the complex dissociation rate $\leq 3.12 \times 10^{-6}\ \underline{M}$/min.

6. Conclusion:

Because iron-reduction rates 100 times higher have been measured, complexed Fe(III) must serve as electron acceptor.

Table 8. Analysis of Mass Transport Across the Hydrodynamic Boundary Layer.

1. Physical situation:

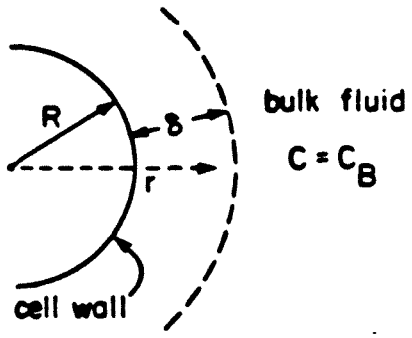

δ = assumed boundary layer thickness, equal to R

R = cell radius, 2.5×10^{-5} cm

ℓ = cell length, 2×10^{-4} cm

C = total soluble Fe(III)

N = cell number, 1.5×10^{9} cells/ml

D = diffusion coefficient, 10^{-5} cm^2/sec

F = observed time rate of change of bulk concentration of ferrous iron, 3.85×10^{-4} M/min.

2. Equation of continuity within the boundary layer:

$$\frac{d}{dr}\left(r\frac{dc}{dr}\right) = 0$$

s.t. (i) @ $r = R$ $\quad \frac{dc}{dr} = \frac{F}{2\pi R\ell ND}$

(ii) @ $r = R + \delta$ $\quad C = C_o$, 2.38×10^{-4} M (MINEQL result, pH 7.0, initial soluble iron concentration)

3. Solution

$$C = C_o + \frac{F}{2\pi\ell ND} \ln\left(\frac{r}{R+\delta}\right)$$

4. Substitute and calculate $C/_{r = R} = C_o$, or

$C \cong C_o$ throughout boundary layer.

5. Conclusion: Mass transport is not a kinetic limitation within the hydrodynamic boundary layer.

CHAPTER 4

REDUCTIVE DISSOLUTION OF Fe(III)-OXIDES BY *PSEUDOMONAS* SP. 200

by

Robert G. Arnold, Thomas J. DiChristina
and Michael R. Hoffmann

Submitted to: Biotechnology & Bioengineering

July 1986

ABSTRACT

The kinetics and mechanism of reductive dissolution of Fe(III) oxides were examined in pure, batch cultures of Pseudomonas sp. 200. Primary factors controlling mineral dissolution kinetics were mineral surface area (or concentration of high-energy surface sites), ligand concentration, and cell number. Saturation kinetics are apparent in the following relationship governing reductive dissolution of hematite:

$$\frac{d[Fe(II)]}{dt} = \frac{V_{max(I)} K_{m(NTA)}\ V_{max(II)}[NTA]}{K_{m(NTA)} + [NTA]} \cdot \frac{[Fe(III)]}{K_{m(Fe)} + [Fe(III)]}$$

where $V_{max(I)} = 2.8 \times 10^{-5}$ M·hr^{-1}

$V_{max(II)} = 6.3 \times 10^{-4}$ M·hr^{-1}

$K_{m(NTA)} = 1.2 \times 10^{-3}$ M

$K_{m(Fe)} = 1.0 \times 10^{-1}$ M (as Fe).

NTA = nitrilotriacetic acid

[Fe(III)] = volume concentration of hematite (as Fe).

Microorganisms were present at an initial concentration of approximately 2×10^9 cells/ml. Addition of NTA resulted in a 20-fold increase in the microbial rate of mineral (reductive) dissolution. Mechanisms in which NTA served as a bridging ligand, shuttling respiratory electrons from the membrane-bound microbial electron transport chain to the metal center of the iron oxide, or accelerated the departure of Fe(II) centers (bound to ligand) from the oxide surface following reduction have been postulated. Separation of microorganisms and iron oxide by a dialysis membrane indicated that cell/mineral contact was essential for reductive dissolution.

INTRODUCTION

The importance of microorganisms in promoting the leaching of metals from naturally occurring ores is well known. Microbial catalysis may be either direct or indirect. Direct bacterial leaching involves an catalyzed change in the oxidation state of one of the mineral components. If the product is soluble, mineral dissolution results. When cellular respiration drives this process, it may be coupled to oxidative phosphorylation. Microbially driven oxidative dissolution has been used for the hydrometallurgical extraction of copper and uranium from low-grade ores; microbial extraction of nickel, lead, and zinc is also feasible due to the nonspecific nature of bacterial substrate requirements. Iron(III) is known to be a major participant in indirect bacterial leaching of copper and uranium; bacterially generated, soluble ferric iron chemically oxidizes mineral components [e.g., U(IV) to U(VI) under acid conditions], resulting in their dissolution.[1]

Bacterially mediated, reductive dissolution of iron- and manganese-bearing ores has also been observed.[2] The process may be of considerable environmental interest due to the limited biological availability of iron in many aquatic settings[3-5] and because Fe(III) reduction can provide an important pathway for mineralization of organic material.[6] In the presence of $Fe(OH)_3$(s,amorph), the solubility of free ferric ion in H_2O at pH 7.0 is about 10^{-18} M[7]; Fe(II), the stable oxidation state of iron under reduced environmental conditions, is much more soluble (and hence biologically available) in the neutral pH range. Reductive dissolution of iron oxide is catalyzed by a variety of microorganisms including Thiobacillus thiooxidans,[8,9]

Bacillus circulans,[10,11] Bacillus polymyxa,[12,13] Clostridium butyricum,[12] Vibrio sp.,[14] Sulfolobus acidocaldarius[8,9] and Pseudomonas sp. 200).[15-18] Dissimilative iron reduction involves a direct transfer of electrons from enzymes of the electron transport system to Fe(III). Evidence for such a transfer includes the enzymatic reduction of Fe(III) by a membrane fraction prepared from Staphylococcus aureus[19] using lactate or glycerol-3-phosphate as substrate.

Details of the mechanism by which microorganisms reduce iron at the surface of Fe(III)-bearing minerals (reductive dissolution) are not clear; the existence of a soluble electron carrier within the periplasmic space of gram-negative bacteria is a possibility. It is also possible that relatively slow mineral dissolution precedes bacterial catalysis of iron reduction. Thus, the rate of reductive dissolution may be controlled by (i) chemical dissolution of the Fe(III) oxide (followed by rapid, bacterially mediated reduction of soluble Fe(II)), (ii) direct electron transport to the oxide surface, or (iii) dissociation and transport of Fe(II) from the particle surface following reduction. When Fe(III) is presented in soluble form, dissimilative iron reduction can be very rapid;[20] reductive dissolution of iron oxides has proven to be much slower. Rates of reductive dissolution of Fe(III)-bearing minerals appear to be inversely related to mineral stability (hematite < goethite < ferric hydroxide).[13,21]

In 1980, Obuekwe[15] isolated bacteria from a Canadian oil pipeline whose iron-reducing capabilities apparently contribute to rapid pipeline corrosion.[22] The best-studied of these isolates, Pseudomonas sp. 200, is capable of catalyzing dissimilative iron reduction at high rates (e.g., 4×10^{-4} M/min in early stationary-phase cultures, A_{600} =

1.0).[20] Under appropriate conditions, the rate of electron transport to Fe(III) approaches that of aerobic respiration, indicating that kinetic control of both respiratory processes lies at the same point.[20] The microorganism possesses both a constitutive (slow) and inducible (fast) iron reductase.[23] Reductase induction is related to both mean cell age and oxygen content or microbial energy status during growth.

At optimal rates, dissimilative iron reduction by Pseudomonas sp. 200 may provide an economically and environmentally attractive means for the extraction of iron from ore. Because such a process would yield Fe(II) in some concentrated form, the microbial product would demand less reductant during high-temperature conversion to elemental iron in subsequent iron-production steps. In addition, iron-reducing microorganisms such as Pseudomonas sp. 200 may be useful for removal of corrosion products from ferrous surfaces. Since commercial viability depends upon reduction of solid-phase Fe(III), we have chosen to explore the kinetics and mechanism of reductive mineral dissolution by Pseudomonas sp. 200. Our primary objectives were (1) to yield mathematical relationships involving reduction rate as a function of component concentrations in pure batch cultures of Pseudomonas sp. 200 and (2) to determine the extent to which reductive dissolution depends on direct mineral/microorganism contact.

MATERIALS AND METHODS

Kinetic Measurements

Kinetic experiments were conducted primarily in pure, 1.5-liter batch cultures (Biostat M reactor, Braun Instrument Co.) of Pseudomonas sp. 200 with temperature and pH held constant at 31°C and 7.0,

respectively. The growth medium is given in Table 1. Species characteristics have been reported previously.[20] Microorganisms were grown aerobically to a target optical density (normally A_{600} = 1.0, cm^{-1}). Dissolved oxygen was then purged using high-purity N_2(g), and Fe(III) oxide and nitrilotriacetic acid (NTA, Pfaltz and Bauer, Inc.) were added to levels dictated by experimental objectives. Fe(II) concentration was measured periodically by adding 1-ml aliquots from the anaerobic culture to a quenching mixture consisting of 2 mls ammonium acetate buffer[24] and 1,10-orthophenanthroline (Sigma Chemical Co.). The total volume was raised to 10 mls with distilled water, and the mixture was centrifuged for 15 minutes at 3000 g in a Sorvall RC3B centrifuge. Centrate color was measured at λ = 510 nm in a Beckman DU7 spectrophotometer. ε_{510} for the $(phenanthroline)_3$-Fe(II) complex is 1.11×10^4 $\underline{M}^{-1}$ cm^{-1}.[20]

When reduction experiments were conducted in tubes, iron oxide or NTA was added incrementally to the 1.5-liter fermentor contents at the conclusion of the growth period. After each addition, 5.5-ml aliquots were removed and sealed in a series of 12 x 75 mm culture tubes. These were incubated at 31°C while continuously mixed on an Eberbach reciprocating shaker table (approximately 120 cycles per second, 2-cm stroke length). At pre-selected intervals, tubes representing each iron oxide level were chilled on ice and centrifuged at 4°C for 15 min. (3000 g). Centrate Fe(II) concentrations were determined as described above.

Electron Microscopy

Cells were fixed for 1 hr. on ice with 2.5% glutaraldehyde in cacodylate buffer (pH 7.2) and collected on an 0.2 μm filter (Nucleopore

Corp., Pleasanton, Calif., or Whatman Ltd., Maidstone, Eng.). After excess fixative was removed with buffer solution, filters were dried in an ethanol gradient. Dehydrated filters were critical-point dried with CO_2 and taped to viewing mounts. An Au-Pd coating was applied using a pulsed-planar, magnetum triode sputtering system (Hummer V, Technics). Scanning electron microscopy observations were made with an ETEC Autoscan.

X-Ray Crystallography

The purity and crystallinity of iron oxides were confirmed via x-ray crystallography using a Norelco vertical diffractometer with Cu(Kα) radiation (λ = 1.5418). Minerals were obtained from the Mineral, Pigments and Metals Division of Pfizer, Inc. Oxide characteristics are summarized in Table 2.

Reduction Activity of Culture Supernatant

The supernatant from growing cultures of Pseudomonas sp. 200 was tested for iron-reducing activity before and immediately after a 30-min. anaerobic period. Cell-free reduction activity would support an indirect mechanism, dependent upon development of a soluble, reduced chemical intermediate. Pseudomonas sp. 200 was grown aerobically (Westlake medium, see above, T = 31°C, pH 6.5 to 7.5) to A_{600} = 0.5 (cm^{-1}). At that point, 100 mls of the culture were chilled on ice and centrifuged at 6400 g for 15 minutes (4°C). Centrate was transferred to a gas-washing bottle. $FeCl_3$ and NTA were added to final concentrations of 1.86×10^{-3} M, and pH was returned to 7.0 with 2 N NaOH. The mixture was continuously purged with N_2(g) while samples were removed periodically for Fe(II) analysis. Additional mixing was provided by a magnetic stirrer. Temperature was held constant at 31°C;

no attempt was made to control pH during the iron-reduction period. A second 100-ml aliquot was removed from the original culture following a 30-min. purge using high-purity N_2(g). After centrifugation, the centrate was treated per above and periodically analyzed for Fe(II). A control culture (no centrifugation step) was monitored for iron reduction in each case (i.e., after 0- and 30-min. anaerobic treatments).

Dialysis Tube Experiments

The existence of soluble, reducing intermediates was investigated by separating Pseudomonas sp. 200 and goethite with a dialysis membrane and monitoring for Fe(II) in the "continuous" liquid medium. Pseudomonas sp. 200 was grown to early stationary phase ($A_{600} \cong 0.4$ cm^{-1}) in two 200-ml cultures of Westlake medium (Table 1), T = 31°C, pH 6.5 to 7.5. At the target optical density, goethite (YL01888D, Table 2) was added to culture no. 1 (control) to a final concentration of 1.86×10^{-3} M (as Fe). An equivalent volume of goethite (sufficient to bring the overall average concentration to 1.86×10^{-3} M) was placed in a dialysis tube (Spectrapor membrane tubing, standard cellulose, 6.4 ml/cm, dry thickness 2.5×10^{-3} cm., molecular weight cutoff 12,000-14,000 or pore diameter $\cong$ 30 Å, Spectrum Medical Ind., Los Angeles) and immersed in culture no. 2. NTA was added to both cultures to 1.86×10^{-3} M, and dissolved oxygen was continuously purged with high purity N_2(g). Aliquots (1 mL) were periodically removed (from tube surroundings) for measurement of [Fe(II)].

A second control was designed to provide assurance that facile membrane transport of soluble iron species was possible during the time course of the experiment. A dense culture (A_{600} = 0.5 cm^{-1}, 100-mls)

was sequestered within the dialysis tube. The membrane and contents were bathed in 200 mls of sterile Westlake medium supplemented with 1.86×10^{-3} M $FeCl_3$ and NTA, pH = 7.0. Samples were periodically removed from the membrane surroundings and analyzed for Fe(II).

Chemical Dissolution Experiments

Solutions (100 mL) of Westlake medium (Table 1), hematite (R1599, Table 2), and NTA were prepared as follows:

(i) 4.0×10^{-3} M α-Fe_2O_3 ; no NTA

(ii) 1.86×10^{-3} M α-Fe_2O_3 ; 5.58×10^{-3} M NTA

(iii) 4.0×10^{-3} M α-Fe_2O_3 ; 5.58×10^{-3} M NTA

Solution pH was adjusted to 7.0 with 2 N NaOH; each mixture was autoclaved for 10 minutes at 121°C. Suspensions were incubated at 31°C while agitated on a reciprocating shaker table. Samples were taken periodically and filtered (0.2 μm filter, Millipore). One mL of filtrate was combined with 1 mL of hydroxylamine solution[24] and a drop of concentrated HCl. After 1-2 min. for chemical reduction of soluble Fe(III), ammonium acetate buffer[24] and 1,10-orthophenanthroline were added to the mixture, and [Fe(II)] was measured spectrophotometrically (Beckman DU7) at λ = 510 nm. To ensure that soluble Fe(III) was rapidly reduced via this procedure, a filter-sterilized solution of 1.86×10^{-2} M $FeCl_3$/NTA was diluted with distilled H_2O to final concentrations of 9.3×10^{-4} M and 4.65×10^{-5} M Fe(III). Each dilution was analyzed for total iron using the procedure outlined above.

Dissolution of Goethite in Solid Media

The spatial distribution of streaked Pseudomonas sp. 200 relative to areas of goethite dissolution in solid media was examined in the following way: Microscope slides were covered with a thin layer of nutrient agar supplemented with goethite (YL01888D, see Table 2) to a final concentration of 7.0×10^{-4} M as Fe. After solidification, the agar was streaked with Pseudomonas sp. 200 and incubated aerobically at 31°C for 36 hours. The slides were then sealed within a BBL Gas Pak jar from which $O_2(g)$ was eliminated via reaction with $H_2(g)$ (Gas Pak Disposable Anaerobic System, Becton Dickinson and Co.). Anaerobic conditions were maintained during an 8-day incubation at 31°C after which the slides were removed and examined with and without phase contrast under a Zeiss (Standard 16) light microscope. Micrographs were taken with a Zeiss Ikon camera.

RESULTS

SEM and X-ray Crystallography

Scanning electron micrographs of Pseudomonas sp. 200 grown in liquid media and in liquid media supplemented with hematite or geothite are provided as Figures 1 through 4. Microorganisms (no mineral) in Figure 1 were withdrawn from Westlake medium after nine hours of growth at 31°C. Although culture optical density at the time of withdrawal was not measured, the culture was in late log or early stationary growth phase. Adjacent microorganisms appeared to be tethered by extra-cellular exopolysaccharides.[15] The extra-cellular polymer develops during the latter stages of log growth; it may be responsible for the characteristic stickiness of Pseudomonas sp. 200 grown to high

cell densities. Cell-solid affinity may also benefit from exopolysaccharide development; cell attachment to both hematite (Figure 2) and goethite (Figure 3) is indicated. Both figures clearly reveal the aggregated nature of iron oxides in cultures of Pseudomonas sp. 200 within the neutral pH range. Shapes of hematite and goethite particles are significantly different (spheroidal vs. acicular). Because iron oxides were hetero-disperse (Table 2b), a few very large particles were apparent upon SEM inspection. One such hematite particle ($D_p \cong 20$ μm) is shown in Figure 4. Inspection of the particle surface reveals both attached microorganisms and small pits. Micrographs showing goethite and Pseudomonas sp. 200 were prepared after a 33-hour anaerobic incubation period at 31°C. Hematite particles had been exposed to cells under similar conditions for 45 hours. NTA was present in both suspensions at a concentration of 1.86×10^{-3} M.

As indicated in Table 3, x-ray crystallographic data confirmed the identity of each mineral. No crystalline impurities were detected, although the background signal precluded identification of mineral impurities present in quantities less than about 5 percent of overall mineral composition.

Particle/Microorganism Contact

Results of kinetic experiments run using (i) intact cultures and (ii) culture centrate are summarized in Figure 5. The relative lack of iron-reducing activities in centrates from growing cultures of Pseudomonas sp. 200 suggests that the presence of a soluble, reducing intermediate is not a major determinant of iron-reduction rates observed in these cultures. Residual activity in culture centrate (Figure 5a, pre-anaerobic curve) is probably due to incomplete removal

of microorganisms during centrifugation; microscopic examination of centrate supported this contention. The centrate obtained from cultures after a 30-min. anaerobic incubation (Figure 5b) exhibited no appreciable iron-reduction activity.

When cells and goethite were separated by a dialysis membrane (Figure 6), essentially no iron reduction was observed. Following a substantial lag period (about 48 hours) a sustained iron-reduction rate of approximately 1.47×10^{-5} M h^{-1} was observed in the control culture (no particle-cell separation). Reductive dissolution in the control was essentially stoichiometric over the 10-day fermentation period. Visual inspection indicated that high rates of iron reduction observed in the dialysis-tube culture near the end of the experiment (2.92×10^{-5} M h^{-1}, or about twice the rate of the control) were accompanied by physical breakdown of the bag. Plate counts reflect rapid inactivation (within the first two days of anaerobiosis) of 95-98% of the aerobically grown cells. The period of rapid cell inactivation was followed by stable cell numbers, or perhaps slow growth, throughout the iron-reduction period. Soluble control data (microorganisms inside tube, Fe(III)-NTA added outside) clearly showed that complexed Fe(III) diffuses rapidly through membrane pores.

No general trend was apparent in data (not shown) representing the time-dependent, chemical dissolution of hematite by NTA. Essentially no increment in total soluble iron was observed in any of the aerobic suspensions over a 48-hour period. At no time did total soluble iron exceed about 0.5% of the total iron in any suspension. Additional control experiments in which $FeCl_3$ and NTA were added to solution indicated that total soluble iron in these suspensions is measured with

reasonable accuracy using the filtration/reduction technique described above.

Micrographs indicating the positions of colonies of Pseudomonas sp. 200 relative to areas of noticeable goethite depletion (solubilization) in solid media are provided as Figures 7 and 8. Mineral-phase iron was solubilized only beneath the bacterial streak, as indicated by the discontinuity in goethite concentration which is visible at the boundary of microbial colonies.

Kinetics of Reductive Dissolution

Preliminary experiments designed to illustrate the effect of mineral type and ligand addition on reductive dissolution kinetics are summarized in Figure 9. The addition of chelators dramatically enhanced rates of reductive dissolution, although the relative accelerations produced by NTA and EDTA were mixed and may depend on mineral identity. The rate of reductive dissolution was found to be a function of mineral identity and degree of crystallinity (hematite < goethite $\cong$ lepidocrocite < $Fe(OH)_3$(s,amorph)).

Dissolution experiments were extended to develop functional relationships between reduction rate and concentrations of microorganisms (Pseudomonas sp. 200), hematite (R1599), ligand (NTA), and substrate (lactate). Results summarized in Figure 10 indicate that saturation of culture iron-reduction capacity was not observed at a hematite concentration of 7.5×10^{-2} M (as Fe), although Figure 10b suggests that saturation kinetics will be encountered at higher mineral levels. In these experiments, NTA concentrations were maintained at or above levels designed to produce maximum rates of reductive dissolution. Culture optical density was 1.0 cm^{-1} (λ = 600 nm) just

prior to mineral addition and establishment of anaerobic conditions. The corresponding cell density was about 2.0×10^9 cells/ml. Plate counts were periodically carried out during each iron-reduction experiment, and typical results are included in Figure 10c. Viable cell counts declined during the first few hours of anaerobic conditions before stabilizing at a level on the order of one percent of the original cell concentration. In a few of the culture-tube experiments, slow growth in cell number seemed evident after the rapid initial decline. Iron-reduction kinetics were apparently unaffected by the decline in cell number.

Dependence of hematite dissolution kinetics on NTA concentration is indicated by Figure 11a. Saturation effects were apparent at high NTA concentrations ($> 1.86 \times 10^{-3}$ M, Figure 11b). The observed iron-reduction rate in 5.5-ml culture tubes (hematite concentration 3.72×10^{-3} M as Fe, Pfizer no. R1599) was accelerated about 13 times by the addition of 1.86×10^{-3} M NTA. Somewhat faster rates should result from higher-level additions. As in previous experiments, iron-reduction rate was independent of cell number down to cell concentrations on the order of 10^7/ml. Solution pH was stable in the range 6.6 to 6.8 during the course of the experiment.

Particle surface area effects were also investigated by generating iron-reduction data using an alternate hematite stock with lower specific surface area (Pfizer no. R8098, see Table 2). In two experiments which were otherwise identical to those described previously, hematite R8098 was added to aerobically grown cultures of *Pseudomonas* sp. 200 to final concentrations of 2.57×10^{-3}M and 3.72×10^{-3}M (as Fe). NTA additions were identical to total iron levels. In

Table 4 measured reduction rates are compared to values calculated on the basis of equal volume concentrations of NTA and hematite from the R1599 Pfizer stock. Discrepancies between observed and predicted rates were apparently related to differences in specific surface areas of the two stocks. Such differences were lower than would be predicted from surface area consideration alone.

Preliminary experiments (results not shown) indicated that variation in lactate concentration up to 2.68×10^{-2} M did not alter the observed rate of mineral dissolution in any systematic way. There were, however, indications that pH is an important kinetic factor in the range 5.0 to 6.0, with relatively high pH favoring reductive dissolution.

When iron-reduction experiments were initiated in low optical density cultures (A_{600} = 0.11 to 0.14, cm^{-1}), rates of hematite dissolution were similar to those observed in denser cultures (A_{600} = 1.0 cm^{-1}). Results summarized in Table 5 reflect the rather weak dependence of iron-reduction rate on cell number in this range. At high mineral concentration (1.26×10^{-2} M, as Fe), low initial cell number appears to be responsible for loss of about 25 percent of the expected iron-reduction capacity. Experiments designed to investigate the dependence of cell survival on hematite surface area are summarized in Figure 12. Steady cell numbers were achieved several hours after hematite addition and establishment of anaerobic conditions. Furthermore, the level at which cell number stabilized was only weakly dependent on hematite concentration: An order-of-magnitude increase in hematite concentration (from 3.72×10^{-4} M to 3.72×10^{-3} M) was

accompanied by a ten-fold increase in the Fe(III) reduction rate but an increase in steady cell number by a factor of only about 2.

Reductive dissolution of $Fe(OH)_3$(s,amorph) by Pseudomonas sp. 200 has been described previously.[20] In the neutral pH range, Fe(III) added to Westlake medium as $FeCl_3$ was present almost entirely as amorphous ferric hydroxide, a metastable intermediate with respect to less reactive iron oxides. Saturation kinetics (zero-order in Fe(III)) were encountered at high concentrations of $Fe(OH)_3$(s,amorph). However, the sharp transition from zero-order to first-order kinetics observed in these experiments is not typical of Michaelis-type processes. No systematic pH dependence was evident in either V_{max} ($\cong 10^{-3}$ M/hr), the maximum rate of Fe(III) reduction in these cultures, or in the pseudo first-order rate constant representing reduction/dissolution kinetics at relatively low Fe(III) concentrations.

ANALYSIS AND DISCUSSION

Contact Requirements

Several lines of experimental evidence indicate that microorganism/particle contact is necessary for the reductive dissolution of iron oxides:

(i) Absence of iron-reducing activity in centrates prepared from cultures of Pseudomonas sp. 200 before and after a brief period of anaerobic fermentation precludes the substantial development of a soluble reducing intermediate.

(ii) Mechanisms of reductive dissolution which depend on such a biologically produced intermediate are unlikely in light of the dialysis-membrane experiments. The membrane barrier between Pseudomonas

sp. 200 and iron oxide (permeable to soluble constituents smaller than m. w. 12,000 to 14,000 daltons) protected goethite particles from reductive dissolution for up to a week (prior to loss of membrane integrity, Figure 6). When microorganisms and soluble Fe(III) ($FeCl_3$ plus NTA) were separated by a dialysis membrane, ferrous iron accumulated in solution at an appreciable rate, providing assurance that transport of soluble iron through membrane pores was possible on a time-scale much shorter than the period of the experiment. Because the Fe(II) concentration after almost 24 hours was only 70% of the initial Fe(III) concentration in the dialysis tube surroundings (there was none inside the tube), it is apparent that iron reduction was not attributable to bacterial contamination in the membrane surroundings. No microorganisms were observed during periodic visual inspections of media outside the membrane.

(iii) The negligible abiotic dissolution of α-Fe_2O_3 by NTA rules out slow chemical dissolution as the rate-limiting step (followed by a fast, biologically catalyzed transformation of soluble Fe(III) to Fe(II)) in reductive dissolution.

(iv) Micrographs of Pseudomonas sp. 200 colonies in relation to areas of goethite depletion in nutrient agar reinforce the idea that reductive dissolution of iron oxides does not depend upon the existence of a diffusible, reducing intermediate. Together these experiments support a mechanism for iron-oxide dissolution which depends upon direct cell/mineral contact (or perhaps contact with the chemically modified surface when NTA is present) for the transfer of biologically produced reducing equivalents to the oxide surface. The affinity of Pseudomonas sp. 200 for mineral surfaces, suggested by scanning

electron micrographs (Figures 2-4), increases the plausibility of such a mechanism. Such findings are consistent with those of Munch and Ottow,[12] who indicated that reductive dissolution of hematite by B. polymyxa and C. butyricum was dependent upon direct cell/particle contact. Other investigators have found that only a portion of the observed iron-reduction activity depends on such contact.[14]

Details concerning the transfer of electrons across the periplasmic space (perhaps 10 nm in thickness[25]) and through the outer membrane to the particle surface are not known. The size of outer membrane pores has been estimated at 1-2 nm in diameter,[26] or large enough to permit pore diffusion of polysaccharides of m. w. < 700 daltons.[27] Possibilities include (i) the presence of soluble cytochromes or other molecules of biological origin which are capable of shuttling electrons across the periplasmic space and (ii) existence of a relatively small number of membrane-bound respiratory proteins which are in direct physical contact with the particle surface via an as-yet-unknown structure or partial intrusion of the oxide surface into the membrane structure.

Direct contact could enhance the rate and extent of reaction by concentrating reduced metabolites at the oxide surface. It does not seem likely, however, that prevention of cell-oxide contact would eliminate iron-reduction activity altogether (Figure 6) if a diffusible intermediate were involved in this manner.

When $Fe(OH)_3$(s,amorph) serves as terminal electron acceptor, it is again possible to envision a mechanism in which chemical dissolution limits the overall rate of dissimilative iron reduction (i.e., the biological reduction of free ferric ion or its hydroxo complexes is

relatively fast). However, saturation kinetics, observed at high total Fe(III) concentration, and lack of a systematic pH dependence[20] are inconsistent with this interpretation. Furthermore, Theis and Singer[28] found that the evolution of Fe(II) in sterile, aqueous suspensions of $Fe(OH)_3$(s,amorph) and tannic acid (neutral pH range) was limited to very low rates by solid-phase dissolution. Less than 10% of the 8.0×10^{-5} M ferric iron initially present was reduced in a 24-hour period. These results suggest that direct contact between Pseudomonas sp. 200 and $Fe(OH)_3$(s,amorph) is required to achieve reduction rates observed in experiments reported here (essentially stoichiometric reduction of 1.86×10^{-3} M Fe(III) in two hours).

Kinetics

Particle Surface Area

Although reactive surface area is more appropriate as a measure of Fe(III) solid-phase concentration, mass units are employed in kinetic analyses described here. The highly aggegated nature of hematite and goethite (Figures 2 and 3) in the neutral pH range makes standard measures of particulate surface area (such as nitrogen adsorption) inappropriate; such measurements would overestimate the surface which is available for microorganism contact. Use of particle mass as an indication of surface area is appropriate when the particle surface-to-volume ratio is reasonably constant, either during the course of a single experiment or (when interexperimental comparison of results necessitates) from experiment to experiment. Despite the heterogeneous nature of iron oxides utilized in these experiments (Table 2b), reasonable precautions should ensure a statistically similar particle-size distribution at the start of each reduction

experiment. Geometric dissimilarities among iron oxides (e.g., goethite and hematite, Figs. 2 and 3) necessitate caution in comparing dissolution data for different minerals.

When data reflect reduction of only a small percentage of the mineral iron initially present in suspension, intraexperimental variation in solid-phase geometry and total surface area is expected to be minor. Since kinetic data reported in Figure 10 reflect the reductive dissolution of < 20% of the iron oxide initially present, data interpretation should be free of problems arising from such variation. However, essentially stoichiometric reduction of Fe(III) was observed in (i) dialysis-bag experiments (reductive dissolution of goethite, Figure 6) and (ii) kinetic experiments involving amorphous ferric hydroxide. Here the particle surface-to-volume ratio should increase as average particle size decreases and pitting occurs. Consequently, an increase in specific reduction rate, defined as the ratio of reduction rate to Fe(III) concentration, might be anticipated over the course of an experiment. No such effect was apparent when Fe(III) was provided as $Fe(OH)_3$(s,amorph),[20] perhaps due to the small initial size of ferric hydroxide particles relative to bacterial dimensions (approximately 80% of solids initially present are filterable using a 0.2 m filter. A cube-root plot[29] of dissolution data $([Fe(III)]^{1/3}$ vs. time, Figure 6b) indicated that surface-area modeling may be appropriate for goethite dissolutions over an extended period.

An Eadie-Hofstee plot (not shown) of hematite-reduction data summarized in Figure 10 indicated that the dependence of initial reduction rate on Fe(III) concentration follows a Michaelis-type

relationship with V_{max} = 4.1 x 10^{-4} M h^{-1} (as Fe) and K_m = 1.05 x 10^{-1} M (as Fe). Substituting these values into the Michaelis expression permits estimation of the Fe(III)

concentration which would result in $\frac{dFe(II)}{dt}$ = 0.9 V_{max} at 9.45 x 10^{-1} M (as Fe). Such results should not be extended to other minerals or to reductive dissolution of hematite particles with a significantly different particle-size distribution, as indicated by results of dissolution using hematite R8098 (Table 4). The observed rate of reductive dissolution is clearly dependent on hematite morphology. However, these differences cannot be rationalized in terms of specific surface area consideration alone, perhaps due to the aggregated nature of hematite particles in the neutral pH range.

NTA Effects

The effect of NTA addition (Figure 11) can also be explained in terms of a saturation model, modified to reflect the non-zero hematite dissolution rate observed at the zero-NTA concentration. Analytical assumptions are as follows:

(i) Reductive dissolution occurs at equivalent high-energy sites on the mineral surface.

(ii) The fraction of high-energy surface sites bound to NTA follows an equilibrium relationship given by:

$$[>S\text{-}NTA] = [>S][NTA]K_{eq} \qquad (1)$$

where [>S] is the volume concentration of uncomplexed iron-reduction sites and [>S-NTA] is the concentration of such sites which are complexed by NTA.

(iii) The overall (observed) iron-reduction rate reflects a combination of rates at free and complexed sites:

$$\frac{d[Fe(II)]}{dt} = k_1[>S] + k_2[>S\text{-}NTA] \qquad (2)$$

where k_1 and k_2 are respective first-order rate constants for the dissolution process. Note that since the chemical rate of iron-reduction is negligible, free and complexed site concentrations actually represent their respective concentrations which are in contact with Pseudomonas sp. 200 or which can accept respiratory electrons from attached microorganisms. At concentrations of solids and microorganisms utilized in these experiments, reduction sites on particle surfaces are apparently saturated in some sense (kinetics are zero-order in microorganisms -- vide infra).

Combination of equations (1) and (2) yields

$$\frac{d[Fe(II)]}{dt} = [>S]\left\{k_1 + k_2K_{eq}[NTA]\right\}. \qquad (3)$$

Since [>S] = S_T - [>S-NTA], where S_T is the total volume concentration of reduction sites, equation (1) may be rewritten:

$$[>S] = \frac{S_T}{1 + K_{eq}[NTA]}. \quad (4)$$

Substituting for [>S] in equation (3) yields:

$$\frac{d[Fe(II)]}{dt} = \frac{k_1 S_T + k_2 S_T K_{eq}[NTA]}{1 + K_{eq}[NTA]} \quad (5)$$

Eqn. (5) consists entirely of terms which can be measured or estimated from kinetic data. At zero-NTA concentration, the iron-reduction rate is $k_1 S_T$ or $V_{max(1)}$ ($V_{max(1)} = 1.0 \times 10^{-6}$ M hr^{-1}). At relatively high iron-reduction rates, $k_1 S_T << k_2 S_T K_{eq}[NTA]$, permitting estimation of additional parameters using an Eadie-Hofstee plot (Fig. 11c). Results indicate that K_m (or Michaelis constant) $\equiv \frac{1}{K_{eq}} = 1.2 \times 10^{-3}$ M and $V_{max(2)} = 2.3 \times 10^{-5}$ M hr^{-1}.

It is emphasized that $V_{max(1)}$ and $V_{max(2)}$ are not intrinsic constants but depend upon S_T, defined as the total volume concentration of active reduction sites. Such sites may be thought of as surface Fe(III) centers, high-energy surface structures (kinks, ledges, etc.), or sites for microbial attachment depending upon one's particular model for reductive dissolution. In any case, S_T is a function of mineral surface area and thus, in these experiments, volume concentration of hematite. Since V_{max} values are specific to the oxide concentration of the experiments, $V_{max(1)}$ and $V_{max(2)}$ do not equal values derived within

a more general rate expression, in which a term is included to account for oxide concentration effects $([Fe(III)]/\{K_{m(Fe)} + [Fe(III)]\}$, where [Fe(III)] is the volume concentration of hematite, as Fe, see summary section). Thus,

$V_{max(1)} = V_{max(I)} \frac{[Fe(III)]}{K_{m(Fe)} + [Fe(III)]}$. The same relationship holds between $V_{max(2)}$ and $V_{max(II)}$. Straightforward calculation indicates that $V_{max(I)} = 2.8 \times 10^{-5}$ M hr^{-1} and $V_{max(II)} = 6.3 \times 10^{-4}$ M hr^{-1}. The latter value is higher than the maximum rate of reductive dissolution derived on the basis of variation in hematite concentration. The seeming discrepancy indicates that NTA concentrations were probably below saturating levels in those experiments. Values derived here for $V_{max(I)}$ and $V_{max(II)}$ are considered more reliable. Thus, the rate law for hematite (R1599) reductive dissolution is as follows:

$$\frac{d[Fe(II)]}{dt} = \frac{V_{max(I)}K_{m(NTA)} + V_{max(II)}[NTA]}{K_{m(NTA)} + [NTA]} \cdot \frac{[Fe(III)]}{K_{m(Fe)} + [Fe(III)]}$$

where $V_{max(I)} = 2.8 \times 10^{-5}$ M hr^{-1}

$V_{max(II)} = 6.3 \times 10^{-4}$ M hr^{-1}

$K_{m(NTA)} = 1.2 \times 10^{-3}$ M

$K_{m(Fe)} = 1.0 \times 10^{-1}$ M (as Fe).

The dependence of V_{max} values on initial concentration of cells is less obvious. Clearly there is a biological limit to the rate at which Fe(III) oxides can be dissolved; however, such a limit is not reflected in equation (5) or more general expressions derived subsequently. Within the range of experimental variables observed here (i.e., oxide

and NTA concentrations) microorganisms are present in saturating quantities. Consequently the relatively minor rate dependence upon cell number is easily hidden in the S_T parameter. Inclusion of a rational term in the rate expression to account for dependence on cell density would require additional experimentation.

To appreciate the role of NTA as a catalyst for reductive dissolution of hematite, it may be helpful to look for analogies in the literature of chemical dissolution of minerals. Rodliffe[30] defined a "simple" dissolution reaction as (i) depending only on the concentration of reagent adjacent to the surface (first-order kinetics), (ii) resulting from dissolution of one solid-phase molecule by one molecule of reagent, and (iii) lacking kinetic limits imposed by either back reaction (dissolution is irreversible) or surface precipitation of reaction products. Momentarily ignoring the biological dependence of our experimental findings, it is evident that NTA effects depart from Rodliffe's model mechanism in several respects: saturation kinetics (Figure 11) force us to recognize that the rate of hematite dissolution depends upon the concentration of ligand bound to the mineral surface, i.e., that NTA adsorption (rapid) is followed by relatively slow loss of metal-ligand complexes from the surface.

Such a mechanism is proposed by Stumm et al.[31] to explain the effects of ligand concentration on the chemical dissolution of hematite and goethite. In Stumm's kinetic model, dissolution proceeds, though at vastly different rates, from both complexed and uncomplexed surface sites, thus providing precedent for our own kinetic treatment. Complexation of specific ligands at mineral oxide surfaces occurs via a ligand-exchange mechanism which may be represented by:

$$>MeOH + L^{n-} \leftrightarrows >MeL^{(n-1)-} + OH^{-}.$$

The catalysis of Fe-oxide dissolution is then attributed to either alteration of surface charge (e.g., Fe-Cl complex formation and iron-oxide dissolution[32]) or elongation and weakening of Fe-O bonds in the mineral lattice.[33]

There is also experimental evidence that formation of surface complexes can accelerate reduction of metal centers at the mineral surface and thus hasten dissolution.[34-35] Chemical (reductive) dissolution of Cr(III) oxides by NTA is thought to occur as follows:[29]

$$Cr(II)L_n + >Cr^{3+} \longrightarrow Cr(III)L_n + Cr^{2+} + >$$

$$Cr^{2+} + nL \longrightarrow Cr(II)L_n$$

Although such a mechanism would provide a non-biological explanation for lag effects observed in several experiments described here (Figs. 10 and 11), it would not account for particle/microorganism contact requirements, established via several lines of experimentation.

A more consistent analogy can be derived from the reductive dissolution of Fe(III)-oxide in the presence of oxalate and ascorbic acids:[31]

$$>Fe(III) = C_2O_4 + H^{+} \xrightarrow{\text{ascorbic acid}} Fe^{2+}(aq) + C_2O_4H^{-} + >$$

Here, ascorbic acid provides reducing power, the function of microorganisms in our experiments. The surface-coordinated ligand ($C_2O_4^{2-}$ or NTA) apparently makes the Fe(III) center more susceptible to reductive dissolution by weakening Fe(III)-O bonds in the mineral. Following reduction the Fe(II) complex provides a kinetically superior leaving group, accelerating the overall process of reductive dissolution. It is also possible that the ligand serves as a bridge for inner-sphere complexation and subsequent electron transfer between the reductant and metal center. Such a mechanism has been suggested for reductive dissolution of Co_2O_3 by Cr^{2+} in the presence of Cl^-.[36]

The rate of reductive dissolution of hematite is accelerated due to addition of saturating amounts of NTA by a factor of $k_2/k_1 = 23$. This enhancement is virtually identical to that which was observed in iron-speciation experiments reported previously[20] in which solubilization of Fe(III) via complexation with NTA increased the observed iron-reduction rate relative to the reduction of colloidal ferric hydroxide. These results suggest that the relative effect of complex formation on iron reduction rate may be independent of the thermodynamic stability of the solid phase.

Respiratory electrons may be transferred to soluble complexes and complexed Fe(III) at surface sites with equal facility; that is, the enormous loss of <u>overall</u> reductive capacity in cultures provided with Fe(III) as iron oxide may result from the relative number of reacting sites and not from the reactivity of those sites. The density of iron centers at the surface of hematite has been estimated at 9 sites per $100(\mathring{A})^2$.[37,38] Since the specific surface area of R1599 hematite is

11.2 m^2/g, the fraction of solid-phase Fe(III) exposed at the surface of these particles is given by:

$$f = \frac{9}{100} \quad \frac{11.2 \times 10^{20}}{N} \quad \frac{159.70}{2} = 0.0133$$

(The molecular weight of α-Fe_2O_3 is 159.70, and N is Avagadro's number). Slightly more than 1 percent of the total iron in these suspensions is present at the particle surface. The maximum rate of reductive dissolution (excess NTA, excess microorganisms) in a hematite/NTA suspension (total Fe = 1.86×10^{-3} M) has been estimated at 7.5×10^{-6} M-hr^{-1} (Figure 10b). This is about 0.03 percent of the maximum rate observed when iron is provided as soluble Fe(III)-NTA complexes.[20] Thus soluble complexes are apparently about 30 times as reactive as Fe(III)-NTA complexes at the particle surface. However, considering the aggregated nature of hematite in these suspensions (Figure 2) it is reasonable to assume that a relatively small fraction the total hematite surface is available for bacterial colonization (or otherwise available to serve as oxidant for bacterial respiration); reactivities of free and surface-bound Fe(III)-NTA complexes may actually be comparable.

Effect of Cell Number

In these experiments the presence of excess microorganisms was indicated by both maintenance of reduction rate throughout periods of significant cell mortality (Figure 10c) and similarity of iron-reduction rates in experiments initiated at significantly different cell numbers (comparative rates from Figure 10a and Table 5).

Furthermore, the steady cellular concentration of microorganisms following the rapid initial decline in cell number was only weakly dependent on initial hematite concentration (Figure 12) and correlated poorly with rate of reductive dissolution. However, data presented in Table 5 (high initial hematite concentration) indicate that iron-reduction rate depends on cell concentration when the ratio of cell number to oxide surface concentration is sufficiently small.

At high levels of colloidal $Fe(OH)_3$(s, amorph), microorganisms were not present in excess. Observed iron reduction rates were limited by microbial electron transport or by the transport of reducing equivalents across the periplasmic space.[20] In either case, constraints arose from microbial physiology as opposed to mineral surface area. The sudden transition from zero- to first-order kinetics at a lower Fe(III) concentration may reflect a shift in the rate-limiting step for reductive dissolution of ferric hydroxide (to control by mineral surface area at low total Fe concentration). The abrupt nature of the transition argues against saturation of the biological surface with bound $Fe(OH)_3$(s,amorph) at high iron concentration.

SUMMARY AND CONCLUSIONS

(1) Evidence presented supports a mechanism in which direct cell/mineral contact is requisite to achievement of observed rates of reductive dissolution of iron oxides. SEM micrographs showing the affinity of microbes for particle surface support this contention.

(2) The rate of reductive dissolution of hematite depends on reactive surface area of the mineral. Although microorganisms were

initially present in excess, viable cell counts decreased rapidly to sustainable levels which appeared to be independent of NTA concentration and reasonably insensitive to particle surface area. At very high mineral loadings, microorganism surfaces can be saturated with particulate iron. A Michaelis-type relationship exists between iron-reduction rate and mineral surface.

(3) At high Fe(III) concentrations, the kinetics of $Fe(OH)_3$(s,amorph) reductive dissolution are subject to constraints imposed by microbial physiology. By way of contrast, reduction kinetics were controlled by mineral surface area in each of the experiments in which Fe(III) was provided as hematite.

(4) A conceptual model for enhancement of reductive dissolution via NTA addition was developed. The rate of reduction of hematite in the presence of NTA is described by the following rate law:

$$\frac{d[Fe(II)]}{dt} = \frac{V_{max(I)}K_{m(NTA)} + V_{max(II)}[NTA]}{K_{m(NTA)} + [NTA]} \cdot \frac{[Fe(III)]}{K_{m(Fe)} + [Fe(III)]}$$

where $V_{max(I)} = 2.8 \times 10^{-5}$ $\underline{M}$ hr^{-1}

$V_{max(II)} = 6.3 \times 10^{-4}$ $\underline{M}$ hr^{-1}

$K_{m(NTA)} = 1.2 \times 10^{-3}$ $\underline{M}$

$K_{m(Fe)} = 1.0 \times 10^{-1}$ $\underline{M}$ (as Fe).

All concentrations are volume concentrations in molar units. Cells are assumed to be present in excess.

(5) NTA surface complexation may accelerate dissimilative iron reduction of iron oxides by: (i) weakening Fe-O bonds in the mineral lattice, accelerating departure of iron-NTA complexes following reduction or (ii) providing a bridge for the transport of bacterial (respiratory) electrons to bound Fe(III). In either case, Fe(II) or the Fe(II)-NTA complex would break free from the lattice, completing a set of events which is consistent with the necessity for particle/microorganism contact.

(6) Results suggest that microbial catalysis of iron leaching has commercial promise. Although observed rates of iron-oxide dissolution are modest in relation to reduction of soluble, complexed Fe(III), it is clear that manipulation of particle surface area and microorganism concentration, based on relationships of the type formulated above, can increase the overall rate of reductive dissolution. Although complexation with NTA results in substantial rate enhancement, other complexing agents may be more effective in this regard.

Efforts designed to promote reductive dissolution of iron oxides should include investigation into the nature of dissolution sites and/or development of physical methods for increasing the concentration of suspended mineral surface. In this regard, comminution of oxide particles might be pursued, but particle-size effects (Table 4) are of secondary importance perhaps due to the highly aggregated nature of hematite and goethite suspensions in the neutral pH range. Since a few acidophiles are capable of promoting iron reduction (Thiobacillus thiooxidans, Sulfolobus acidocaldarius), use of such microorganisms for iron leaching would capitalize on the stability of colloidal iron oxide in the acid pH range.

(7) In light of the very significant enhancement of iron-oxide dissolution rate attributable to microbial catalysis, both in the presence and absence of NTA, dissimilative iron reduction may play an important role in mineral weathering and biogeochemical iron transformations.

Acknowledgements

This work was supported under United States Department of Energy Contract No. DE-AS03-83ER13125 administered within the Division of Advanced Energy Projects, Office of the Basic Energy Sciences. We appreciate the support and encouragement of Drs. Ryszard Gajewski and Duane L. Barney.

The authors further acknowledge Dr. D. W. S. Westlake of the Department of Microbiology, University of Alberta, Canada, for generously providing the microorganism used in this study, Pseudomonas sp. 200.

Electron micrographs were prepared with the direct assistance and advice of Mr. Pat Koen of the Caltech Biology Division Staff.

Our thanks to Ms. Sandy Brooks, Ms. Elaine Granger, and Ms. Nancy Tomer of the Caltech Environmental Engineering Science staff for secretarial and drafting assistance during manuscript preparation.

REFERENCES

1. C. L. Brierley, Scientific American, August 1982, p. 44 (1982).

2. H. L. Ehrlich, Geomicrobiology, (Marcel Dekker, New York, 1981) pp. 187-194.

3. M. A. Anderson and M. M. Morel, Limnology and Oceanography, 27, 789 (1982).

4. J. H. Ryther and R. R. L. Guillard, Deep-Sea Res., 6, 65 (1959).

5. D. W. Menzel and J. H. Ryther, Deep-Sea Res., 7 276 (1961).

6. D. R. Lovley and E. J. P. Phillips, Appl. Environ. Microbiol., 51, 683 (1986).

7. W. Stumm and J. J. Morgan, Aquatic Chemistry, 2nd ed. (Wiley-Interscience, New York, 1983), pp. 418-463.

8. T. D. Brock and J. Gustafson, Appl. Environ. Microbiol., 32, 567 (1976).

9. K. Kino and S. Usami, Ag. Biol. Chem., 46, 803 (1982).

10. E. P. Troshanov, Mikrobiol., 37, 934 (1968).

11. E. P. Troshanov, Mikrobiol., 38, 634 (1969).

12. J. C. Munch and J. C. G. Ottow, In: Environmental Biogeochemistry, R. Hallberg (ed.), Ecol. Bull. (Stockholm) 35, 383 (1983).

13. J. C. Munch and J. C. G. Ottow, Z. Pflanzenernähr. Dung. Bodenkd., 145, 66 (1982).

14. J. G. Jones, S. Gardener, and B. M. Simon, J. Gen. Microbiol., 129, 131 (1983).

15. C. O. Obuekwe, Ph.D. dissertation, University of Alberta, Edmonton, Alberta, 1980.

16. C. O. Obuekwe, D. W. S. Westlake, and F. D. Cook, Can. J. Microbiol., 27, 692 (1981).

17. C. O. Obuekwe and D. W. S. Westlake, Can. J. Microbiol., 28, 989 (1982).

18. C. O. Obuekwe and D. W. S. Westlake, Microbios Lett., 19, 57 (1982).

19. J. Lascelles and K. A. Burke, J. Bact., 134, 585 (1978).

20. R. G. Arnold, T. M. Olson, and M. R. Hoffmann, Biotechnology and Bioengineering, in press.

21. A. F. DeCastro and H. L. Ehrlich, Antonie van Leeuwenhoek, 36, 317 (1970).

22. C. O. Obuekwe, D. W. S. Westlake, F. D. Cook, and J. W. Costerton, Applied and Environ. Microbiol., 41, 766 (1981).

23. R. G. Arnold, T. J. DiChristina, and M. R. Hoffmann, Appl. & Envr. Microbiol., in press.

24. American Public Health Association, American Water Works Association, Water Pollution Control Federation, Standard Methods for the Examination of Water and Wastewater, 15th ed. (APHA, Washington, D.C., 1981), pp. 201-205.

25. W. Van Iterson (ed.) Outer Structures of Bacteria (Van Nostrand Reinhold Co., N.Y., 1984) pp. 48-99.

26. A. C. Steven, B. Ten Heggeler, R. Müller, J. Kistler, and J. P. Rosenbusch, J. Cell Biol., 72, 292 (1977).

27. T. Nakae, J. Biol. Chem., 251, 2176 (1976).

28. T. L. Theis and P. L. Singer, In: Trace Metals and Metal-Organic Interactions in Natural Waters, ed. P. L. Singer (Ann Arbor, Michigan, 1973), pp. 303-320.

29. M. G. Segal and R. M. Sellers, Advances in Inorganic and Bioinorganic Mechanisms, 3, 97 (1984).

30. R. S. Rodliffe, Water Chemistry of Nuclear Reactor Systems 2, (British Nuclear Energy Society: London, 1981), p. 383.

31. W. Stumm, G. Furrer, E. Wieland, and B. Zinder, In: The Chemistry of Weathering, J. Drever, ed. NATO ASI Series C Vol. 149 (D. Reidel Publ., Dordrecht, Holland, 1985).

32. R. M. Cornell, A. M. Posner, and J. P. Quirk, J. Inorg. Nucl. Chem., 38, 563 (1976).

33. P. S. Sidhu, R. J. Gilkes, R. M. Cornell, A. M. Posner, and J. P. Quirk, Clays and Clay Minerals, 29 269 (1981).

34. A. T. Stone and J. J. Morgan, Environ. Sci. Technol., 18, 450 (1984).

35. A. T. Stone and J. J. Morgan, Environ. Sci. Technol., 18, 617 (1984).

36. B. A. Zabin and H. Taube, Inorg. Chem., 3, 963 (1964).

37. T. Morimoto, T. Nagao, and F. Tokuda, J. Phys. Chem., 73. 243 (1969).

38. E. S. Dana and W. E. Ford, A Textbook on Mineralogy (John Wiley and Sons, Inc., N.Y., 1960).

FIGURE CAPTIONS

Figure 1. SEM micrograph of Pseudomonas sp. 200 during late logarithmic growth phase.

Figure 2. SEM micrograph of Pseudomonas sp. 200 cells and hematite (R1599, Table 2) particles after 45-hour incubation under anaerobic conditions. Cell-particle adhesion and particle aggregation are apparent.

Figure 3. SEM micrograph of Pseudomonas sp. 200 cells and goethite (YL01888D, Table 2) particles after 33-hour incubation under anaerobic conditions. Cell-particle adhesion and particle aggregation are apparent.

Figure 4. Anomalously large hematite (R1599, Table 2) particle under SEM. Individual Pseudomonas sp. 200 cells are visible on particle surface as are pits and smaller hematite particles.

Figure 5. Concentration of Fe(II) vs. time in whole cultures of Pseudomonas sp. 200 and culture centrate following -- (a) centrifugation at the onset of anaerobic conditions; (b) centrifugation after a 30-minute, anaerobic period. A_{600} = 0.50 (cm^{-1}) at establishment of anaerobic conditions. [Fe(III)], [NTA] added to 1.86×10^{-3} M.

Figure 6a. Fe(II) concentration and cell number vs. time (after establishment of anaerobic conditions) in cultures of Pseudomonas sp. 200 with goethite added to 1.86×10^{-3} M (as Fe); [NTA] = 1.86×10^{-3} M. In dialysis-tube experiment, cells and goethite particles were separated by a membrane. In the second control, cells and soluble Fe(III)-NTA complexes were initially separated by the dialysis membrane.

Figure 6b. Cube-root plot of goethite concentration to the one-third power versus time. Geothite concentration data are from Figure 6a (control no. 1) assuming the initial goethite concentration was 1.86×10^{-3} M (as Fe).

Figure 7. Light micrograph showing discontinuous depletion of goethite particles from thin agar beneath streaked cells of Pseudomonas sp. 200. Dashed line lies slightly above the boundary of the streak. (Microscope enlargement, 20x.)

Figure 8. Light micrographs showing spatial relation between streak of Pseudomonas sp. 200 colonies (Figure (a), above solid line) and area of goethite particle depletion (Figure (b)). The interface from (a) is overlaid on (b). Both photographs were taken via a Zeiss light microscope at 128x; Figure (a) with phase contrast to highlight cells; Figure (b) without phase contrast so that only goethite particles are evident.

Figure 9. Preliminary experimental results -- dependence of iron-reduction rate on Fe(III)-oxide identity and NTA concentration.

Figure 10a. Reductive dissolution of hematite (R1599) by Pseudomonas sp. 200 as a function of time and mineral concentration (sufficient NTA and microorganisms present to maximize Fe(III) reduction rate; initial cell density corresponding to A_{600} = 1.0, cm^{-1}). All concentrations are as Fe.

Figure 10b. Fe(III) reduction rate as a function of hematite (R1599) concentration -- from Figure 10a data.

Figure 10c. Hematite dissolution and cell number in anaerobic cultures of Pseudomonas sp. 200. (Initial hematite concentration, 1.86×10^{-3} M as Fe; NTA concentration, 9.3×10^{-3} M.)

Figure 11a. Hematite reduction by Pseudomonas sp. 200 as a function of time and NTA concentration. $[\alpha\text{-}Fe_2O_3] = 3.72 \times 10^{-3}$ M (as Fe) in all cultures. Initial cell density corresponding to A_{600} = 1.0 (cm^{-1}). Results of cell counts are provided at the end of each experiment.

Culture No.	[NTA]
0	none
1	9.3×10^{-5} M
2	1.86×10^{-4} M
3	2.79×10^{-4} M
4	3.72×10^{-4} M
5	4.65×10^{-4} M
6	6.51×10^{-4} M
7	9.30×10^{-4} M
8	1.86×10^{-3} M

Figure 11b. Rate of reductive dissolution as a function of NTA concentration. Based on data provided as Figure 11a.

Figure 11c. Eadie-Hofstee plot based on iron-reduction rate/NTA concentration data of Figs. 11a and 11b.

Figure 12. Cell number as a function of initial hematite (R1599) concentration (M, as Fe) and time in anaerobic cultures of Pseudomonas sp. 200. NTA was present in excess concentration in each case. Numbers in parentheses represent measured rates of iron reduction in these cultures ($M \cdot hr^{-1}$)

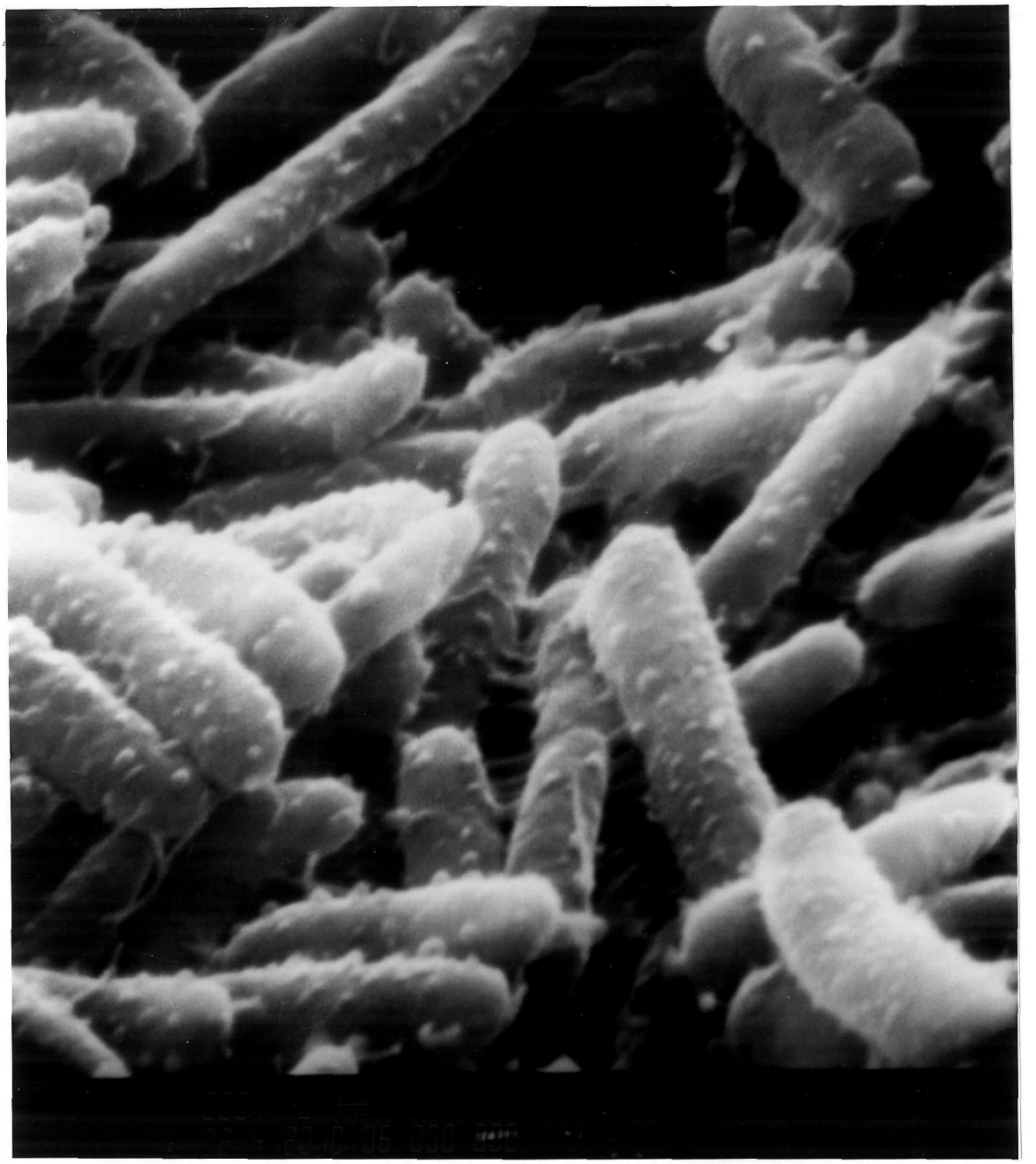

Figure 1

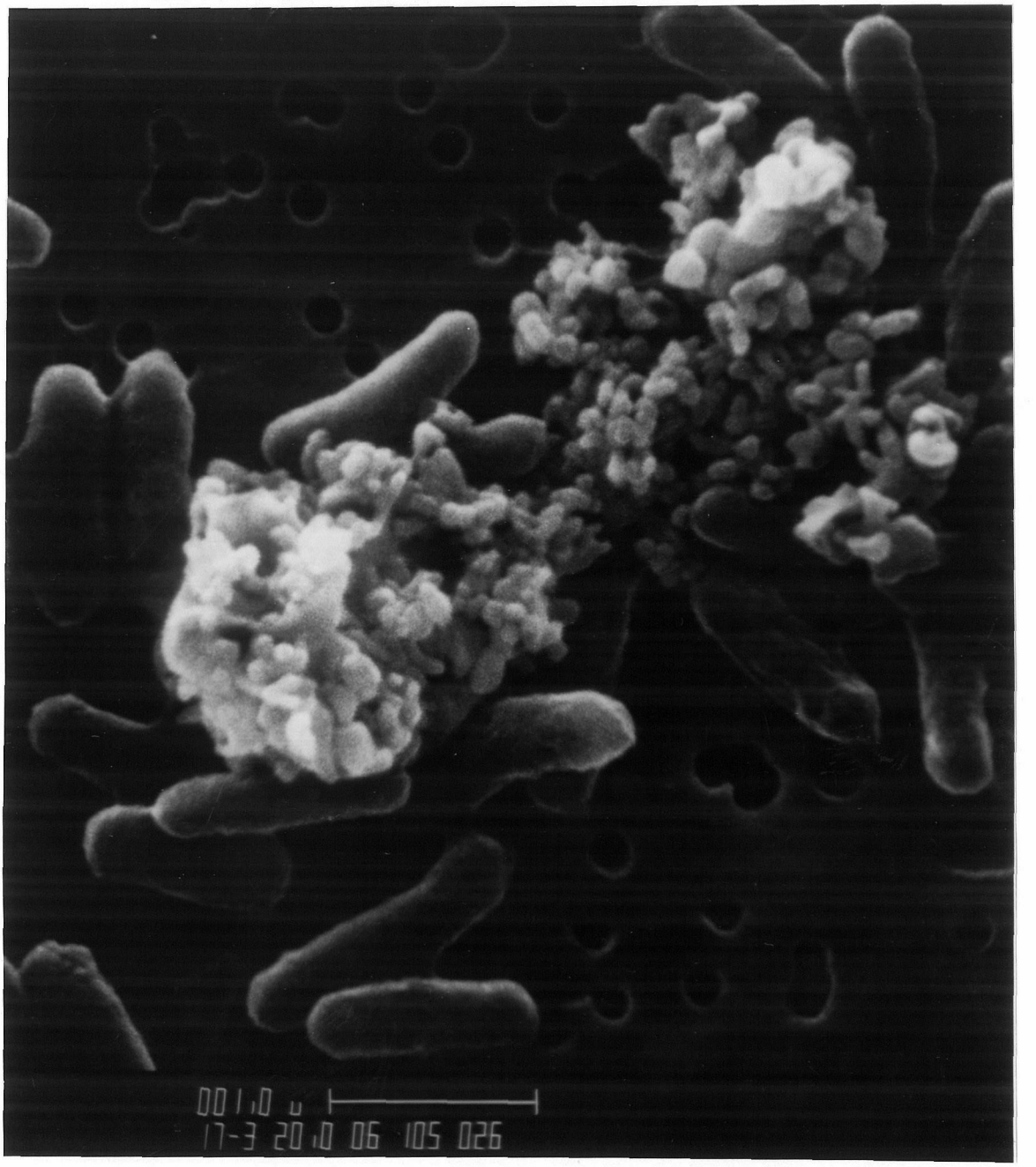

Figure 2

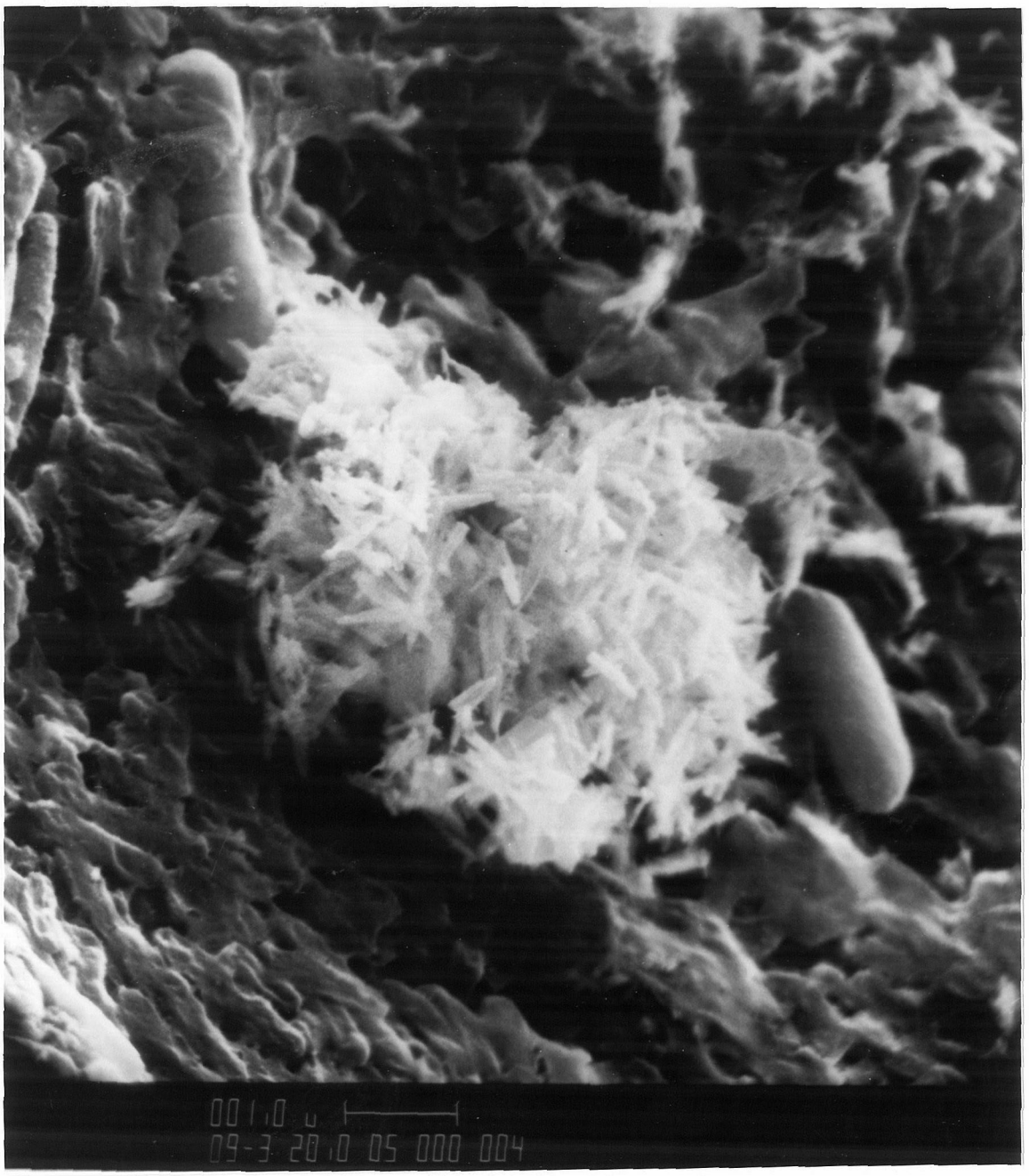

Figure 3

Figure 4

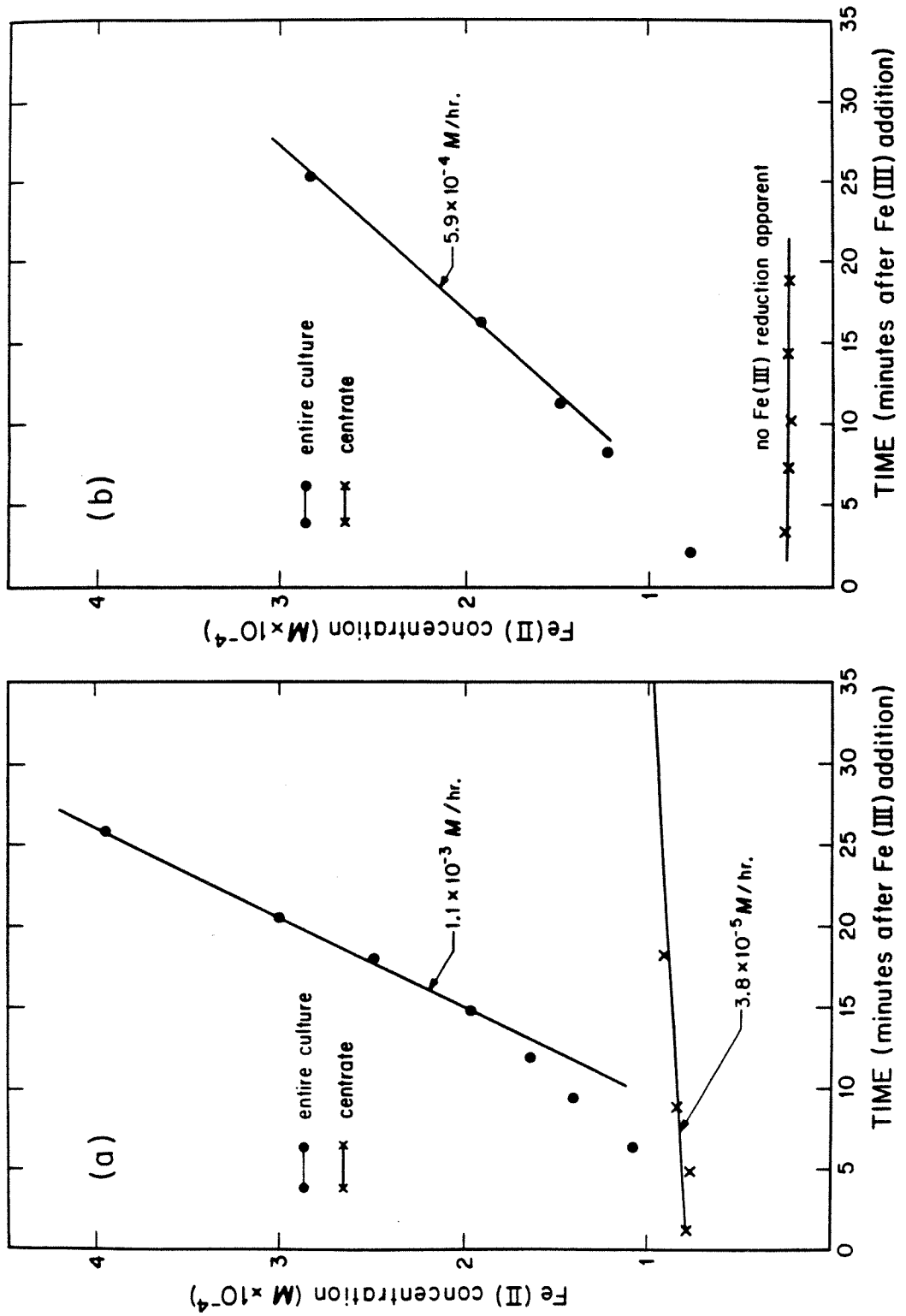
(a)
entire culture
centrate
1.1 × 10⁻³ M/hr.
3.8 × 10⁻⁵ M/hr.
Fe (II) concentration (M × 10⁻⁴)
TIME (minutes after Fe (III) addition)
(b)
entire culture
centrate
5.9 × 10⁻⁴ M/hr.
no Fe(III) reduction apparent
Fe(II) concentration (M × 10⁻⁴)
TIME (minutes after Fe(III) addition)

Figure 5

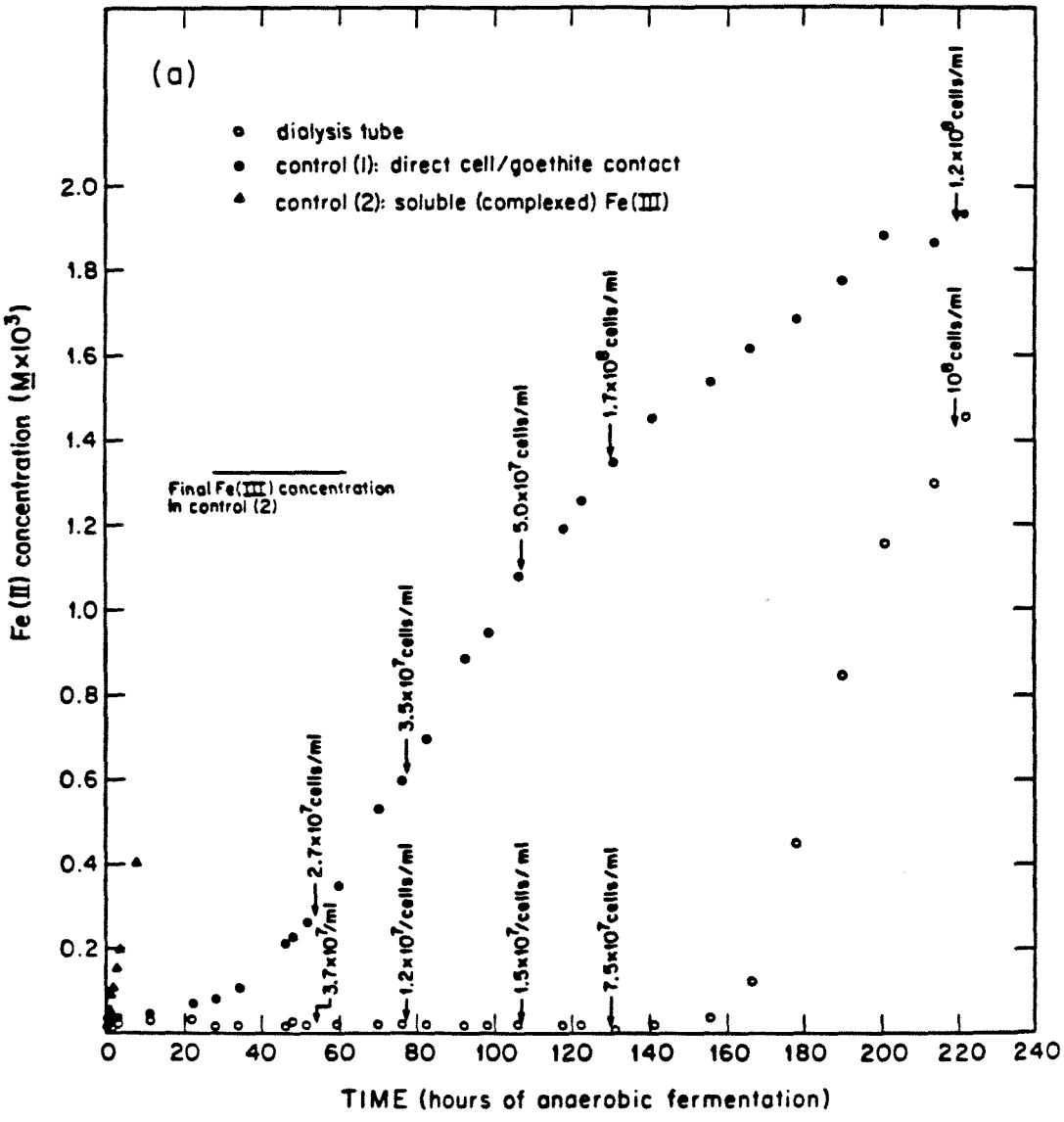
(a)
dialysis tube
control (1): direct cell/goethite contact
control (2): soluble (complexed) Fe(III)
Final Fe(III) concentration in control (2)
2.7x10^7 cells/ml
3.7x10^7/ml
1.2x10^7/cells/ml
3.5x10^7 cells/ml
5.0x10^7 cells/ml
1.5x10^7/cells/ml
1.7x10^8 cells/ml
7.5x10^7 cells/ml
10^8 cells/ml
1.2x10^8 cells/ml
Fe (II) concentration (M×10^3)
TIME (hours of anaerobic fermentation)
0
20
40
60
80
100
120
140
160
180
200
220
240
0.2
0.4
0.6
0.8
1.0
1.2
1.4
1.6
1.8
2.0

Figure 6(a)

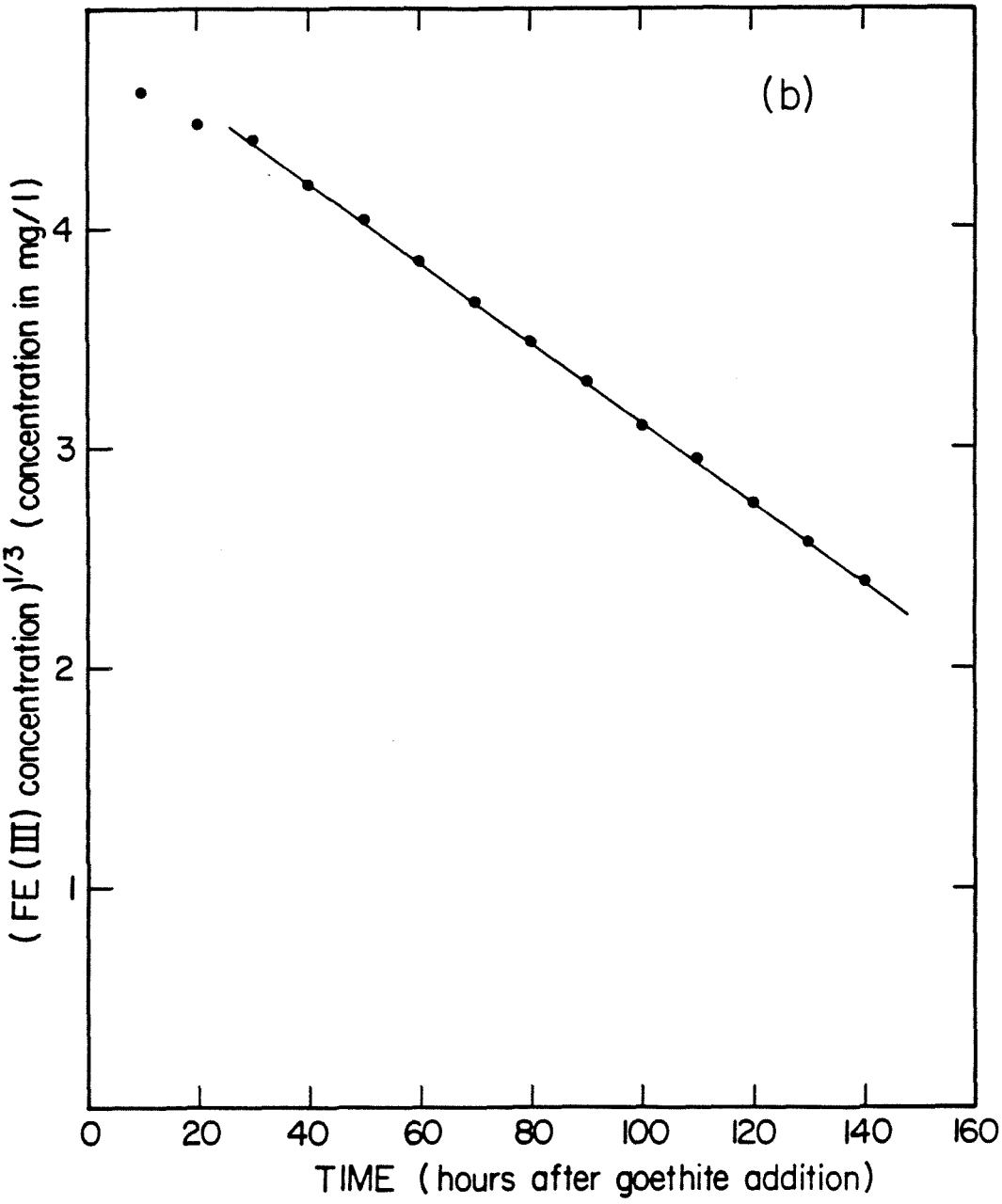
(b)
(FE (III) concentration)$^{1/3}$ (concentration in mg/l)
1
2
3
4
0
20
40
60
80
100
120
140
160
TIME (hours after goethite addition)

Figure 6(b)

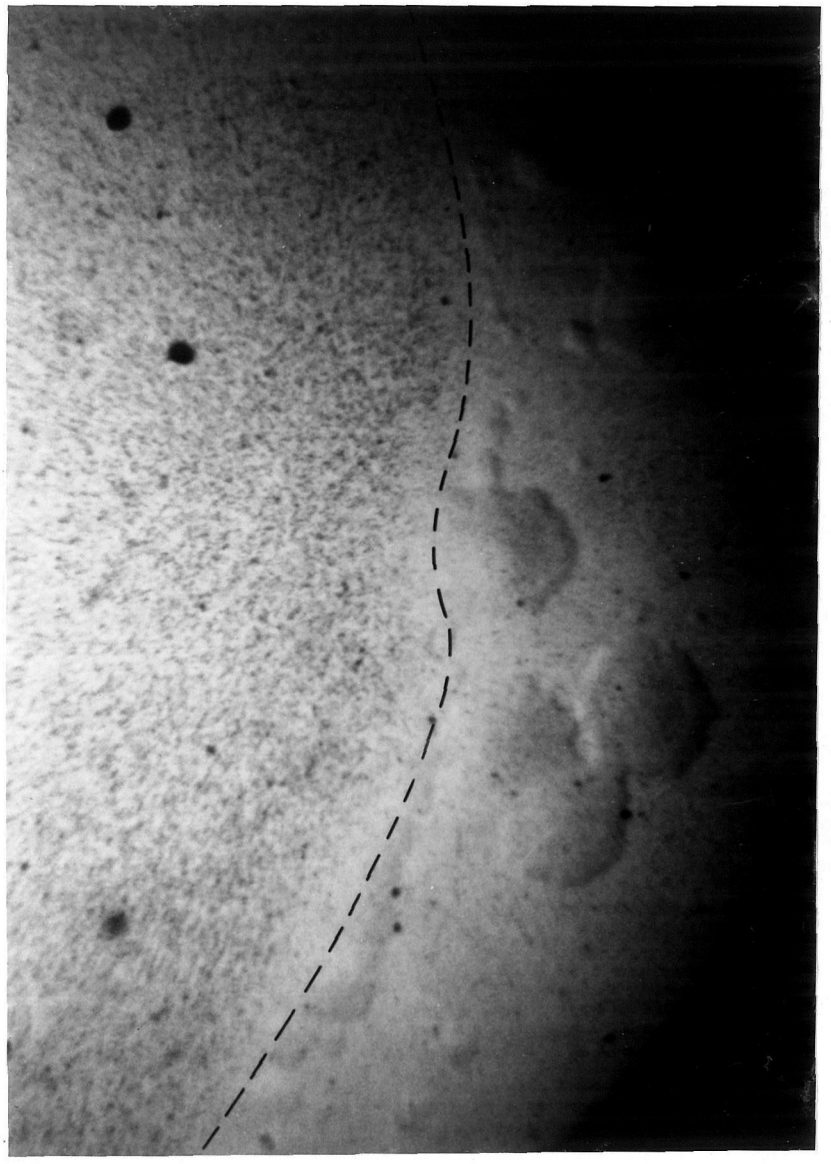

Figure 7

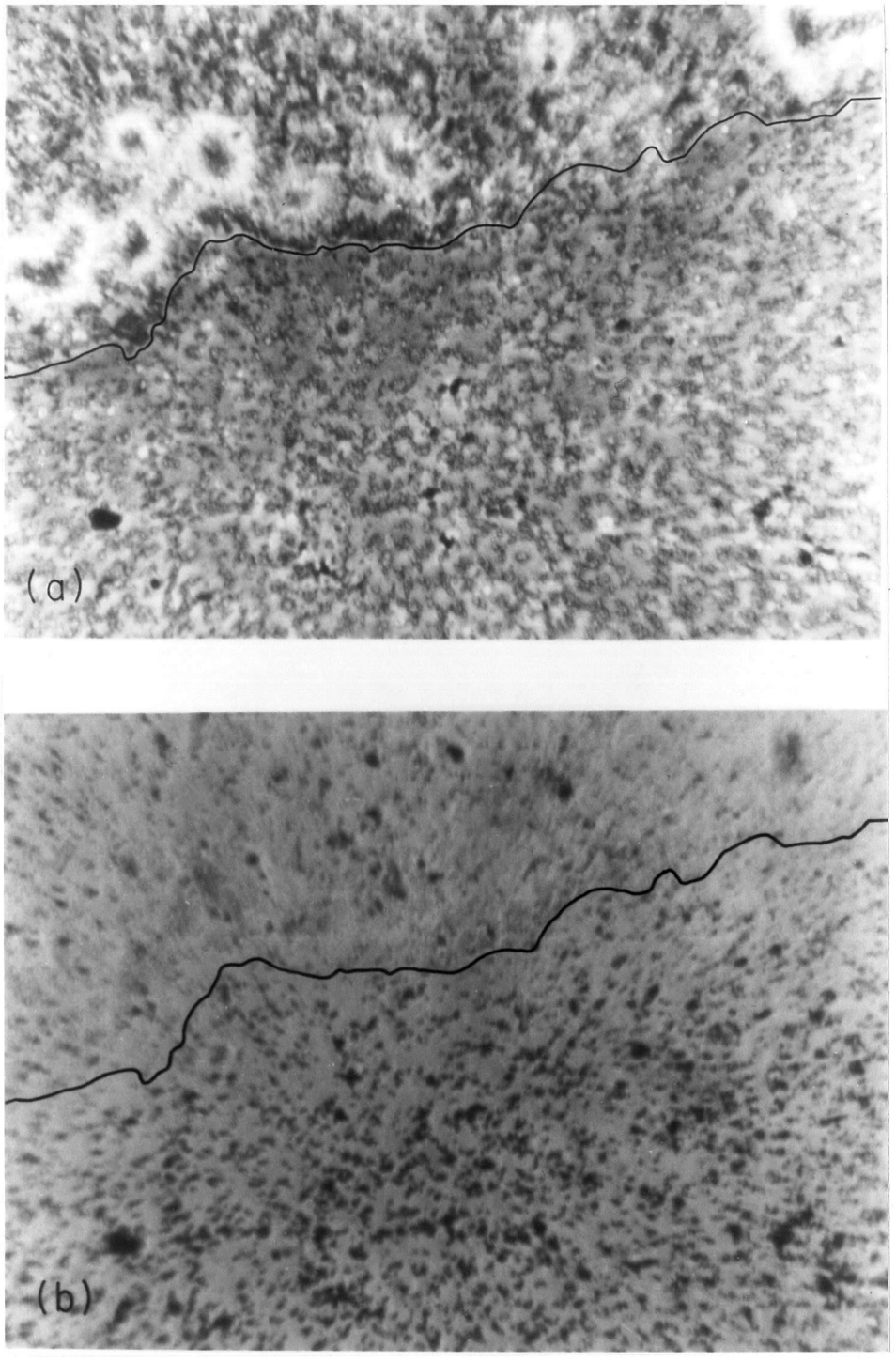

Figure 8

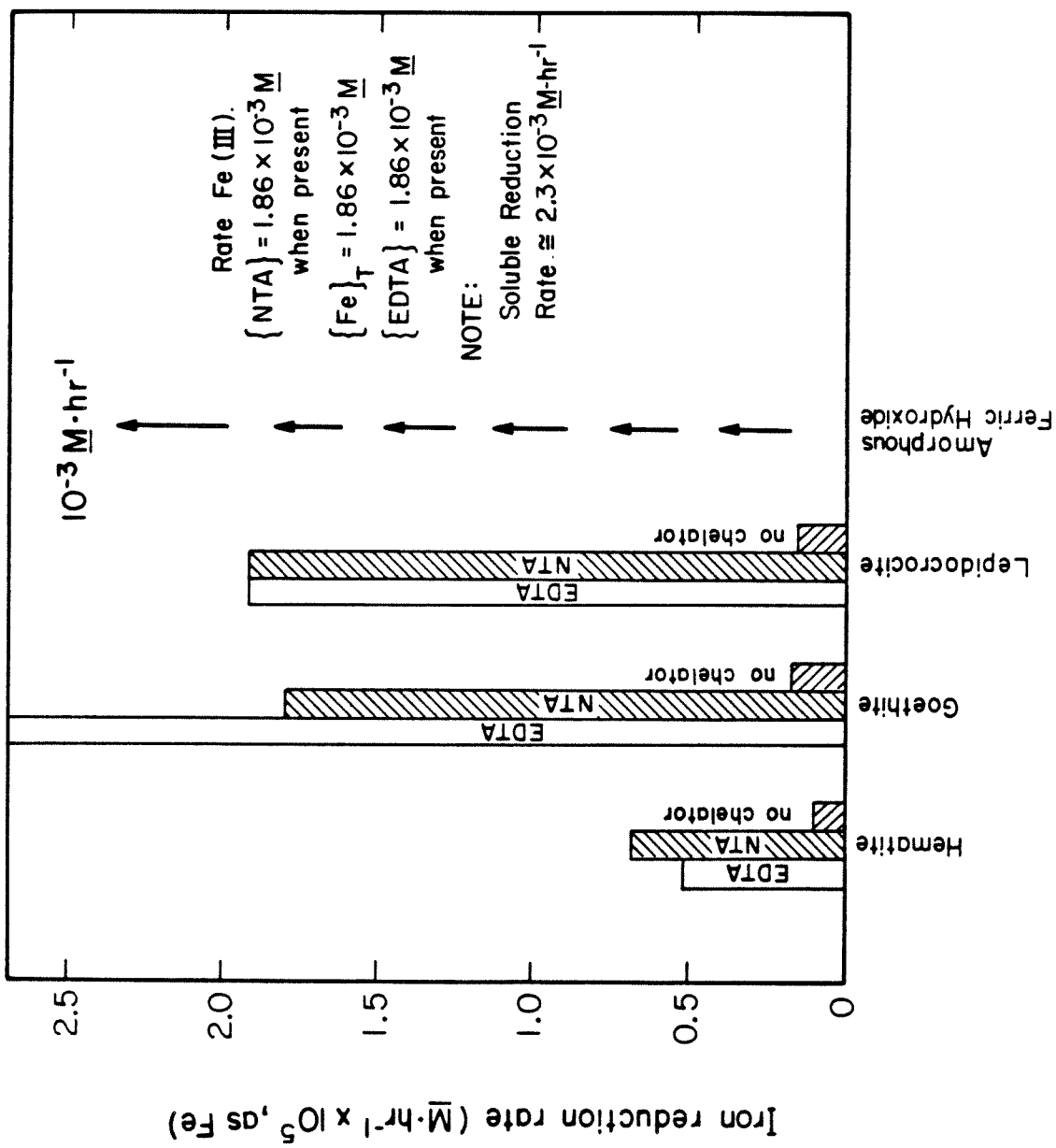
Iron reduction rate ($\underline{M}\cdot hr^{-1} \times 10^5$, as Fe)
2.5
2.0
1.5
1.0
0.5
0
Hematite
EDTA
NTA
no chelator
Goethite
EDTA
NTA
no chelator
Lepidocrocite
EDTA
NTA
no chelator
Amorphous Ferric Hydroxide
$10^{-3}\ \underline{M}\cdot hr^{-1}$
Rate Fe (III). {NTA} = $1.86\times10^{-3}\ \underline{M}$ when present
$\{Fe\}_T = 1.86\times10^{-3}\ \underline{M}$
{EDTA} = $1.86\times10^{-3}\ \underline{M}$ when present
NOTE:
Soluble Reduction Rate $\cong 2.3\times10^{-3}\ \underline{M}\cdot hr^{-1}$

Figure 9

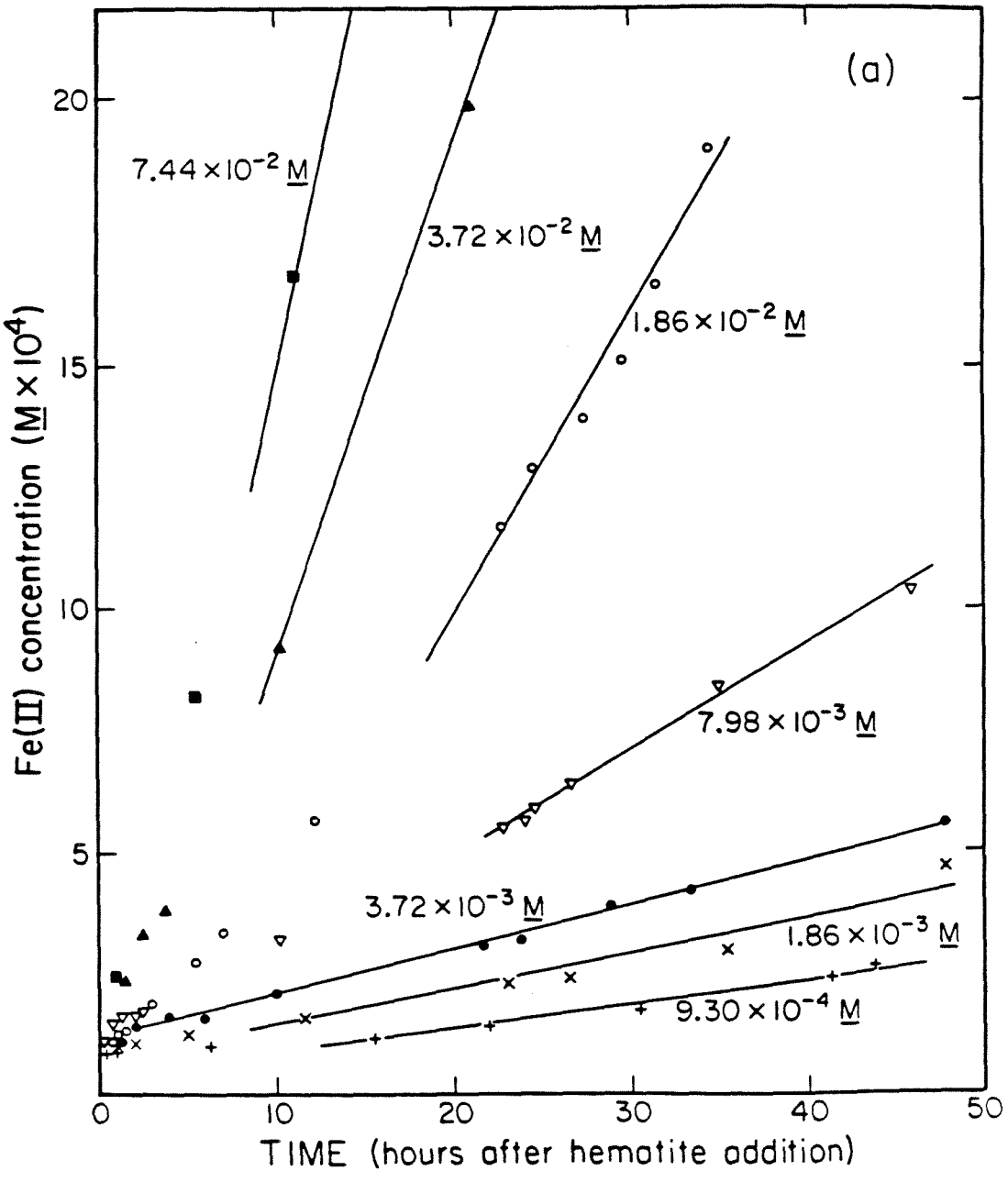
(a)
7.44 × 10⁻² M
3.72 × 10⁻² M
1.86 × 10⁻² M
7.98 × 10⁻³ M
3.72 × 10⁻³ M
1.86 × 10⁻³ M
9.30 × 10⁻⁴ M
Fe(II) concentration (M × 10⁴)
TIME (hours after hemotite addition)
0
10
20
30
40
50
5
10
15
20

Figure 10(a)

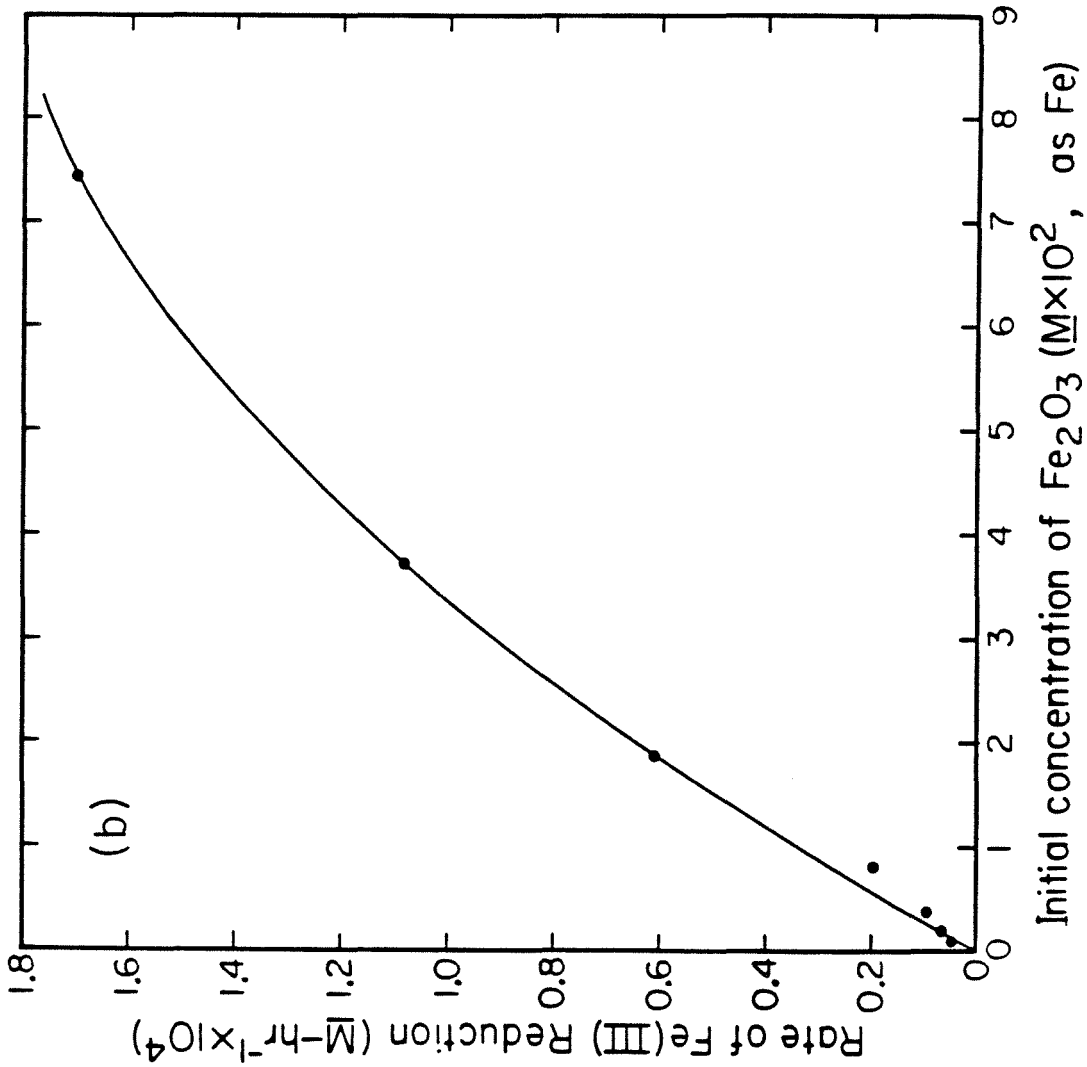
(b)
Rate of Fe(III) Reduction (M-hr^{-1}x10^4)
Initial concentration of Fe_2O_3 (Mx10^2, as Fe)
0
0.2
0.4
0.6
0.8
1.0
1.2
1.4
1.6
1.8
1
2
3
4
5
6
7
8
9

Figure 10(b)

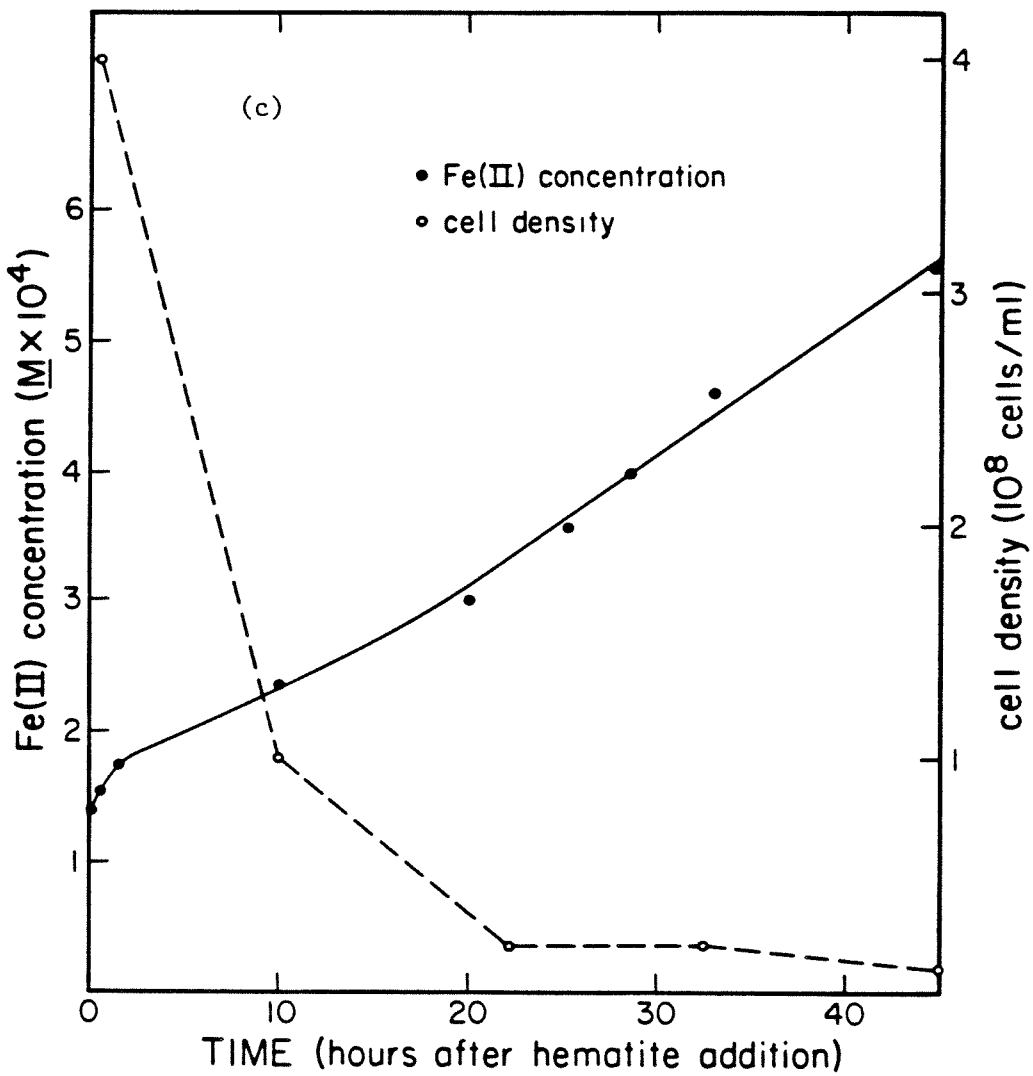
(c)
• Fe(II) concentration
∘ cell density
Fe(II) concentration (M×10⁴)
cell density (10⁸ cells/ml)
TIME (hours after hematite addition)
0
10
20
30
40
1
2
3
4
5
6

Figure 10(c)

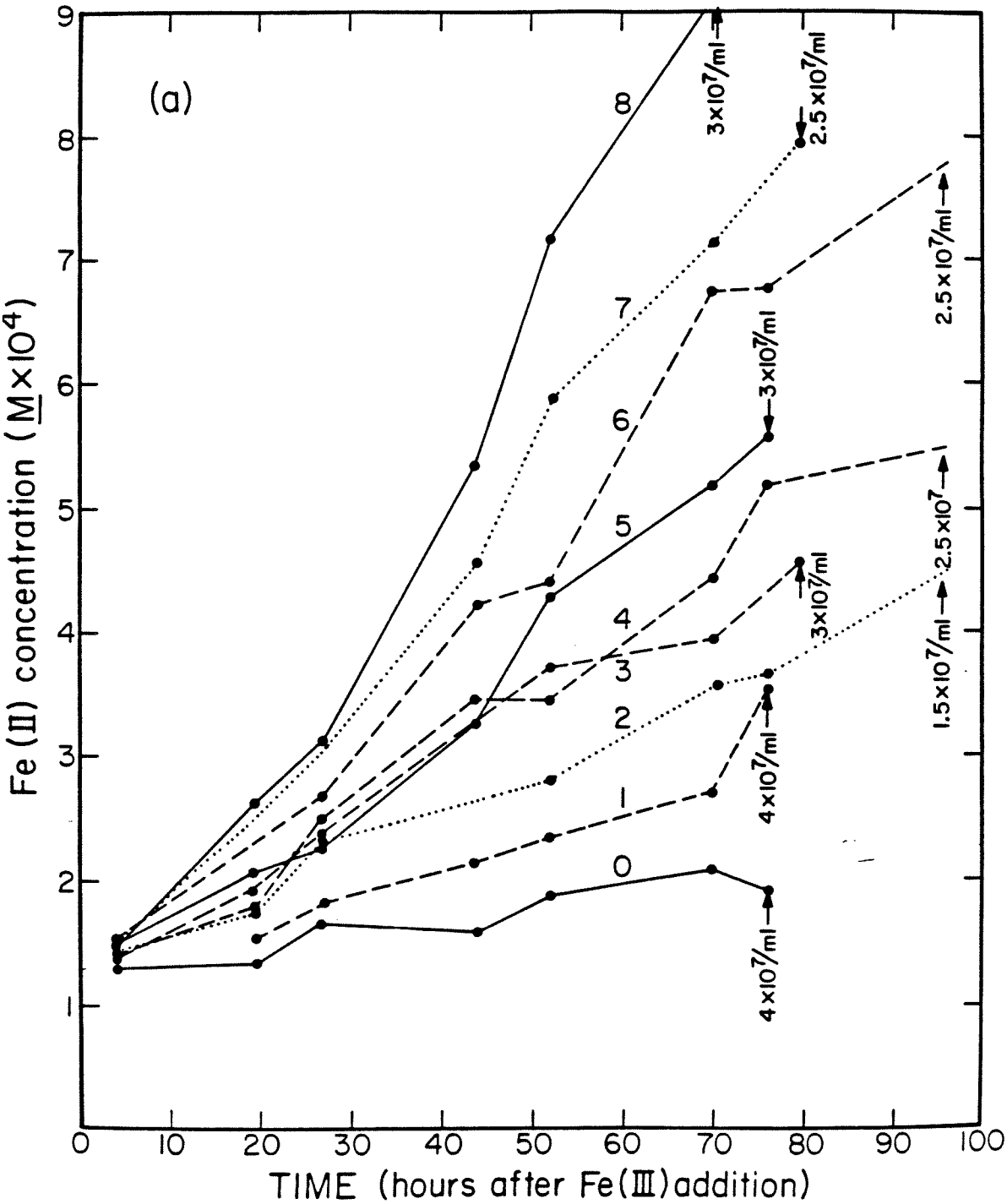
(a)
Fe (II) concentration (M×10⁴)
TIME (hours after Fe(III) addition)
0
10
20
30
40
50
60
70
80
90
100
1
2
3
4
5
6
7
8
9
8
7
6
5
4
3
2
1
0
3×10⁷/ml
2.5×10⁷/ml
2.5×10⁷/ml
3×10⁷/ml
2.5×10⁷
1.5×10⁷/ml
3×10⁷/ml
4×10⁷/ml
4×10⁷/ml

Figure 11(a)

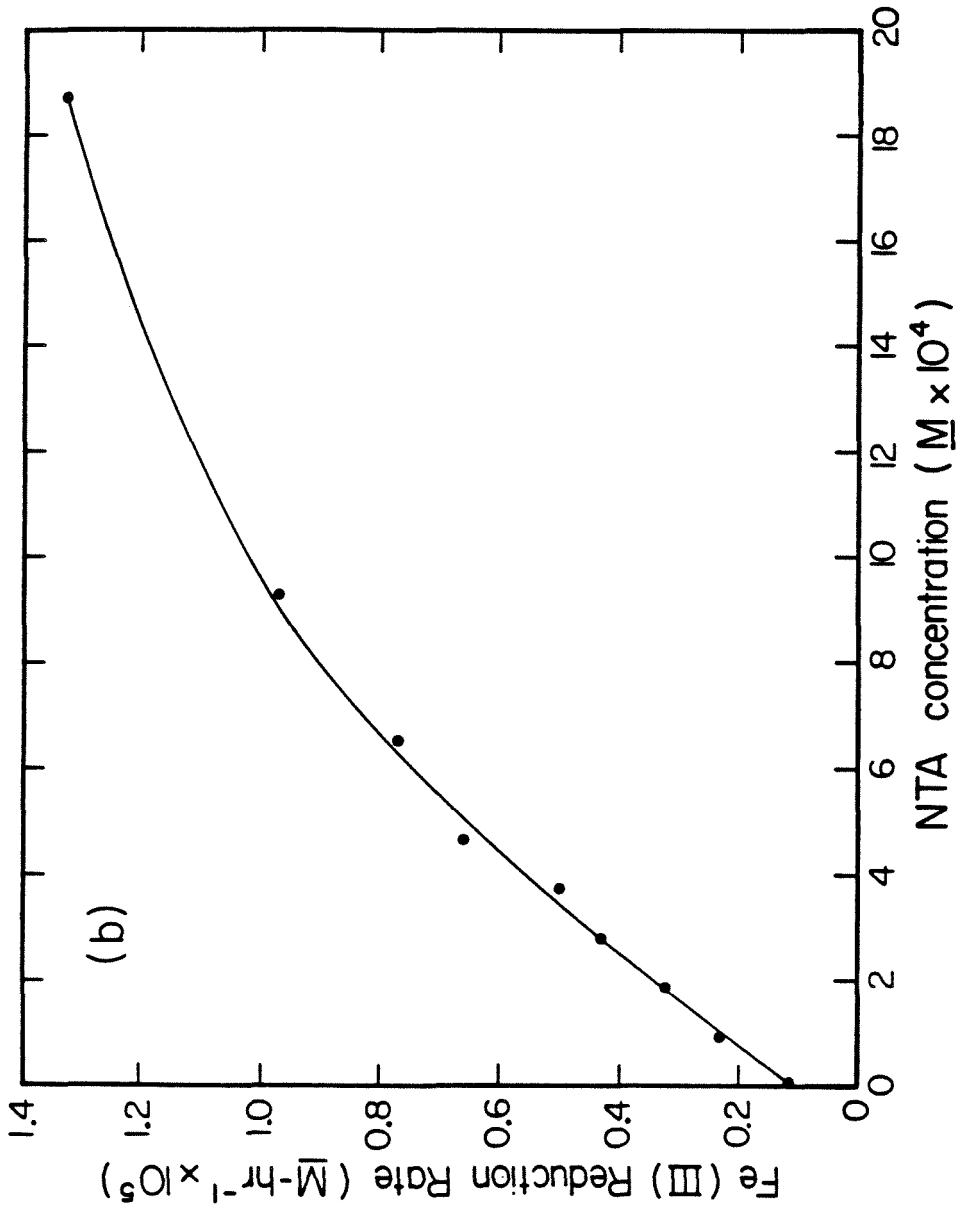
(b)
Fe (III) Reduction Rate (M-hr^{-1} x 10^5)
NTA concentration (M x 10^4)
0
0.2
0.4
0.6
0.8
1.0
1.2
1.4
0
2
4
6
8
10
12
14
16
18
20

Figure 11(b)

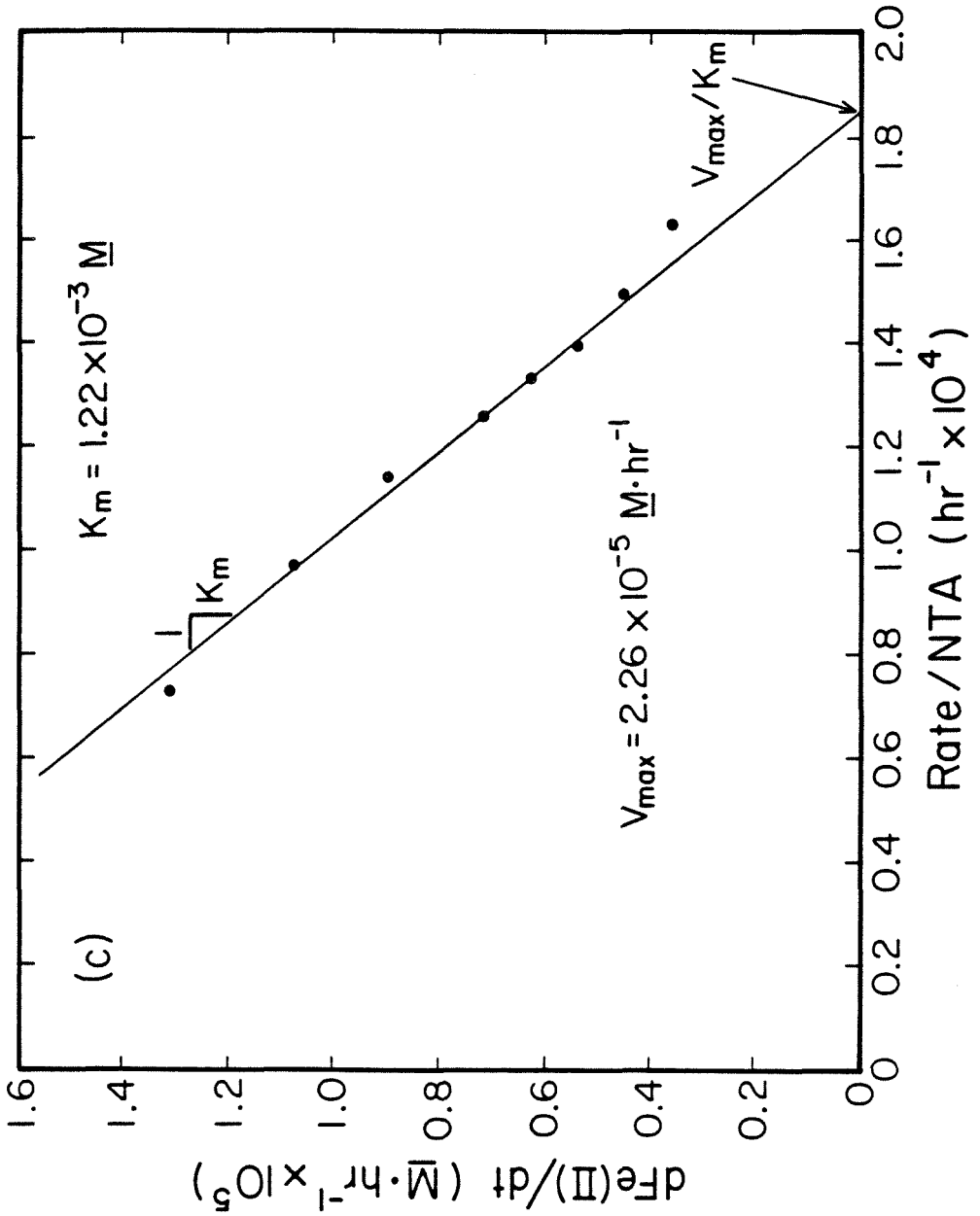
(c)
$K_m = 1.22 \times 10^{-3}$ M
K_m
1
$V_{max} = 2.26 \times 10^{-5}$ M·hr^{-1}
V_{max}/K_m
$d[Fe(II)]/dt$ (M·hr^{-1} x 10^5)
Rate/NTA (hr^{-1} x 10^4)
0
0.2
0.4
0.6
0.8
1.0
1.2
1.4
1.6
1.8
2.0

Figure 11(c)

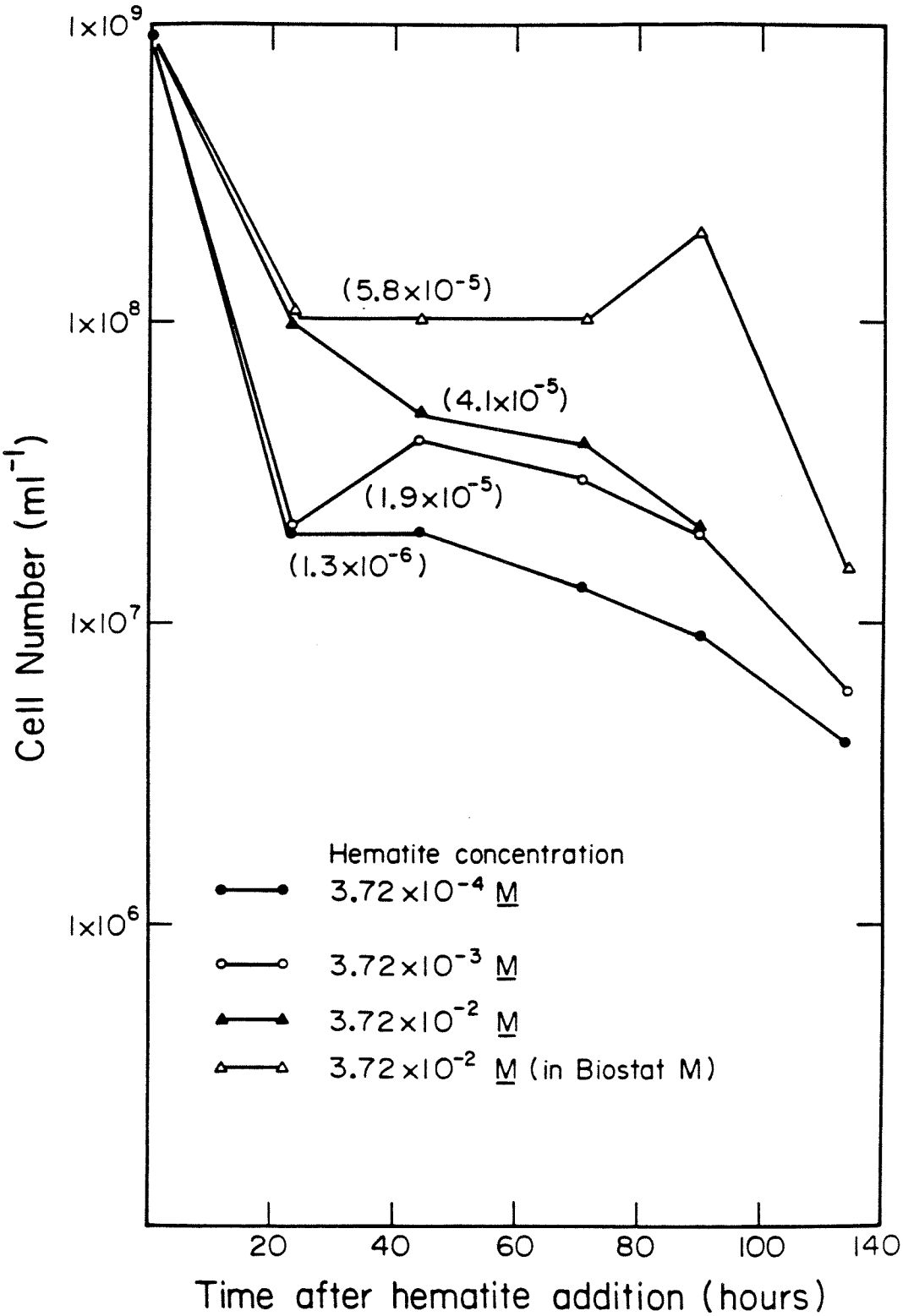
1x10^9
1x10^8
1x10^7
1x10^6
Cell Number (ml^-1)
(5.8x10^-5)
(4.1x10^-5)
(1.9x10^-5)
(1.3x10^-6)
Hematite concentration
3.72x10^-4 M
3.72x10^-3 M
3.72x10^-2 M
3.72x10^-2 M (in Biostat M)
20
40
60
80
100
140
Time after hematite addition (hours)

Figure 12

Table 1. Medium for growth and iron reduction by Pseudomonas sp. 200[16].

K_2HPO_4	0.5 g
Na_2SO_4	2.0 g
NH_4Cl	1.0 g
$CaCl_2$	0.15 g
$MgSO_4.7H_2O$	0.1 g
$FeCl_3$	4.0 mg (as Fe) (filter sterilized and added after autoclaving other medium contents)
Yeast extract	0.5 g
Sodium lactate	3 mls from 60% syrup
H_2O	to 1 ℓ total volume

Note: Major organic components of yeast extract include amino acids and B-complex vitamins (Difo Laboratories, personal communication). Major inorganic constituents include iron, potassium, sodium, and chloride ion. Inorganics represent only a small percentage of overall growth medium concentrations. Independent calculations (not reviewed here) indicate that organic components do not appreciably alter iron speciation.

Table 2a. Description of iron oxides utilized in reductive dissolution experiments.(1)

Product No.	Mineral Identity	Purity	Particle Shape	Average Particle Size (μm)	Specific Gravity	Surface Area (m^2/g)
R1599	hematite	>99%	spheroidal	0.25	5.15	11.2
R8098	hematite	>99%	spheroidal	0.90	5.15	3.2
YL01888D	goethite	>85%	acicular	0.35	4.03	23.0
M02228	lepidocrocite					26.0

Table 2b. Iron oxide particle heterogeneity data.

Product No.	Weight % < Size Indicated (diameters in microns)															
	20	10	5	4	3	2.5	2	1	.8	.75	.6	.5	.4	.3	.2	.1
R1599	-	100	100	-	-	-	99	97	-	-	-	94	-	77	50	17
R8098	99	98	95	-	-	85	-	48	-	35	-	16	-	5	-	-
YL01888D		-	-	100	100	100	-	99	97	-	94	-	85	-	35	-
M02228	data not available															

Notes:

(1) All data and information from Pfizer Inc. -- Minerals, Pigments and Metals Division.

(2) Surface area measurements by B.E.T. method.

Table 3. Confirmation of Iron-Oxide Identity via X-ray Crystallography[1],[2]

α-Fe_2O_3 -- hematite						α-FeO(OH) -- goethite			
Reference		Pfizer #R1599		Pfizer #19377		Reference		Pfizer #YL01888	
Lattice spacing (Å)	Relative peak[3] intensity (I/I_o)	Lattice spacing (Å)	I/I_o	Lattice spacing (Å)	I/I_o	Lattice spacing (Å)	Relative peak intensity (I/I_o)	Lattice spacing (Å)	I/I_o
3.686	0.33	3.70	0.30	3.66	0.30	4.98	0.10	not scanned	
2.703	1.00	2.71	1.00	2.69	1.00	4.18	1.00	4.15	1.00
2.519	0.70	2.53	0.70	2.51	0.90	3.38	0.10	not observed	
2.295	0.02	not observed		not observed		2.69	0.35	2.68	0.60
2.208	0.17	2.22	0.20	2.20	0.30	2.58	0.08	2.58	0.15
2.080	0.02	not observed		not observed		2.49	0.10	not observed	
1.8428	0.31	1.84	0.30	1.84	0.50	2.45	0.50	2.44	1.00
1.6966	0.36	1.70	0.60	1.69	0.70	2.25	0.14	not observed	
1.6013	0.08	1.61	0.10	not observed		2.19	0.18	2.18	0.15
1.4873	0.22	1.49	0.30	1.48	0.50	1.92	0.05	1.92	0.10
1.4543	0.21	1.46	0.30	1.45	0.40	1.80	0.06	not observed	
						1.72	0.20	1.72	0.20
						1.564	0.10	1.56	0.10
						1.561	0.08		

Notes:
(1) Data were obtained using a Norelco vertical diffractometer with Cu($K\alpha$) radiation (λ = 1.5418).
(2) Reference data are from Selected Powder Diffraction Data for Minerals, 1st edition (Joint Committee on Powder Diffraction Standards, Swarthmore, PA, 1976).
(3) Relative peak intensity is a measure of peak height relative to that of the most intense peak in the scan.

Table 4. Effect of hematite specific surface area on observed rate of dissimilative iron reduction.

Hematite Identity (Pfizer designation)	[Fe(III)] (M)	Specific Surface Area (from Table 2, m^2/g)	[NTA](M)	Observed Fe(III) Reduction Rate ($M.hr^{-1}$)	Predicted[1] designation Reduction Rate ($M.hr^{-1}$)
R8089	2.57×10^{-3}	3.2[2]	2.57×10^{-3}	5.19×10^{-6}	7.14×10^{-6}
R8089	3.92×10^{-3}	3.2	3.92×10^{-3}	7.61×10^{-6}	1.13×10^{-5}

Notes:

(1) Predictions are based upon semi-empirical formulae relating iron-reduction rate to hematite (R1599) and NTA concentrations. Figures represent calculated rates of reductive dissolution at the concentrations of hematite (R1599 vice R8089) and NTA shown.

(2) Specific surface area of hematite R1599 is 11.2 m^2/g.

Table 5. Relationships among initial cell number, hematite concentration, and the observed rate of reductive dissolution.

Culture Optical Density[1] (λ = 600, cm^{-1})	Hematite (R1599) Concentration ($\underline{M}$ as Fe)	Observed Rate of Reductive Dissolution ($\underline{M}.hr^{-1}$, as Fe)	Predicted Rate of Reductive Dissolution ($\underline{M}.hr^{-1}$)[2]
0.135	1.26×10^{-2}	2.7×10^{-5}	3.5×10^{-5}
0.116	3.72×10^{-3}	1.2×10^{-5}	1.1×10^{-5}

Notes:

(1) An indication of cell density at the onset of anaerobic conditions (point of hematite addition).

(2) Predictions were based on semi-empirical formulae relating iron-reduction rate to hematite (R1599) and NTA concentrations. NTA was at 3.72×10^{-3} $\underline{M}$ in both experiments and calculations. For computational purposes, cells were assumed to be present in excess.

CHAPTER 5

Dissimilative Fe(III) Reduction by *Pseudomonas* sp. 200, (*Pseudomonas ferrireductans*) -- Inhibitor Studies

by

Robert G. Arnold, Thomas J. DiChristina and
Michael R. Hoffmann

Submitted to: Applied and Environmental Microbiology

February 1986

Abstract

Aerobic respiration and dissimilative iron reduction were studied in pure, batch cultures of Pseudomonas sp. 200 (P.ferrireductans). Specific respiratory inhibitors were utilized to identify elements of electron transport chains involved in reduction of molecular oxygen and Fe(III). When cells were grown at high oxygen concentration, dissimilative iron reduction occurred via an abbreviated electron transport chain. Induction of alternative respiratory pathways resulted from growth at low oxygen tension (<0.01 atm.). Induced cells were capable of O_2 utilization at moderately increased rates; dissimilative iron reduction was accelerated by a factor of 6 to 8. In cells grown at low oxygen tension, dissimilative iron reduction appears to be uncoupled from oxidative phosphorylation. Models of induced and uninduced electron transport chains are presented including a mathematical treatment of chemical inhibition within the uninduced, aerobic electron transport system. In uninduced cells respiring anaerobically, electron transport is limited by ferri-reductase activity. This limitation may disappear among induced cells.

Introduction

According to Mitchell's chemiosmotic hypothesis (16, 17) electron transport is coupled to oxidative phosphorylation by the following mechanism: Reducing equivalents enter the respiratory chain via one of several dehydrogenases (often flavin-containing enzymes, e.g., NADH and succinate dehydrogenases) and are passed sequentially down a chain of carriers which includes iron-sulfur proteins, coenzyme Q, and a series of cytochromes (9). In mitochondria, molecular oxygen serves as the final electron acceptor. Energy available from electron transport supports an electrochemical proton-motive force which drives ADP phosphorylation (coupled to proton retranslocation via membrane-bound ATPase).

Similarities between mitochondrial and bacterial respiration have prompted speculation that mitochondria originated as bacterial endosymbionts (9) or fragments of specialized bacterial membranes (25). However, there are fundamental differences in bacterial systems including: (i) species- and strain-dependent variations in transport-chain composition; (ii) intra-strain dependence of transport-chain composition on growth conditions; (iii) the branched nature of bacterial respiratory systems, which provides a measure of metabolic flexibility absent in their mitochondrial counterpart (26,32), (iv) their respective H^+/ATP ratios (11) [this despite similarities (3) between mitochondrial and bacterial membrane-bound ATPases] and (v) structural differences between mitochondrial and bacterial cytochrome oxidases including aa_3-type oxidases (25). Bacterial respiration can terminate with a number of electron acceptors including O_2, NO_3^-, NO_2^-, SO_3^{2-}, SO_4^{2-}, and Fe(III) (10). The

development of alternative electron transport pathways is often inducible in the absence of more thermodynamically favorable routes.

Pseudomonas sp. 200 (hereinafter referred to as Pseudomonas ferrireductans), is capable of catalyzing dissimilative iron reduction [Fe(III) + e^- ———> Fe(II)] at rates considerably faster than those reported for other capable bacteria, e.g., Thiobacillus thiooxidans (2,12), Bacillus circulans (30,31), Bacillus polymyxa (19), and Clostridium butyricum (19). Previous experiments in this laboratory have shown that electron transport to Fe(III) can proceed at a rate comparable to that observed during aerobic respiration (1). Iron-reduction activity in P. ferrireductans is known to respond to growth medium composition. Furthermore, Fe(III) reduction is directly related to cell pigmentation and can be inhibited by HOQNO (2-n-heptyl-4-hydroxyquinoline N-oxide) (20,21). Cytochrome content is directly corelated with ferri-reductase activity.

A variety of reagents are known to interfere with electron transport. When the site and/or mechanism of electron-transport inhibition is known, inhibitor studies offer insights into the character of the electron-transport chain and identities of individual electron carriers (7). However, respiratory inhibitors frequently act at more than one site (14).

Kinetic data for oxygen-utilization and Fe(III) reduction by P. ferrireductans are reported here. These data are used to (i) identify (and contrast) electron carriers involved in aerobic respiration versus dissimilative iron reduction, (ii) identify inducible elements of the electron transport chain, (iii) support models of electron transport

kinetics and inhibitor activity and (iv) determine whether dissimilative iron reduction can support oxidative phosphorylation.

Materials and Methods

Four types of experiments were conducted: Dissolved oxygen utilization was monitored in (i) uninduced and (ii) induced cultures of P. ferrireductans which differed only in the dissolved oxygen concentration maintained during aerobic growth (see below). Similarly, dissimilative iron reduction was examined under anaerobic conditions in uninduced and induced cultures (experiment types (iii) and (iv)).

(i) Aerobic Respiration (uninduced)

Oxygen utilization experiments were conducted in a 2-liter Biostat M batch reactor (Braun Instrument Co.) with automatic temperature (± 0.2°C) and pH (± 0.05) control (pH-stat.). Dissolved oxygen concentration was measured continuously using an O_2 probe (Ingold, Type 82) fitted through the head plate of the Biostat M. In a typical experiment, the reactor was filled to 1.5 liters with lactate medium (21) (per liter: 0.5 g K_2HPO_4; 2.0 g Na_2SO_4; 1.0 g NH_4Cl; 0.15 g $CaCl_2$; 0.1 g $MgSO_4.7H_2O$; 0.5 g yeast extract; Na-lactate, 3 mls from 60% syrup) and autoclaved at 121°C for 30-60 minutes. Iron was added to a final concentration of 72 μM from a filter-sterilized $FeCl_3$ solution for satisfaction of microbial nutritional requirements. Aerobic growth was initiated by adding approximately 1.5 mls from a dense overnight culture (identical medium) of P. ferrireductans Species characteristics have been summarized previously (1). Gas flow (Q_{AIR} 0.5 L/min) and mechanical agitation (250 rpms) provided mixing energy, and temperature was maintained at 31°C. Dissolved oxygen concentration

remained at or above 80% of saturation throughout the period of aerobic growth.

Microbial growth was monitored via periodic measurement of light absorbance at λ = 600 nm. At a target optical density of 0.10 cm^{-1}, the air supply to the culture was cut off and agitation speed reduced to 150 rpm in order to minimize entrainment of air from the culture head space while still providing mixing energy. The concentration of dissolved oxygen was measured at 15-second intervals before and after chloramphenicol addition to 0.23 mM; when a steady rate of O_2 depletion was observed, inhibitor addition was initiated. Thereafter, the concentration of inhibitor was increased periodically while continuously monitoring O_2 concentration. There was sufficient time between successive additions to establish a steady oxygen-utilization rate at each inhibitor concentration. A list of chemical inhibitors and ranges of addition, probable inhibition sites, and inhibitor solvents is provided as Table 1.

(ii) Aerobic Respiration (induced)

Procedures were essentially the same as those described above. However, cultures were grown to an absorbance of A = 0.25 (cm^{-1}, λ = 600 nm) while maintaining dissolved oxygen at $\leq$ 2% of the saturation level. At the target optical density, chloramphenicol was added to 0.46 mM and profiles of dissolved oxygen concentration versus time were generated at pre-selected inhibitor levels.

(iii) Dissimilative Iron Reduction (uninduced)

P. ferrireductans was grown aerobically (dissolved oxygen concentration $\geq$ 0.8 x saturation) to a target optical density of A_{600} = 0.25, chosen to provide an appreciable baseline iron-reduction rate.

At that point, O_2-utilization rate was measured before and after chloramphenicol addition to 0.46 mM. The culture was then purged of residual oxygen with N_2(g), and nitrilotriacetic acid (NTA) and $FeCl_3$ were added to final concentrations of 1.86×10^{-3} M. Thermodynamic calculations indicate that NTA substantially increases the overall solubility of Fe(III) (1); the rate of dissimilative iron reduction by P. ferrireductans is also increased dramatically. Aliquots of 120 mls were immediately transferred from the Biostat M into 250-ml flasks in a water bath/shaker ($31^{o}C$). Flasks were continuously purged with high purity nitrogen gas. Respiratory inhibitors were added to pre-selected concentrations ranging over at least two orders of magnitude. The highest concentration was reserved for the Biostat M, in which pH changes due to inhibitor addition were offset. One flask was used as a control (no inhibitor). Thereafter, reaction flasks and the Biostat M were periodically sampled for determination of total ferrous iron concentration. During the iron-reduction period, pH control in the Biostat M was terminated since similar control in the flasks was not feasible. The culture remained in the neutral pH range throughout, drifting $\leq$ 0.3 pH units.

(iv) Iron Reduction (induced)

Preliminary experiments (Figure 1) showed that iron-reduction activity in cultures of P. ferrireductans is enhanced by growth under O_2-limited conditions. Experiments were undertaken to see if inducible and constitutive iron reductases could be differentiated on the basis of response to chemical inhibition. Procedures were identical to those of iron-reduction experiments described above, except that dissolved

oxygen levels were maintained at less than 2% saturation during the aerobic growth period (to A_{600} = 0.25) preceding iron addition.

Carbon Monoxide Inhibition

Carbon monoxide inhibition experiments represent a special case since inhibitor concentration was not measured and could not be varied systematically. CO inhibition of dissimilative iron reduction was tested in induced and uninduced cultures grown to A_{600} = 0.25 (cm^{-1}) in the Biostat M.

Whole-Cell Spectra

P. ferrireductans was grown in complex lactate medium to A_{600} = 0.75 (cm^{-1}) at high- and low-level O_2 concentrations (per above). Cells were harvested by centrifugation for 30 minutes at 3000xg (4°C) in a Sorvall Model RC-3B centrifuge, then washed and resuspended to (1/50) x original volume in cold saline solution (0.15 M NaCl; 1 mM $MgCl_2$). Dithionite-reduced-minus-oxidized spectra were obtained using a Model MPS-2000 Shimadzu recording spectrophotometer (1-cm pathlength cuvettes positioned adjacent to the photomultiplier). The oxidized sample was prepared by bubbling pure O_2 through the suspension; reduced conditions were developed via addition of a few grains of sodium dithionite ($Na_2S_2O_4$; Sigma Co.).

Analytical Procedures

Optical density (an indication of cell density) was measured using a Beckman Model DU7 spectrophotometer at λ = 600 nm and a 1-cm-pathlength, reduced-volume cuvette.

To eliminate the possibility of Fe(II) autoxidation (13) following sample removal, 1 ml of anaerobic fermentation medium was rapidly added (within five seconds of sample withdrawal) to a quenching medium

consisting of 0.5% w/v 1,10-phenanthroline (sufficient volume to provide excess phenanthroline) and 2 mls of ammonium acetate buffer (35). (Phenanthroline is itself a potent inhibitor (7) of electron transport.) After adding 50 µl of a 2 M NH_4F solution to mask color produced by complexed Fe(III) (29), samples were diluted to 10 mls with distilled water and centrifuged at 3000xg for 20-30 minutes in a model RC-3B Sorvall centrifuge. Centrate color was immediately assayed spectrophotometrically at λ = 510 nm. Preliminary work in this lab showed that ε_{510} for the Fe(II)-(phenanthroline)$_3$ complex is 1.11×10^4 $(M\text{-cm})^{-1}$.

Inhibitor Description

Relevant information pertaining to individual chemical inhibitors is summarized in Table 1. The primary sites of inhibitor activity are indicated in Figure 10.

Results

Uninduced O_2 Utilization

Two examples of $[O_2]$ vs. time profiles are provided in Figure 2. Points of inhibitor (azide or quinacrine) addition correspond to discontinuities in the rate of oxygen disappearance $(-d[O_2]/dt)$. Stable respiration rates were reestablished within 1-2 minutes after the addition of inhibitors. In the absence of inhibitors, oxygen-utilization rates at the target optical density (A_{600} = 0.10 cm^{-1}) were approximately 5×10^{-4} M hr^{-1}.

Oxygen utilization rates, determined at various points along the $[O_2]$ vs. time profile, were used to calculate percent inhibition as a function of inhibitor concentration. Results are summarized in Figure

3. The effects of DCCD and DNP additions are not included due to their time-dependent mode of inhibition. Results indicate that all the inhibitors tested except rotenone are capable of completely inhibiting electron transport to molecular oxygen. HOQNO is almost an order of magnitude more effective than dicumarol, which was the next most potent respiratory inhibitor. With the exception of rotenone, sodium azide was the least effective; it was approximately an order of magnitude less potent than quinacrine dihydrochloride and almost 10^3 less effective than HOQNO.

After 40 minutes of exposure to 10^{-4} M DCCD, respiratory activity by P. ferrireductans was essentially nil (data not shown). Stimulation of O_2-utilization was not observed at any of the DNP levels investigated ($\geq 10^{-6}$ M). Respiration was inhibited to a significant degree at DNP concentrations $\geq 10^{-4}$ M (data not shown). Cell density was much less important than DNP concentration as a determinant of inhibitor efficiency.

O_2 Utilization by Induced Microorganisms

Representative oxygen-utilization data are also provided for the induced case of P. ferrireductans grown at low oxygen tension (Figure 3). It is apparent that cells grown at low oxygen concentrations are considerably less sensitive than uninduced cells to all respiratory inhibitors tested.

Iron Reduction (uninduced and induced cases)

Dissimilative iron reduction by induced cells was unaffected by DCCD ($\leq 10^{-4}$ M). Among uninduced cells, both DCCD and DNP were potent inhibitors of iron reduction (though somewhat less effective than during aerobic respiration).

Examples of kinetic data for Fe(III) reduction are provided in Figure 4. These and similar, unplotted results are summarized in dose-response curves (Figure 5) which are similar to those generated for aerobic respiration. The effect of rotenone on dissimilative iron reduction was not tested.

Comparison of Figures 3 and 5 indicates that, in general, the reagents used in this study are less effective inhibitors of electron transport to Fe(III) than to molecular oxygen. Neither cyanide nor azide appears to inhibit dissimilative iron reduction appreciably, while quinacrine, dicumarol and HOQNO are all less efficient when Fe(III) is electron acceptor.

No general trend is apparent from a comparison of iron reduction inhibition among uninduced versus induced cells. When cyanide or azide is present, inhibition efficiency appears to be independent of the iron-reduction competence of the cells. While HOQNO and dicumarol are more effective among uninduced cells, the reverse is true for quinacrine inhibition.

CO Inhibition (uninduced and induced cells)

Constitutive iron reductase was completely inhibited by CO treatment although the inducible system seemed unaffected.

Whole-Cell Spectra

Reduced-minus-oxidized spectra corresponding to induced and uninduced, whole-cell suspensions are provided as Figure 6. In both curves, strong maxima are apparent at 550 and 521 nm; there are inflections near 512 and 528 nm. In the Soret region, there is a strong peak at 420 nm and trough at about 382 nm. Differences between the two Figure 6 spectra include the appearance in the induced culture

of (i) elevated levels of cytochrome expression and (ii) a 630-nm peak and 646-nm trough.

Discussion

Inhibition of O_2 Utilization (uninduced case)

The data of Figure 3 are consistent with the postulated mechanisms by which specific inhibitors interfere with electron transport to molecular oxygen. Assuming that (i) successive electron transfer reactions are governed by Michaelis-type kinetics, and (ii) inhibitors block electron transport by binding at a single site, the kinetics of electron transport can be reduced to two simplified cases:

(a) A site of inhibition is also the rate-limiting step for electron transport in the absence of inhibitor.

(b) An inhibitor acts at a site other than the rate-limiting site or enzyme. Case (a) would hold, for example, if (i) electron transport were limited at the dehydrogenase level and quinacrine dihydrochloride were inhibitor or (ii) respiration rate limits were imposed by cytochrome oxidase and inhibition were by sodium azide or cyanide. Case (b) would hold for all inhibitors if the uninhibited respiration rate were limited to the rate of dissipation of proton-motive force.

The mathematics of these two situations is fundamentally different at low inhibitor levels since, in case (b), some level of inhibitor addition can be tolerated without diminishing the overall (observed) respiration rate. In case (a), any level of inhibitor binding would, in theory, lower the observed rate.

When the inhibitor acts on the rate-limiting enzymatic reaction:

$$\frac{d\{e^-\}}{dt} \equiv \phi = k_1 E_{red} \qquad (1)$$

where $\frac{d\{e^-\}}{dt}$ is the rate of electron transport, E_{red} is the concentration of reduced enzyme (i.e., prepared to transfer an electron), and k_1 is the pseudo first-order rate constant for electron transfer between successive carriers. We have assumed that electron-transport <u>from</u> the active site is rate-limiting. The same mathematical form would result were transport <u>to</u> the critical enzyme rate-limiting.

In the presence of inhibitor, a balance on enzyme yields:

$$E_T = E_{red} + E_{ox} + [EI] \qquad \text{where}$$

E_T is total enzyme concentration,

E_{ox} is the concentration of enzyme in its <u>oxidized</u> form, and

[EI] is the concentration of enzyme-inhibitor complex (inactive enzyme).

When electron transport is limited at this step, $E_{ox} << E_{red}$ and

$$E_T \cong E_{red} + [EI] \qquad (2)$$

At equilibrium, the concentration of enzyme bound to inhibitor conforms to

$$K_I = \frac{[EI]}{E_{red} \cdot I} \qquad \text{where} \qquad (3)$$

I is the bulk concentration of inhibitor, and

K_I is the association constant for enzyme and inhibitor.

Combining (2) and (3) we obtain:

$$E_{red} \cong \frac{E_T}{1 + K_I \cdot I}$$

and if:

$E_T = k_2\theta$, where $\theta \equiv$ cell density, then

$$\phi = \frac{k_3}{1 + K_I \cdot I} \qquad (4)$$

for experiments run at a single cell density. Note that K_I retains its physical significance, and k_3 is a combination of physical constants ($k_1 \cdot k_2 \cdot \theta$).

By inverting both sides of expression (3) and multiplying by ν_o, the uninhibited O_2-utilization rate:

$$\frac{\nu_o}{\phi} = \frac{\nu_o}{k_3} + \frac{\nu_o K_I}{k_3}[I] \qquad (5)$$

From equation (5), a plot of (ν_o/ϕ) versus inhibitor concentration (Figure 7) will yield estimates of ν_o/k_3 (intercept) and K_I (slope/intercept). It should be noted that at <u>high</u> concentrations of

inhibitors, which are known to interfere with electron transport to oxygen, transport past the site of inhibition is always rate-limiting. Departures from model predictions are expected at low inhibitor concentrations.

Fitted kinetic parameters are summarized in Table 2. When substituted back into equation (5), these permit prediction of inhibitor efficiency as a function of concentration. Such predictions are compared to experimental observations in Figure 8 (CN^-, quinacrine). Results support the general validity of the model. The analysis was extended to inhibition by N_3^-, dicumarol, and HOQNO with similar results.

At high inhibitor concentration, predictions are generally lower than observed inhibition rates, perhaps due to secondary effects arising from loss of cellular energy-generation capacity. At low inhibitor concentrations, results are less consistent. When model predictions are higher than observations (e.g., inhibition by quinacrine), the inhibitor probably acts at a site which does not control the (uninhibited) rate of electron transport. Quinacrine and azide appear to fit this pattern, as indicated by ν_o/k_3 values which exceed unity. Nothing more can be stated with confidence relative to the source of kinetic limits in the uninhibited case. However, since all intercept values are close to unity, we are encouraged to suspect that cellular production of electron transport chain components is well regulated -- that no component is enormously overproduced or underproduced to the extent that it limits the uninhibited rate of electron transfer.

O_2 Utilization in Induced Cultures

In preliminary experiments (results not shown) it was observed that aerobic respiration capacity is significantly enhanced by prolonged growth at low oxygen tension. Enhancement could result from induction of branches within the electron transport chain, similar to induction of an alternate cytochrome oxidase in Escherichia coli (5), and Pseudomonas putida (28). This hypothesis is supported by inhibition studies, which show that induced cells are less susceptible to inhibition by cyanide and azide than are cells grown at near-saturation oxygen levels. More direct evidence is provided by reduced-minus-oxidized spectra: reduced cytochrome oxidase d has a characteristic spectral peak near 632 nm; in its oxidized form it absorbs in the range 647-652 nm (25). Spectral characteristics induced under low oxygen tension (Figure 6) are consistent with this pattern, offering evidence on behalf of an induced aerobic electron transport branch. Cytochrome oxidase d is relatively resistant to CN^- inhibition (25) due to poor CN^- binding characteristics and provides competitive advantages under low-O_2 conditions (due to high O_2-affinity relative to other cytochrome oxidases).

Figure 9 permits a more detailed comparison of inhibition by cyanide versus HOQNO in cultures of P. ferrireductans grown at low oxygen tension. The figure contains profiles of O_2-utilization rate as a function of oxygen concentration at several inhibitor concentrations. Although respiration rate was sensitive to HOQNO concentration, O_2-utilization rate is essentially a constant (independent of O_2 concentration in the range shown) at each inhibitor concentration. This would be expected when the inhibitor acts at a site other than

cytochrome oxidase (i.e., transfer from cytochrome oxidase to O_2 is not rate limiting). In direct contrast, electron transport in the presence of cyanide is sensitive to oxygen concentration (Figure 9b). At CN^- concentrations below 4×10^{-5} M, there is no apparent loss in electron transport due to inhibitor addition, indicating that uninhibited respiration is not limited at the level of the cytochrome oxidase. (This idea is supported by the apparent independence of rate on O_2 concentration at low cyanide levels.) At higher inhibitor levels, a dependence on dissolved oxygen concentration is evident. The similarity of the slopes for these curves suggests that the electron transport chain in these cells is branched. One of these branches is completely inhibited at cyanide levels approaching 3×10^{-3} M, while the other appears to be less sensitive to CN^- inhibition (either due to lower CN^- or higher O_2 affinity). Since uninduced cells are completely inhibited by 10^{-3} M CN^- (Figure 3), it is possible that the branched chain develops in response to low-O_2 concentration. Enhancement of cytochrome d relative to other cytochrome oxidases has been observed in a variety of gram-negative heterotrophs in response to low-O_2 or related conditions (25).

Differences in susceptibility of alternative cytochrome oxidases to inhibition by CN^- or N_3^- can be explained as follows: The active site on one of the terminal oxidases lies in a relatively hydrophobic region of the folded protein which excludes highly solvated CN^- (i.e., $CN(H_2O)_n^-$), while permitting access of O_2 via diffusion. Alternatively, resistance could be conferred by much higher affinity for O_2.

Other explanations for Figure 9 data are possible. The slopes of individual curves in Figure 9b could result from time-dependent cyanide activity. Alternatively, one might postulate the existence of a single cytochrome oxidase whose electron-transfer kinetics are affected by competitive cyanide binding in the available apical coordination site of an iron-porphyrin prosthetic group. The latter explanation would not account for complete cyanide inhibition among uninduced cells.

From Figure 3 it is evident that respiratory inhibitors are less potent in cultures of induced cells than among their uninduced counterparts, perhaps due to a general strengthening of the respiratory chain in cells grown at low oxygen tension. Augmentation of cytochrome densities in response to low-O_2 conditions is evident in reduced-minus-oxidized spectra (Figure 6). It is also possible that induction of parallel respiratory chain elements (branched chains) at low dissolved oxygen concentration accounts for resistance to inhibitors. Both quinacrine and dicumarol appear capable of completely inhibiting respiration in both induced and uninduced cultures, perhaps because transport chain branch points lie downstream from the sites of inhibition by these drugs.

In no case did DNP, an uncoupler of electron transport and oxidative phosphorylation, stimulate respiration. Acceleration of electron transport would be expected only if transport kinetics were limited by the rate of dissipation of proton-motive force. Membrane distortion or steric interference due to DNP addition may be responsible for the drug's observed inhibitory effect. Lack of dependence of inhibitory efficiency on cell number suggests that a low

percentage of the added chemical is taken up by cells at DNP concentrations near 10^{-4} M.

Dissimilative Iron Reduction

Rates of dissimilative iron reduction in both induced and uninduced cultures of P. ferrireductans show little dependence on cyanide or azide addition, suggesting that the terminal oxidase(s) for dissimilative iron reduction is not a cytochrome. Thermodynamic considerations indicate that dissimilative iron reduction is less energetically favorable than aerobic respiration (1). Thus, transport to ferric iron via an abbreviated electron transport chain is consistent with results of both inhibitor studies and energetic calculations.

The induction of iron-reduction capacity among cells grown at low oxygen tension (Figure 1) has already been noted. Electron transport to Fe(III) among induced cells (A_{600} = 0.25 cm^{-1}) is 6-8 times faster than iron reduction in similar, uninduced cultures. Thus, inhibitor efficiency curves by themselves (Figure 5) do not permit comparison of electron transport rates in induced and uninduced cultures. Nevertheless, inhibition studies support a qualitative picture of transport to Fe(III) in these cases. HOQNO, dicumarol, and carbon monoxide are effective inhibitors of iron reduction in cells grown at high oxygen tension but have only a minor impact on induced cultures. The implication is that cells grown at low oxygen concentration transport electrons to Fe(III) via two branches. Because the induced path is not substantially affected by HOQNO or dicumarol, it may be considerably shorter than the constitutive branch (refer to Figure 10). On the other hand, quinacrine, which is a more potent inhibitor in

induced cells, appears to act on both pathways, ahead of the branch point present under low-oxygen conditions. Because electron transport is more rapid among induced cells, quinacrine inhibition is more effective in such cultures.

Comparison of rates of electron transfer to O_2 and Fe(III) among uninduced cells indicates that anaerobic respiration is limited by ferri-reductase activity. This limitation may disappear among induced cells. In such cultures (Figure 1) it is evident that rates of electron transfer to Fe(III) can approach those of aerobic respiration.

Since DCCD inhibits electron transport in uninduced but not induced cells, oxidative phosphorylation is probably linked to iron reduction via the constitutive pathway only. This result supports the physical picture of an induced and constitutive branch for electron transfer to Fe(III). The more energetically favorable branch (constitutive) is linked to oxidative phosphorylation via proton translocation; the shorter (induced) branch serves only as a sink for cellular reducing power.

Summary

Taken together, inhibition data support the postulated mechanism for electron transport and inhibition in P. ferrireductans which is summarized in Figure 10. Differences in inhibition pattern and energetic considerations indicate that ferric iron is not reduced by a cytochrome oxidase in uninduced cells.

A second cytochrome oxidase and a second iron reductase are induced in P. ferrireductans by prolonged growth under low-oxygen conditions. Induced cells can utilize oxygen somewhat faster than their uninduced

counterparts. Iron reduction by induced cells is almost an order of magnitude faster than measured rates in uninduced cultures.

Although the constitutive iron reductase in P. ferrireductans is completely inhibited by 10^{-4} M DCCD after 60 minutes, the induced system is unaffected. Iron reduction by the induced system is probably not linked to oxidative phosphorylation, while the constitutive iron reductase does drive ATP synthesis.

Because electron transfer to dissolved oxygen is apparently more rapid than to Fe(III) among uninduced cells, we conclude that iron reduction is limited kinetically at the level of Fe(III) reductase. When dissolved oxygen is the electron acceptor, the interpretation is less clear. Our analysis indicated that neither azide nor quinacrine acts at the rate-limiting site in uninduced cells. Several potential control points remain along the postulated transport chain; control could also reside with metabolic processes ahead of the electron transport chain or in limits imposed by dissipation of transmembrane proton-motive force. Since respiration is not accelerated by DNP (uncoupler) addition, control by the proton-motive force seems less likely.

Striking differences in inhibition pattern (and electron transport chain configuration) between induced and uninduced cells are related to the dissolved oxygen level in the growth medium. The importance of controlling environmental variables while investiating bacterial metabolism/energetics is apparent.

Acknowledgement

The authors are grateful to Dr. D. W. S. Westlake of the Department of Microbiology, University of Alberta, Canada, for generously providing the microorganism used in this study, Pseudomonas sp. 200. Taxonomic studies leading to species identification were undertaken and reported on by Drs. Westlake and C. O. Obuekwe; we have changed its name to Pseudomonas ferrireductans (upon request of a reviewer) with some reluctance. Hopefully its new name will provide the microorganism with deserved distinction without causing excessive confusion.

This work was supported by United States Department of Energy Contract No. DE-AS03-83ER13125 administered within the Division of Advanced Energy Projects, Office of the Basic Energy Sciences. We appreciate the support and encouragement of Drs. Ryszard Gajewski and Duane L. Barney.

Our thanks to Ms. Sandy Brooks, Ms. Elaine Granger, and Ms. Nancy Tomer of the Caltech Environmental Sciences and Engineering staff for secretarial and drafting assistance during manuscript preparation.

LITERATURE CITED

1. Arnold, R. G., T. M. Olson, and M. R. Hoffmann. 1986. Kinetics and mechanism of dissimilative Fe(III) reduction by Pseudomonas sp. 200. Biotech. Bio. (in press).
2. Brock, T. D. and J. Gustafson. 1976. Ferric iron reduction by sulfur- and iron-oxidizing bacteria. Appl. Environ. Microbiol. 32: 567-571.
3. Futai, M. and H. Kanazawa. 1983. Structure and function of proton-translocating adenosine triphosphatase (F_0F_1): biochemical and molecular biological approaches. Microbiol. Rev. 47: 285-312.
4. Ghiorse, W. C. and H. L. Ehrlich. 1976. Electron transport components of the MnO_2 reductase system and the location of the terminal reductase in a marine Bacillus. Appl. Environ. Microbiol. 31: 977-985.
5. Haddock, B. A. and C. W. Jones. 1977. Bacterial respiration. Bact. Rev. 41: 47-99.
6. Harold, F. M. 1970. Antimicrobial agents and membrane function. p. 45-104. In: A. H. Rose and J. F. Wilkinson (eds.), Adv. Microb. Physiol. Vol. 4. Academic Press, New York.
7. Heinen, W. 1971. Inhibitors of electron transport and oxidative phosphorylation. p. 383-393. In: J. R. Norris and D. W. Ribbons (eds.), Methods in Microbiology, Vol. 6A. Academic Press, New York.

8. Hewitt, E. J. and D. J. D. Nicholas. 1963. Cations and anions: inhibitions and interactions in metabolism and in enzyme activity. p. 311-427. In: R. M. Hochster and J. H. Quastel (eds.), Metabolic Inhibitors. A Comprehensive Treatise. Vol. II. Academic Press, New York.

9. Hinkle, P. C. and R. E. McCarty. 1978. How Cells Make ATP. Scient. Amer. 228, No. 3: 104-123.

10. Jones, C. W. 1983. Bacterial Respiration and Photosynthesis. American Society of Microbiology, Washington, D.C.

11. Kashket, E. R. 1982. Stoichiometry of the H^+-ATPase of growing and resting, aerobic Escherichia coli. Biochem. 21: 5534-5538.

12. Kino, K. and S. Usami. 1982. Biological reduction of ferric iron by iron- and sulfur-oxidizing bacteria. Agric. Biol. Chem. 46: 803-805.

13. Kurimura, Y., R. Ochiai, and N. Matsuura. 1968. Oxygen oxidation of ferrous ions induced by chelation. Bull. Chem. Soc. Japan 41: 2234-2239.

14. Lemberg, R. and J. Barrett. 1973. Cytochromes. Academic Press, New York.

15. McLaughlin, S. 1972. The mechanism of action of DNP on phospholipid bilayer membranes. J. Membr. Bio. 9: 361-372.

16. Mitchell, P. 1961. Coupling of phosphorylation to electron and hydrogen transfer by a chemi-osmotic type of mechanism. Nature 191: 144-148.

17. Mitchell, P. 1966. Chemiosmotic coupling in oxidative and photosynthetic phosphorylation. Biol. R. 41: 445-502.

18. Mitchell, P. and J. Moyle. 1967. Acid-base titration across the membrane system of rat-liver mitochondia. Catalysis by uncouplers. Biochem. J. 104: 588-599.

19. Munch, J. C. and J. C. G. Ottow. 1983. Reductive transformation mechanism of ferric oxides in hydromorphic soils. In: R. Hallberg (ed.), Environmental Biogeochemistry, Ecol. Bull. (Stockholm) 35: 383-394.

20. Obuekwe, C. O. 1980. Microbial corrosion of crude oil pipeline. Ph.D. dissertation, University of Alberta, Edmonton, Alberta, Canada.

21. Obuekwe, C. O. and D. W. S. Westlake. 1982. Effects of medium composition on cell pigmentation, cytochrome content, and ferric iron reduction in a Pseudomonas sp. isolated from crude oil. Can. J. Microbiol. 28: 989-992.

22. Obuekwe, C. O., D. W. S. Westlake, and F. D. Cook. 1981. Effect of nitrate ion on reduction of ferric iron by a bacterium isolated from crude oil. Can. J. Microbiol. 27: 692-697.

23. Pestka, S. 1975. Chloramphenicol. p. 370-395. In: J. W. Corcoran and F. E. Hahn (eds.), Antibiotics, Vol. III, Mechanism of action of antimicrobial and antitumor drugs. Springer-Verlag, New York.

24. Pongs, O. 1979. Chloramphenicol. p. 26-42. In: F. E. Hahn (ed.), Antibiotics, Vol. V-1, Mechanism of action of antimicrobial agents. Springer-Verlag, New York.

25. Poole, R. K. 1983. Bacterial cytochrome oxidases a structurally and functionally diverse group of electron-transfer proteins. Biochim. Biophys. Acta 726: 205-243.

26. Smith, L. 1968. The respiratory chain system of bacteria. p. 55-122. In: T. P. Singer (ed.), Biological oxidations. Interscience Publishers, New York.

27. Stryer, L. 1981. Biochemistry. W. H. Freeman and Co., San Francisco.

28. Sweet, W. J. and J. A. Peterson. 1978. Changes in cytochrome content and electron transport patterns in Pseudomonas putida as a function of growth phase. J. Bact. 133: 217-224.

29. Tamura, H., K. Goto, T. Yotsuyanagi, and M. Nagayama. 1974. Spectrophotometric determination of iron(II) with 1,10-phenanthroline in the presence of large amounts of iron(III). Talanta 21: 314-318.

30. Troshanov, E. P. 1968. Iron- and manganese-reducing microorganisms in ore-containing lakes of the Karelian Isthmus. Mikrobiol. 37: 934-940.

31. Troshanov, E. P. 1969. Conditions affecting the reduction of iron and manganese by bacteria in the ore-bearing lakes of the Karelian Isthmus. Mikrobiol. 38: 634-643.

32. White, D. C. and P. R. Sinclair. 1971. Branched electron-transport systems in bacteria. Adv. Microbiol. Physiol. 5: 173-211.

33. Wright, C. I. and J. C. Sabine. 1944. The effect of atabrine on the oxygen consumption of tissues. J. Biol. Chem. 155: 315-320.

34. Wolfe, A. D. 1975. Quinacrine and other acridines. p. 203-233. In: J. W. Corcoran and F. E. Hahn (eds.), Antibiotics, Vol. III, Mechanism of Action of Antimicrobial and Antitimor Agents. Springer-Verlag, New York.

35. American Public Health Association, American Water Works Association, Water Pollution Control Federation. 1981. Standard Methods for the Examination of Water and Wastewater, 15th edition.

Figure Captions

Figure 1. Uninhibited O_2-utilization and iron-reduction rates "normalized" on the basis of culture optical density (λ = 600 nm, cm^{-1}).

Figure 2. Inhibition of aerobic respiration in cultures of Pseudomonas ferrireductans (A_{600} = 0.10 cm^{-1}) by azide and quinacrine. Cultures were grown at near-saturation O_2 concentrations (uninduced).

Figure 3. Inhibition of electron transport to molecular oxygen as a function of inhibitor concentration in cultures of Pseudomonas ferriductans (A_{600} = 0.10 in uninduced experiments; A_{600} = 0.25 in induced experiments.) Q,q -- quinacrine dihydrochloride; D,d -- dicumarol; H,h -- HOQNO; C,c -- NaCN; N,n -- NaN_3; R -- rotenone; (solid lines, upper-case letters -- cells grown at high O_2; dotted lines, lower-case letters -- cells grown at low O_2 tension).

Figure 4a. Inhibition of Fe(III) reduction by NaN_3 in uninduced cultures of Pseudomonas ferrireductans (A_{600} = 0.25, cells grown at near-saturation O_2 levels.)

Figure 4b. Inhibition of Fe(III) reduction by HOQNO in uninduced cultures of Pseudomonas ferrireductans (A_{600} = 0.25, cells grown at near-saturation O_2 levels.)

Figure 5. Inhibition of electron transport to ferric iron as a function of inhibitor concentration in cultures of Pseudomonas ferrireductans (A_{600} = 0.25 in all experiments.) Q,q -- quinacrine dihydrochloride; D,d -- dicumarol; H,h -- HOQNO; C,c -- NaCN; N,n -- NaN_3 (solid lines, upper-case letters -- cells grown at high O_2; dotted lines, lower-case letters -- cells grown at low O_2 tension).

Figure 6. Reduced-minus-oxidized spectra corresponding to induced and uninduced cultures of Pseudomonas ferrireductans. Cells were harvested at A_{600} = 0.75 (cm^{-1}).

Figure 7. Reciprocal rate of O_2 utilization (normalized) versus inhibitor concentration. Data points are from inhibition curves (Figure 3). Slope/intercept information forms the basis of parameter estimates summarized in Table 2.

Figure 8. Comparison of predicted and observed inhibition of aerobic respiration rates in (uninduced) cultures of Pseudomonas ferrireductans (A_{600} = 0.10.)

Figure 9a. HOQNO inhibition of aerobic respiration in induced culture of Pseudomonas ferrireductans (A_{600} = 0.25, cm^{-1}.)

Figure 9b. Cyanide inhibition of aerobic respiration in induced culture of Pseudomonas ferrireductans (A_{600} = 0.25, cm^{-1}.)

Figure 10. Schematic representation of electron transport to O_2 or Fe(III) and transport inhibition in Pseudomonas ferrireductans (Fig. 10a) Notes:

1. O_2 utilization and iron reduction are both blocked by 10^{-4} M DCCD.
2. DNP is a strong inhibitor of O_2 utilization. Fe(III) reduction is inhibited less efficiently.
3. Order of inhibitor efficiency:
   a) Aerobic respiration - HOQNO > dicumarol ≅ CN^- > quinacrine > N_3^-.
   b) Iron reduction - HOQNO > dicumarol > quinacrine (N_3^- and CN^- are not effective inhibitors; CO inhibits completely.)
4. At A_{600} = 0.25 (cm^{-1}) (culture optical density) electron transport proceeds at (uninhibited) rates of 8×10^{-5} M e^-/min to O_2 and 9×10^{-6} M e^-/min to Fe(III).

(Fig 10b) Notes:

1. Dotted lines represent induced electron transport pathways.
2. Iron reduction is unaffected by DCCD.

3. Order of inhibitor efficiency in cells:

   a) Aerobic respiration - HOQNO > CN^- > dicumarol > quinacrine > N_3^-.

   b) Iron reduction - only quinacrine has a major effect on electron transport in the concentration ranges tested.

4. At A_{600} = 0.25 (cm^{-1}) (culture optical density) electron transport proceeds at (uninhibited) rates of 1.3×10^{-4} M e^-/min to O_2 and 6.6×10^{-5} M e^-/min to Fe(III).

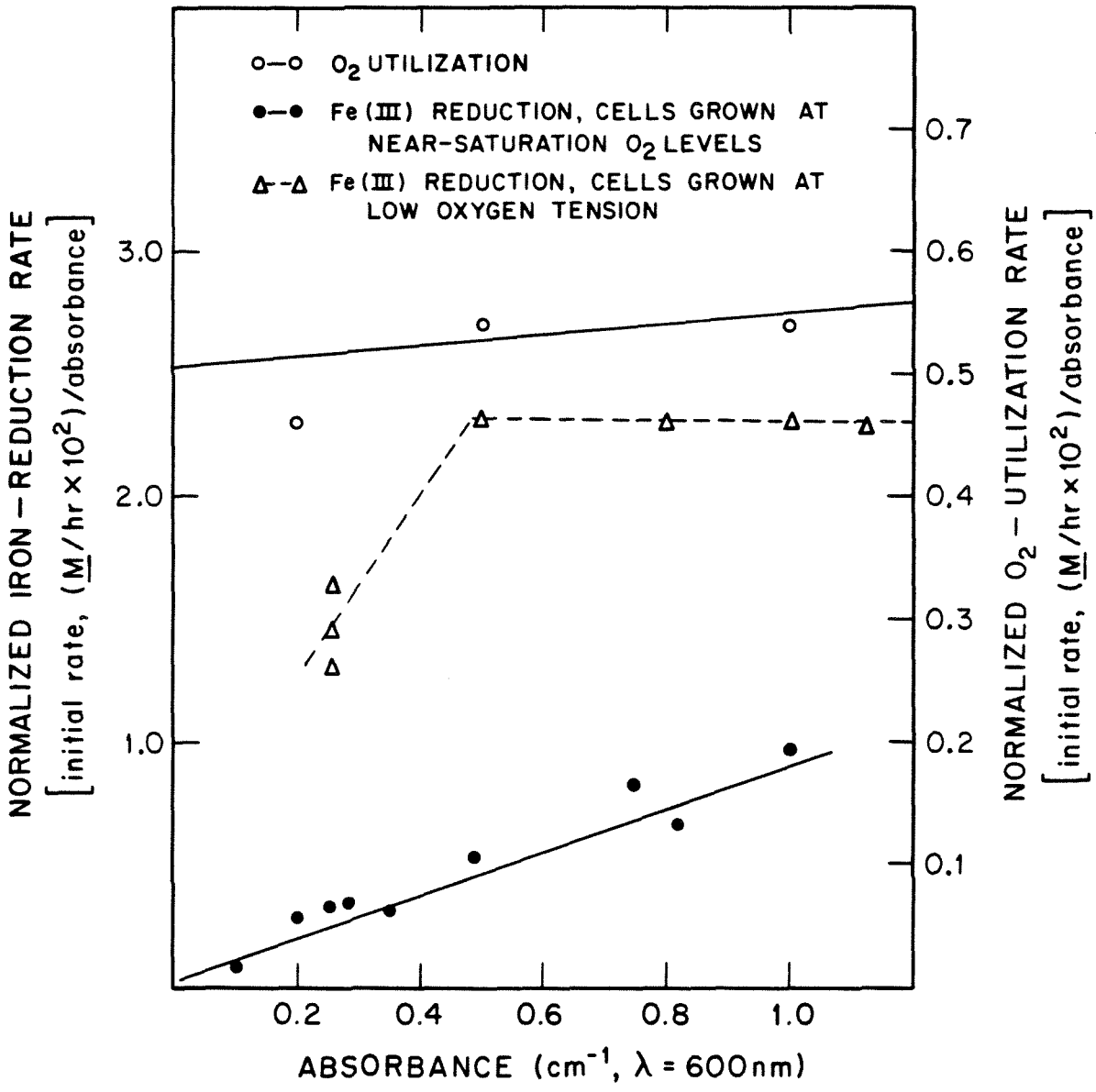
o—o O2 UTILIZATION
●—● Fe(III) REDUCTION, CELLS GROWN AT NEAR-SATURATION O2 LEVELS
Δ--Δ Fe(III) REDUCTION, CELLS GROWN AT LOW OXYGEN TENSION
NORMALIZED IRON-REDUCTION RATE [initial rate, (M/hr x 10²)/absorbance]
NORMALIZED O2-UTILIZATION RATE [initial rate, (M/hr x 10²)/absorbance]
3.0
2.0
1.0
0.7
0.6
0.5
0.4
0.3
0.2
0.1
0.2
0.4
0.6
0.8
1.0
ABSORBANCE (cm⁻¹, λ = 600nm)

Figure 1

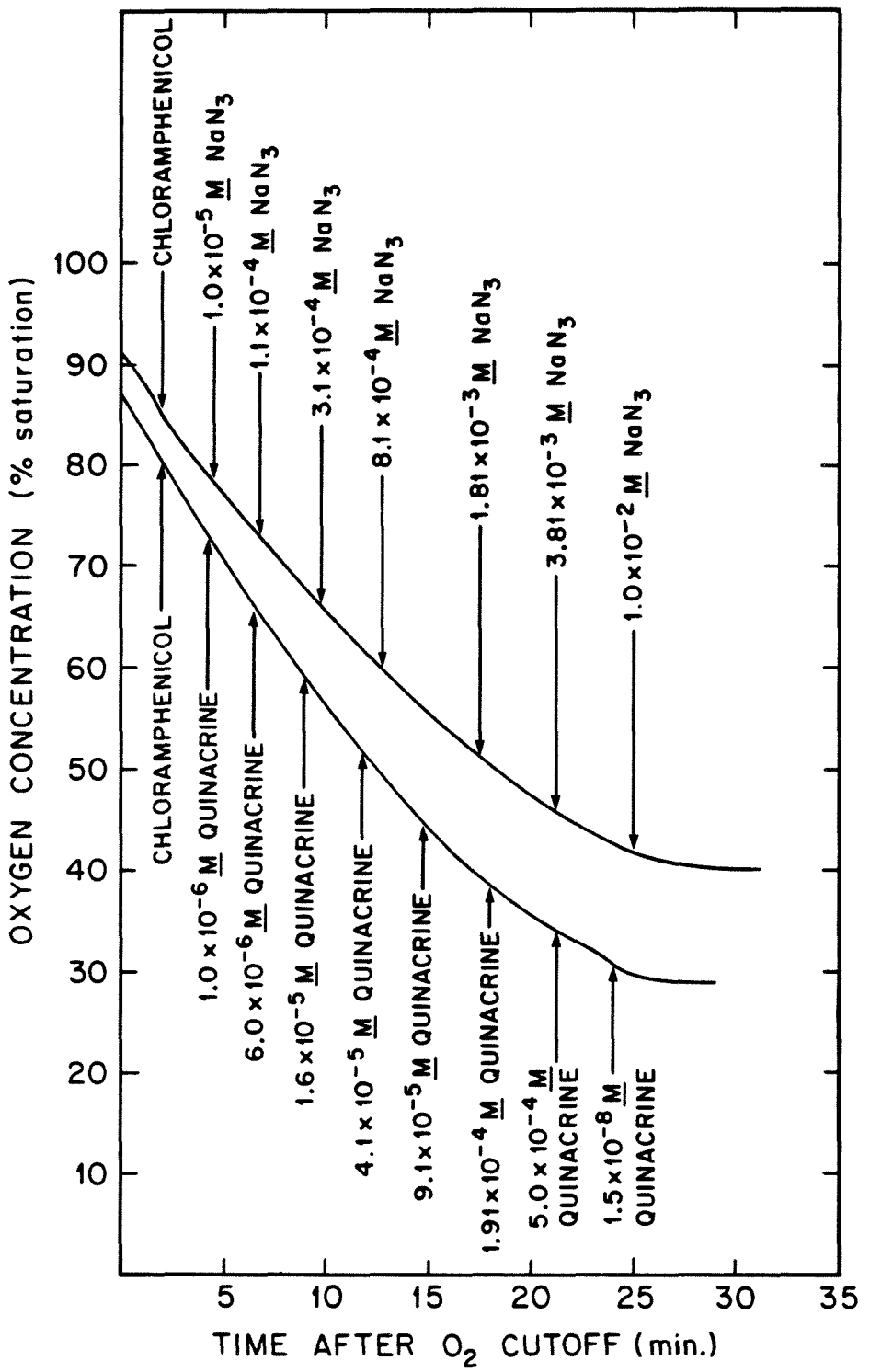
OXYGEN CONCENTRATION (% saturation)
100
90
80
70
60
50
40
30
20
10
5
10
15
20
25
30
35
TIME AFTER O_2 CUTOFF (min.)
CHLORAMPHENICOL
1.0×10^{-5} M NaN_3
1.1×10^{-4} M NaN_3
3.1×10^{-4} M NaN_3
8.1×10^{-4} M NaN_3
1.81×10^{-3} M NaN_3
3.81×10^{-3} M NaN_3
1.0×10^{-2} M NaN_3
CHLORAMPHENICOL
1.0×10^{-6} M QUINACRINE
6.0×10^{-6} M QUINACRINE
1.6×10^{-5} M QUINACRINE
4.1×10^{-5} M QUINACRINE
9.1×10^{-5} M QUINACRINE
1.91×10^{-4} M QUINACRINE
5.0×10^{-4} M QUINACRINE
1.5×10^{-8} M QUINACRINE

Figure 2

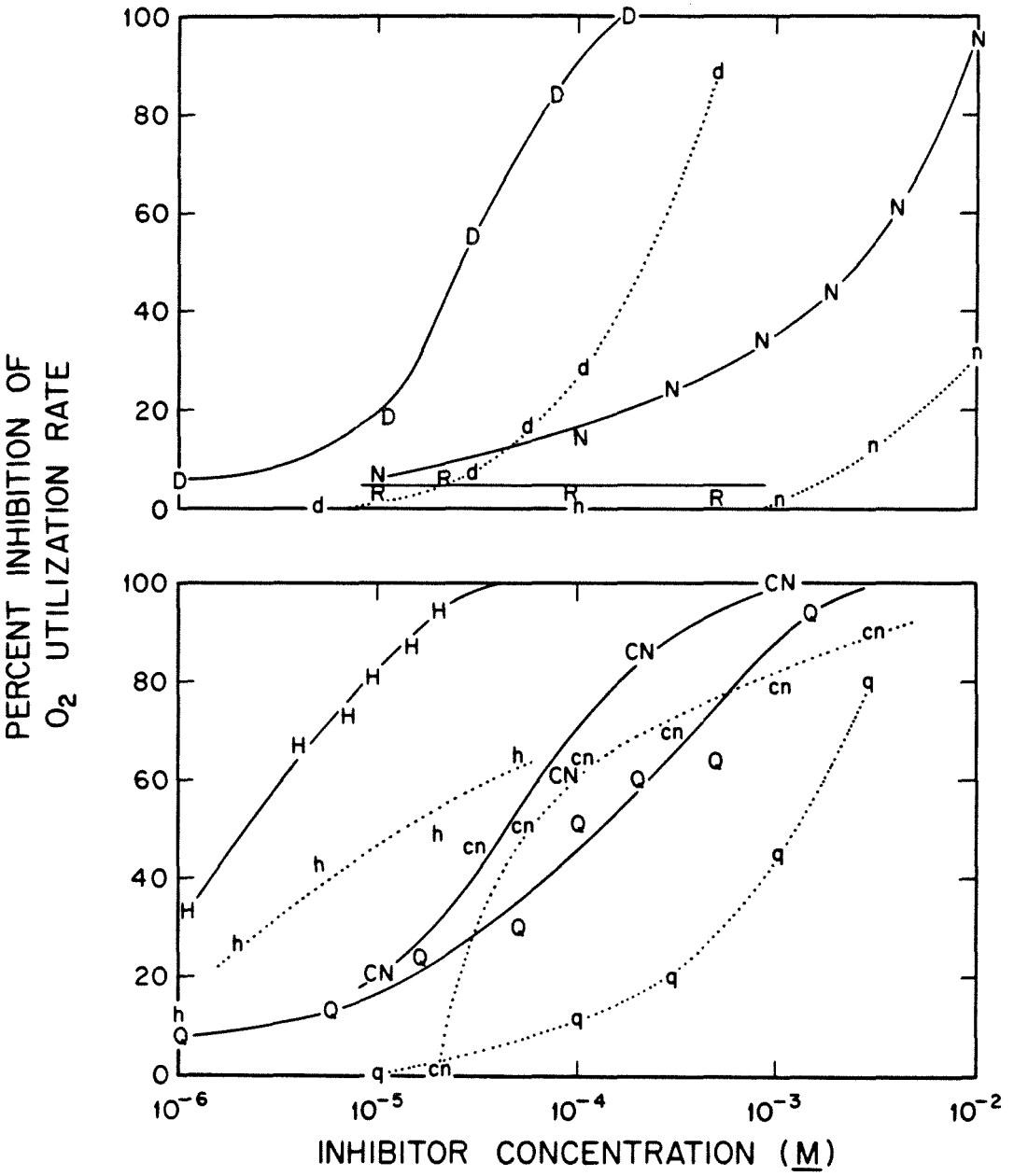
PERCENT INHIBITION OF O_2 UTILIZATION RATE
100
80
60
40
20
0
D
d
N
R
n
H
h
CN
cn
Q
q
10^{-6}
10^{-5}
10^{-4}
10^{-3}
10^{-2}
INHIBITOR CONCENTRATION (M)

Figure 3

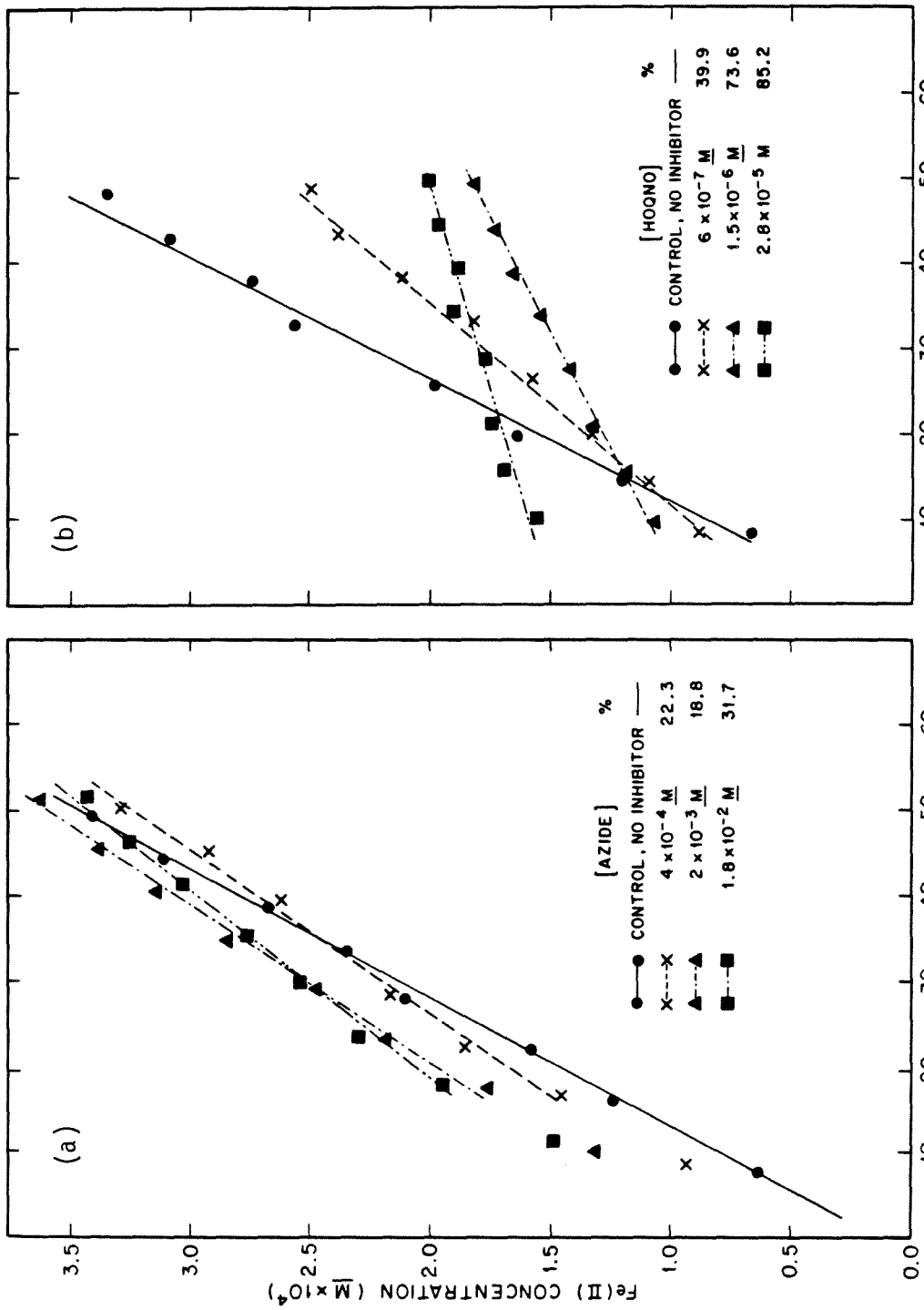
(a)
(b)
Fe(II) CONCENTRATION (M x 10⁴)
TIME AFTER Fe(III) ADDITION (min.)
[AZIDE]
%
CONTROL, NO INHIBITOR
4 x 10⁻⁴ M 22.3
2 x 10⁻³ M 18.8
1.8 x 10⁻² M 31.7
[HOQNO]
%
CONTROL, NO INHIBITOR
6 x 10⁻⁷ M 39.9
1.5 x 10⁻⁶ M 73.6
2.8 x 10⁻⁵ M 85.2

Figure 4

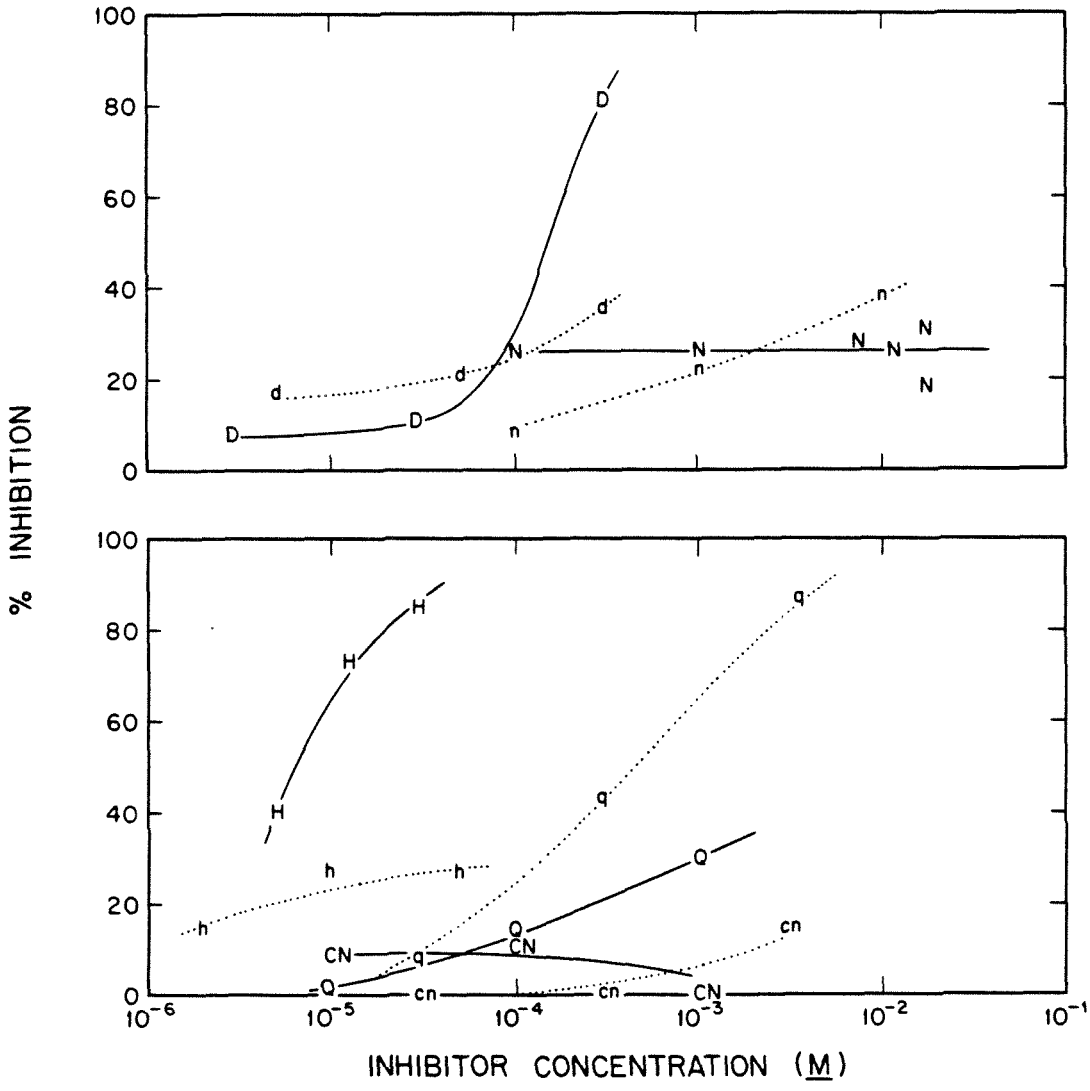
% INHIBITION
100
80
60
40
20
0
D
d
N
n
H
h
q
Q
CN
cn
=Q
10^{-6}
10^{-5}
10^{-4}
10^{-3}
10^{-2}
10^{-1}
INHIBITOR CONCENTRATION (M)

Figure 5

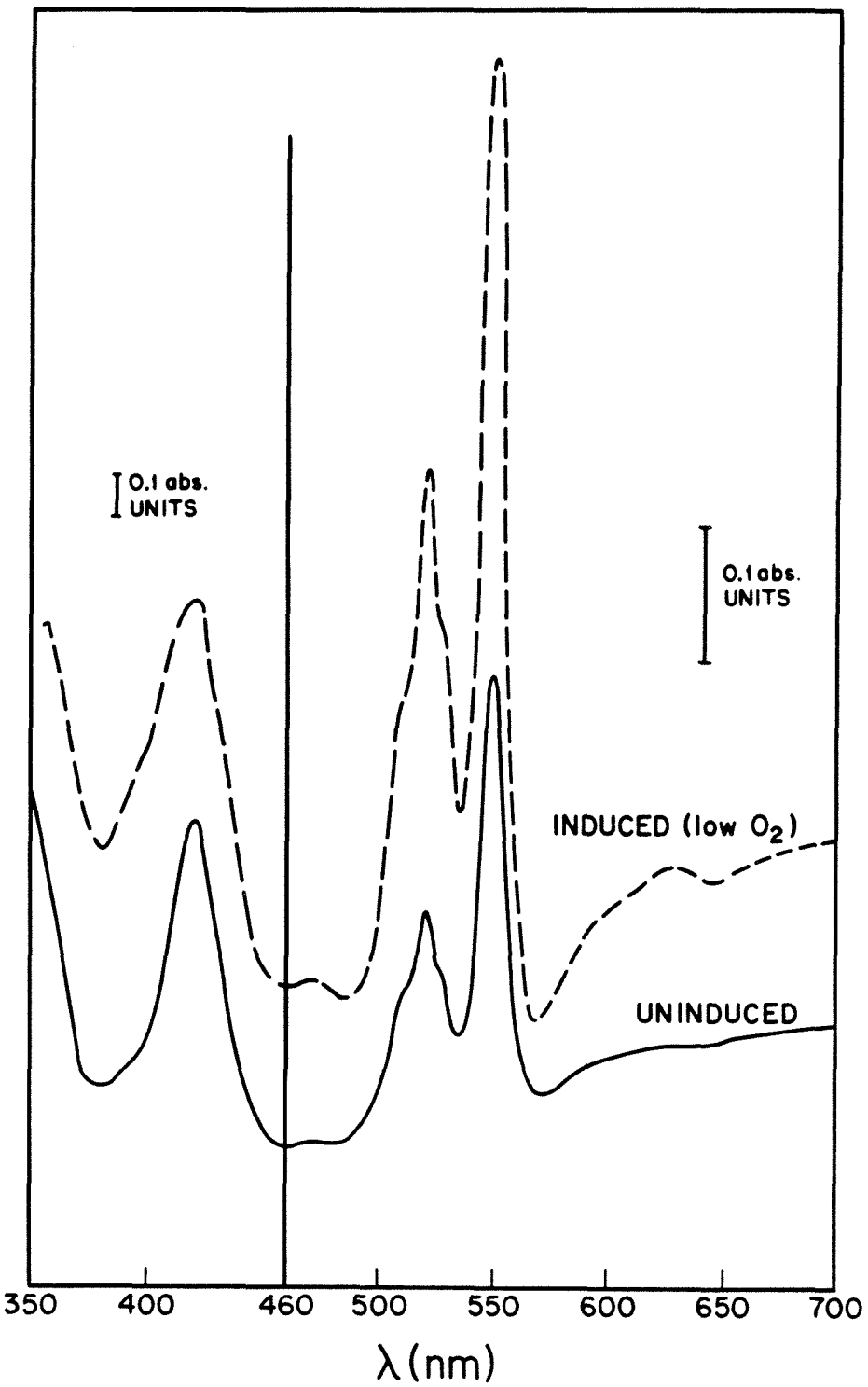
0.1 abs. UNITS
0.1 abs. UNITS
INDUCED (low O_2)
UNINDUCED
350
400
460
500
550
600
650
700
λ(nm)

Figure 6

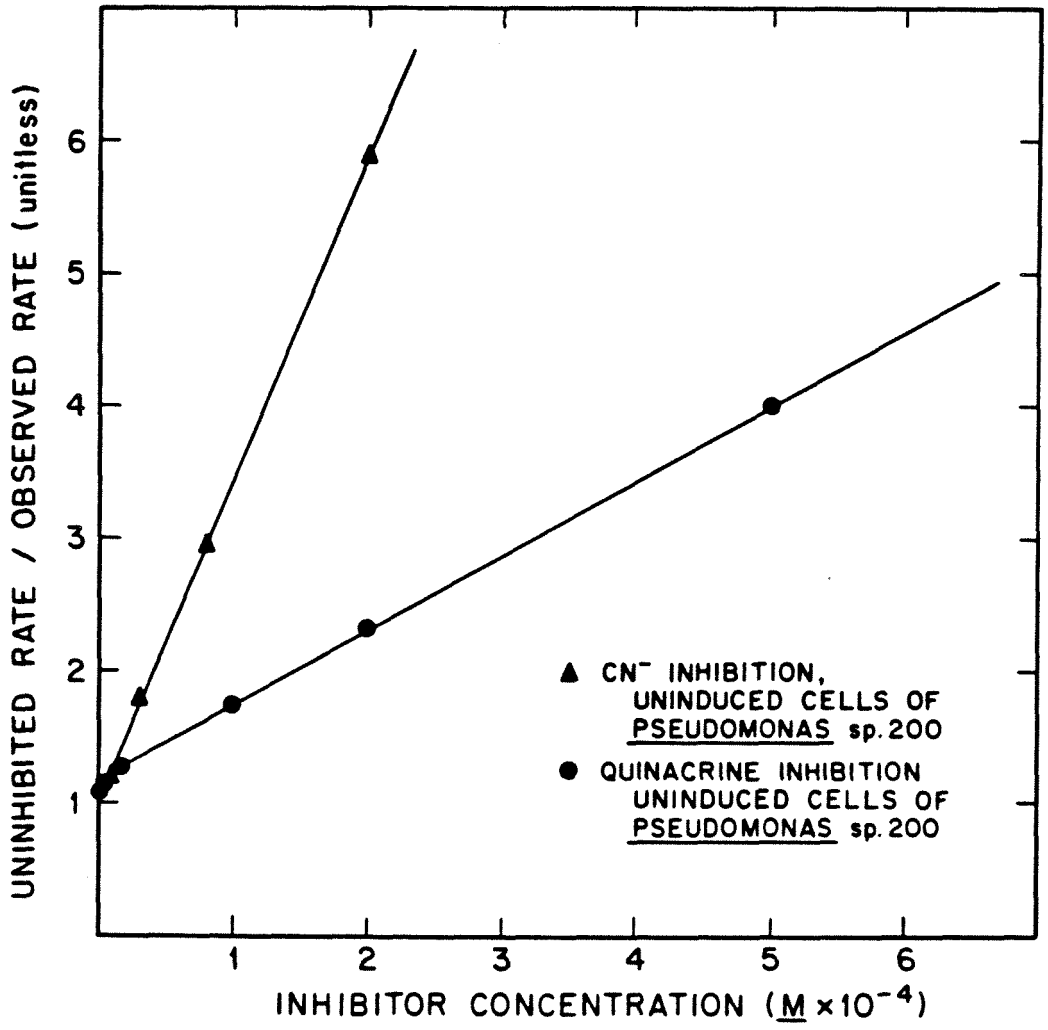
UNINHIBITED RATE / OBSERVED RATE (unitless)
1
2
3
4
5
6
1
2
3
4
5
6
INHIBITOR CONCENTRATION (M x 10⁻⁴)
▲ CN⁻ INHIBITION, UNINDUCED CELLS OF PSEUDOMONAS sp. 200
● QUINACRINE INHIBITION UNINDUCED CELLS OF PSEUDOMONAS sp. 200

Figure 7

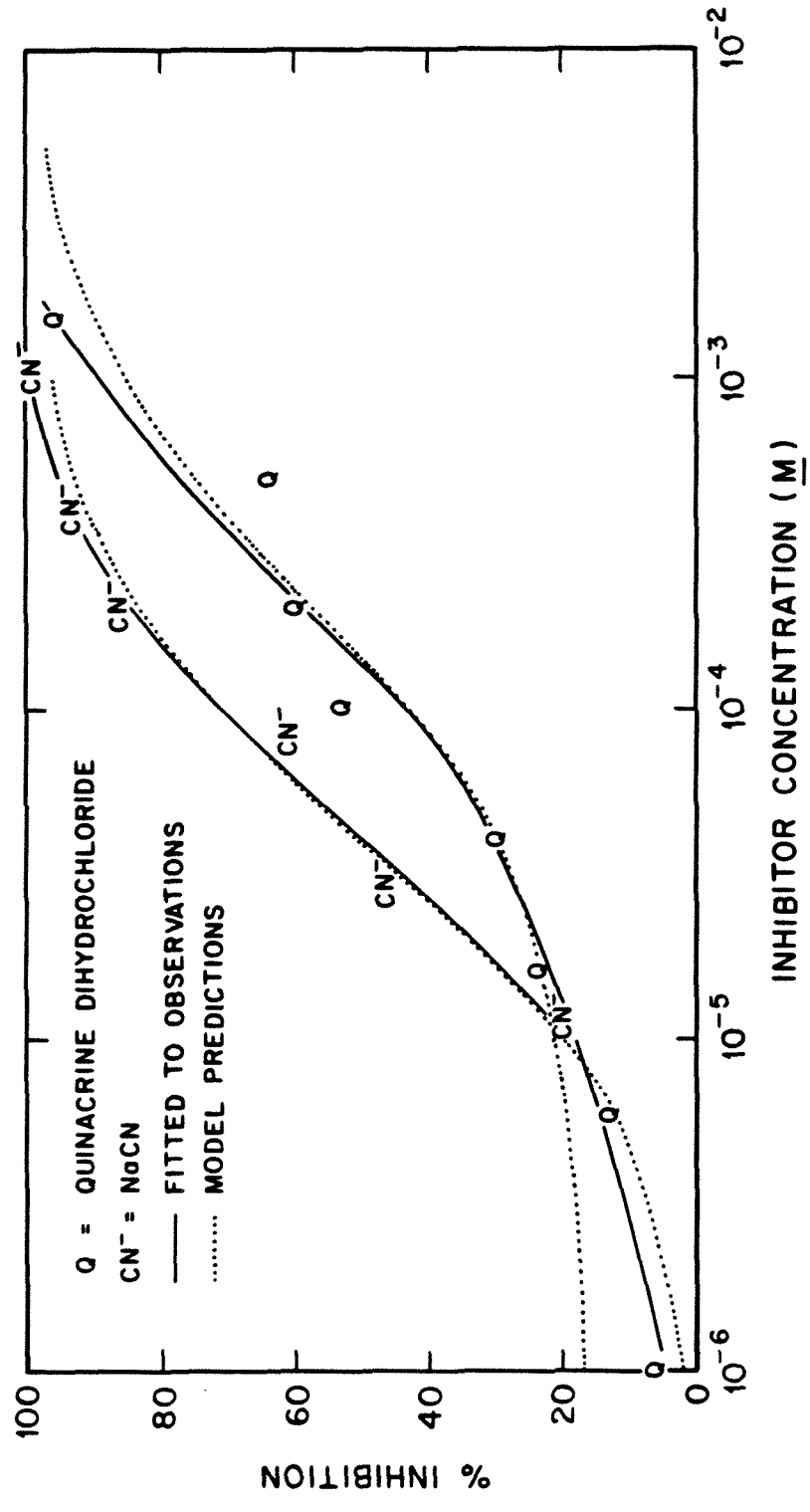
Q = QUINACRINE DIHYDROCHLORIDE
CN⁻ = NaCN
FITTED TO OBSERVATIONS
MODEL PREDICTIONS
% INHIBITION
INHIBITOR CONCENTRATION (M)
100
80
60
40
20
0
10⁻⁶
10⁻⁵
10⁻⁴
10⁻³
10⁻²
Q
CN⁻

Figure 8

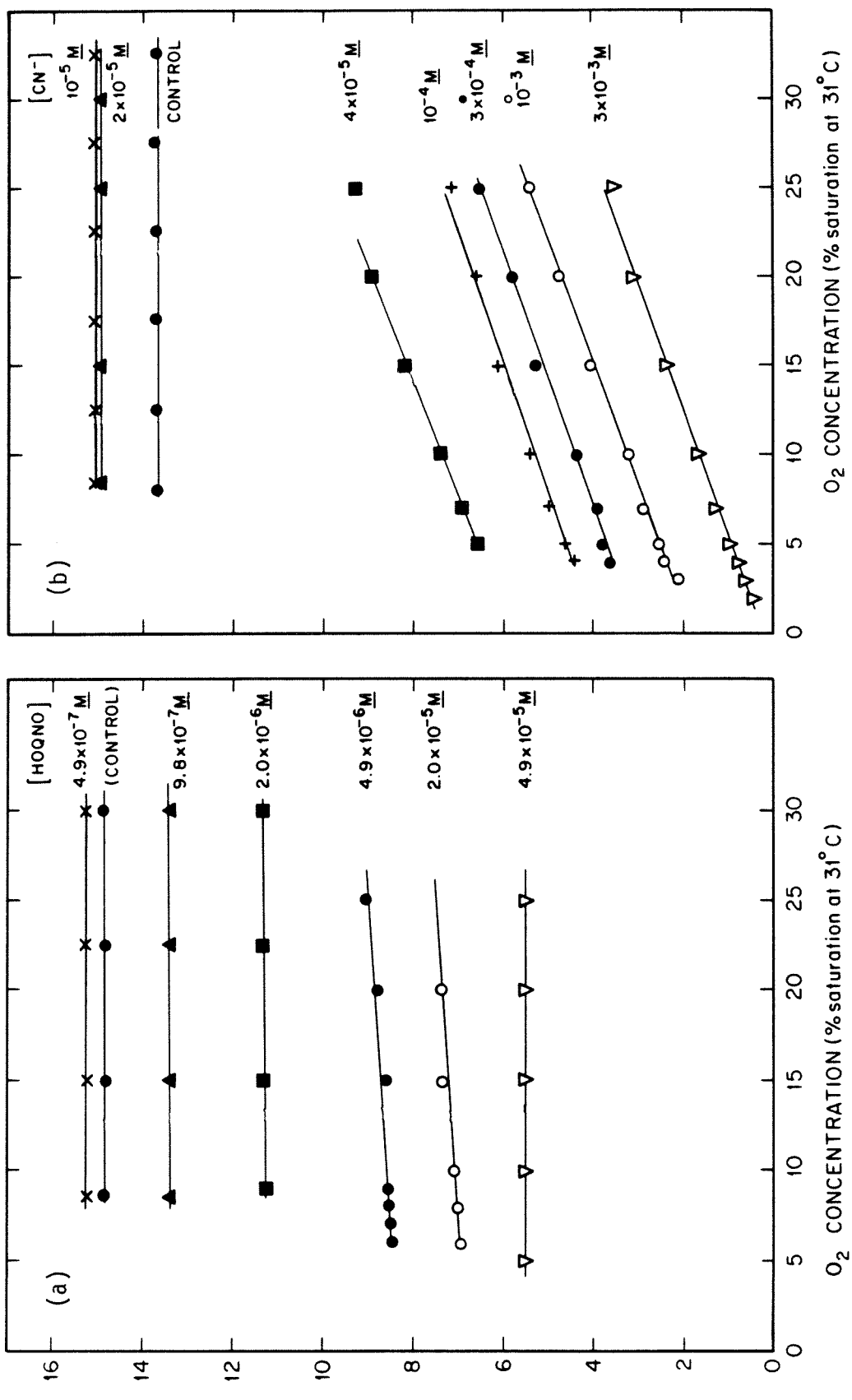
RATE OF O2 UTILIZATION (%sat./min.)
(a)
[HOQNO]
4.9x10-7 M
(CONTROL)
9.8x10-7 M
2.0x10-6 M
4.9x10-6 M
2.0x10-5 M
4.9x10-5 M
O2 CONCENTRATION (% saturation at 31° C)
(b)
[CN-]
10-5 M
2x10-5 M
CONTROL
4x10-5 M
10-4 M
3x10-4 M
10-3 M
3x10-3 M
O2 CONCENTRATION (% saturation at 31° C)

Figure 9

(a) CELLS GROWN AT NEAR-SATURATION O_2 LEVEL (uninduced)

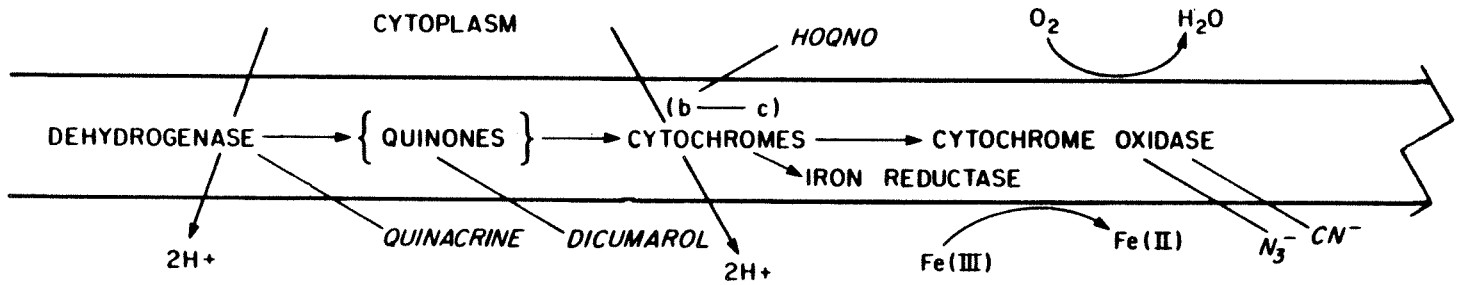

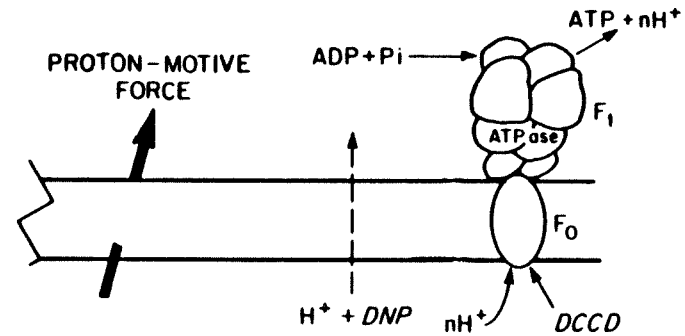

DCCD DICYCLOHEXYLCARBODIIMIDE
DNP 2,4 DINITROPHENOL
HOQNO 2-n-HEPTYL-4-HYDROXYQUINOLINE-N-OXIDE
(INHIBITORS IN ITALICS)

(b) CELLS GROWN AT LOW O_2 LEVEL (induced)

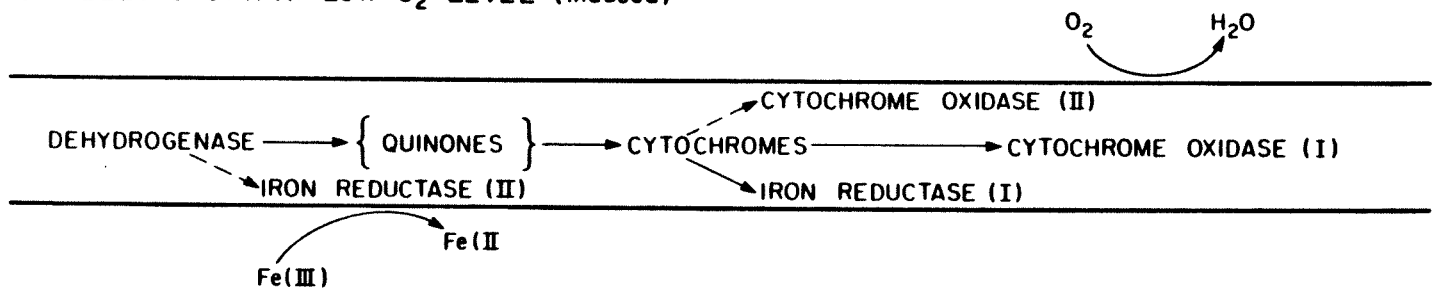

Figure 10

Table 1. Respiration-inhibiting drugs used in these experiments.

Drug	Concentration Range	Source	Solvent	Inhibition Site	Refs.
Rotenone (1,2,12,12a-Tetrahydro-8,9-dimethoxy-2-(1-methylethenyl)-[1]benzopyrano [3,4-6]furo[2,3-h] [1]-benzopyran-6(6aH)-one)	10^{-5}-$5x10^{-3}$ M	Sigma	Acetone	NADH dehydrogenase	(6)
Quinacrine dihydrochloride (N^4-(6-chloro-2-methoxy-9-acridinyl-N',N'-diethyl-1,4 pentanediamine dihydrochloride)	10^{-6}-$4x10^{-3}$ M	Sigma	H_2O	Flavins (dehydrogenases)	(33, 34)
Dicumarol (3,3'-Methylene-bis-(4-hydroxy-2H-1-benzopyran-2-one)	10^{-6}-$5x10^{-5}$ M	Sigma	Pyridine	Quinones	(4)
2-Heptyl-4-hydroxyquinoline-N-oxide (HOQNO)	$6x10^{-7}$-$5x10^{-5}$ M	Sigma	Ethanol	Cytochrome b	(20)
Sodium cyanide (NaCN)	10^{-5}-$3x10^{-3}$ M	Mallinkrodt	H_2O	Cytochrome oxidase	(8, 27)
Sodium azide (NaN_3)	10^{-5}-$2x10^{-2}$ M	Sigma	H_2O	Cytochrome oxidase	(8, 27)
Dicyclohexyl-carbodiimide (DCCD)	10^{-6}-10^{-4} M	Sigma	Acetone	F_0 subunit of ATPase (blocks oxidative phosphorylation)	(3)
2,4 Dinitrophenol (DNP)	10^{-6}-$5x10^{-4}$ M	Sigma	Acetone	uncoupler (renders cytoplasmic membrane permeable to H^+)	(6, 15, 18)

Chloramphenicol (2,2-dichloro-N-[2-hydroxy-1-hydroxymethyl)-2-(4-nitrophenyl)ethyl] acteamide)	$2x10^{-4}$-$5x10^{-4}$ M	Sigma	Ethanol	(bacterio- static agent -- blocks protein synthesis) (23, 24)

Notes:
(1) Inhibitors were dissolved in as little solvent as possible to minimize the chances of secondary effects attributable to solvent addition. Controls were run to ensure that solvents were not themselves inhibitory at levels added.

(2) Preliminary experiments (not shown) indicated that chloramphenicol addition to 0.46 mM did not impede dissimilative iron reduction. A minor, temporary reduction in O_2-utilization rate was observed, however.

(3) DCCD blocks proton retranslocation by binding specifically to the F_o subunit of membrane-bound ATPase. Inhibition follows due to proton-motive back pressure.

(4) DNP uncouples electron transport from oxidative phosphorylation by rendering the cytoplasmic membrane permeable to hydrogen ions and thereby dissipating proton-motive force.

Table 2. Summary of Fitted Kinetic Parameters for Inhibition of Electron Transport by Respiratory Poisons (uninduced cells, $A_{600} = 0.1$).

General model: $\frac{\nu_o}{\phi} = \frac{\nu_o}{k_3} + \frac{\nu_o K_I}{k_3} [I]$

(see text for explanation of symbols)

Inhibitor	$\frac{\nu_o}{k_3}$ (intercept, unitless)	K_I (slope/intercept, M^{-1})
quinacrine dihydrochloride	1.2	4.6×10^3
dicumarol	0.8	7.5×10^4
HOQNO	0.9	5.0×10^5
azide	1.2	2.9×10^2
cyanide	1.0	2.5×10^4

Note: Intercept predictions higher than one arise when low-level inhibitor additions are less effective than expected. It is likely that the active site of such inhibitors does not provide the rate-limiting step for uninhibited electron transport. Because none of the predictions is much greater than unity, it is probable that individual electron transport steps are kinetically in balance -- i.e., that there is no severe bottleneck in the electron transport chain prior to inhibitor addition.

Chapter 6

KINETICS AND MECHANISM (PART II)

6.1 Introduction

The chapter is a compilation of experiments not described elsewhere whose collective results bear upon the kinetics and mechanism of dissimilative iron reduction in Pseudomonas sp. 200. Investigation of electron transport chain composition is also described. Experiments fall into two categories:

(i) investigation of electron-transport kinetics when alternative electron acceptors (Fe(III) and O_2) are present in solution simultaneously; and

(ii) exploration of the Pseudomonas sp. 200 cytochrome content including changes attributable to low-oxygen conditions during growth.

6.2 Simultaneous Reduction of Dissolved Oxygen and Fe(III)

6.2.1 Background

Thermodynamic analysis (Chp. 2) has shown that considerably less energy is available from dissimilative iron reduction than from aerobic respiration, a mechanism which directs electron transport to cytochrome oxidase when alternate electron acceptors are present in solution would benefit the microorganism immensely. For reasons explained previously, Fe(III) provides a kinetically significant alternative to aerobic respiration (in terms of overall rate of electron transport) among cells induced for ferrireductase (again, see Chapter 5) when sufficiently high concentrations of soluble Fe(III) are provided. Results of kinetic

experiments in which Fe(III) is provided in soluble, complexed form (Chapter 3) indicated that among induced cells electron transport to Fe(III) is ultimately limited by the same kinetic factors as aerobic respiration.

Detection of dissimilative iron reduction in the presence of molecular oxygen is complicated by rapid autoxidation of Fe(II) in the neutral pH range (Sung and Morgan, 1980), particularly in the presence of chelating agents such as NTA (Kurimura et al., 1968). To overcome this problem, 3-(2-pyridyl)-5,6-bis-(4-phenylsulfonic acid)-1,2,4-triazine (ferrozine) was used as a ferrous iron trap following the procedure of Carter (1971). Ferrozine forms a stable 1:3 (Fe:ferrozine) bidentate complex with ferrous iron on a time scale faster than that of autoxidation. Stookey (1970) indicated that the stability constant for ferrozine-Fe(II) association is too large to measure via conventional methods. Thus, in the presence of excess ferrozine, essentially all ferrous iron should be complexed. The ferrozine-Fe(II) complex is magenta in color; ε_{562} for the complex is 2.8×10^4 $(\underline{M} \cdot cm)^{-1}$.

6.2.2 Procedures

The overall procedure followed in ferrozine-trap experiments was very similar to that of iron-reduction and O_2-utilization work described in Chapter 5. That is, Pseudomonas sp. 200 was grown in 1.5-liter batch cultures to a target optical density of $A_{600} = 0.15$ (cm^{-1}) under either high-O_2 or low-O_2 (inducing) conditions. At that point, chloramphenicol was added to a final concentration of 2.3×10^{-4} $\underline{M}$ to halt protein synthesis and bacterial growth. NTA and $FeCl_3 \cdot 6H_2O$ were added to final

concentrations of 1.86×10^{-3} M; addition of 2.79×10^{-3} M ferrozine provided excess ligand during the time frame of the biological reaction.

During O_2-utilization measurements, molecular oxygen was initially present at levels which maximized cytochrome oxidase activity. Following interruption of airflow to the reactor, dissolved-oxygen was continuously monitored using the Ingold probe and meter (Chapter 5) provided with the Biostat M reactor. O_2-utilization rates were derived from tangents to the time-dependent O_2 profile.

For measurement of Fe(II), aliquots were periodically withdrawn from the Biostat M and quick-frozen in dry ice to halt the Fe(III) ----> Fe(II) conversion. Prior to spectrophotometric measurement of color intensity at λ = 562 nm, samples were quickly thawed and centrifuged for 5 minutes at 3000 xg in a Sorvall Model RC-3B refrigerated centrifuge (4°C).

6.2.3 Results and Conclusions

Preliminary experiments were run to see if ferrozine either (i) reduced Fe(III) chemically under experimental conditions or (ii) inhibited electron transport when added to aerobically respiring cultures of *Pseudomonas* sp. 200. In the abiotic iron-reduction experiment, 1.86×10^{-3} M $FeCl_3 \cdot 6H_2O$, 1.57×10^{-3} M NTA, and 1.78×10^{-3} M ferrozine were added to Westlake medium (Table 1, Chapter 3). O_2 was purged from solution with high-purity N_2 gas, and aliquots were periodically removed for measurement of A_{562}. Results (Figure 6.1) indicate that abiotic reduction of Fe(III) by ferrozine is slow (7.0×10^{-6} M-hr^{-1}) compared to biologically catalyzed rates (Chapter 3). When the experiment was repeated in the presence of dissolved oxygen, no iron

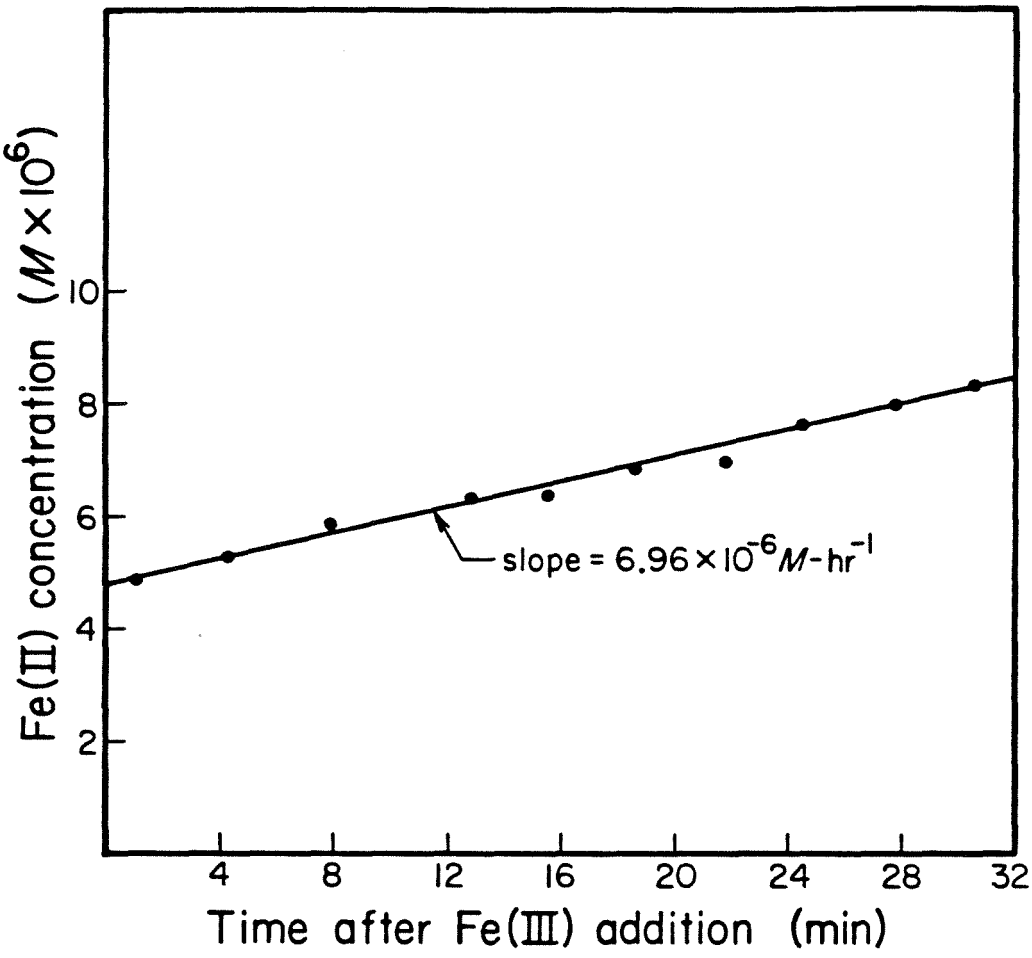

Figure 6.1 Abiotic iron reduction as a function of time in Westlake medium plus 1.86 x 10^{-3} M $FeCl_3$, 1.57 x 10^{-3} M NTA, and 1.78 x 10^{-3} M ferrozine. Dissolved oxygen was purged from the system with high-purity N_2(g).

reduction was observed. Furthermore, the measured rate of O_2-utilization among cells grown to A_{600} = 0.15 (cm^{-1}) under highly aerobic conditions (1.7×10^{-5} M $O_2 \cdot min^{-1}$) was similar to rates measured in the absence of ferrozine.

Duplicate experiments (Figure 6.2) using uninduced cultures (grown under highly aerobic conditions) indicated that: (i) in the presence of even small concentrations of dissolved oxygen, dissimilative iron reduction was slow. Expected rates of iron reduction (based on previous experiments, see Chapters 3 and 5) were not achieved until residual oxygen was purged from the medium; (ii) assuming that O_2 utilization involves a 4-electron transfer, the observed rate of electron transport to O_2 was an order of magnitude faster than electron transport to Fe(III) following O_2 exhaustion; (iii) experimental results were highly reproducible; and (iv) the presence of ferrozine in solution did not interfere with attainment of expected rates of dissimilative iron reduction among uninduced cultures of Pseudomonas sp. 200. Subsequent experiments (results not shown) indicated that the apparent relationship between the onset of high-rate iron reduction and initiation of the N_2 purge was almost certainly due to interference from molecular oxygen which was entrained from the reactor head space up to the point of $N_2(g)$ addition.

A similar experiment was carried out in an induced culture of Pseudomonas sp. 200 (grown at low oxygen tension). Fe(III), NTA, and ferrozine were again added at A_{600} = 0.15. Results are summarized in Figure 6.3. Once again it is apparent that dissimilative iron reduction proceeds after dissolved oxygen is exhausted. It was not necessary, however, to purge residual O_2 in order to achieve high-rate Fe(III)

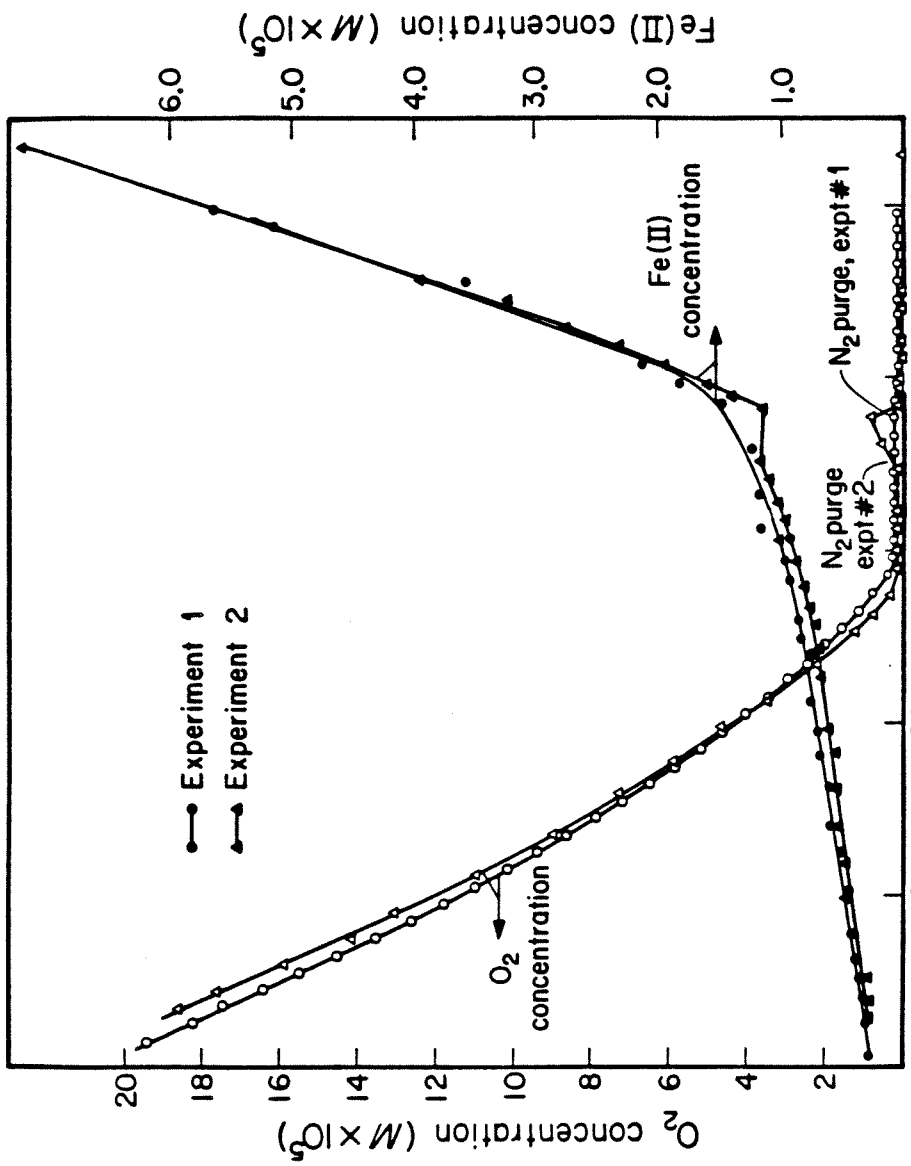

Figure 6.2 Duplicate ferrozine-trap experiments in which dissolved oxygen utilization and iron reduction were measured simultaneously. Cells were grown to A_{600} = 0.15 (cm^{-1}) under highly aerobic conditions prior to the introduction of high-level Fe(III), NTA, and ferrozine.

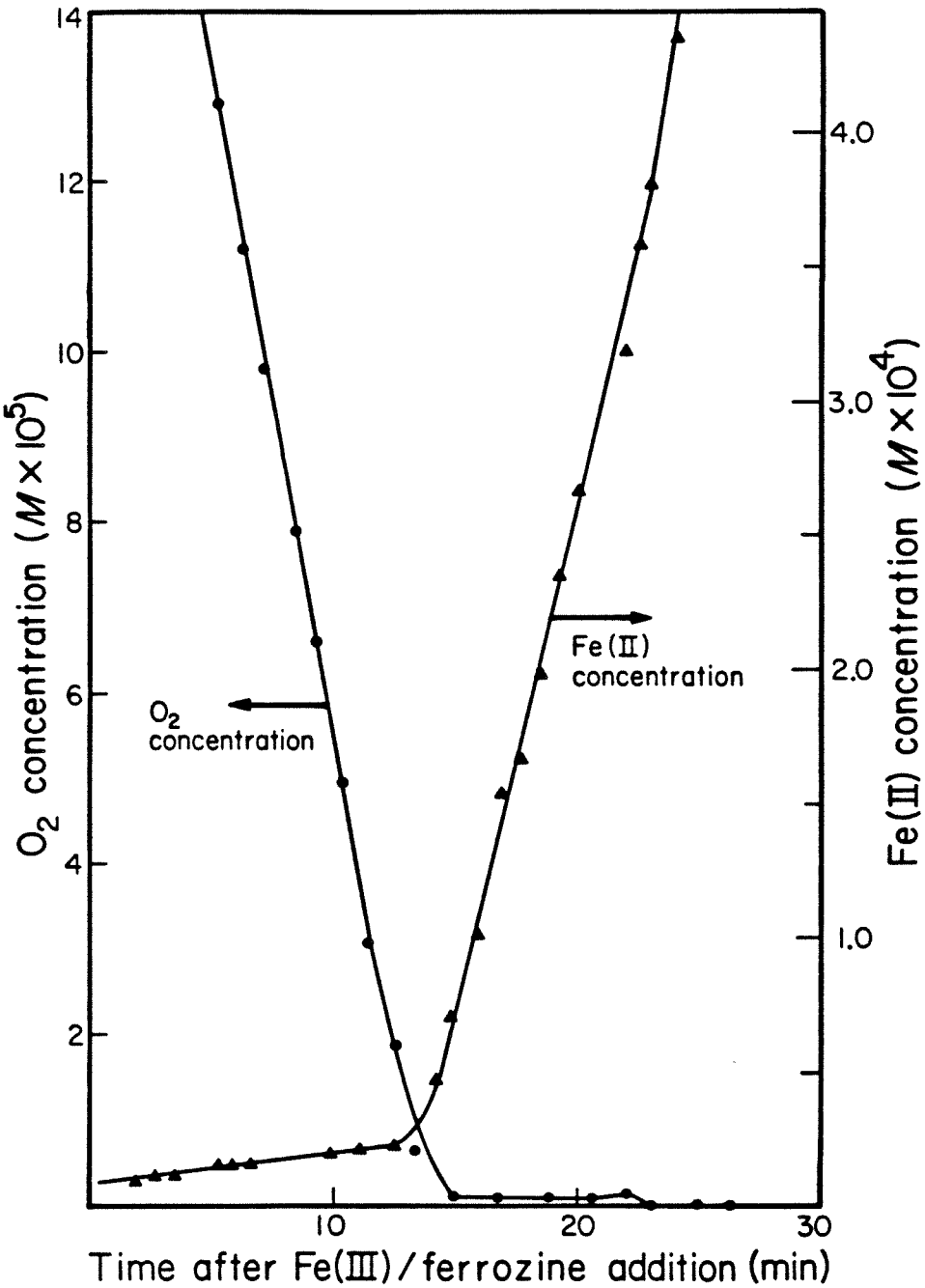

Figure 6.3 Simultaneous O_2 utilization and Fe(III) reduction in a pure, batch culture of Pseudomonas sp. 200 (A_{600} = 0.15, cm^{-1}) grown under low-O_2 (inducing) conditions. ([Fe_T] = 1.86 x 10^{-3} M; [NTA] = 1.86 x 10^{-3} M; [ferrozine] = 2.79 x 10^{-3} M).

reduction. At the fastest rates of iron reduction observed, electron transport to Fe(III) proceeds at essentially the same rate as aerobic respiration (again assuming a 4-electron transfer is required for O_2 ----> $2H_2O$). The estimated rate of electron transport to O_2 was 6.3 x 10^{-5} M $e^{-}\cdot min^{-1}$; that of dissimilative iron reduction was 5.3 x 10^{-5} M $e^{-}\cdot min^{-1}$. The difference is probably within experimental error.

Having established (i) the effectiveness of the ferrozine trap as a method for stabilizing and measuring Fe(II) in the presence of O_2 and (ii) the relationship between dissimilative iron reduction and O_2 concentration, it was possible to explore the effect of cyanide addition on simultaneous oxygen utilization and iron reduction. Experiments were carried out in the manner described above. Cells were aerobically grown to A_{600} = 0.15 at either high or low (inducing) oxygen levels. At the target optical density, Fe(III), NTA, and ferrozine were added to predetermined levels (see above), and O_2 concentration was manipulated in a manner consistent with experimental objectives. Cyanide was added incrementally at several points during the iron-reduction period.

Results of the first such experiment are summarized in Figure 6.4. Cells were grown at high oxygen concentration (uninduced). At the target optical density, the measured rate of O_2 utilization was 1.8 x 10^{-5} M$\cdot min^{-1}$. Prior to O_2 exhaustion and the onset of Fe(III) reduction, dissolved oxygen was restored to near-saturation levels, and CN^- was added to 7.14 x 10^{-5} M (first increment). Table 6.1 contains a brief summary of O_2-utilization-rate measurements (and percent inhibition) in relation to CN^- level. Fe(III) reduction rate, which remained essentially constant throughout the period of CN^- addition (up to the point at which dissolved oxygen was purged from solution), is

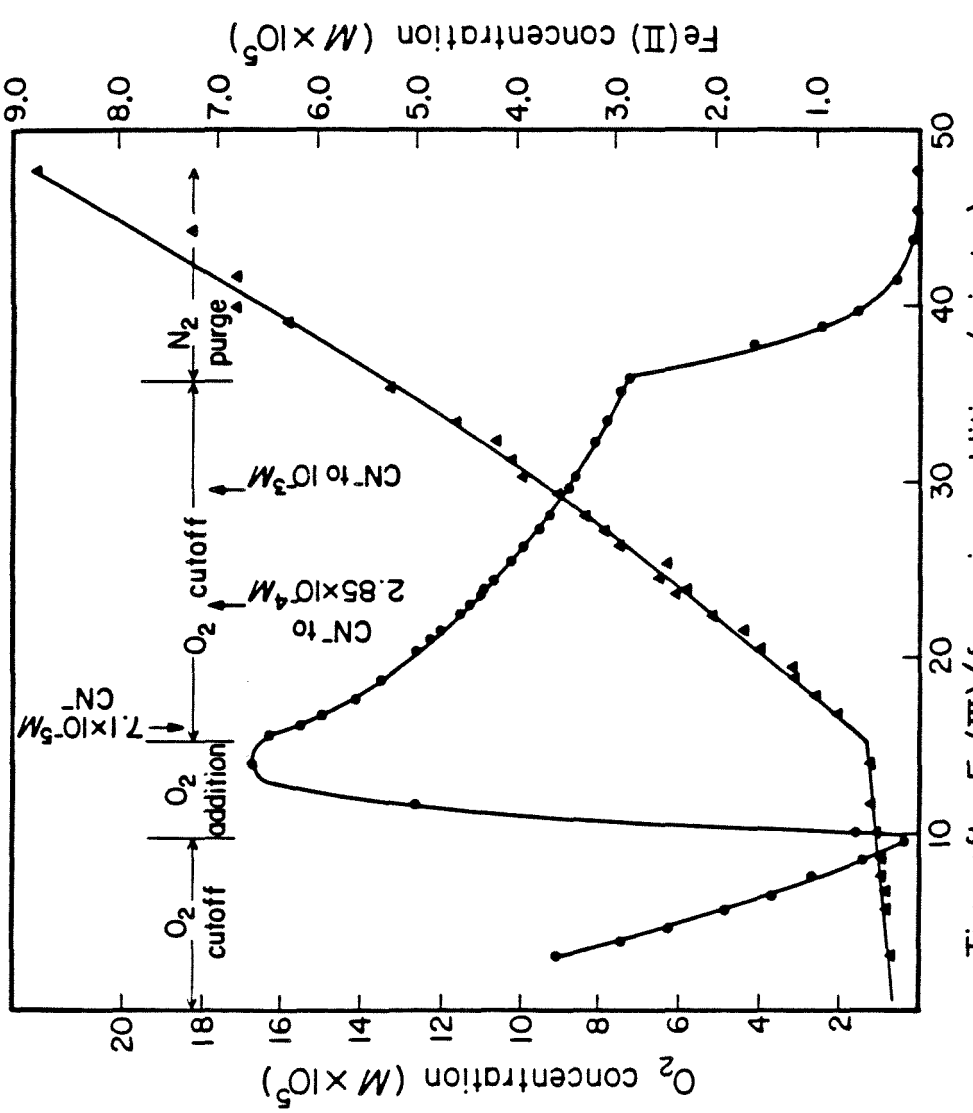

Figure 6.4 Simultaneous O_2 utilization and Fe(III) reduction as a function of CN^- and O_2 concentrations in an uninduced culture of Pseudomonas sp. 200 (A_{600} = 0.15 cm^{-1}). Iron reduction was measured in the presence of dissolved oxygen using ferrozine as an Fe(II) trap. ($[Fe_T]$ = 1.86 x 10-3 M; NTA = 1.86 x 10-3 M; [ferrozine] = 2.79 x 10-3 M).

Table 6.1 Simultaneous Measurements of O_2-utilization and Fe(III) Reduction as a Function of CN^- Concentration in an Uninduced Culture of Pseudomonas sp. 200. A_{600} = 0.15 (cm^{-1}).

$[CN^-]$(M)	$\frac{-d[O_2]}{dt}$ (M·min^{-1})	% Inhibition of O_2-utilization Rate	$\frac{dFe(II)}{dt}$ (M·hr^{-1})
0	1.8×10^{-5}	0	--
7.14×10^{-5}	5.2×10^{-6}	71	1.3×10^{-4}
2.85×10^{-4}	3.9×10^{-6}	78	1.4×10^{-4}
1.0×10^{-3}	2.3×10^{-6}	87	1.5×10^{-4}

Table 6.2 Dependence of (simultaneous) O_2-utilization and Fe(III) Reduction on CN^- Concentration in an Induced Culture of Pseudomonas sp. 200. A_{600} = 0.05 (cm^{-1}).

$[CN^-]$(M)	$\frac{-d[O_2]}{dt}$ (M·min^{-1})	% Inhibition of O_2-utilization Rate	$\frac{dFe(II)}{dt}$ (M·hr^{-1})
0	9.6×10^{-6}	0	~ 0
3×10^{-5}	4.1×10^{-6}	57	3.1×10^{-4}
3×10^{-4}	2.7×10^{-6}	72	3.1×10^{-4}
3×10^{-3}	2.2×10^{-6}	77	3.1×10^{-4}

included as well. Notice that (i) the iron-reduction rate increased only slightly (to 1.8×10^{-4} $\underline{M}$•hr^{-1}) in response to the purge of residual O_2 (although the experiment extended only to the point of O_2 exhaustion since measurement of Fe(II) using the ferrozine method becomes increasingly unreliable at high-Fe(II) concentrations) and (ii) at no point did the iron-reduction rate reach the level observed (2.7×10^{-4} $\underline{M}$•hr^{-1}) in previous experiments of this type. Partial loss of culture dissimilative iron-reduction capacity could have been due to CN^- inhibition of (constitutive) ferrireductase activity, kinetic interference by preferential electron transfer to molecular oxygen or these effects in combination. Inhibition of dissimilative iron reduction at $[CN^-] = 1.0 \times 10^{-3}$ $\underline{M}$ was crudely estimated to be 35% by comparing the rate of iron reduction following O_2 exhaustion with the uninhibited, zero-O_2 rate from Figure 6.2. Cyanide inhibition of Fe(III) reduction at lower concentrations of CN^- should have been somewhat lower. Consequently, a portion of the overall inhibition of ferrireductase activity at low CN^- concentration may have been due to competition for electrons by the aerobic branch of the respiratory chain.

Electron-transport kinetics reflect the nature of enzyme interaction in bacterial respiration. When electron transport to molecular oxygen is limited by cytochrome-oxidase activity (e.g., when CN^- inhibition is apparent), upstream electron carriers must be primarily in their reduced forms. Were cytochromes ahead of the terminal oxidase free to interact in the manner of soluble, chemical reactants, CN^- inhibition would create pools of reduced electron carriers upstream from the terminal oxidase. Under these circumstances, maximal dissimilative

iron-reduction activity would be expected despite a residual level of aerobic respiration. However, if cytochromes interact as fully associated, multi-enzyme complexes, CN^- inhibition at the cytochrome oxidase level would affect electron transport to O_2 in only a portion of these complexes. (It is assumed that the time required for electron transfer across a cytochrome complex is much shorter than the characteristic time for inhibitor-oxidase association/dissociation.) Prior to O_2 exhaustion, enzyme complexes not bound to CN^- would continue to transport electrons to molecular oxygen at the expense of iron reduction. In only the latter scheme would partial development of ferrireductase activity be anticipated when (i) O_2 concentration reaches levels at which aerobic respiration is limited by cytochrome oxidase activity or (ii) inhibitory levels of CN^- are added. If respiratory enzymes act as independent pools of reactants subject to laws of mass action, a partial reduction in aerobic respiration rate should result in the immediate, full-capacity transport of respiratory electrons to Fe(III) via the constitutive ferrireductase.

Essentially the same experiment (simultaneous measurement of O_2 utilization and dissimilative iron reduction in the presence of CN^-) was run using a culture of Pseudomonas sp. 200 grown to $A_{600} = 0.05$ (cm^{-1}) under low-O_2 (inducing) conditions. The low culture density was selected to permit manipulation of dissolved-oxygen and CN^- levels prior to development of large concentrations of Fe(II) in solution.

Due to the induction of the high-rate ferrireductase there were potentially important differences between this and the previous experiment: (i) since the maximum activity of the inducible ferrireductase is comparable to that of cytochrome oxidase, simultaneous

Fe(III) reduction and O_2 utilization might be anticipated in the absence of CN^-, even at high O_2 concentrations; and (ii) since CN^- is not an effective inhibitor of the inducible ferrireductase (Chapter 5), kinetic inhibition of iron reduction by transport to oxygen could be studied without interference from CN^- competition for enzyme active sites.

Results of the experiment are summarized in Figure 6.5 and Table 6.2. The following points deserve mention:

(1) When both molecular oxygen and complexed Fe(III) are present as potential electron acceptors (no CN^-), electron transport is to O_2 exclusively. Because high-rate iron reduction is later observed in the presence of molecular oxygen and CN^-, it is certain that O_2 neither competitively inhibits ferrireductase activity by binding at the enzyme active site nor does it exert a negative influence in an allosteric relationship. Control of electron transport in the presence of alternate electron acceptors must arise from a competition for reducing equivalents at the transport-chain branch point. The competition is resolved in favor of the aerobic branch.

(2) Iron reduction is observed at the same time that CN^- inhibition of aerobic respiration becomes apparent, i.e., when aerobic respiration becomes limited at the level of the cytochrome oxidase and upstream respiratory enzymes are essentially completely reduced. Results imply that the ferrireductase does not receive respiratory electrons until more favorable respiratory pathways are partially blocked.

(3) Ferrireductase activity is maximized by CN^- additions $\geq 3 \times 10^{-5}$ M. Electron transport to Fe(III), however, does not compensate (in terms of an electron balance) for the observed loss of O_2-utilization capacity in the culture, indicating that kinetic control lies within the

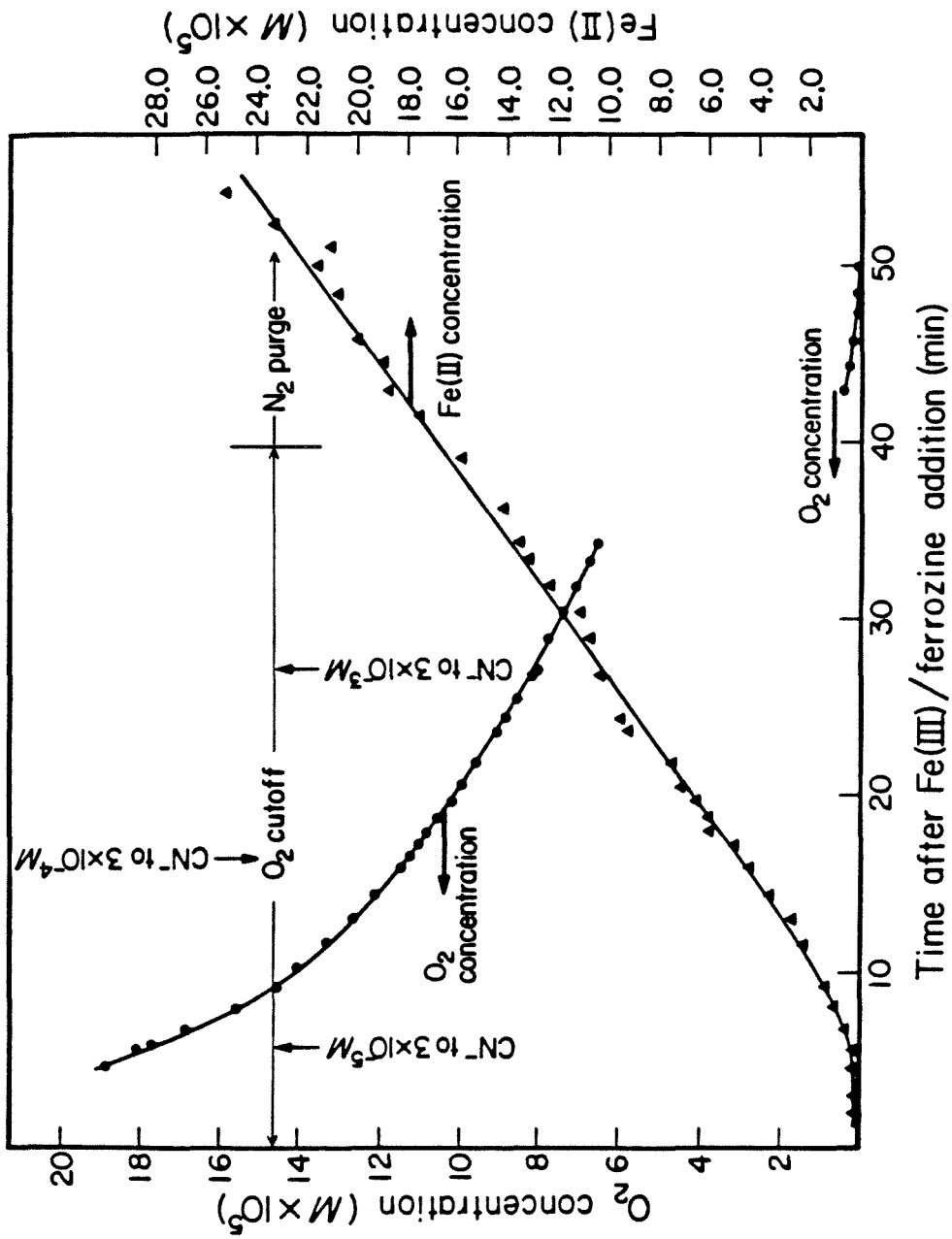

Figure 6.5 Simultaneous O_2 utilization and Fe(III) reduction as a function of O_2 and CN^- concentrations in an induced culture of Pseudomonas sp. 200 (A_{600} = 0.05, cm^{-1}). Iron reduction was measured in the presence of dissolved O_2 using ferrozine as a ferrous-iron trap ($[Fe_T]$ = 1.86 x 10^{-3} M; NTA = 1.86 x 10^{-3} M; [ferrozine] = 2.79 x 10^{-3} M).

electron transport chain (ferrireductase branch) following inhibitor addition.

(4) Full ferrireductase activity (5.1×10^{-6} M e^- transferred per hour) is not as large as anticipated from previous induction experiments conducted at higher cell densities (Chapters 3 and 5). Evidently both mean cell age and oxygen tension during growth play roles in (high-rate) ferrireductase induction.

6.3 Spectrophotometric Investigation of Respiratory-Chain Composition

6.3.1 Objectives and Background

Many investigators have studied the composition of the bacterial electron transport chain spectroscopically. Cytochromes typically absorb in the visible range in their reduced states; flavin groups (FAD/FMN), common to dehydrogenases, absorb when oxidized (Chance, 1957). Thus, reduced-minus-oxidized spectra of whole-cell or membrane preparations provide signatures representing partial composition of the electron transport chain. These are interpretable on the basis of numerous previous studies of the same nature. A compilation of bacterial cytochromes and absorption bands identified via previous studies is available in the CRC Handbook of Microbiology, Vol. IV (1982).

Here reduced-minus-oxidized and, to a lesser extent, CO-reduced-minus-reduced spectra are used to: (i) investigate the response of respiratory chain composition to variation in the steady-state O_2 level during growth and mean cell age in batch cultures of Pseudomonas sp. 200; (ii) identify membrane-bound components whose concentrations, as determined by light absorbance measurements,

correlate with culture iron-reduction capacity; and (iii) determine the degree to which electron-transport-chain components are associated with the cytoplasmic membrane of Pseudomonas sp. 200.

This investigation was designed to supplement the results of previous experiments described by Obuekwe (1980) and Obuekwe and Westlake (1982) which established the dependence of membrane cytochrome concentrations on growth medium composition. It was determined that the Pseudomonas sp. 200 respiratory chain included multiple c- and b-type cytochromes following growth in a rich medium with sufficient iron. Cells grown in an iron-deficient medium exhibited both a diminished cytochrome content (cytochrome absorption maxima disappeared in cells grown in a synthetic medium without iron) and a loss of iron-reduction capacity, leading to speculation that electron transport to Fe(III) is a function of cell pigmentation in this species.

6.3.2 Procedures

Cells were grown to target optical densities in 1.5-liter batch cultures. Temperature and pH were maintained at 31°C and 7.0, respectively, in a Biostat M bench-scale fermentor. Chapter 3 contains a complete description of fermentation conditions. Cells were grown in Westlake medium, Table 1, Chp.3. Air flow rate and mixing energy were varied to maintain either highly aerobic ($[O_2] \geq 10^{-4}$ M) or microaerophilic conditions ($[O_2] \leq 2$ μM) throughout. Culture optical density was monitored by periodically withdrawing samples for measurement of light absorbance at 600 nm using a Beckman DU7 spectrophotometer equipped with a 1-cm pathlength cuvette. At a preselected optical density, the remaining culture volume was withdrawn

and chilled on ice. Cells were washed by repeated centrifugation (20 minutes at 6400X g, 4°C in a Sorvall RC-3B refrigerated centrifuge) and resuspended in saline buffer (0.15 M NaCl; 1 mM $MgCl_2$). Final suspension volumes and calculated cell concentration factors are summarized in Table 6.3.

A description of physical treatments afforded individual (concentrated) suspensions of Pseudomonas sp. 200 prior to spectrophotometric analysis follows:

(i) Freeze/thaw. Most cultures were temporarily stored at -50°C and subsequently thawed at room temperature prior to analysis of respiratory chain components. Other treatments followed these steps.

(ii) Ultrasonic treatment. Concentrated suspensions of whole cells (2-5 mL) were disrupted with a Branson Model 200 cell disruptor (20 kHz, power variable) equipped with a double-step microtip and coupler. To avoid excessive sample heating, the cell disruptor was operated in pulsed mode, 25% duty cycle. Sonication times were 4 min. for a total ultrasonic exposure of 1 min. Disruptions were run at power outputs between 3 and 13 watts without significant differences in terms of centrate pigmentation.

(iii) Centrifugation. Several centrifugation techniques were employed for cell or membrane separation. Selection was based upon experimental objectives, machine capabilities, convenience and equipment availability.

(a) Low-speed centrifugation. Concentrated cell suspensions were centrifuged for 20 minutes at 6400x g in a Sorvall RC-3B refrigerated centrifuge (4°C). Centrate was analyzed spectrophotometrically for cytochrome content.

Table 6.3. Summary of culture concentration factors during cell washing and resuspension steps preceding spectrophotometric analysis of cytochrome content.

Culture description[1]	V_o/V_f[2]	Relative cellular concentration[3] Normalized to most concentrated resuspension
highly aerobic; A_{600} = 0.30 (cm^{-1})	120.7	0.45
highly aerobic; A_{600} = 0.50	110.0	0.69
highly aerobic; A_{600} = 0.75	92.4	0.87
highly aerobic; A_{600} = 1.0	79.8	1.00
O_2-limited; A_{600} = 0.255	135.0	0.43
O_2-limited; A_{600} = 0.50	88.2	0.55
O_2-limited; A_{600} = 0.75	81.2	0.76
O_2-limited; A_{600} = 1.0	73.8	0.92

[1] Oxygen conditions during growth; optical density when cells were harvested (1-cm pathlength cuvette).

[2] Culture volume when cells were harvested divided by final volume of washed resuspended cells.

[3] Culture optical density times concentration factor (V_o/V_f) normalized on the basis of most concentrated resuspension.

(b) Mid-speed centrifugation. Two techniques were employed in this range: Thawed cells were centrifuged for 45 min. at 30,000x g in a Sorvall RC-2B refrigerated centrifuge (4°C), and centrate was analyzed for pigment content spectrophotometrically. Alternatively, disrupted or whole-cell suspensions were spun for 30 min. at 15,600x g in an Eppendorf Model 5415 microfuge (room temperature). Microfuge centrate and resuspended cell fragments (original volume restored) were analyzed spectrophotometrically.

(c) Ultracentrifugation. Either whole-cell or suspensions of disrupted cells were spun at 140,000x g for 120 min. (10°C) in a Beckman Model L8-70 ultracentrifuge. Centrifugation RCF and run duration were selected on the basis of membrane separation procedures, derived by Hunt et al. (1959). Both centrate and resuspended pellet were analyzed spectrophotometrically for pigment content. Sonication was necessary for pellet dispersal.

Spectrophotometric studies were conducted using a Shimadzu (MPS-2000) dual-beam recording spectrophotometer. Cuvettes (1-cm pathlength) were positioned immediately adjacent to the photomultiplier in order to minimize light attenuation due to scattering. Since measurements with cuvettes in this position were virtually identical to those obtained using the same spectrophotometer equipped with a Shimadzu light-integrating sphere assembly, use of the sphere assembly was considered unnecessary. Samples were reduced by adding a few grains of sodium dithionite ($Na_2S_2O_4$) or oxidized by bubbling high-purity oxygen through the appropriate cuvette for 1 minute immediately prior to measurement of light absorbance. To obtain CO-reduced-minus-reduced spectra, carbon monoxide (Linde specialty gases, div. of Union Carbide)

was bubbled through one of the dithionite-reduced samples for 1 minute prior to absorbance measurement against the dithionite-reduced "blank".

In the absence of cell lysis, respiratory chain components were expected to separate with the whole cell. However, the freeze-thaw procedure apparently caused partial lysis and membrane fragmentation. Consequently, high-rate centrifugation treatments were carried out to settle even small membrane fragments, producing a centrate which could contain only soluble or loosely bound peripheral membrane proteins. Bacterial cytochromes c are frequently soluble periplasmic enzymes or weakly bound to the plasma membrane (periplasmic side) (Gel'man et al., 1975). Previous studies indicate that c-type cytochromes are sometimes partially solubilized by freeze-thaw procedures.

6.3.3 Results and Conclusions

Representative spectrophotometric scans shown in Figures 6.6 and 6.7 permit tentative identification of respiratory system components present in preparations of whole cells grown under highly aerobic versus O_2-limited conditions. Figure 6.6 consists of reduced-minus-oxidized spectra obtained using cells harvested at A_{600} = 0.75 (cm^{-1}). Figure 6.7 contains CO-reduced-minus-reduced spectra developed using the same cultures.

From comparison of these spectra, it is evident that the cytochrome contents of Pseudomonas sp. 200 cultures grown under highly aerobic and oxygen-limited conditions are qualitatively similar. Implications of the relatively minor differences between these curves are addressed below. Reduced-minus-oxidized spectra reveal distinct maxima at 551 and 521 nm and relatively minor shoulders or inflections at wavelengths of

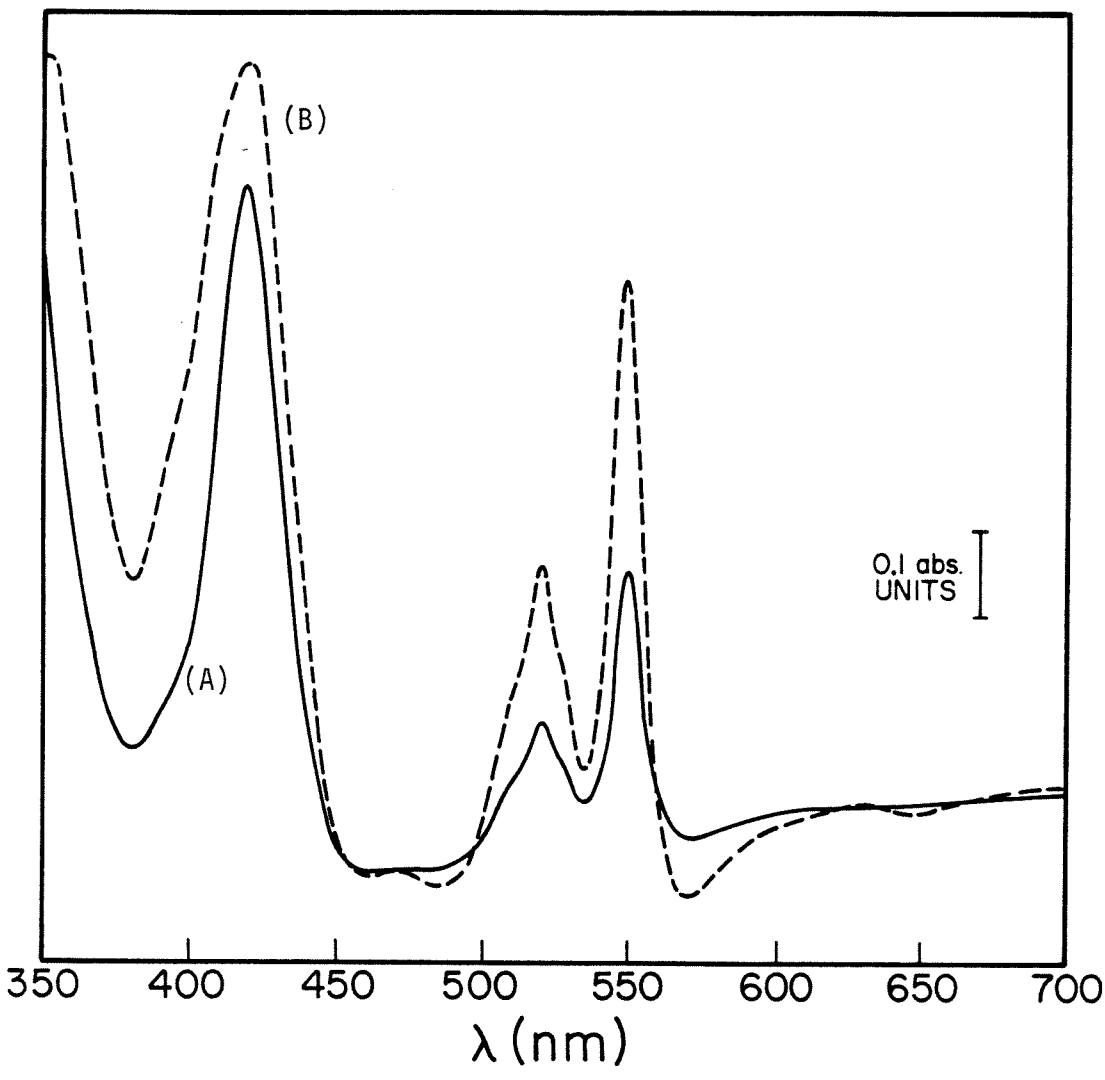

Figure 6.6 Dithionite-reduced-minus-oxidized spectra corresponding to whole-cell suspensions of Pseudomonas sp. 200 grown to A_{600} = 0.75 (cm^{-1}) under highly aerobic (non-inducing, curve A) and O_2-limited (inducing, curve B) conditions. Both suspensions were frozen at -50°C for storage and thawed prior to analysis.

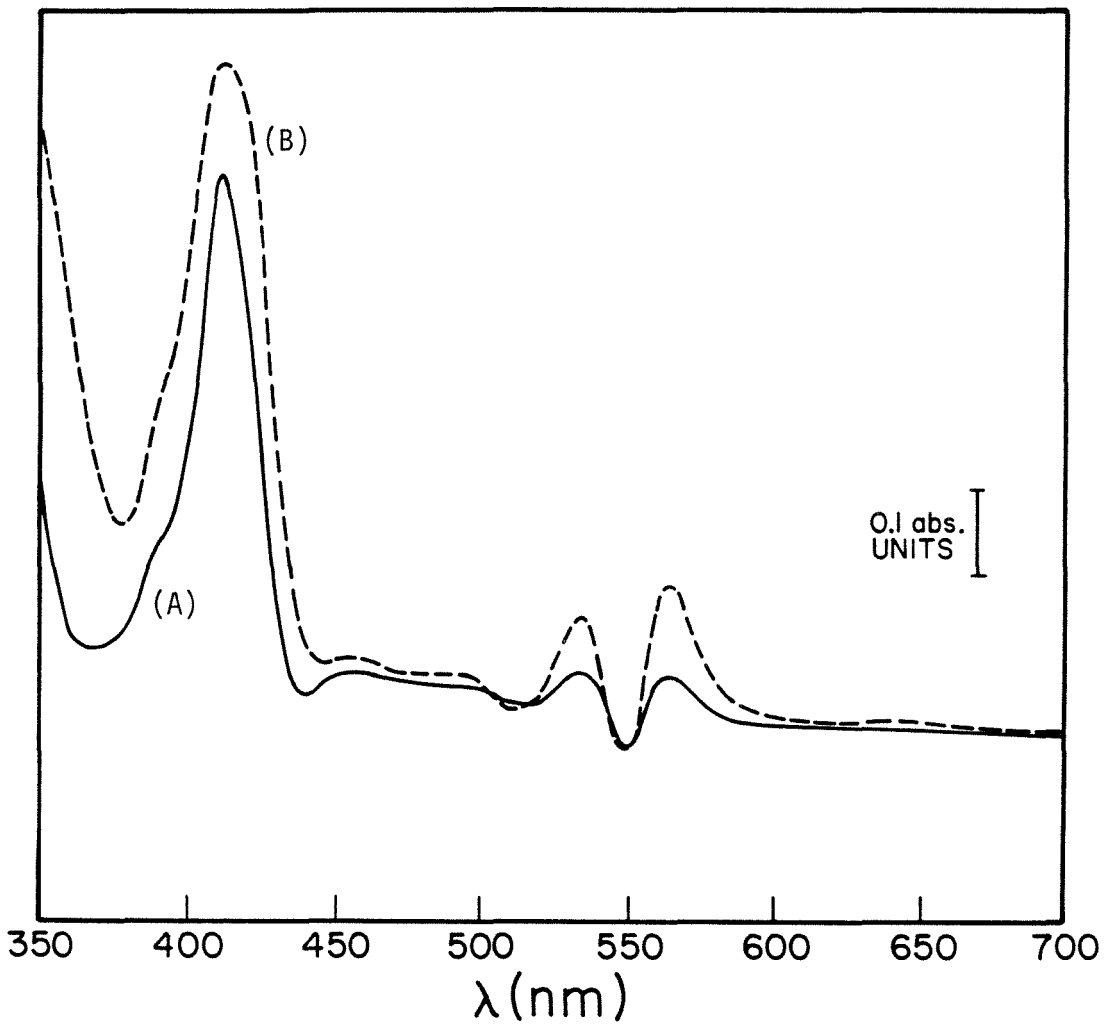

Figure 6.7 Reduced-plus CO-minus-reduced spectra corresponding to whole-cell suspensions of Pseudomonas sp. 200 grown to A_{600} = 0.75 (cm^{-1}) under highly aerobic (non-inducing, curve A) and O_2-limited (inducing, curve B) conditions. Both suspensions were frozen at -50°C for storage and thawed prior to analysis.

510 and 527 nm. Both of the large peaks have been attributed to cytochrome c in previous studies (Lemberg and Barrett, 1973). The small shoulders may reflect the presence of a b-type cytochrome, although other bands which are typically associated with cytochrome b are missing. The trough present in reduced-minus-oxidized spectra at about 460 nm may be attributable to a flavoprotein.

The CO-reduced-minus-reduced peak in the Soret region at 412 nm may be due to cytochrome o (Jones and Poole, 1985). This speculation is supported by the 420 nm band in reduced-minus-oxidized spectra (two-component peak, see below); a peak at 420 nm (absolute-reduced spectrum) has been observed in studies involving Vitreoscilla (Choc et al., 1982) and attributed to cytochrome o. The CO-complexed form of cytochrome(s) o is also a source of α and β bands in the regions 531-543 and 565-575 nm, respectively (Poole, 1983). Consequently, three major peaks of Figure 6.7 spectra suggest that cytochrome o is present in both induced and uninduced cultures (for ferrireductase) of Pseudomonas sp. 200.

Cytochrome d, previously cytochrome a_2, is commonly found in gram-negative heterotrophic bacteria, where it frequently coexists with cytochrome o (Poole, 1983). In Azotobacter the oxidase has a reduced band at 632 nm which shifts to 647 nm upon aeration (Negelein and Gerischer, 1934). The process proved reversible upon establishment of anaerobic conditions, and CO shifted the 632 nm band to 637 nm. All of these observations are consistent with the pattern observed in spectra of Figure 6.6 and 6.7 corresponding to induced cells. That is, the reduced-minus-oxidized spectrum of whole cells grown under O_2-limited conditions (Figure 6.6) shows a peak at 630 nm and trough at 646 nm.

The corresponding CO-reduced-minus-reduced spectrum (induced curve, Figure 6.7) has a peak at about 638 nm reflecting the CO-complexed form of the oxidase. Cytochrome d is apparently not present among uninduced cultures of Pseudomonas sp. 200. The pattern of cytochrome oxidase development suggested by these data (constitutive cytochrome o; cytochrome d induced under low-O_2 or low-energy conditions) has been observed in a variety of microorganisms including Escherichia coli (Poole, 1983).

Because concentration factors for these preparations were similar (Table 6.3), intercomparison of peak amplitudes in Figures 6.6 and 6.7 permits estimation of the relative concentrations of individual electron transport chain components in cells grown under highly aerobic and low-O_2 conditions. A general strengthening of the electron-transport-chain is evident in response to low-O_2 conditions as well as induction of the second cytochrome oxidase. Quantitative estimates of cellular cytochrome content are tentatively offered in Table 6.5 based on estimates of extinction coefficients summarized in Table 6.4. Figures reflect extrapolation from literature values for extinction coefficients corresponding to each cytochrome type. Enormous uncertainty is tolerated in this procedure; calculated values represent order-of-magnitude estimates of actual cytochrome concentrations. The average area "available" to a single cytochrome in the cytoplasmic membrane (final column, Table 6.5) was estimated using cellular cytochrome concentrations and the estimated surface area of cells in these cultures. Preliminary studies (Appendix) indicated that the approximate cell number in cultures of Pseudomonas sp. 200 at A_{600} =

Table 6.4 Selected wavelengths and extinction coefficients for quantification of cytochrome content in optical spectra.

Cytochrome	Type of spectrum	Wavelength[1] (both in nm)	Extinction coefficient $(mM\ cm)^{-1}$	References
c	reduced minus oxidized	550 (540)	14.3	van Gelden (1978)
d	reduced minus oxidized	630 (615)	8.5	Jones and Redfearn (1966)
o	reduced + CO minus reduced	417 (432)	170	Daniel (1970)

[1]Reference wavelength is in parentheses.

Table 6.5 Summary of computational procedures for estimating cytochrome content in Pseudomonas sp. 200 based on optical spectra presented in Figures 6.6 and 6.7.

Growth conditions (optical density)[1]	Cytochrome	Spectrum used	Wavelength[2] (nm)	Cytochrome concentration (M)[3]	Surface concentration (mols/cm^2)[4]	$\{$Surface concentration (Å^2/cytochrome)$\}^{-1}$
Highly aerobic (A_{600} = 0.75)	c	reduced minus oxidized	550 (540)	4.7×10^{-7}	9.5×10^{-12}	1.8×10^{3}
	d	reduced minus oxidized	632 (615)	(no peak)	--	
	o	reduced + CO minus reduced	412 (438)	9.5×10^{-8}	1.9×10^{-12}	8.7×10^{3}
O_2-limited (A_{600} = 0.75)	c	reduced minus oxidized	550 (540)	9.6×10^{-7}	1.4×10^{-11}	1.2×10^{3}
	d	reduced minus oxidized	632 (615)	6.8×10^{-8}	1.0×10^{-12}	1.7×10^{4}
	o	reduced + CO minus reduced	412 (438)	1.1×10^{-7}	1.6×10^{-12}	1.0×10^{4}

(1) Optical density at the point at which cells were harvested, washed, and resuspended.

(2) Reference wavelength in parentheses.

(3) Calculated using $\Delta A = \varepsilon C \ell$, ℓ = 1 cm, $\varepsilon \equiv$ extinction coef. (from Table 6.4, $\Delta A \equiv$ difference in light absorbance between the peak and reference wavelengths, Figure 6.6 or 6.7, as appropriate. Calculated concentration represents that of the original culture, prior to concentration via centrifugation/resuspension.

(4) Cytochrome concentration normalized on the basis of cell surface area. Assumed cell number at A_{600} = 0.75 is 10^9/ml; concentration factors from Table 6.3, assumed surface per cell is 5×10^{-8} cm^2.

0.75 (cm^{-1}) is 10^9/ml. From electron micrographs (Chapter 4), the surface area of an individual microorganism is about 5×10^{-8} cm^2.

Calculated results indicate that cytochrome c is present in considerable molar excess relative to cytochrome oxidase (about 5-fold excess if one considers both cytochrome o and cytochrome d in such calculations. Assuming that (i) the Pseudomonas sp. 200 cytochrome c is globular with molecular weight similar to that of mitochondrial cytochrome c and (ii) the entire cellular complement of cytochrome c is peripherally bound to the periplasmic surface of the cytoplasmic membrane, straightforward geometric calculations indicate that roughly one-half of the membrane is covered with this protein in cells grown under highly aerobic conditions. Following O_2-limited growth, surface coverage would be about 70 percent. While such figures are decidedly high, they may be reasonable in light of uncertainties associated with this type of analysis in general. However, it is also possible that both the high apparent surface concentration and lack of stoichiometric compatibility with cytochrome oxidase arise because surface-bound cytochrome c is in equilibrium with soluble protein in the periplasmic space (see below).

It is apparent from Table 6.6 that O_2 level during batch growth is more important than growth stage as a determinant of cellular cytochrome composition. Concentrations were normalized to account for differences in culture density and cell concentration factors during washing and resuspension steps. Mean cell age and growth stage were unrelated to cytochrome content in cultures grown under O_2-limited conditions. See also Figure 6.8.

Table 6.6 Calculated cytochrome c content and culture iron-reduction capacity as a function of growth stage and oxygen tension during growth in batch fermentations of Pseudomonas sp. 200. Cytochrome figures represent surface concentrations assuming measured quantities are entirely membrane bound.

Culture[1] Description	Surface Concentration[2] of Cytochrome c (mols/cm^2)	Normalized Culture Iron[3] Reduction Capacity (M/h - abs. unit)
highly aerobic; A_{600} = 0.30	3.2×10^{-12}	2.2×10^{-3}
highly aerobic; A_{600} = 0.50	6.4×10^{-12}	5.0×10^{-3}
highly aerobic; A_{600} = 0.75	7.8×10^{-12}	7.5×10^{-3}
highly aerobic; A_{600} = 1.00	6.0×10^{-12}	1.0×10^{-2}
O_2-limited; A_{600} = 0.255	1.5×10^{-11}	1.4×10^{-2}
O_2-limited; A_{600} = 0.50	1.5×10^{-11}	2.3×10^{-2}
O_2-limited; A_{600} = 0.75	1.5×10^{-11}	2.3×10^{-2}
O_2-limited; A_{600} = 1.00	1.5×10^{-11}	2.3×10^{-2}

(1) Oxygen status during growth: highly aerobic -- $[O_2] \geq 10^{-4}$ M; O_2-limited -- $[O_2] \leq 2$ μM. A_{600} value represents optical density at the point of cell harvest (1-cm pathlength cuvette).

(2) Per computational procedure illustrated in Table 6.5.

(3) Normalized on the basis of culture optical density measured as A_{600} (cm^{-1}). These data are summarized in Figure 1, Chapter 5.

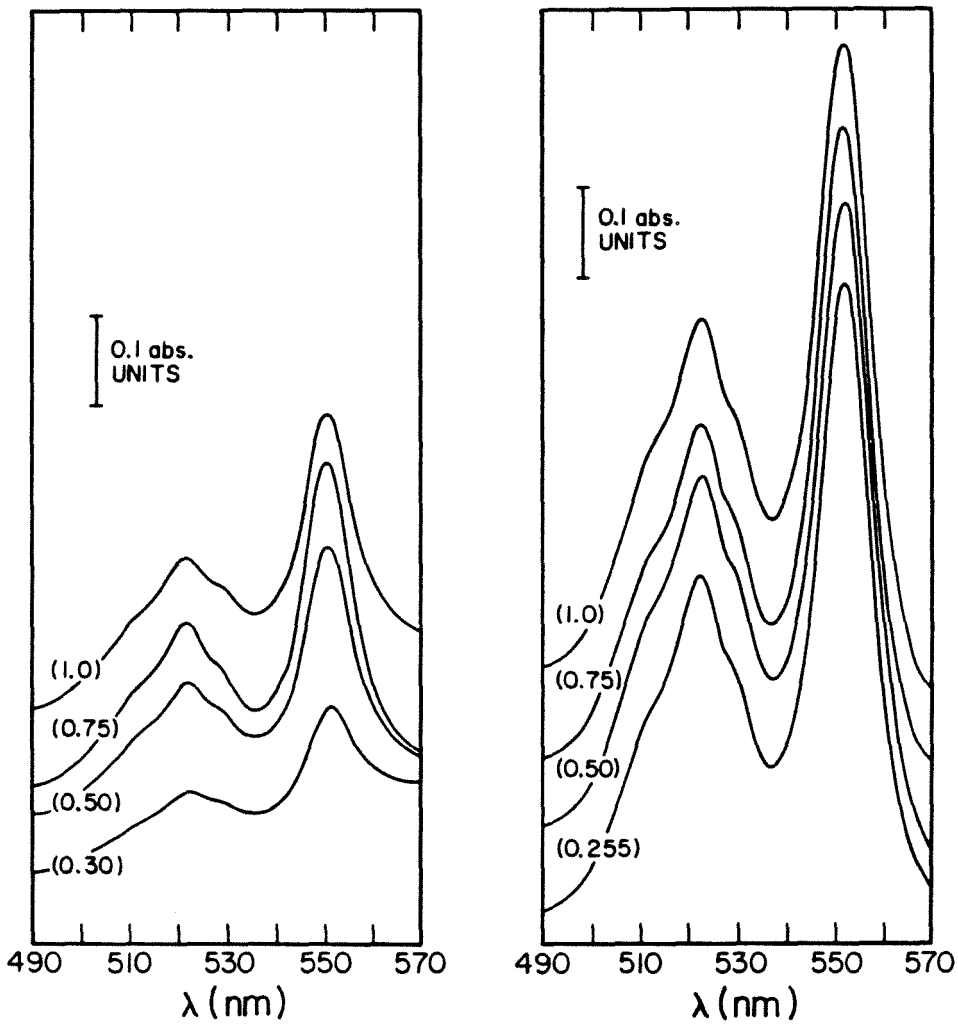

Figure 6.8 Whole-cell reduced-minus-oxidized spectra corresponding to batch cultures of Pseudomonas sp. 200 grown under (a) highly aerobic (non-inducing) and low-O_2 (inducing) conditions. Cell densities in all suspensions were "normalized" to a cell dry weight of approximately 20 mg/mL prior to analysis. Figures in parentheses represent culture optical densities (A_{600}, cm^{-1}) when culture growth was arrested.

Cell cytochrome content correlated poorly with culture iron-reduction capacity (Table 6.6) indicating that strengthening of the electron transport chain is not a primary factor in the striking enhancement of iron-reduction rate which is associated with growth under O_2-limited conditions. The inducible ferrireductase (Chapter 5) either does not absorb in the visible range or is not reduced by dithionite addition.

Whole cells grown to A_{600} = 0.75 (cm^{-1}) under O_2-limited conditions were treated via several combinations of sonic disruption and centrifugation prior to generation of corresponding spectra. Results are summarized in Figures 6.9 through 6.12. From Figure 6.9 it is clear that centrate from low-speed centrifugation (4000x g for 20 min.) of cells treated by freezing and thawing retains an appreciable fraction of the original, whole-cell cytochrome c content. A subsequent centrifugation step at 30,000x g removed no additional pigment suggesting that these cytochromes are not associated with small membrane fragments liberated during earlier treatments. The figure also indicates that cytochrome d, induced during growth under low-O_2 conditions, is tightly bound to bacterial membranes, which are virtually all removed via centrifugation. A correlation between the peak heights at 551 and 521 nm reinforces the notion that these peaks are attributable to a single constituent, or perhaps a multienzyme complex.

Figure 6.10 shows the results of a similar experiment in which a reduced-minus-oxidized spectrum corresponding to whole cells (induced culture; A_{600} = 0.75 when harvested) is compared to that of culture centrate obtained following centrifugation at 15,600x g for 30 min. It is important to note that these cells were not frozen and stored prior

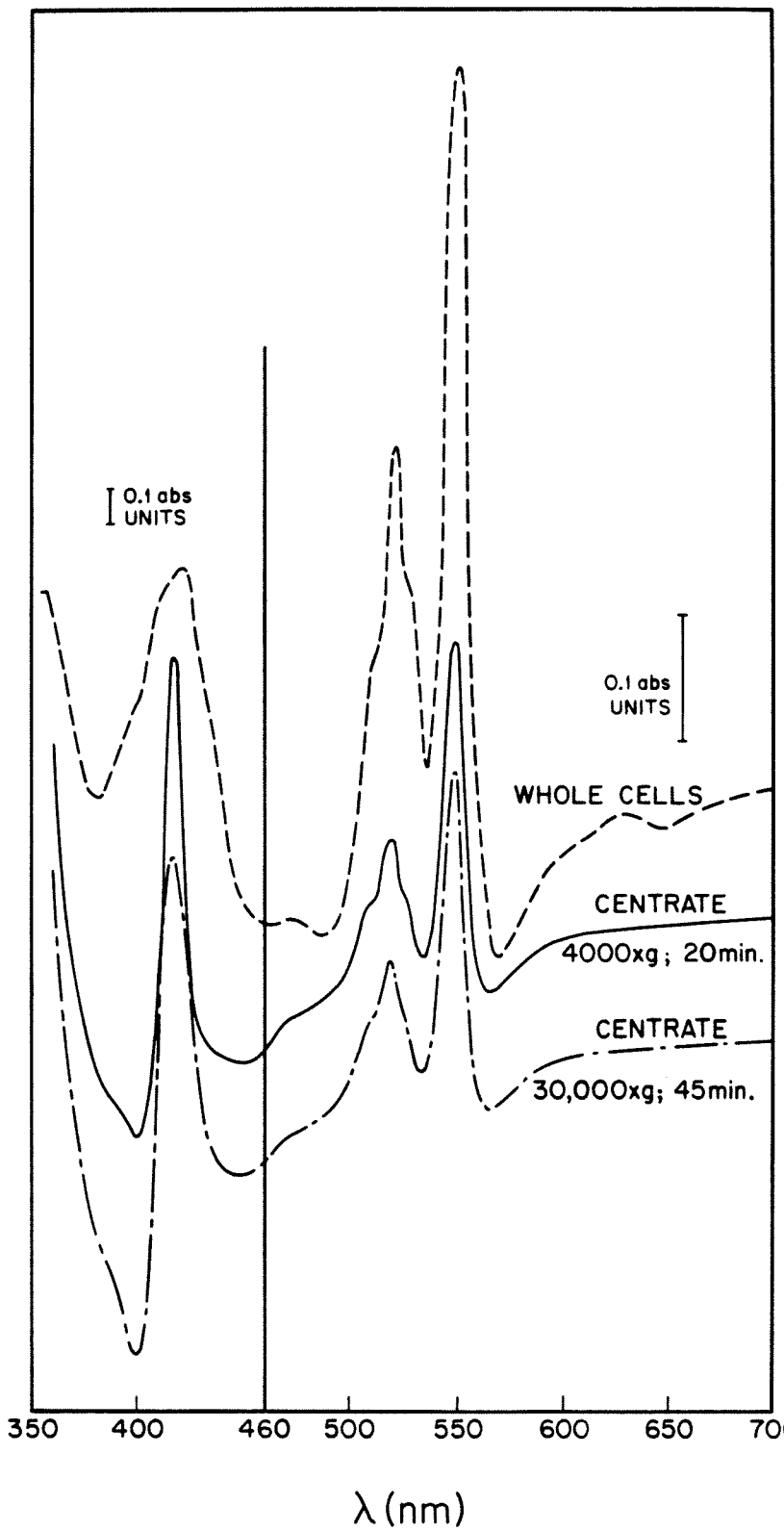

Figure 6.9 Comparison of reduced-minus-oxidized spectra for a whole-cell suspension of Pseudomonas sp. 200 and centrate from centrifugations at low and intermediate speeds. Original culture was grown to A_{600} = 0.75 (cm^{-1}) under O_2-limited (inducing) conditions.

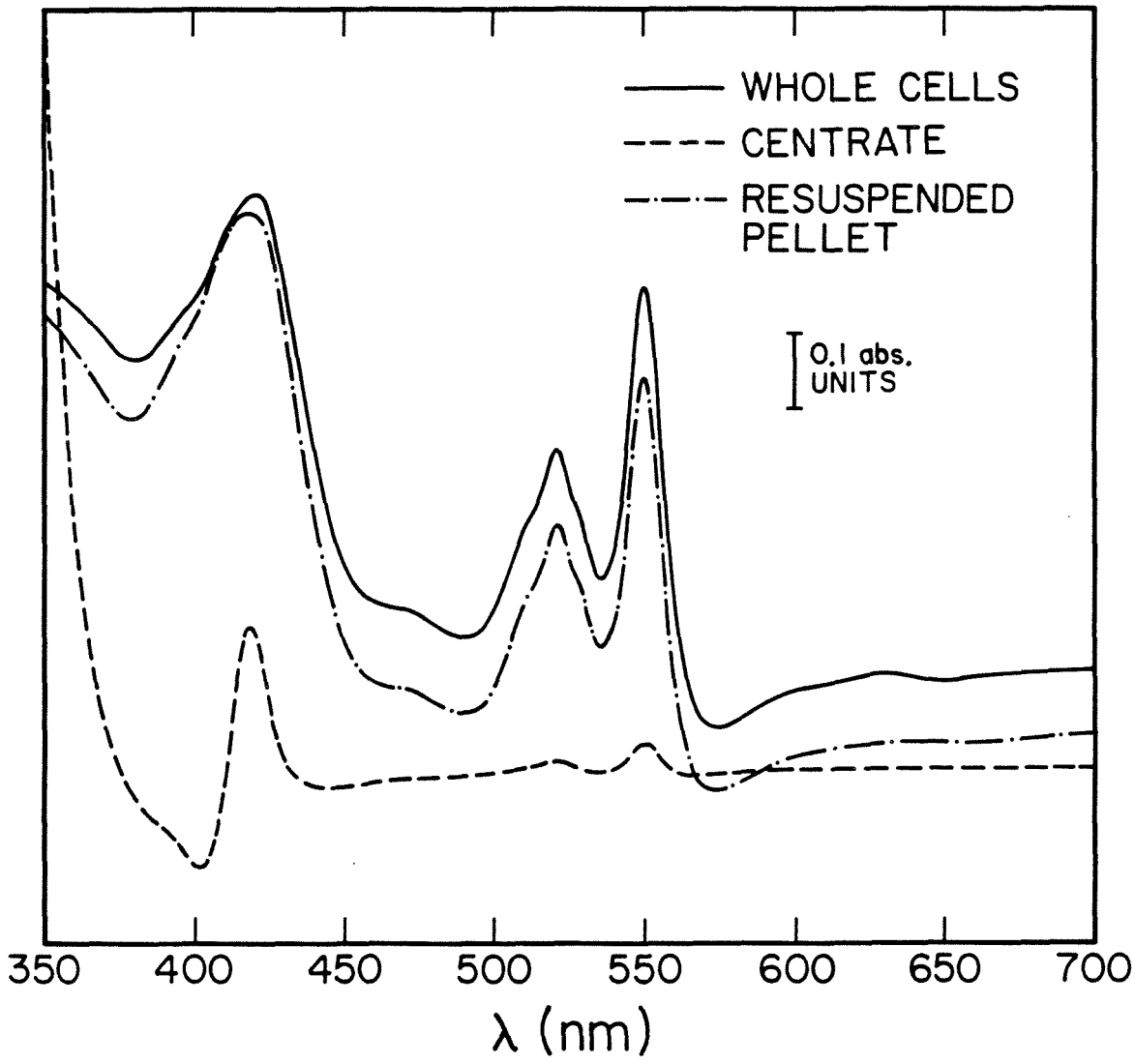

Figure 6.10 Comparison of reduced-minus-oxidized spectra corresponding to (i) a whole-cell suspension of Pseudomonas sp. 200, (ii) suspension centrate (15,600x g, 30 min.), and (iii) pellet (resuspended to original volume). Cells were grown to A_{600} = 0.75 (cm^{-1}), harvested, and treated without an intervening freeze-thaw step.

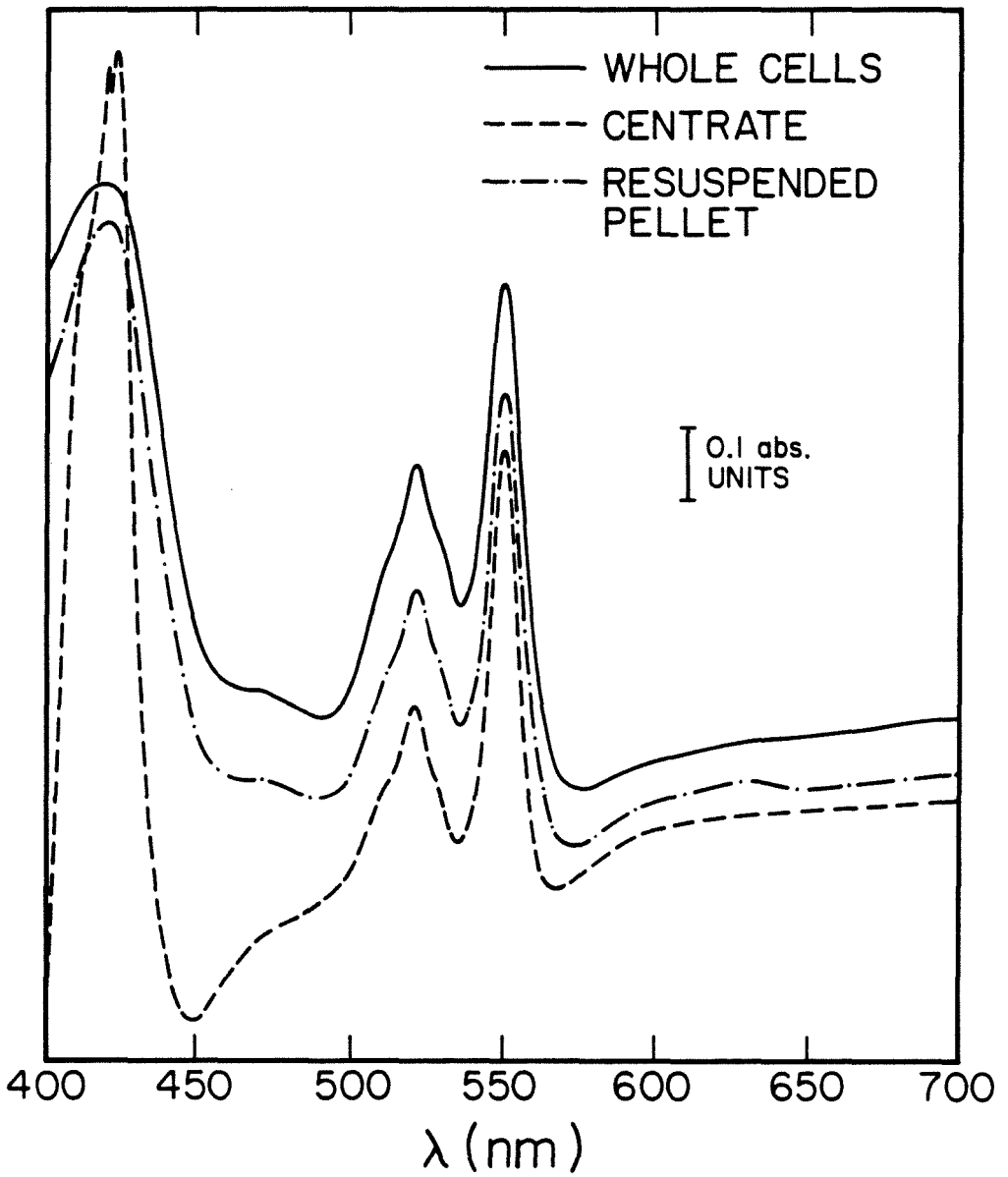

Figure 6.11 Comparison of reduced-minus-oxidized spectra corresponding to (i) a whole-cell suspension of Pseudomonas sp. 200, (ii) suspension centrate (15,600x g, 30 min.), and pellet (resuspended to original volume). Cells were grown to A_{600} = 0.75 (cm^{-1}), harvested, and sonicated (3 W., 1 min.) prior to centrifugation.

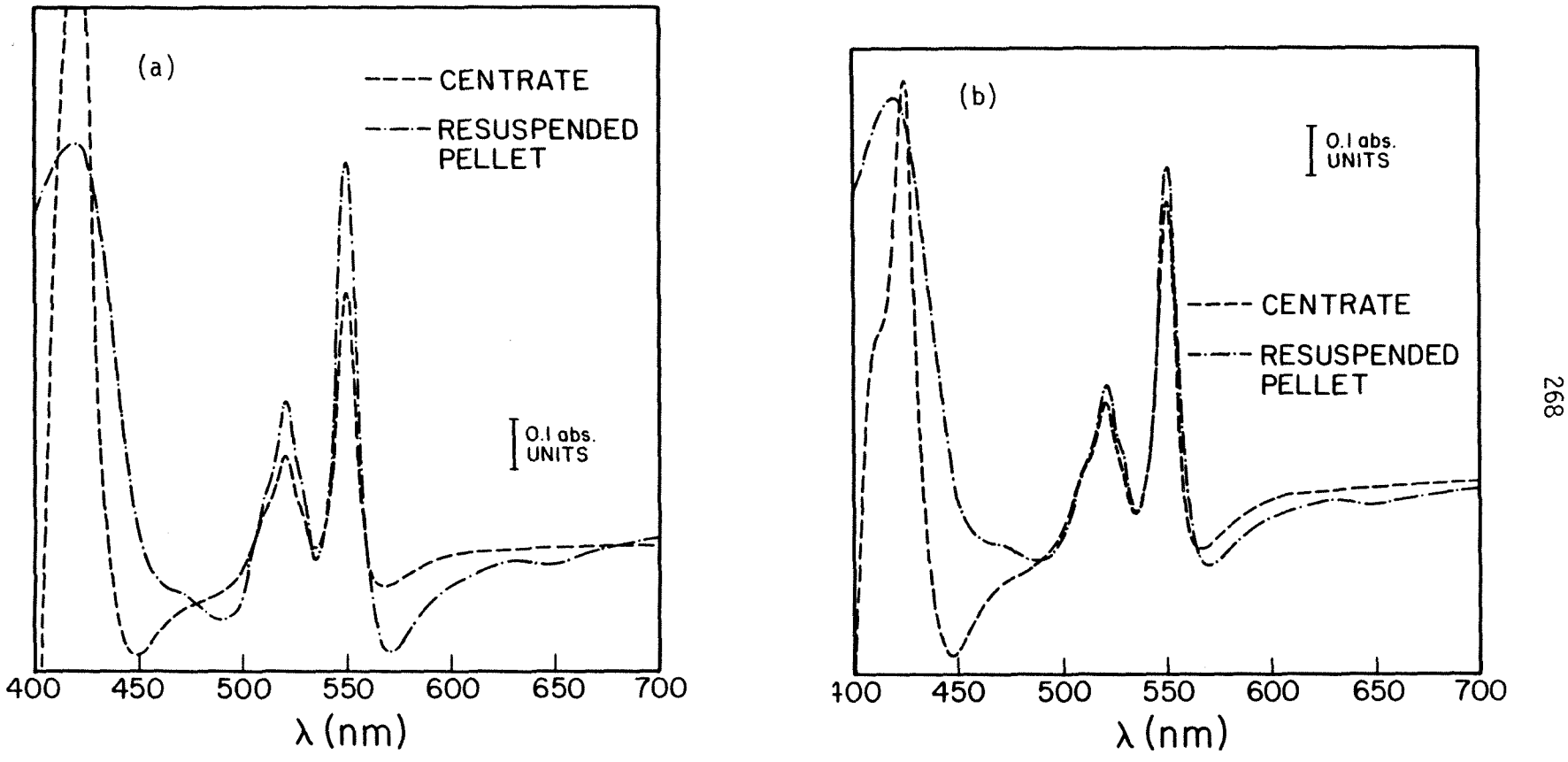

Figure 6.12 Comparison of reduced-minus-oxidized spectra corresponding to centrate and (resuspended) pellet fractions when (a) freeze-thaw and (b) freeze-thaw and mild sonication (3W., 1 min.) precede centrifugation (15,600x g, 30 min.) of whole cells.

to analysis. Here membranes and/or whole cells were resuspended and analyzed yielding a third spectrum for comparison. Results indicate that the cellular cytochrome content settles with whole cells when cellular membranes are not disrupted by such treatments as freeze-thaw procedures. Resuspended whole cells showed virtually the same absorption signature as the suspension prior to centrifugation. Cytochrome c is evident in the centrate at a comparatively low concentration, perhaps due to unavoidable membrane damage during washing and resuspension steps. This and other spectra tend to show that the (untreated) whole-cell peak at 420 nm (reduced-minus-oxidized spectra) is comprised of two components -- one is tightly bound to cell membranes; the other (probably cytochrome c, as suggested by Obuekwe and Westlake (1982)) readily escapes from the particulate fraction upon mild treatment.

The same set of spectra (whole preparation, centrate, resuspended pellet) were developed using cells subjected to mild sonic disruption (1 min. at 3 W., see above) prior to centrifugation steps. Results are summarized in Figure 6.11. It is clear that sonication "solubilizes" a reasonable fraction of the cytochrome c present in the whole-cell preparation. Furthermore, the cytochrome d peak appears to be missing from the centrate fraction indicating that membrane-bound components are associated primarily with the pellet following centrifugation at 15,600x g (i.e., that cytochrome c in the centrate is truly soluble as opposed to being bound to small membrane fragments produced via treatment with ultrasound).

Finally, it is apparent from Figure 6.12(a) that soluble pigments (cytochrome c and others) are liberated from resuspended cells which are frozen for storage. These pigments did not settle during centrifugation at 140,000x g for 2 hrs. Sonication of the same (original) suspension for 1 min. at 3 W. resulted in solubilization of a greater fraction of the cellular cytochrome c content (Figure 6.12(b)).

6.3.4 Summary

Spectrophotometric studies of electron transport chain components in Pseudomonas sp. 200 support the following conclusions:

1. The constitutive respiratory chain of the species includes c-type and perhaps b-type cytochromes. Cytochrome o serves as the constitituve cytochrome oxidase. These findings are reasonably consistent with those of Obuekwe and Westlake (1982).

2. Growth under O_2-limited conditions results in a general strengthening of the constitutive aerobic electron transport chain and induction of a second cytochrome oxidase (cytochrome d).

3. Results do not permit identification of respiratory chain components which are involved in electron transport to Fe(III). There is limited correlation between estimated concentrations of transport-chain elements identifiable via these techniques and culture iron-reduction capacity.

4. An appreciable fraction of the cytochrome c content of Pseudomonas sp. 200 is released by relatively mild cell treatment such as freezing and thawing. Solubilized cytochrome c remains in the centrate following ultracentrifugation indicating that association with small membrane fractions is not a factor in its release. Although this

enzyme appears to be only partially membrane-bound, assignment of soluble cytochrome c to the periplasmic space is not possible without additional study. The existence of a soluble c-type cytochrome in the periplasmic space would offer a potential mechanism for transport of cellular reducing power from the cytoplasmic membrane to oxide surfaces which could not otherwise accept respiratory electrons due to steric limitations.

6.4 References

Carter, P. Spectrophotometric determination of serum iron at the submicrogram level with a new reagent (ferrozine). Analyt. Biochem. 40: 450-458 (1971).

Chance, B. Cellular oxygen requirements. Federation Proceedings. Federation of American Biological Societies 16: 671-680 (1957).

Choc, M. G.; Webster, D. A. and Caughey, W. S. Oxygenated intermediate and carbonyl species of cytochrome o (Vitreoscilla). J. Biol. Chem. 257: 865-869 (1982).

Daniel, R. M. The electron transport system of Acetobacter suboxydans with particular reference to cytochrome o. Biochim. Biophys. Acta 216: 328-341 (1970).

Gel'man, N. S.; Lukoyanova, M. A. and Ostrovskii, D. N. Biomembranes, Vol. 6. Plenum, New York (1975).

Hunt, A. L.; Rodgers, A. and Hughes, D. E. Sub-cellular particles and the nicotinic acid hydrolase system in extracts of Pseudomonas fluorescens KB_I. Biochim. Biophys. Acta 34: 354-372 (1959).

Jones, C. W. and Redfearn, E. R. Electron transport in Azotobacter vinelandii. Biochim. Biophys. Acta 113: 467-481 (1966).

Jones, C. W. and Meyer, D. J. The distribution of cytochromes in bacteria. In: CRC Handbook of Microbiology, Vol. IX. Eds. A. I. Larkin and H. A. Lechevalier. CRC Press; Boca Raton, Florida (1982).

Jones, C. W. and Poole, R. K. The analysis of cytochromes. In: Methods in Microbiology, Vol. 18, Chapter 10. Academic Press, New York (1985).

Kurimura, Y.; Ochiai, R. and Matsuura, N. Oxygen oxidation of ferrous ions induced by chelation. Bull. Chem. Soc. Japan 41: 2234-2239 (1968).

Lemberg, R. and Barrett, J. Cytochromes. Academic Press, New York (1973).

Negelein, E. and Gerischer, W. Biochem. Z. 268: 1-7 (1934).

Obuekwe, C. O. Microbial corrosion of crude oil pipeline. Ph.D. dissertation. Univ. of Alberta, Edmonton, Alberta (1980).

Obuekwe, C. O. and Westlake, D. W. S. Effects of medium composition on cell pigmentation, cytochrome content, and ferric iron reduction in a Pseudomonas sp. isolated from crude oil. Can. J. Microbiol. 28: 989-992 (1982).

Poole, R. K. Bacterial cytochrome oxidases, a structurally and functionally diverse group of electron-transfer proteins. Biochim. Biophys. Acta 726: 205-243 (1983).

Stookey, L. L. Ferrozine - a new spectrophotometric reagent for iron. An. Chem. 42: 779-781 (1970).

Sung, W. and Morgan, J. J. Kinetics and product of ferrous iron oxygenation in aqueous systems. Environ. Sci. Technol. 14: 561-568 (1980).

van Gelder, S. R. Optical properties of cytochromes from beef heart mitochondria, submitochondrial vesicles, and derived preparations. In: Methods in Enzymology, Vol. 53. pp. 126-128. Academic Press, New York (1978).

Chapter 7

CONCLUSIONS AND PERSPECTIVE

Introducing the Unknowns

The experiments, analyses, and discussion offered to this point provide a broad, though non-comprehensive view of dissimilative iron reduction by *Pseudomonas* sp. 200. This work adds to our collective understanding of the process, but a true mechanistic understanding remains to be established.

From previous studies described in Chapter 1 and screening experiments conducted in this laboratory, it is clear that bacteria of diverse genera are capable of catalyzing dissimilative iron reduction at rates which are decidedly in excess of their nutritional requirements for iron. In the majority of these studies, the dissimilative nature of bacterial iron reduction was established by circumstantial evidence. The work of Lascelles and Burke (1978), in which membrane preparations of *Staphylococcus aureus* catalyzed reduction of complexed Fe(III) in a defined medium, stands out as the lone exception.

In most studies, direct transfer of electrons from membrane-bound respiratory enzymes (ferrireductases) to Fe(III) has not been established. Such transfer could depend upon a diffusible intermediate of metabolic origin. Similarly, it is seldom known whether dissimilative iron reduction supports oxidative phosphorylation and cellular growth or merely provides a sink for excess cellular reducing capacity.

The availability of Fe(III) as electron acceptor for bacterial respiration is extremely sensitive to the form in which iron is provided. Much evidence suggests that complexed and less crystalline

insoluble forms are favored in this regard. Overall process thermodynamics seem to correlate with iron reduction kinetics, though work in this area has been qualitative.

In general, a predictive kinetic description of dissimilative iron reduction has proven difficult to formulate because the mechanics of electron transport to Fe(III) are potentially complex. For instance, when Fe(III) is provided in soluble, complexed form, it is easy to envision a direct transfer of respiratory electrons from membrane-bound ferrireductase to Fe(III). Under these circumstances, however, the number of potentially important iron species makes development of a rational rate expression very difficult. Furthermore, at high total Fe(III) concentrations it is probable that rate limitations lie not with ferrireductase activity but with that of upstream elements of the electron transport chain or in metabolic pathways upon which respiration depends for the development of reductant. Thus, kinetic control arises from factors which may be considered primarily chemical (Fe(III) speciation, ferrireductase affinity, etc.) or biological, increasing the potential complexity of kinetic models.

When Fe(III) is provided in insoluble form, the role of ligand addition is no less important to reduction kinetics, but potential kinetic limitations include mass transport from cell to particulate surface and solid dissolution in addition to bacterial electron transport or other biological factors. The mechanics of electron transport to Fe(III) at an oxide surface are difficult to envision due to steric problems potentially imposed by the outer membrane (Gram-negative bacteria) and cell wall. A soluble metabolic intermediate capable of shuttling reducing equivalents across the

periplasmic space and through outer membrane pores would solve this problem. However, the true mechanism may depend on contact between cells and iron oxides of such intimacy that barriers to direct electron transport are partially obliterated.

Our imperfect understanding of bacterial respiratory chains contributes to the scarcity of plausible models of electron transport kinetics. On one hand, it is possible to envision electron transport chain components as permanently associated, multienzyme complexes -- conduits for electron transport, the pieces of which interchange or exchange infrequently with unincorporated enzyme pools. At the other extreme, individual respiratory enzymes may be thought of as essentially unassociated pools, components of which interact in the same manner as reactive, soluble chemical compounds. Mass action laws would apply strictly only in the latter case. In the former, only the number of intact (complete) complexes, as opposed to concentrations of individual enzymes, would be of importance to the formulation of kinetic models, and rate constants for electron transport processes could exceed limits imposed by mass transport requirements. A true representation of bacterial electron transport chains probably lies between these extremes. Multienzyme complexes consisting of cytochromes or flavoproteins plus iron-sulfur proteins are consistently isolated following membrane disruption. On the other hand, quinones are frequently present in considerable molar excess over other respiratory components and may serve as an independent pool connecting the cytochrome and dehydrogenase complexes. Uncertainties of this nature undermine the reliability of efforts to model respiration kinetics and identify kinetic limitations to electron-transport processes including

dissimilative iron reduction.

This work was undertaken to approach areas of mechanistic uncertainty in a single bacterial system. Pseudomonas sp. 200 was selected primarily for convenience. The microorganism grows rapidly in the neutral pH range and under proper conditions reduces Fe(III) much more rapidly than other capable bacteria. Results and conclusions are summarized below in much the same order as they were developed in the preceding text.

Results and Conclusions

Findings are conveniently divided into the several primary areas of inquiry.

Energetics

1. Thermodynamic considerations indicate that there is sufficient energy in the transfer of electrons from either lactate ion or NADH to Fe(III) (as $Fe(OH)_3$(s,amorph) or soluble Fe-NTA-hydroxo complexes) to drive oxidative phosphorylation. When ferric iron is provided as hematite, the energy requirements of oxidative phosphorylation are similar to or below the level of energy available from dissimilative iron reduction, indicating that either electron transport is efficiently coupled to ADP phosphorylation or iron reduction is used only as a sink for excess cellular reducing power.

2. Although provision of Fe(III) as Fe(III)-NTA-hydroxo complexes or amorphous ferric hydroxide improves the thermodynamics of dissimilative iron reduction considerably (relative to Fe(III) oxides), there is significantly more energy available from aerobic respiration than from electron transport to Fe(III) in any of the forms considered. Consequently, one should expect electron transport to Fe(III) to occur

via an abbreviated electron transport chain. E_m (defined as the potential at which half the cellular complement of a particular redox component is reduced -- nearest equivalent to E_o' which can be measured among membrane-bound electron carriers) for respiratory enzymes near the cytochrome oxidase would overpower the Fe(III)/Fe(II) redox pair. Because anaerobic respiration must occur via an abbreviated chain, the number of proton translocation sites involved in dissimilative iron reduction (and thus H^+/e^-, ATP/$2e^-$, etc.) should be lower than that of aerobic respiration. Growth yield parameters will necessarily be lower as well.

3. Results of thermodynamic calculations are sensitive to assumptions regarding process stoichiometry and concentrations chosen to represent physiological conditions. Energetic and topological considerations dictate that reducing equivalents enter the electron transport chain via NADH or lactate dehydrogenase on the cytoplasmic side of the plasma membrane and exit via ferrireductase on the periplasmic side. Consequently, redox half reactions which comprise the overall transfer of electrons from NADH or lactate to Fe(III) should not be combined prior to substitution of physiological concentrations and calculation of free energy changes. That is, because physiological concentrations are expected to differ across the cytoplasmic membrane (e.g., a transmembrane proton gradient is necessary to sustain oxidative phosphorylation), energy changes should be calculated from half-reaction potentials and local concentrations and then combined to yield an overall free energy change. Resultant values are significantly larger than those obtained using procedures applicable to non-vectorial processes.

Screening Experiments and Selection of Pseudomonas sp. 200.

4. Among the microorganisms tested for growth characteristics and iron reduction capacity, only Pseudomonas sp. 200 both grew rapidly (doubling times slightly greater than 30 min. under optimal growth conditions) and exhibited high specific Fe(III) reduction rates (normalized on the basis of cell dry weight). Acidophilic strains of Thiobacillus thiooxidans also proved capable of rapid iron reduction catalysis. In screening experiments, Fe(III) was added to solution as either $FeCl_3$ or $Fe_2(SO_4)_3$; Fe(III) solubility was significantly greater in experiments involving acidophiles, perhaps fostering higher bacterial iron-reduction rates.

5. Indicators of bacterial growth (light attenuation, cell dry weight, total protein, cell number, O_2 utilization rate) in batch cultures of Pseudomonas sp. 200 are reasonably well correlated. Relationships developed in preliminary growth experiments follow:

$$A_{600} = 1.8\ (CDW)\ ;\ A_{600} \text{ in } cm^{-1},\ \text{cell dry weight in } g \cdot L^{-1}.$$

$$\frac{d[O_2]}{dt} = 9.0 \times 10^{-5}\ (A_{600})\ ;\ \frac{d[O_2]}{dt} \text{ in } \underline{M} \cdot min^{-1}.$$

$$[cells] = 10^9\ (A_{600})\ ;\ [cells] \text{ in } cells \cdot mL^{-1}.$$

Kinetics of Electron Transport in Pseudomonas sp. 200.

6. Growth of Pseudomonas sp. 200 under O_2-limited conditions ($[O_2] \leq 2$ $\underline{M}$) leads to a moderate increase in culture O_2-utilization capacity. The same growth conditions increase the culture

iron-reduction capacity by almost an order of magnitude. Kinetic results suggest that Pseudomonas sp. 200 produces both a low- (constitutive) and high-rate (inducible) ferrireductase. Ferrireductase induction in response to conditions of low dissolved oxygen concentration or perhaps low cellular energy level would eliminate unnecessary protein synthesis in the presence of more energetically favorable electron acceptors. Such a mechanism has been postulated among nitrate reducers.

7. The kinetics of high-rate (fully induced) iron reduction by Pseudomonas sp. 200 are not light sensitive.

8. The abiotic rate of iron reduction in cell-free, anaerobic cultures of identical initial chemical composition is essentially zero.

9. When Fe(III) is provided at sufficient total iron concentrations as either freshly precipitated $Fe(OH)_3(s,amorph)$ or soluble Fe(III)-NTA-hydroxo complexes, saturation kinetics limit the observed rate of dissimilative iron reduction in cultures of Pseudomonas sp. 200. NTA addition increases V_{max} in cultures which are otherwise identical by a factor of more than 20 (from 1.0×10^{-3} to 23×10^{-3} M Fe/hr in fully induced cultures at $A_{600} = 1.0$ (cm^{-1})).

10. Following a series of experiments in which NTA addition and solution pH were systematically varied, measured iron reduction rates in cultures of Pseudomonas sp. 200 were modeled as a function of the equilibrium concentrations of individual Fe(III) species. In the most successful and simplest of these models, it was hypothesized that there exist two types of iron-reduction sites on the surface of the microorganism. These differ only in their accessibility to solid Fe(III) forms -- affinities for Fe(III) species and catalytic rate

constants are otherwise identical. Model results indicated that (i) soluble Fe(III) species are not equivalent in terms of their contributions to overall iron reduction rate; (ii) $FeNTA(OH)_2^{2-}$ concentration correlated best with the observed iron reduction rate; (iii) low culture iron-reduction capacity, observed when Fe(III) is present primarily as ferric hydroxide (zero-NTA cases), may arise from the limited number of ferrireductase sites in contact with insoluble iron; and (iv) although two-site, multisubstrate, Michaelis-type models offer a reasonable fit for iron-reduction rate data, goodness-of-fit is limited by the inability of rate expressions to match observations at high (saturated) iron-reduction rates.

The final observation suggests that Michaelis-type kinetic expressions are not appropriate at high rates of dissimilative iron reduction. This contention is supported by an abrupt transition from zero-order kinetics at high Fe(III) concentrations to a first-order relationship at low concentrations. Such kinetics are more readily explained in terms of a shift in the rate-limiting step from ferrireductase activity at low Fe(III) concentrations to an earlier reaction (e.g., NADH dehydrogenase activity) at higher ferric iron levels (when total ferrireductase activity is sufficiently great).

Models of electron transport chain activity were explored by Chance (1957) and by Chance and Williams (1956), who observed a sharp transition from zero- to first-order kinetics in aerobic experiments involving a preparation of heart muscle mitochondria. Rates computed as a function of O_2 concentration using their model fit the observed pattern. Chance indicated that such a functional relationship results from a complex pattern of interaction among electron transport chain

elements, as opposed to a shift in the rate-controlling elementary reaction.

11. At the highest rates of dissimilative iron reduction observed, the rate of electron transport to Fe(III) (2.3×10^{-2} M e^-/hr) approaches the aerobic electron transport capacity of Pseudomonas sp. 200 (assuming a 4-electron transfer is necessary for the complete reduction of O_2 to H_2O). Above the critical O_2 concentration, aerobic electron transport is routinely limited by dehydrogenase activity (as opposed to cytochrome oxidase activity). Thus, similarity between maximal rates of O_2 utilization and iron reduction supports a shift to kinetic control at the dehydrogenase level at sufficiently great ferric iron concentrations.

The sudden transition from zero- to first-order reduction kinetics is more difficult to rationalize when Fe(III) is presented as $Fe(OH)_3$(s,amorph) since a shift in rate-limiting step to an "upstream" reaction at a relatively low overall iron reduction rate at first seems implausible. However, if the electron transport chain from dehydrogenase to ferrireductase acts as a single multienzyme complex, then the postulated limitations on Fe(III)/ferrireductase contact imposed by provision of Fe(III) as a solid would be directly reflected in the number of functional dehydrogenases. (Those not in contact would simply not transport electrons.) Under those circumstances, a shift to kinetic control at the dehydrogenase level might be expected at a much lower overall iron reduction rate.

Other explanations for these rate data are possible. When Fe(III) is provided primarily as ferric hydroxide, initial rate limitations could arise from diffusion of a reduced intermediate (soluble carrier

shuttling reducing power from membrane-bound respiratory components to $Fe(OH)_3$(s,amorph) at the cell exterior). At lower total Fe(III) concentrations, following reductive dissolution of an appreciable fraction of the $Fe(OH)_3$(s,amorph) initially provided, a shift in kinetic control to reduction of Fe(III) at the outer membrane might be expected. Beyond this point, iron reduction rate would be proportional to Fe(III) remaining.

12. Direct contact between cells (or ferrireductase) and Fe(III) seems necessary for achievement of iron reduction rates observed in experiments in which Fe(III) was provided either as amorphous ferric hydroxide or in soluble form (complexed with NTA). For the soluble Fe(III) case, potential limits imposed by mass transport across the hydrodynamic boundary layer surrounding the cell and by a (hypothetical) slow chemical dissociation step (Fe(III)-NTA ---> Fe^{3+} + NTA^{3-}) were examined mathematically and dismissed.

Electron-Transport-Chain Composition in Pseudomonas sp. 200.

13. Inhibitor studies of the Pseudomonas sp. 200 electron transport chain support the existence of both a constitutive (low-rate) and inducible (high-rate) ferrireductase. The high-rate enzyme is induced by low O_2 conditions, or perhaps low cellular energy levels. Whereas the constitutive enzyme system is inhibited by atebrine, dicumarol, and HOQNO, the inducible system is blocked only by atebrine. DCCD addition inhibits dissimilative iron reduction by the constitutive, but not the inducible enzyme indicating that dissimilative iron reduction via only the constitutive enzyme is linked to oxidative phosphorylation. Thus, kinetic and inhibitor studies present a uniform picture of the iron reduction mechanism in Pseudomonas sp. 200.

14. Differences in inhibition pattern indicate that Pseudomonas sp. 200 can also express both a constitutive and an inducible cytochrome oxidase. Reduced-minus-oxidized spectra developed using whole-cell preparations suggest that cytochrome o is the constitutive oxidase while cytochrome d is induced in response to low-O_2 conditions or low cellular energy levels. This pattern of cytochrome oxidase synthesis has been observed in other microorganisms. Cytochrome d permits respiration under microaerophilic conditions or perhaps scavenging of residual O_2 due to its relatively high affinity for molecular oxygen. Again, a reinforced picture of respiration in Pseudomonas sp. 200 is provided by several types of experiments -- in this case, by complementary kinetic, inhibitor, and spectrophotometric studies of aerobic electron transport system components.

Rate Limitations.

15. Analysis of O_2 utilization kinetic data obtained in the presence of various electron transport chain inhibitors does not permit identification of a rate-limiting redox reaction for uninhibited respiration. Furthermore, production of aerobic electron transport chain components is apparently well balanced, without an excess of any particular respiratory enzyme. Results of inhibitor studies are consistent with a respiratory mechanism in which transport chain elements are associated in multienzyme complexes which interchange components infrequently.

16. In the presence of soluble Fe(III) (complexed with NTA), observed rates of electron transport to the constitutive ferrireductase were modest in comparison to the aerobic respiration rate indicating that under these circumstances iron reduction is kinetically limited by

ferrireductase activity. Consequently, one might anticipate a true Michaelis-type relationship between iron reduction rate and Fe(III) concentration in uninduced cultures of Pseudomonas sp. 200.

Reductive Dissolution of Iron Oxides.

17. Catalysis of reductive dissolution of iron oxides such as hematite and goethite by Pseudomonas sp. 200 depends upon direct contact between cells and mineral. These findings provide indirect support for Michaelis-type kinetic models developed using data for the reduction of $Fe(OH)_3$(s,amorph) and soluble Fe(III)-NTA-hydroxo species.

18. NTA addition can accelerate the reductive dissolution of hematite by Pseudomonas sp. 200 by a factor of 20. Since direct particle/cell contact is required for reductive dissolution of goethite in the presence of NTA, it is apparent that overall process acceleration is not due to enhancement of a slow dissolution step followed by relatively rapid, microbially catalyzed reduction of soluble Fe(III). For cultures of the same initial cell concentration and particle surface area, there is a Michaelis-type dependence of iron reduction rate upon total NTA addition. NTA addition undoubtedly increases the free energy change associated with reductive dissolution of hematite by decreasing both the stability of Fe(III) bound at the particle surface and the concentration of free ferrous iron in solution. However, the mechanism for NTA acceleration of oxide (reductive) dissolution is unclear. NTA attached to particle surfaces may act as a bridge, shuttling electrons from membrane-bound respiratory enzymes to surface-coordinated Fe(III) centers, or the ligand may improve overall process kinetics by accelerating the departure of Fe(II) as an Fe(II)-NTA complex from the particle surface following electron transport.

19. For a given initial cell density and total NTA concentration, there is a Michaelis-type relationship between particle surface area and culture iron-reduction activity. For a given initial particle surface area, reduction in cell number from 2×10^9/ml to 2×10^7/ml has little effect on the culture iron reduction rate, indicating that (i) at the concentrations of hematite (surface area) and initial cell densities employed in these experiments, oxide surface area is in some sense saturated with microorganisms and (ii) the sustainable culture cell number is a weak function of total particle (oxide) surface area in the ranges investigated.

20. It is difficult to reconcile the role(s) of NTA addition in enhancement of reductive dissolution kinetics when Fe(III) is presented as (i) $Fe(OH)_3$(s,amorph) as opposed to (ii) more stable iron oxides. The NTA-driven dissolution of amorphous ferric hydroxide is fast compared to the observed iron reduction rate (if, in fact, $Fe(OH)_3$(s,amorph) forms at all since NTA and $FeCl_3$ were added almost simultaneously in these experiments). Consequently, rate enhancement in the former case is primarily due to an increase in the equilibrium concentration of soluble ferric iron species. The apparent non-equivalence of soluble species, in terms of their effect on overall iron reduction rate, may be due to steric specificities of the ferrireductase, charge effects, etc. When Fe(III) is provided as hematite or other stable oxides, however, chemical dissolution is slow in comparison to observed rates of reductive dissolution. In this case, NTA either facilitates the transfer of respiratory electrons from cell to oxide surface or assists in the departure of Fe(II) centers following electron transfer.

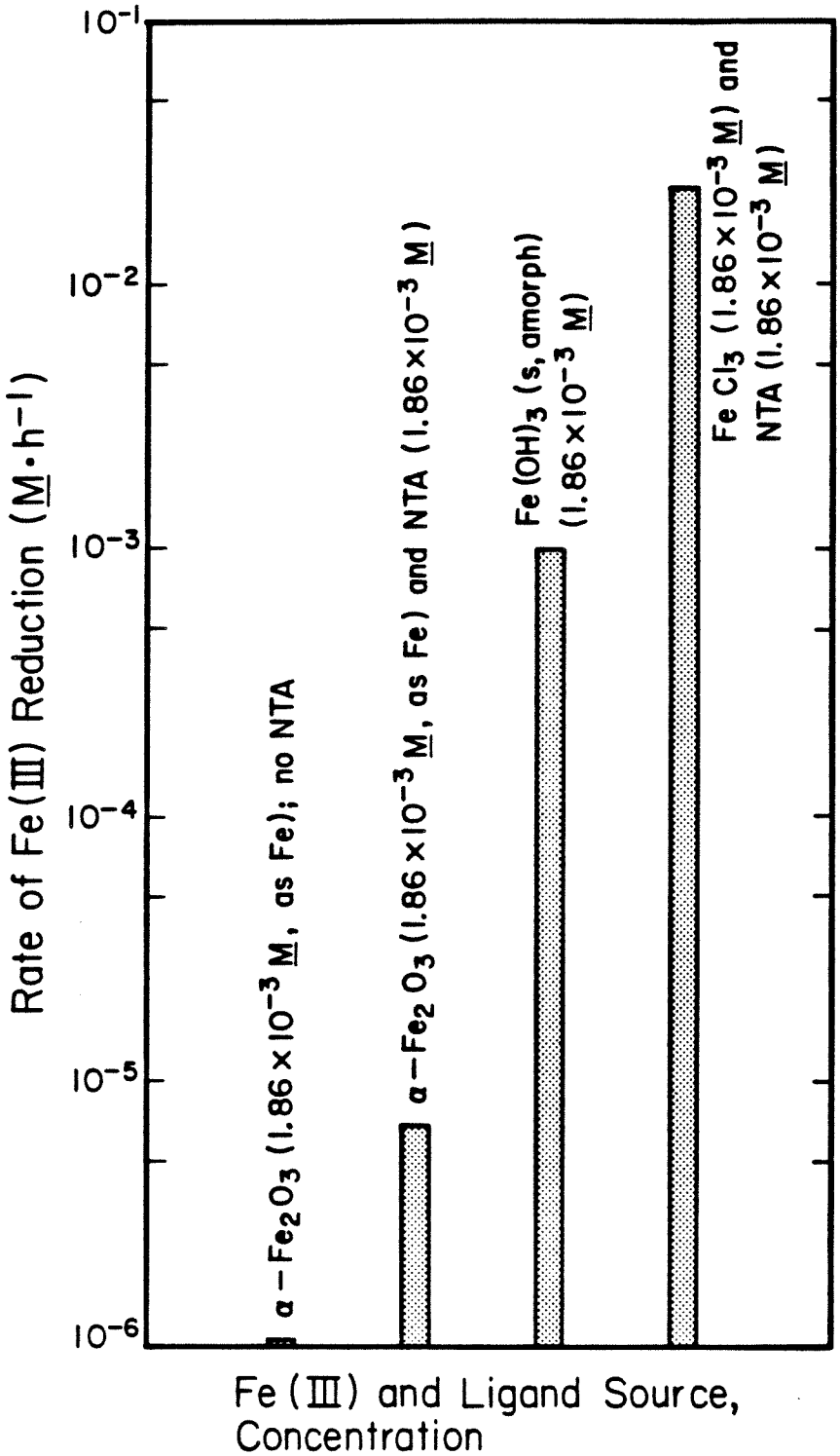

Figure 7.1 Variation in observed rate of dissimilative iron reduction by Pseudomonas sp. 200 as a function of Fe(III) aqueous chemistry.

21. Observed iron reduction rates vary over several orders of magnitude in response to the form in which Fe(III) is provided to otherwise similar cultures. As indicated in Figure 7.1, the observed rate of reduction of soluble, complexed Fe(III) is more than 10^3 times as fast as the rate of reductive dissolution of hematite (same total Fe concentration, saturating concentration of NTA). However, if these rates are normalized on the basis of Fe(III) accessibility (when Fe(III) is provided as iron oxide, only surface iron centers are considered exposed) they differ by a factor of about 30. The unexplained difference may be due to the aggregated nature of oxides such as hematite and goethite in growth media at neutral pH. That is, when only the concentration of ferric iron in solution or suspension which can be directly contacted by microorganisms is considered, it becomes clear that the bacterium is virtually indifferent to the form in which Fe(III) is encountered as long as oxidant can be contacted directly and is present in sufficient quantity.

Control of Ferrireductase Activity in the Presence of Dissolved O_2.

22. Experiments in which ferrozine, a non-inhibitory ligand which forms a colored tris complex with Fe(II), was used to measure the bacterial iron reduction rate in the presence of dissolved oxygen indicate that in batch cultures of Pseudomonas sp. 200 electron transport to Fe(III) does not proceed until dissolved oxygen is virtually exhausted. This is relatively easy to reconcile within the framework of a branched electron transport chain when cells are grown at high O_2 concentration (uninduced). Such cells are incapable of catalyzing iron reduction at rates approaching that of aerobic electron transport; electrons can be directed kinetically to O_2 without throwing

any sort of biological switch within the respiratory chain. The aerobic branch simply outcompetes the constitutive branch to Fe(III) for reducing equivalents which reach the branch point. On the other hand, one might expect simultaneous reduction of O_2 and Fe(III) among induced cells since the activity of the high-rate ferrireductase approaches that of cytochrome oxidase. However, ferrozine experiments indicated that dissimilative iron reduction is also virtually nil until O_2 is exhausted from induced cultures. A mechanism for control of this sort over electron transport offers considerable benefit to the organism by maximizing the useful energy potentially available from substrate metabolism despite the presence of electron acceptors less energetically favorable than O_2. Mechanistic details, however, are unclear. Among the simplest possibilities is competitive inhibition of the high-rate, inducible ferrireductase by molecular oxygen. Such a mechanism is unlikely, however, in light of experiments in which iron reduction was observed in the presence of O_2 and CN^-.

23. It is clear from the foregoing that at least two levels of control govern the kinetics of dissimilative iron reduction in Pseudomonas sp. 200. A high-rate ferrireductase is induced by low-O_2 or low-energy conditions, avoiding needless protein synthesis in the presence of more thermodynamically favorable electron acceptors. Since dissimilative iron reduction via the inducible ferrireductase is probably not coupled to oxidative phosphorylation, electron transport to Fe(III) would prove to be an extremely inefficient use of cellular reducing power when induced cells again enter an aerobic environment. A second control mechanism, directing respiratory electrons toward molecular oxygen, apparently enables the cell to avoid this potentially

wasteful practice. Such control makes the microorganism particularly well adapted to microaerophilic environments in which there is an ample supply of ferric iron.

24. Reduced-minus-oxidized spectra of whole-cell preparations of Pseudomonas sp. 200 indicate that the cell cytochrome content includes a number of c- and b-type cytochromes. Cytochrome o is the constitutive cytochrome oxidase, but during growth under O_2-limited conditions a second cytochrome oxidase, cytochrome d, is induced. The high-rate, inducible ferrireductase is apparently not a cytochrome or other pigmented enzyme inasmuch as the spectral signature of induced cells is qualitatively unchanged (with the exception of cytochrome d synthesis) relative to that of cells grown under highly aerobic conditions.

References

Chance, B. and Williams, G. R. The respiratory chain and oxidative phosphorylation. Adv. Enzymol. 17: 65-134 (1956).

Chance, B. Cellular oxygen requirements. Fed. Proc. Fedn. Am. Socs. Exp. Biol. 16: 671-680 (1957).

Lascelles, J. and Burke, K. A. Reduction of ferric iron by lactate and DL-glycerol-3-phosphate in membrane preparations from Staphylococcus aureus and interaction with nitrate reductase system. J. Bacteriol. 134: 585-589 (1978).

APPENDIX

SCREENING EXPERIMENTS AND PRELIMINARY STUDIES INVOLVING *PSEUDOMONAS* SP. 200

A.1 Screening Experiments

A.1.1 General

Although a number of microorganisms are capable of catalyzing dissimilative iron reduction (Chapter 1), intercomparison of iron reducers on the basis of process kinetics is not yet possible. However, experiments involving pure cultures of select, iron-reducing bacteria allow comparison of their growth and iron-reduction characteristics. As explained below, the screening experiments have common objectives and structural similarities which make their description relatively simple.

The list of microorganisms selected, although by no means exhaustive, includes those offering the greatest potential from the standpoint of iron-reduction kinetics. Ottow (1968) indicated that at least two mechanisms for direct dissimilative reduction of Fe(III) are represented among the species selected for screening. In addition, *Thiobacillus thiooxidans* is thought to reduce Fe(III) via an indirect mechanism involving a chemical intermediate. Relevant characteristics of microorganisms tested are summarized in Table A.1.

Screening experiments were designed to yield data in three areas:

(i) Batch growth experiments provided an estimate of the rate constant for logarithmic growth or doubling time for each bacterial species screened. Growth curves were generated under near-optimal

Table A.1 Iron-reducing Bacteria Included in Screening Experiments; Classification and Comment. (American Type Culture Collection Designations in Parenthesis.)

Classification & Species	O_2(g) Utilization	Energy Source	Mechanism for Iron Reduction[a]	References
A. Genus Bacillus				
Bacillus circulans (E4513)	Facultative Anaerobic	Heterotroph (various sources)	Enzymatic	Silverman & Ehrlich (1964) Ehrlich (1981) Bromfield (1954a) Bromfield (1954b) Troshanov (1968) Troshanov (1969) Ottow (1969)
Bacillus polymyxa (842)	Facultative Anaerobic	Heterotroph; grew well on glucose and fructose only	Enzymatic	Silverman & Ehrlich (1964) Ehrlich (1981) Bromfield (1954a) Troshanov (1968) Ottow (1969) Hammann & Ottow (1974)
Bacillus pumilus (E72)	Facultative Anaerobic	Heterotroph	Enzymatic	Ehrlich (1981) Ottow (1968) Ottow (1969)
B. Genus Pseudomonas				
Pseudomonas aeruginosa (E10145)	Will not grow in absence of respiration	Heterotroph	Enzymatic	Ottow (1968) Ottow (1969)
Pseudomonas sp. 200[b] (isolated from crude oil)	Will not grow fermentatively	Heterotroph; lactate, glucose, succinate	Enzymatic	Obuekwe, Westlake & Cook (1981)

Table A.1 (continued)

Classification & Species	O_2(g) Utilization	Energy Source	Mechanism for Iron Reduction[a]	References
C. Genus *Thiobacillus*				
Thiobacillus thiooxidans (19377 & E8085)	Obligate Aerobic	Reduced sulfur forms	Non-enzymatic	Silverman & Ehrlich (1964) Ehrlich (1981) Brock & Gustafson (1976) Kino & Usami (1982)

[a] "Enzymatic" implies that the microorganism is capable of utilizing some form of ferric iron as terminal electron acceptor for the electron transport chain. "Non-enzymatic" implies that iron reduction is not directly related to bacterial respiration.

[b] Source of all bacterial cultures except *Pseudomonas* sp. 200 were the American Type Culture Collection. *Pseudomonas* sp. 200 was obtained from Dr. D. W. S. Westlake of the University of Alberta, Edmonton, Alta., Canada.

conditions in media developed for respective microorganisms by other investigators. For the most part, the level of effort associated with the overall screening program precluded an investigation of kinetic effects atributable to systematic variation of such environmental variables as temperature, pH, nutrient concentration, and energy source.

(ii) The kinetics of iron reduction were investigated at or immediately following the cessation of the log-growth phase (onset of early-stationary phase). Fe(III) was invariably provided as $FeCl_3$ or $FeNH_4(SO_4)_2$; in the neutral pH range, Fe(III) precipitates rapidly to form colloidal $Fe(OH)_s$(s,amorph). Consequently, growth measurements based on suspension optics were not possible during the iron-reduction phase of these experiments. With the exception of experiments involving acidophiles, molecular oxygen was excluded from solution during iron-reduction phase in order to avoid reoxidation of Fe(II) (Sung and Morgan, 1980). For both of these reasons, measurements of growth and iron-reduction kinetics did not generally overlap.

(iii) Although measurement of nutrient levels and utilization rates was generally confined to organic substrates and molecular oxygen, estimation of a few yield parameters was possible. These and other yield factors bear upon the commercial viability of microbial iron-extraction schemes.

A.1.2 Procedures

All screening experiments were conducted in 1.5-liter batch cultures in a Biostat M fermentor purchased from Braun Instrument Company. A reactor schematic is provided as Figure A.1. The Biostat M is equipped for continuous measurement of temperature, pH, and dissolved oxygen

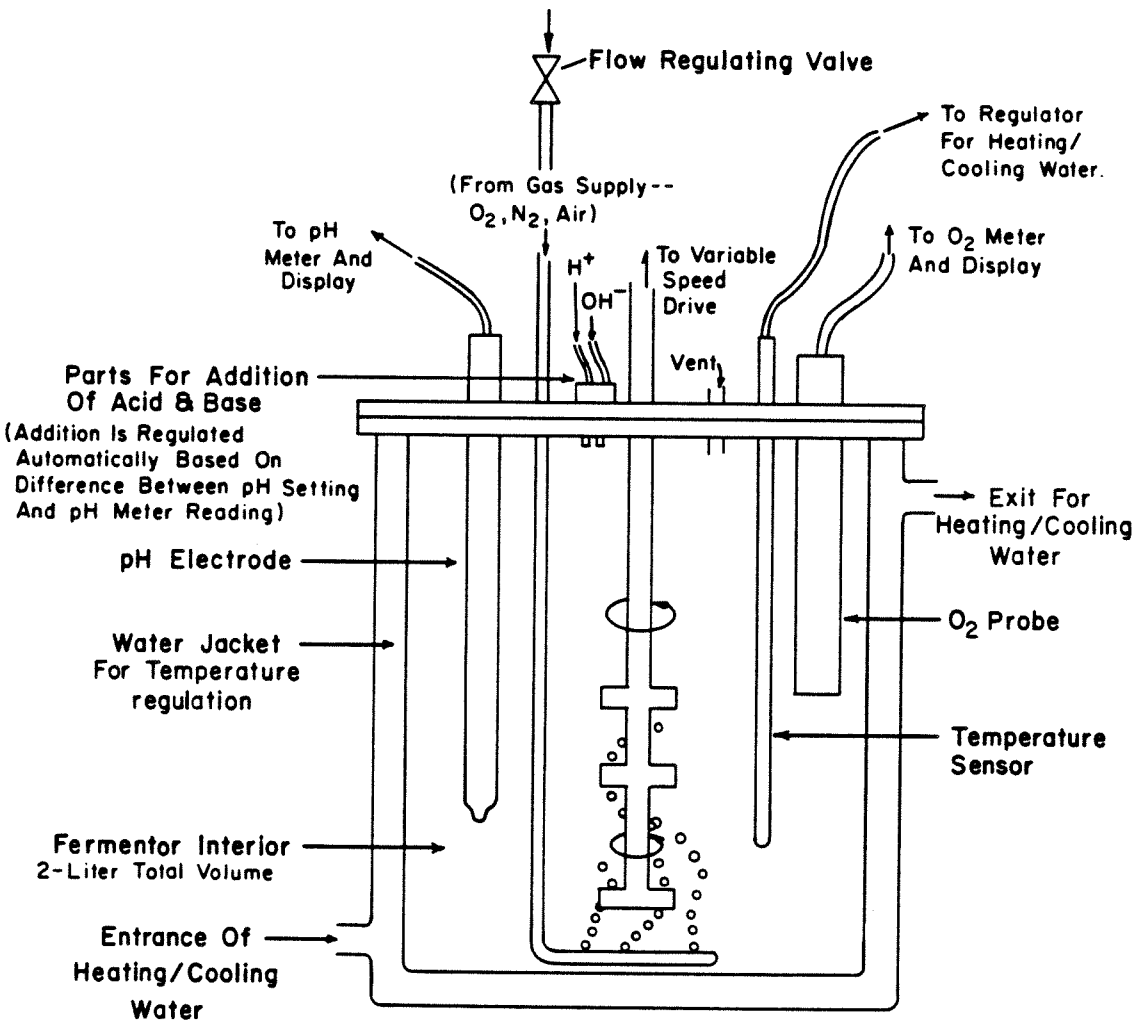

Figure A.1. Schematic diagram of Biostat M 2-liter laboratory fermentor (Braun Instrument Co.).

concentration. Both temperature and pH can be regulated automatically; culture dissolved oxygen levels can be controlled, albeit somewhat crudely, by adjusting the culture agitation speed or the gas flow rate and composition. Routine fermentation procedures (summarized schematically in Figure A.2) follow:

(i) The Biostat M was filled to 1.5 liters with growth medium, and reactor and contents were autoclaved at 121°C for approximately 30 minutes. Equipment for pH measurement was routinely calibrated before autoclaving; the O_2 probe and meter were calibrated after sterilization.

(ii) Growth was initiated by adding 1.5 mls from a dense overnight or stock culture of microorganisms. Culture optical density was monitored in real-time by periodically withdrawing aliquots for measurement of light attenuation at 600 nm in a 1-cm pathlength cuvette (Beckman DU-7 spectrophotometer). A portion of each aliquot was saved for measurement of particulate-phase total organic carbon and total protein (after centrifugation and washing). Substrate levels were monitored in the liquid phase. The rate of dissolved-oxygen utilization following periodic interruption of gas flow to the reactor was also measured as an indication of culture activity.

(iii) When real-time measures of culture growth and activity (optical density and O_2-depletion rate) indicated that the culture was in early stationary growth phase, the culture was purged of oxygen with $N_2(g)$, and high levels of ferric iron ($1.8\text{-}3.6 \times 10^{-3}$ M) were added from either $FeCl_3$ or $Fe(NH_4)(SO_4)_2$ stock solutions. Thereafter, although optical density and oxygen utilization measurements were discontinued, meaurements of particulate-phase TOC, protein levels, and liquid-phase substrate concentration were carried out to completion of the

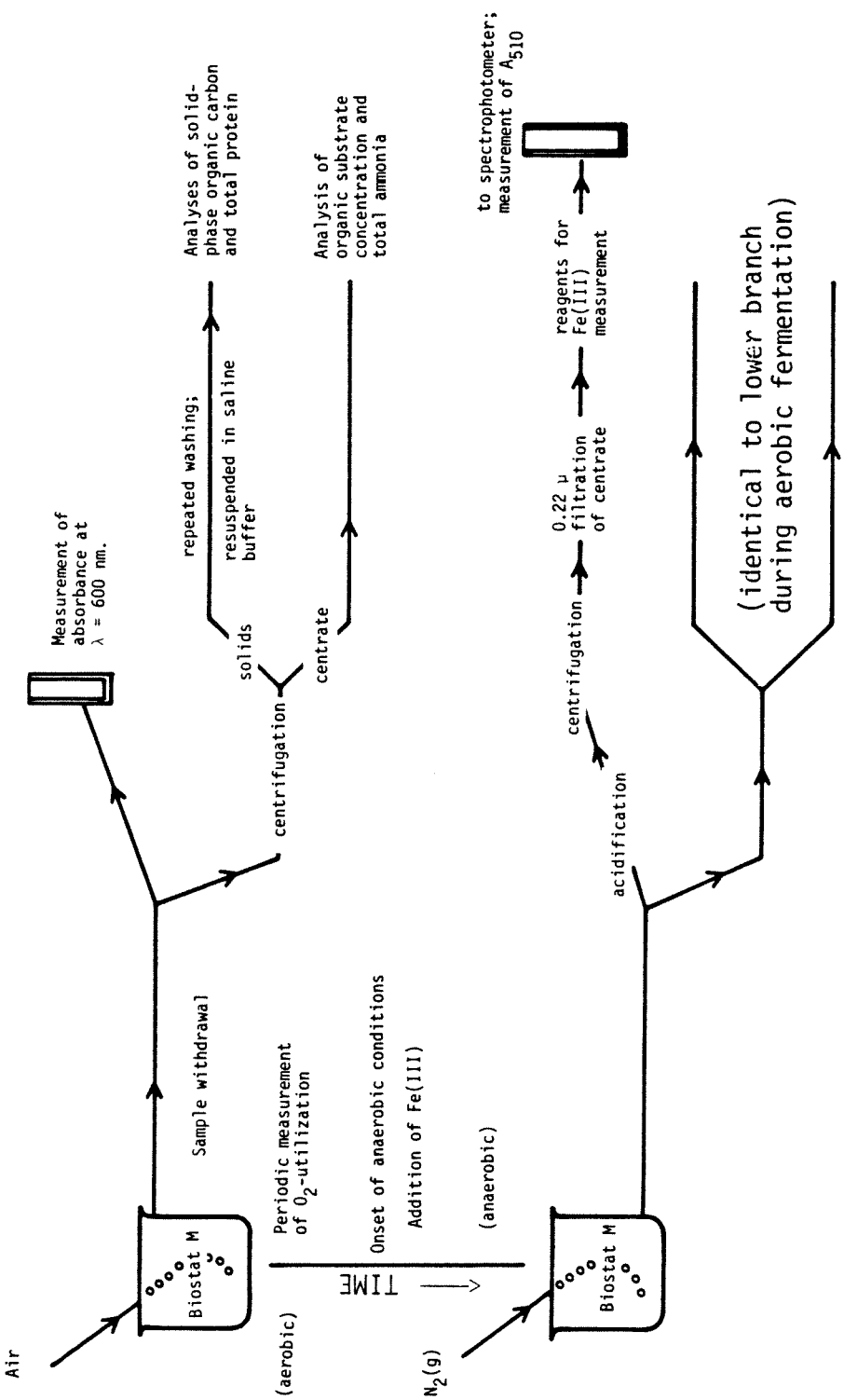

Figure A.2. Schematic representation of procedures which normally comprised iron-reduction screening experiments (exceptions, per text).

fermentation. Periodic measurement of ferrous iron concentration was initiated at the point of addition of high-level Fe(III) to solution and continued to the end of the experiment.

There were significant exceptions to the general experimental scheme outlined above. These involved primarily experiments conducted with Thiobacillus thiooxidans. In these fermentations, low solution pH stabilized ferrous iron in the presence of dissolved oxygen; maintenance of anaerobic conditions was not essential during the iron-reduction phase of these experiments, and oxygen-depletion rate could be measured throughout the fermentation as an indicator of microbial activity.

In those experiments in which elemental sulfur served as energy source for microbial growth (again, T. thiooxidans), optical density measurements were never a meaningful indicator of biomass. Consequently, the only available real-time indicator of culture activity was oxygen-utilization rate. Other departures from the general scheme will be discussed as necessary.

A detailed description of procedures for individual measurements follows:

(1) Optical density (A_{600}) - Light attenuation measurements were carried out in a Model DU7 Beckman spectrophotometer, λ = 600 nm, using a 1-cm-pathlength cuvette. Growth curves (A_{600} vs. time) reflect absorbance values after correction for a medium blank.

(2) Total organic carbon (TOC) - In general, samples were prepared by repeated centrifugation at 3500 rpms (3200 x g) in a model RC-3B Sorvall centrifuge. The solid phase was resuspended in saline buffer (0.15 M NaCl, 1 mM $MgCl_2$ in distilled H_2O). After two such washing steps, the solid phase was sufficiently free of dissolved organics to

permit analysis for the organic-carbon component of microbial biomass. TOC measurements were carried out in a model DC-50A Dohrmann TOC analyzer.

(3) Rate of $O_2(g)$ utilization - The Ingold probe and O_2 meter built into the Biostat M permit continuous measurement of culture dissolved oxygen. During this procedure, airflow to the reactor was briefly cut off and dissolved oxygen concentration measured as a function of time following its interruption. The slope of the $O_2(g)$ versus time curve was used to estimate the rate of dissolved-oxygen utilization.

(4) Total protein - Total solid-phase protein (TSPP) was measured as an alternative indicator of microbial biomass. The relationship between TSPP and TOC during various growth phases was also a matter of interest. Measurements were preceded by the several washing steps described earlier for analysis of insoluble TOC. Sample preparation also included steps designed to extract membrane-bound protein. Following the general procedure of Herbert et al. (1971), NaOH was added to washed-cell preparations to a concentration of about 1.0 N, and the mixture was heated at 100°C for 10-15 minutes to dissolve cell membranes. Following pH restoration (via HCl addition) and centrifugation, centrate protein was measured using reagents and methods available in kit form from Sigma Chemical Company (Sigma diagnostics - catalog no. 690-A).

(5) Glucose analysis - A commerically available kit (Sigma Chemical Company catalog no. 16-UV) and recommended protocol were also used for glucose analyses. Glucose was measured in centrate from the first cell-washing step (see Figure A.2). Results were used in carbon balances to estimate bacterial yield coefficients.

(6) Ferrous iron - To preclude reoxidation of Fe(II), samples were acidified to pH 1 to 2 by addition of one or two drops of 25% hydrochloric acid immediately upon withdrawal. Solids were removed via centrifugation in a Sorvall model RC-3B centrifuge for 15 minutes at 3500 rpms (3200 x g). Centrate was filtered (0.2 μm filter, Millepore) and filtrate was assayed for Fe(II) by adding successively: (1) 1 ml of filtrate, (2) 1-2 mls of a 0.5% w/v solution of 1,10-phenanthroline (sufficient volume to provide excess phenanthroline), and (3) 1-2 mls of ammonium acetate buffer solution (250 g $NH_4CH_3CO_2$ dissolved in 150 mls distilled H_2O plus 200 mls glacial acetic acid). All samples were diluted to 10 mls prior to color measurement. When analysis for total iron was required, 2 mls of hydroxylamine solution (10 g $NH_2OH \cdot HCl$ in 100 mls distilled H_2O) were substituted for 2 mls of dilution water. Reagents were prepared as described in Standard Methods for Analysis of Water and Wastewater, 15th editon (1980). Under conditions of the test, the intensity of the deep red color attributable to the Fe(II)-phenanthroline complex is proportional to the concentration of ferrous iron in the sample. Color development was measured in a Model DU-7 Beckman spectrophotometer at $\lambda = 510$ nm. The extinction coefficient for light absorption by the Fe(II)-phenanthroline complex is 1.11×10^4 $(M\ cm)^{-1}$, verified by separate experiment.

(7) In experiments involving Pseudomonas sp. 200, lactate concentration was measured via ion-exchange chromatography using a Dionex 2020i ion chromatograph. Lactate was separated on a standard anion column using a CO_3^{2-}/HCO_3^- eluent. Quantification was by peak area.

Unless otherwise indicated, procedures described above apply to all screening experiments. Departures are described as necessary in the following sections. Culture media for all bacteria screened are defined in Table A.2.

A.1.3 Results and discussion

Results are provided largely as a series of Figures and Tables designed to facilitate inter-species comparison of growth and iron-reduction rates. Fermentation conditions which may have differed slightly from one experiment to another, including air flow, temperature, agitation rate, etc., are routinely summarized on the same figure as the results. Table A-3, Table A-4, and Figure A-10 offer summarized estimates of growth and iron-reduction parameters. In the following discussion, experiments are arbitrarily grouped by bacterial genus.

A.2.3.1 Genus Bacillus (B. pumilus, B. polymyxa, B. circulans).

Experiments involving these microorganisms produced similar results (Figures A.3 through A.5). All three species grow at a moderate rate; during log growth, cell divisions occur with an average period of 1.0 to 1.5 hours. B. polymyxa is unique among the three in its ability to oxidize glucose and continue to assimilate carbon following the onset of anaerobic conditions (see Figure A.4(b)). Both carbon assimilation and iron-reduction rate are clearly a function of glucose concentration; the decline in insoluble TOC and protein is precipitous upon glucose exhaustion, and iron reduction seems to depend upon glucose

Table A.2 Growth Media for Microorganisms Included in Iron-reduction Screening Experiments.

Thiobacillus thiooxidans (on a per-liter basis)	
$(NH_4)_2SO_4$	1.32 g
KH_2PO_4	0.27 g
$MgSO_4$	0.12 g
$CaCl_2$	0.0555 g
$MnSO_4 \cdot H_2O$	1.54 mg
H_3BO_4	2.86 mg
$ZnSO_4 \cdot 7H_2O$	0.22 mg
$CuSO_4 \cdot 5H_2O$	0.079 mg
$VOSO_4 \cdot 2H_2O$	0.039 mg
$Na_2MoO_4 \cdot 2H_2O$	0.025 mg
Na_2SeO_3	0.017 mg
$FeCl_3 \cdot 6H_2O$	19.36 mg
precipitated sulfur (10 grams) final pH 2.0 to 4.0	

Pseudomonas sp. 200 (on a per liter basis)	
K_2HPO_4	0.5 g
Na_2SO_4	2.0 g
NH_4Cl	1.0 g
$CaCl_2$	0.15 g
$MgSO_4 \cdot 7H_2O$	0.1 g
$FeCl_3 \cdot 6H_2O$	19.36 mg
Yeast extract	(0.5 grams)
Na-lactate (3 mls, 60% syrup)	
final pH 6.5 to 7.5	

Pseudomonas aeruginosa (on a per liter basis)	
KH_2PO_4	0.8 g
K_2HPO_4	3.0 g
$MgSO_4 \cdot 7H_2O$	0.2 g
$CaCl_2$	0.01 g
Asparagine	5.0 g
Yeast extract	0.5 g
Succinic acid	9.8 g
$FeCl_3 \cdot 6H_2O$	19.36 mg
final pH = 7.0	

Bacillus polymyxa, B. circulans, B. pumilus (on a per liter basis)	
$(NH_4)_2SO_4$	1.0 g
$MgSO_4 \cdot 7H_2O$	0.2 g
Na_2HPO_4	3.58 g
KH_2PO_4	1.5 g
$FeCl_3 \cdot 6H_2O$	19.36 mg
$CaCl_2$	0.01 g
Yeast extract	0.15 g
Glucose (25 mls of a 20% syrup)	
final pH = 7.0	

Sterilization Notes (general)

(1) In general, media were sterilized by autoclaving at 121°C for 20-30 min.

(2) Iron chloride was prepared in 1000x solutions and filter-sterilized prior to addition.

(3) Glucose was sterilized separately (20-30 min. @ 121°C) and added to the previously autoclaved media.

(4) Thiobacillus medium was sterilized by tyndallization. Precipitated sulfur was floated on the liquid medium and autoclaved at 100°C, 1 atm. for one hour on three successive days.

Table A.3 Growth and Iron-reduction Characteristics of Bacteria Screened for Dissimilative Iron-reduction Capacity.

Species/strain	Log-growth Rate Constant (hr^{-1})	Log-growth Doubling Time (hours)	Iron Reduction Rate ($\underline{M}$-hr^{-1}) (2)	Fe(III) Reduction Rate/ Biomass ($\underline{M}$/hr-g insoluble carbon)
Bacillus pumilus ATCC #E72	0.46	1.5	8.95×10^{-7}	3.58×10^{-5}
Bacillus polymyxa ATCC #842	0.63	1.1	1.79×10^{-5}	1.34×10^{-4}
Bacillus circulans ATCC #E4513	0.63	1.1	8.95×10^{-6}	6.98×10^{-5}
Thiobacillus thiooxidans ATCC #19377	0.055	12.7	1.79×10^{-5}	9.63×10^{-4}
Thiobacillus thiooxidans ATCC #E8085	0.075	9.3	2.5×10^{-5}	5.01×10^{-4}
Pseudomonas aeruginosa ATCC #E10145	1.26	0.55	2.5×10^{-6}	1.59×10^{-5}
Pseudomonas sp. 200	0.84	0.83(1)	1.99×10^{-4}	5.23×10^{-4}

Notes:
(1) Represents doubling time during early log growth. Exponential growth was biphasic (see text) perhaps reflecting exhaustion of preferred nutrient supply at $A_{600} \cong 0.2$ (cm^{-1}).
(2) Cells were grown to early stationary phase prior to establishment of anaerobic conditions and addition of high-level Fe(III).

Table A.4 Yield Factors Associated with Growth and Respiration by Bacteria Screened.

Species/strain	Carbon assimilated / Carbon utilized (a) [1]	Fe(III) reduced / 4(1-a)(C util.) [2]	Protein/TOC (gram/gram)			$Y_{(C/O_2)}$ [3]		$Y_{(O_{2/S})}$ [4]	$Y_{(O_{2/C})}$ [5]
			Log Phase	Stationary	Anaerobic	Log Phase	Stationary		
Bacillus pumilus	0.13 (glucose)	8.76×10^{-4}	1.8	1.4	1.1	O_2 not measured		NA	NC
Bacillus polymyxa	0.21 (glucose)	6.95×10^{-4}	1.4	1.7	2.4	O_2 not measured		NA	NC
Bacillus circulans	0.28 (glucose)	not measured	2.6	1.8	1.	O_2 not measured		NA	NC
Thiobacillus thiooxidans ATCC #19377	NA	NA	total insoluble protein not measured			0.053	0.084	NC	NA
Thiobacillus thiooxidans ATCC #E8085	NA	NA	total insoluble protein not measured			0.072	0.113	0.27	NA
Pseudomonas aeruginosa	not measured	not measured		0.1		not measured			
Pseudomonas sp. 200	0.8 (lactate)	3.22×10^{-2}	0.12	0.13	0.12	1.04	O_2 msmt. not feasible		0.26

NA (not applicable)

NC (not calculated)

Table A.4 (continued)

Notes:

(1) Primary substrate in parentheses. Ratio applies to growth up to early stationary phase.

(2) Molar ratio. Complete oxidation of 1 mole of organic carbon (as glucose or lactate) requires transfer of 4 moles of electrons. Therefore, if a = the fraction of substrate carbon assimilated, 4(1-a) represents the number of moles of electrons transferred per mole of substrate carbon utilized 'when organic carbon is either mineralized or assimilated into biomass of average oxidation state zerc).

(3) Yield factor defined as molar ratio of carbon assimilated to molecular oxygen utilized. If conversion of CO_2 to organic carbon requires 4 moles of reducing equivalent per mole of carbon assimilated (i.e., for chemolithotrophs), this factor is equal to the fraction of substrate reducing power which is converted to biomass.

(4) Defined as molar ratio of sulfur oxidized to molecular oxygen utilized. Complete oxidation of elemental sulfur would require 1.5 moles O_2/mole of SO_4^{2-} formed. Calculation is based on data up to the assumed point of sulfur exhaustion.

(5) Defined as molar ratio of substrate carbon oxidized to molecular oxygen utilized. Complete oxidation of lactate would require 1 mole of O_2/mole of CO_2 formed.

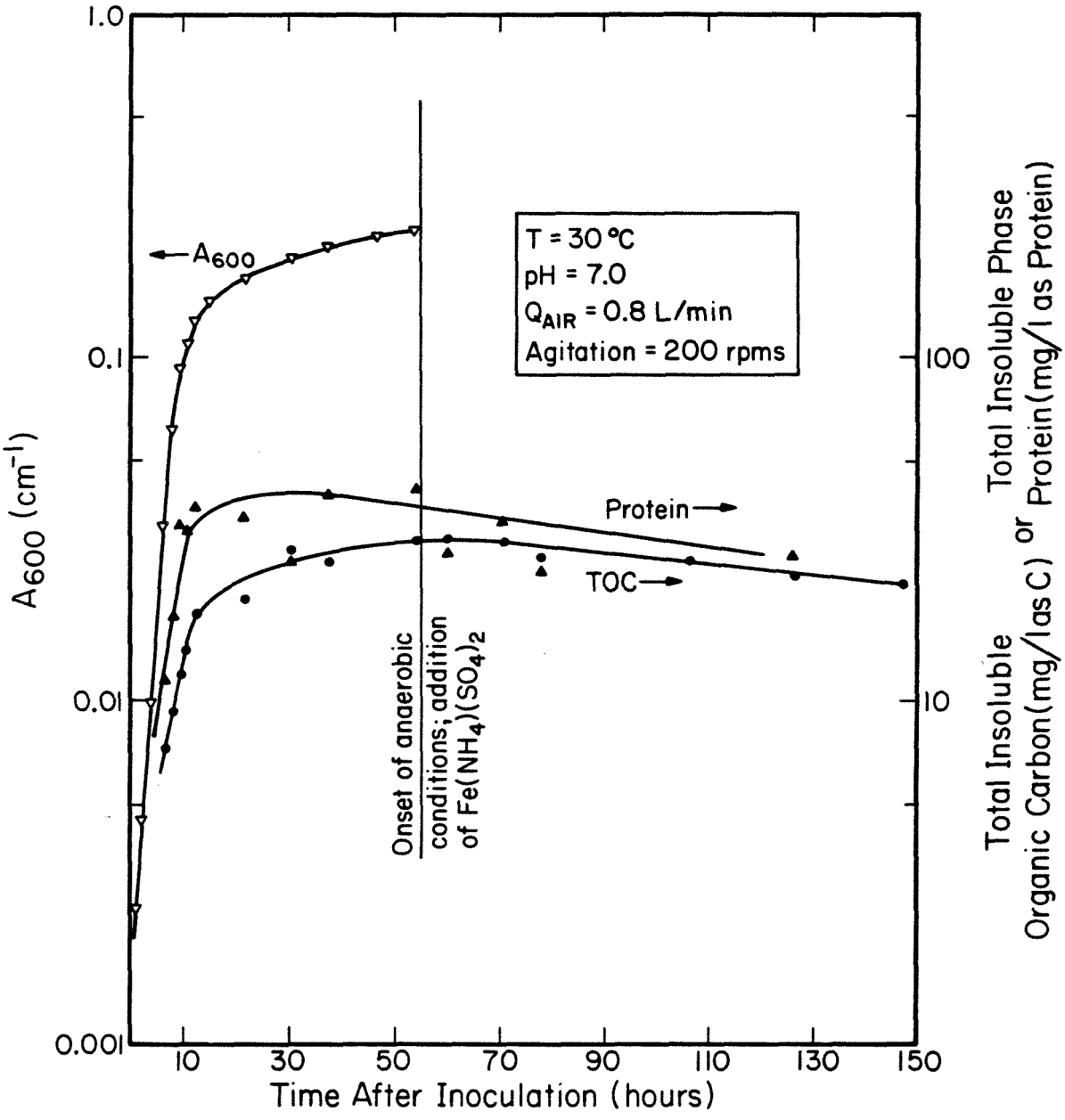

Figure A.3(a). Indicators of microbial biomass as functions of time during a batch fermentation of Bacillus pumilus.

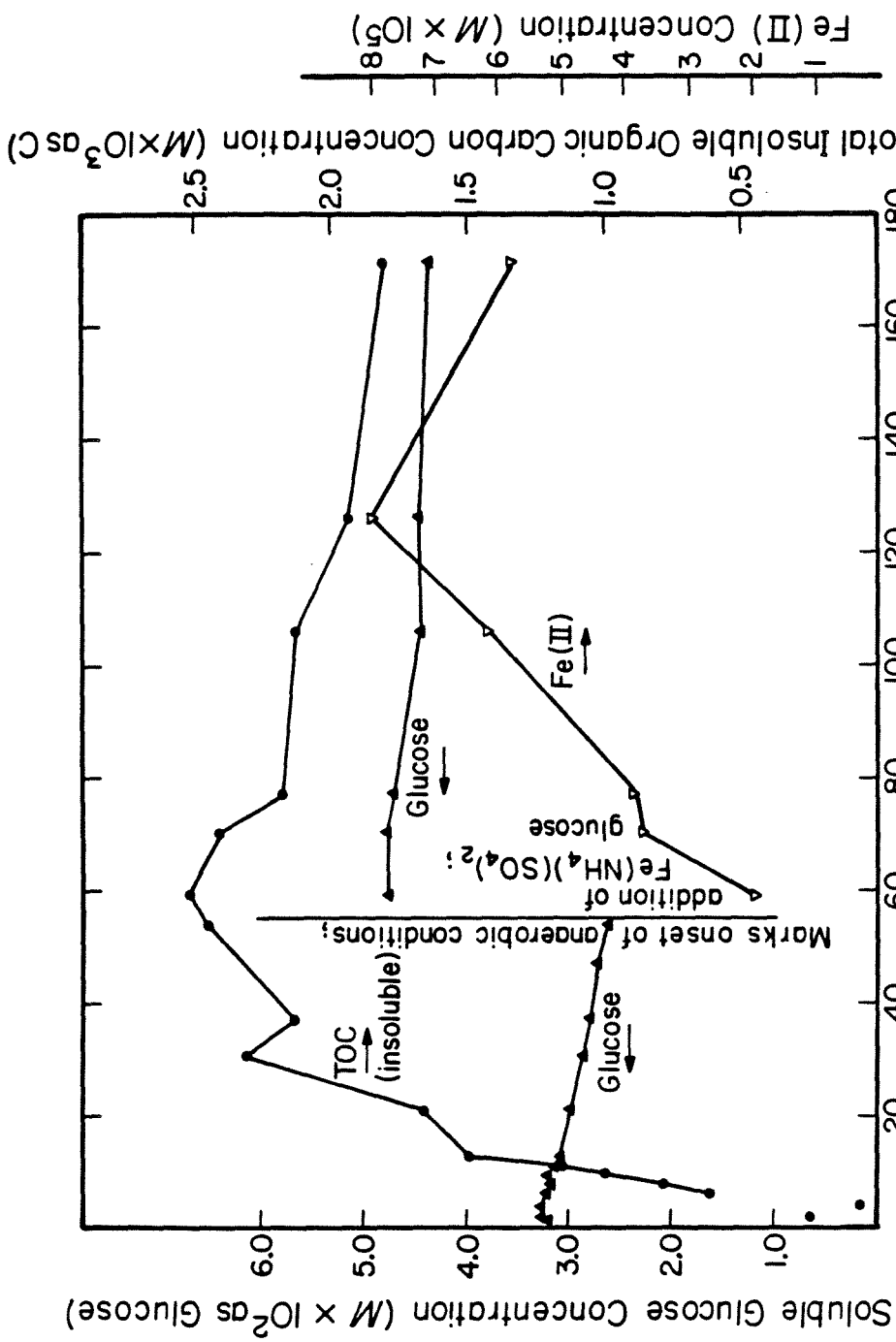

Figure A.3(b). Growth (TOC), substrate utilization, and iron reduction as functions of time during a batch fermentation of Bacillus pumilus.

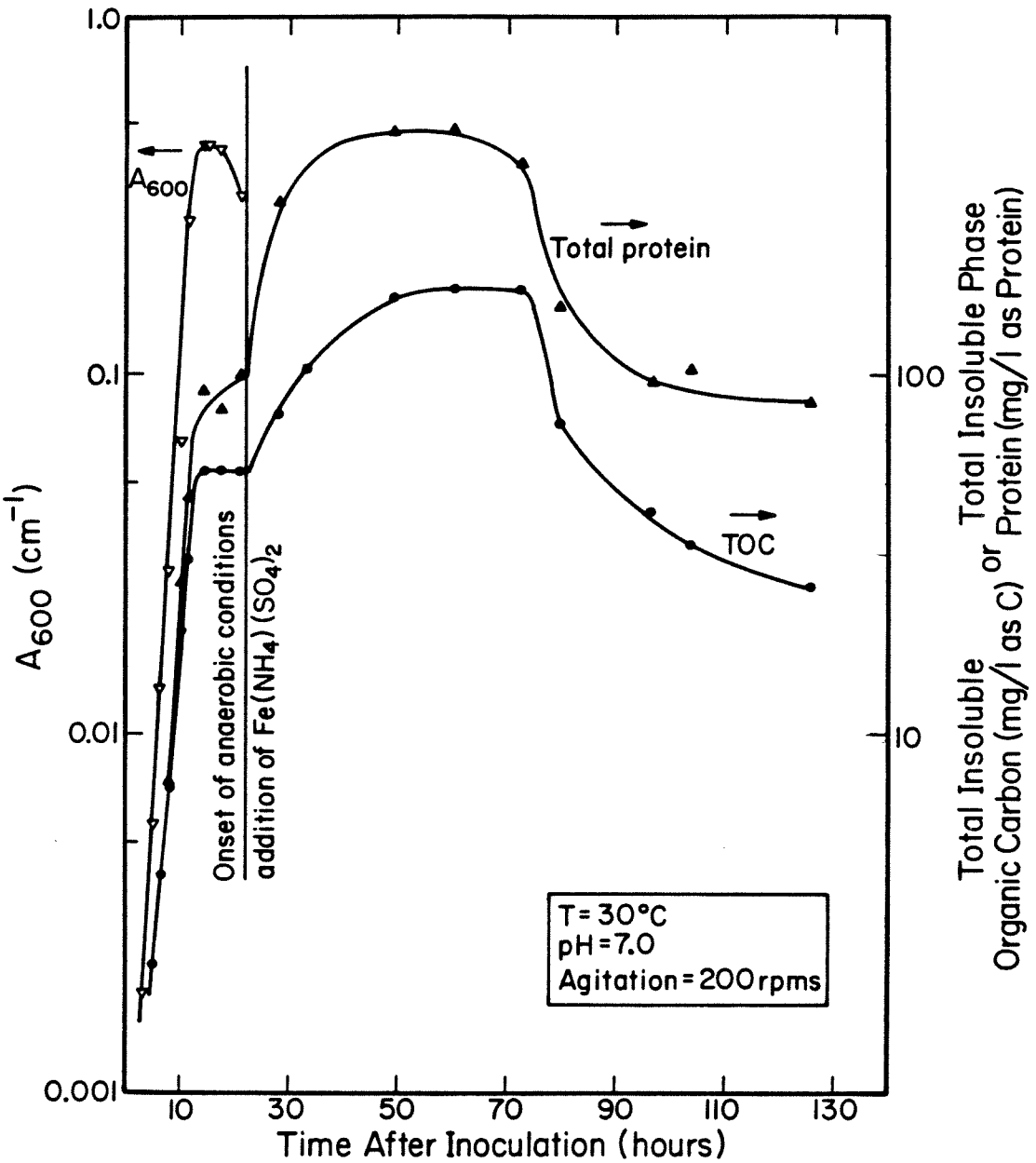

Figure A.4(a). Indicators of microbial biomass as functions of time during a batch fermentation of Bacillus polymyxa.

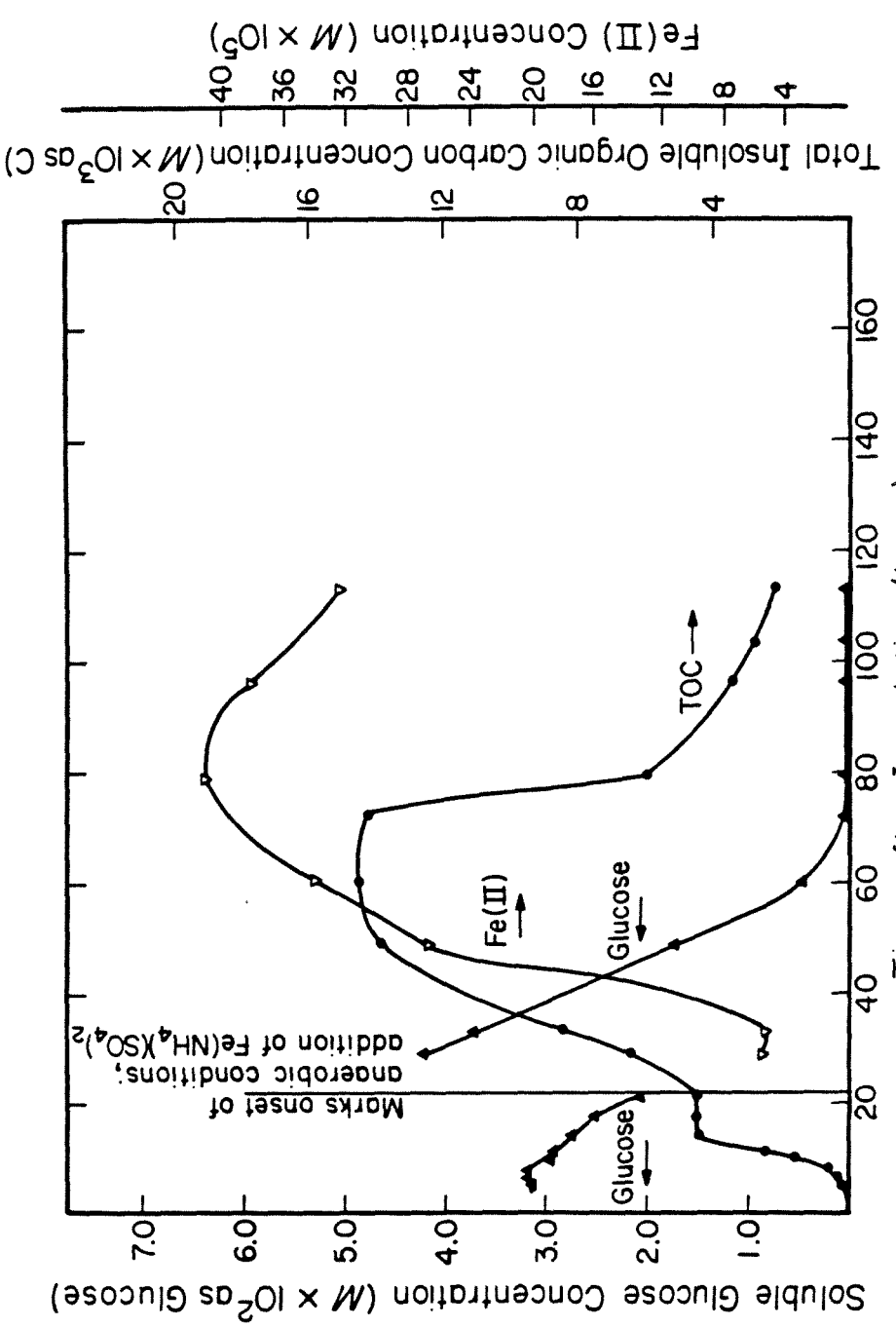

Figure A.4(b). Growth (TOC), substrate utilization, and ferrous iron as functions of time during a batch fermentation of Bacillus polymyxa.

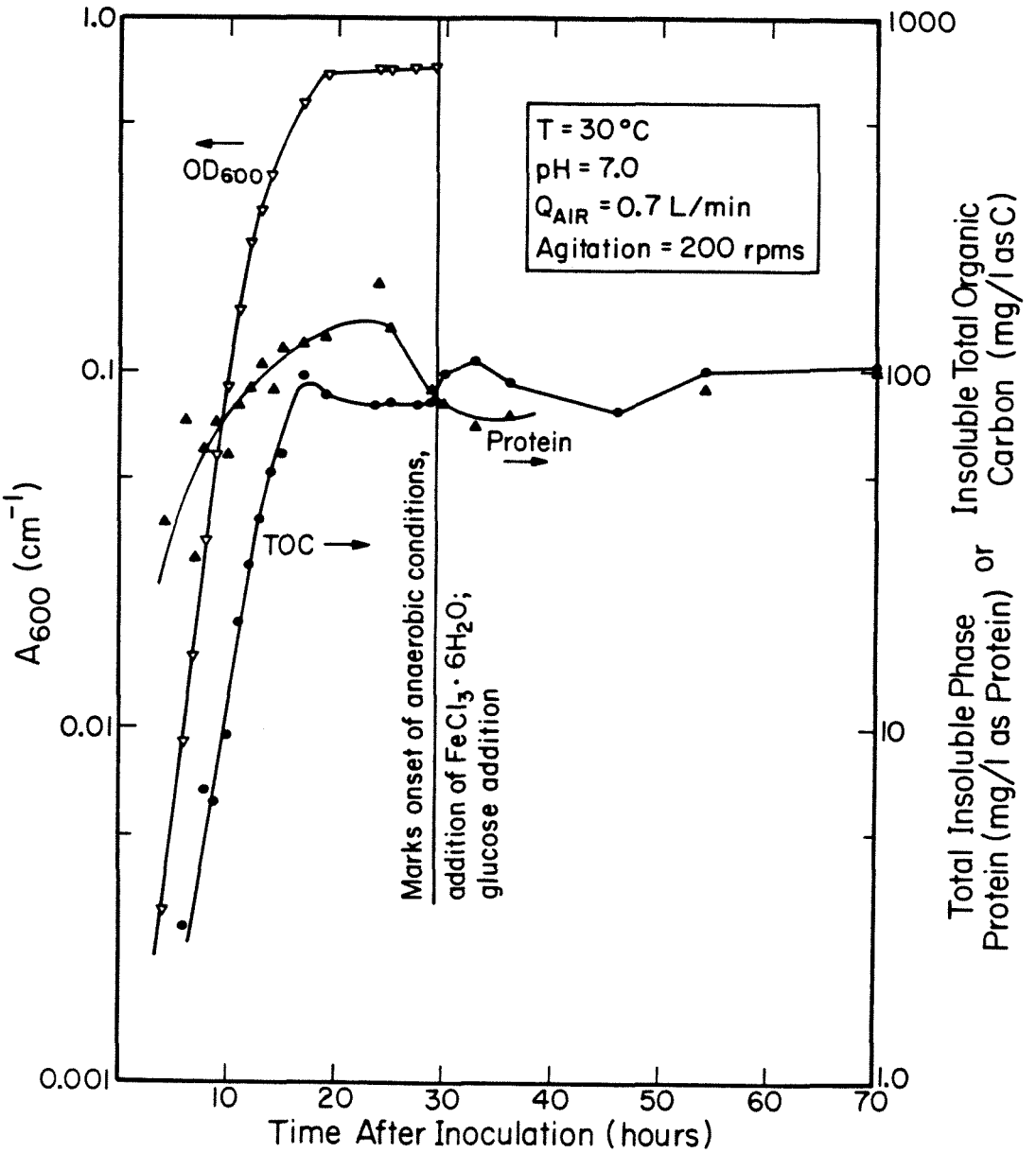

Figure A.5(a). Indicators of microbial biomass as functions of time during a batch fermentation of Bacillus circulans.

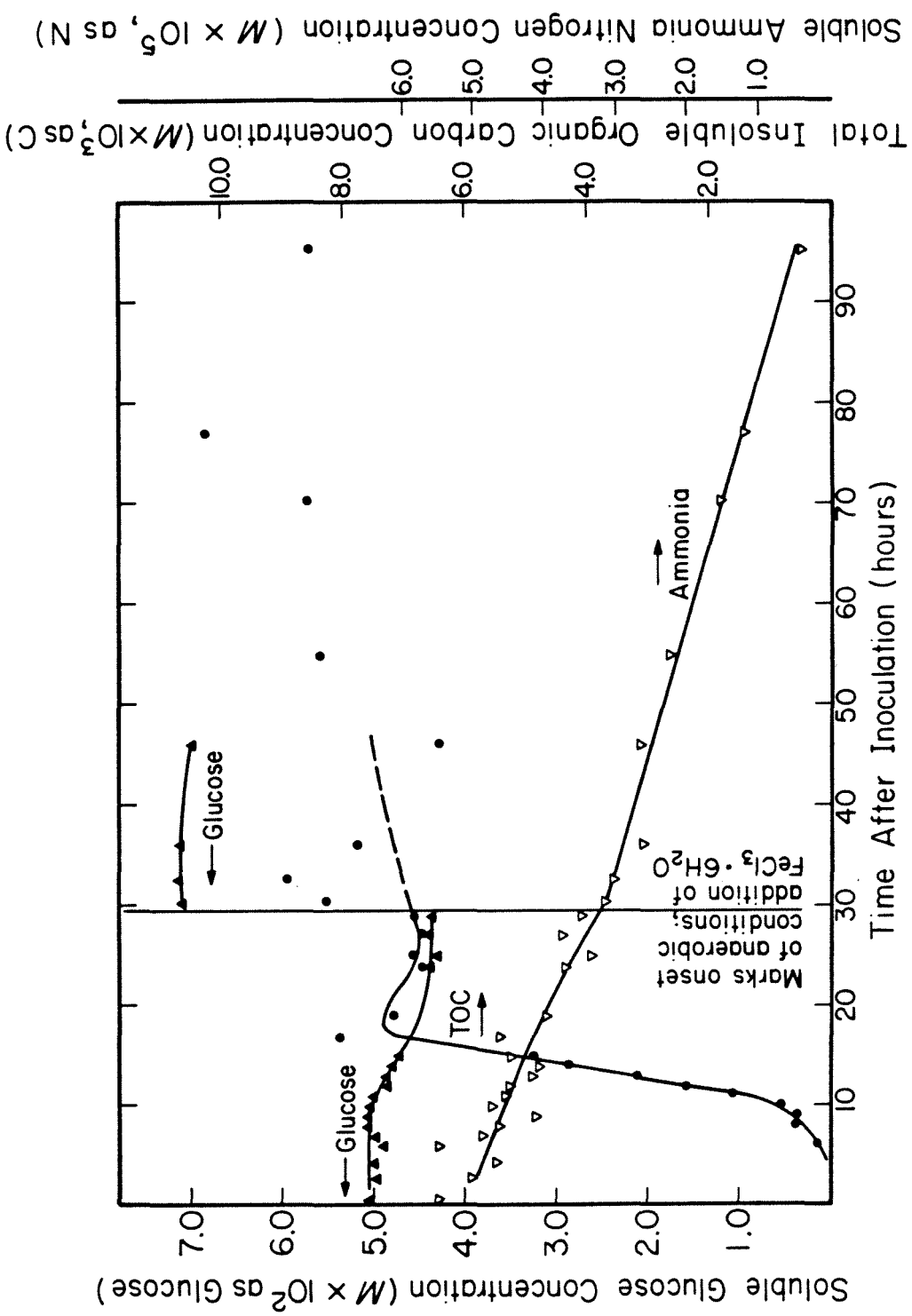

Figure A.5(b). Growth (TOC) and nutrient utilization as functions of time during a batch fermentation of Bacillus circulans.

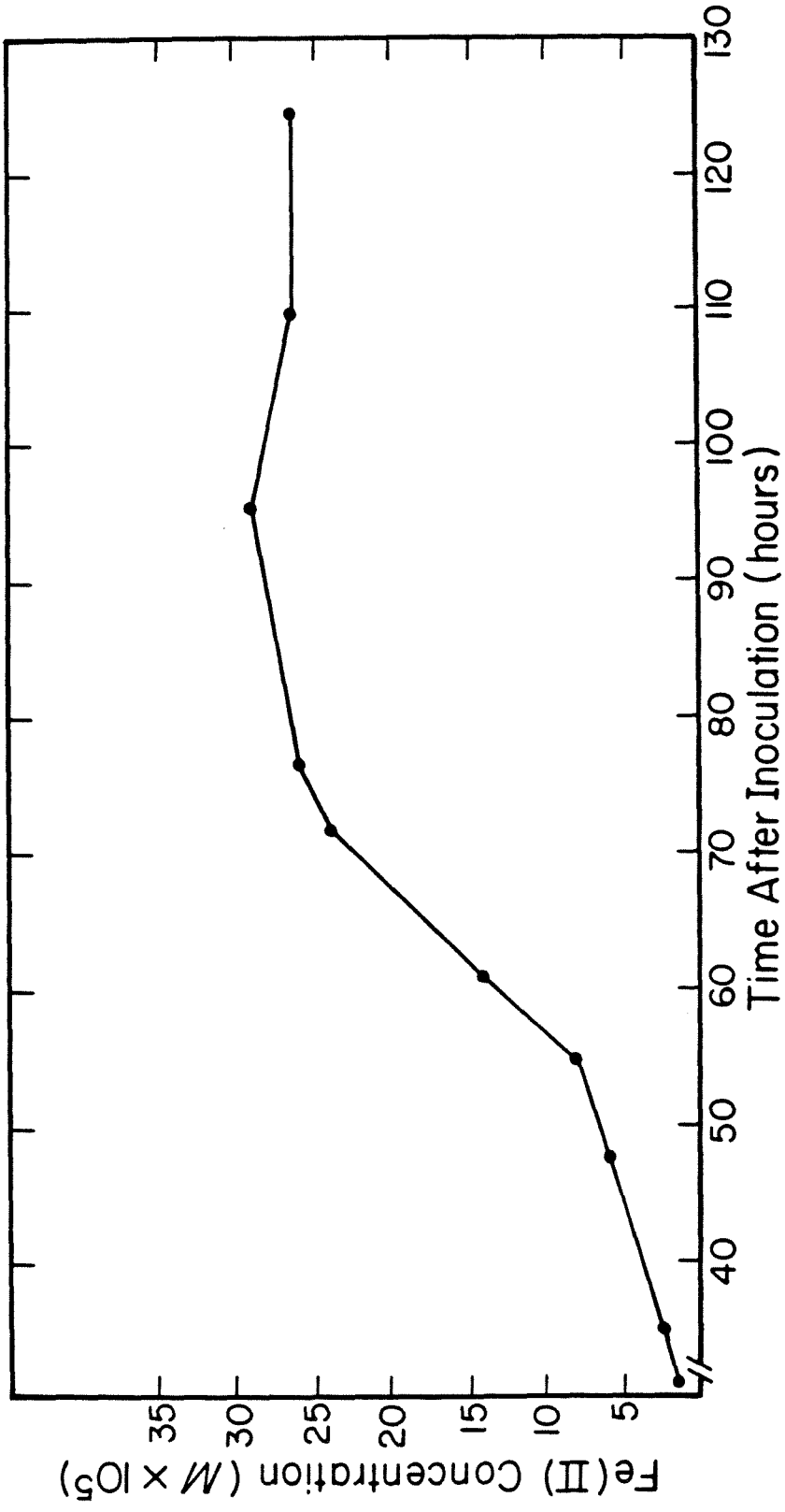

Figure A.5(c). Ferrous iron versus time in a pure batch culture of Bacillus circulans. (High-level Fe(III) addition and establishment of anaerobic conditions at about 30-hour mark.)

mineralization as opposed to some form of endogenous respiration or breakdown of long-lived organic intermediates. Iron-reduction rates were slow in comparison to both literature values and rates measured in subsequent experiments involving other genera.

As indicated in Table A.4, carbon assimilation during exponential growth is somewhat less efficient in B. pumilus than in the other Bacilli tested. Efficiency, as employed here, is defined as the ratio of carbon assimilated to glucose carbon utilized over a representative period of exponential growth. Differences in efficiency could account for most of the inter-species variation in growth rate, although the absolute rate of glucose utilization must be considered as well.

It is also clear from Table A.4 that dissimilative iron reduction plays a minor role at best in the respiratory metabolism of these species. At observed rates of glucose utilization and iron reduction, Fe(III) cannot serve as a major terminal oxidant for respiration. Even if cells are assumed to subsist off substrate-level phosphorylation during periods of anaerobiosis, with no Krebs cycle involvement, stoichiometry dictates that Fe(III) cannot provide a significant sink for excess cellular reductant.

As indicated in Figure A.5(b), soluble ammonia nitrogen was measured throughout the fermentation involving B. circulans. Results indicate that ammonia is continuously, albeit slowly, stripped from solution during the course of the fermentation. As a consequence, yield parameters based on nitrogen utilization measurements are considered untrustworthy, and soluble nitrogen was not monitored in subsequent experiments.

A.1.3.2 Genus Thiobacillus.

Two strains of T. thiooxidans (ATCC nos. 19377 and E8085) were screened for growth and iron-reduction characteristics (Table A.1). Elemental sulfur served as energy source, thus prohibiting the use of light-attenuation as a measure of culture density. Furthermore, protein measurement proved difficult in these fermentations, probably due to high levels of sulfate. Consequently, total solid-phase organic carbon and oxygen utilization rate were relied upon as indicators of culture growth and activity (Figures A.6(a) and A.7(a)). Experimental results indicate that growth of T. thiooxidans on elemental sulfur is about an order of magnitude slower (doubling times are ten times longer) than aerobic growth by heterotrophs screened (Table A.3).

Because autoxidation of Fe(II) is slow at low pH (T. thiooxidans, unlike T. ferrooxidans, has no iron oxidase) aerobic conditions were maintained during both the growth and iron-reduction phases of these experiments, and O_2-utilization rate was monitored throughout the fermentations. As indicated by Figures A.6(a) and A.7(a), oxygen utilization is considerably more useful than total organic carbon as an indicator of culture activity. Restoration of bacterial respiration following sulfur addition (see Figure A.7(a)) indicates that activity can be lost due to substrate exhaustion during the time frame of these experiments ($\sim$ 2 weeks). A yield parameter of sorts can be estimated without direct measurement of elemental sulfur or change in sulfate concentration by comparing (i) the integrated area under the curve of $\frac{-d[O_2]}{dt}$ versus time up to the point of substrate exhaustion with (ii) the

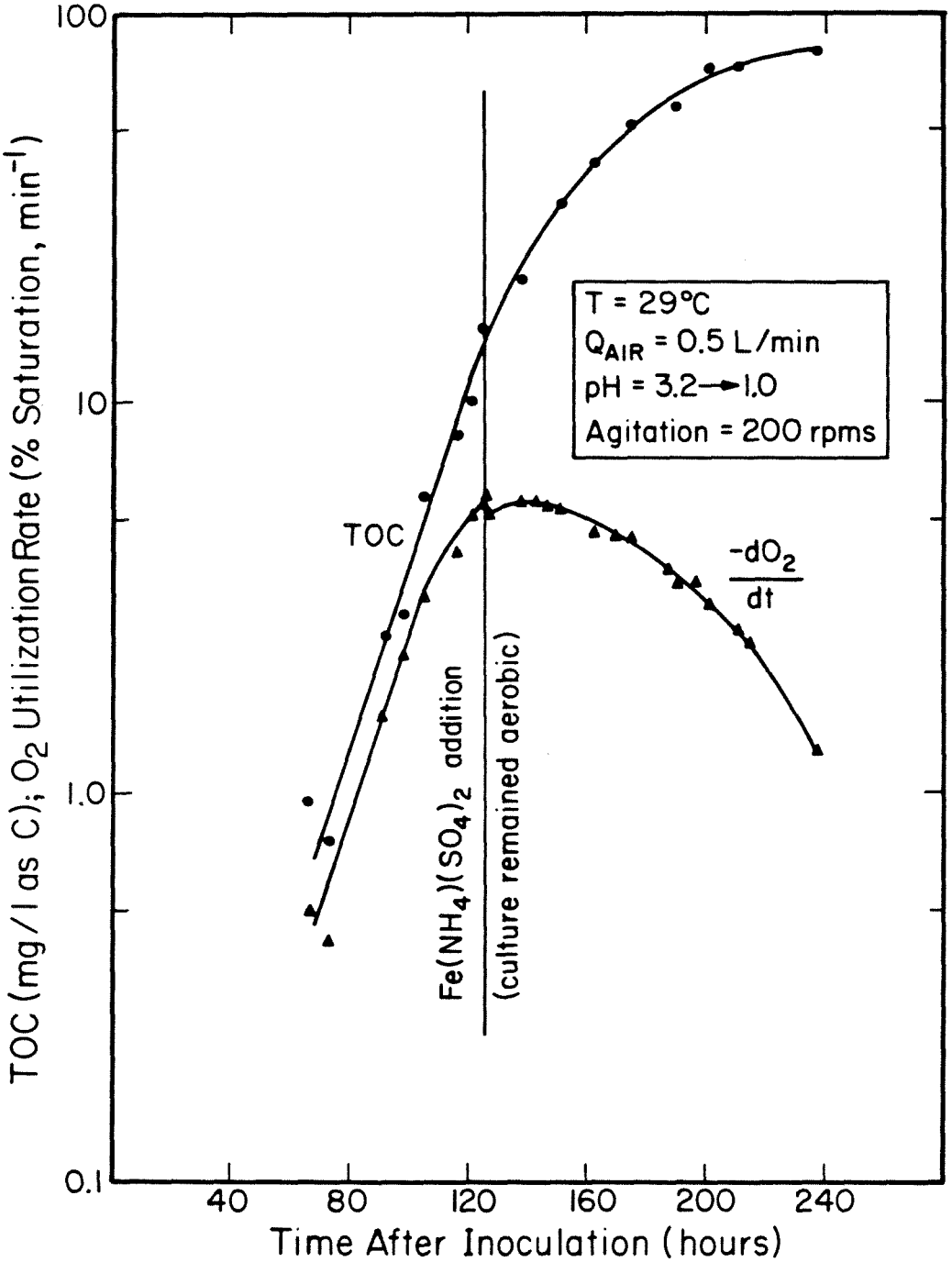

Figure A.6(a). Indicators of microbial biomass and activity as functions of time in a pure, batch culture of Thiobacillus thiooxidans (ATCC strain no. 19377).

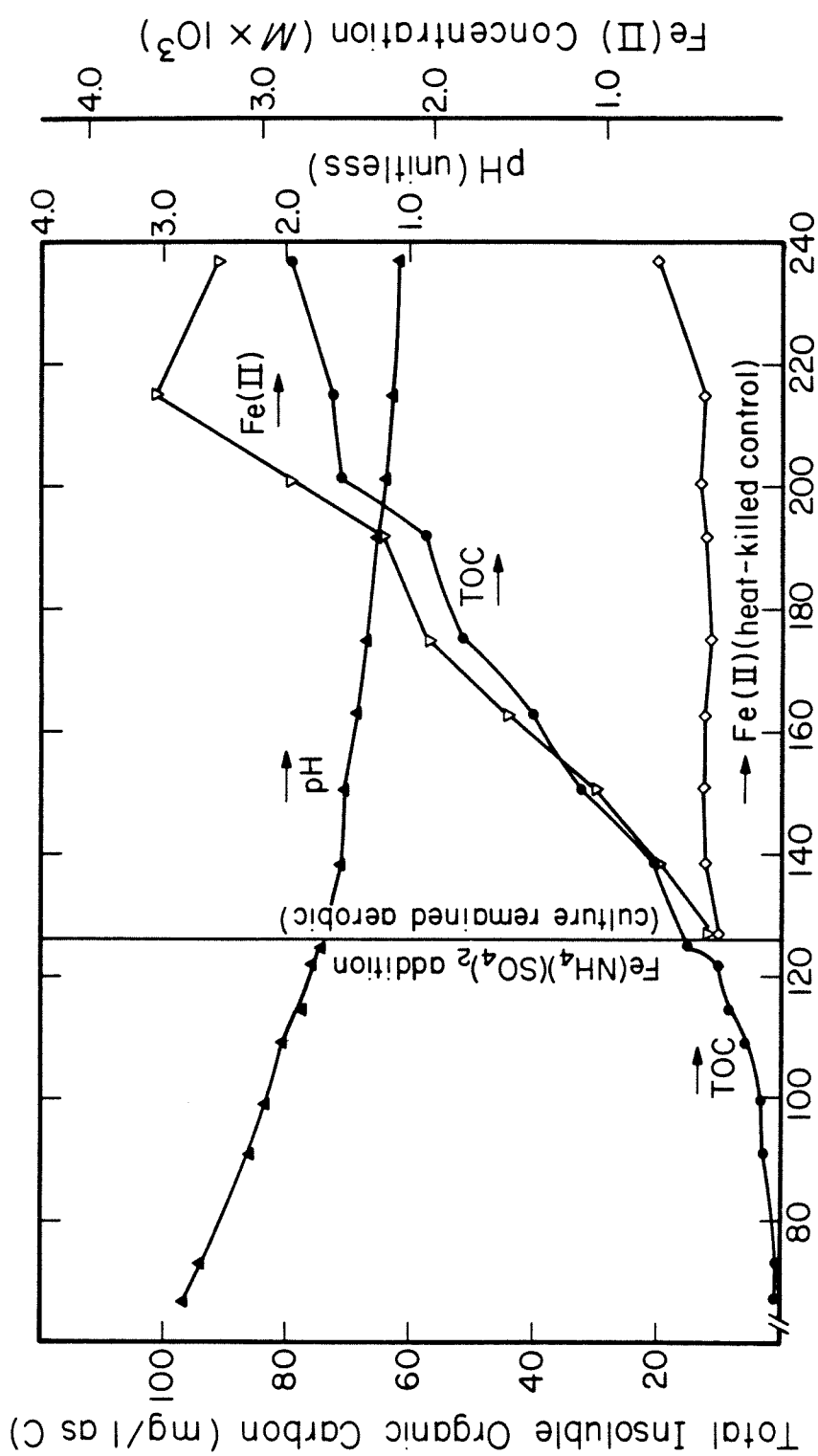

Figure A.6(b). Growth (TOC), iron reduction, and pH as functions of time in a pure, batch culture of Thiobacillus thiooxidans (ATCC strain no. 19377).

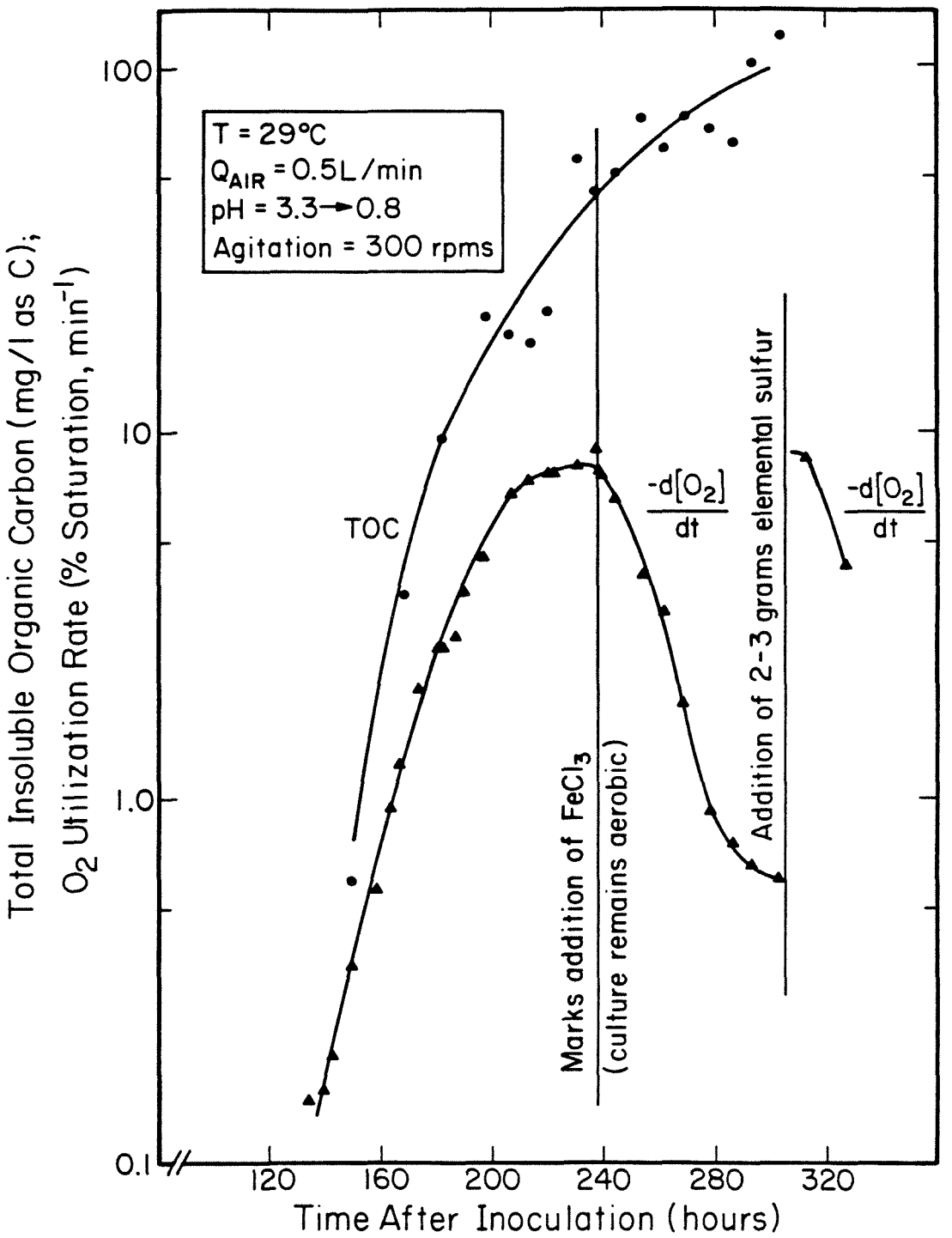

Figure A.7(a). Indicators of microbial biomass and activity as functions of time in a pure, batch culture of Thiobacillus thiooxidans (ATCC strain no. E8085).

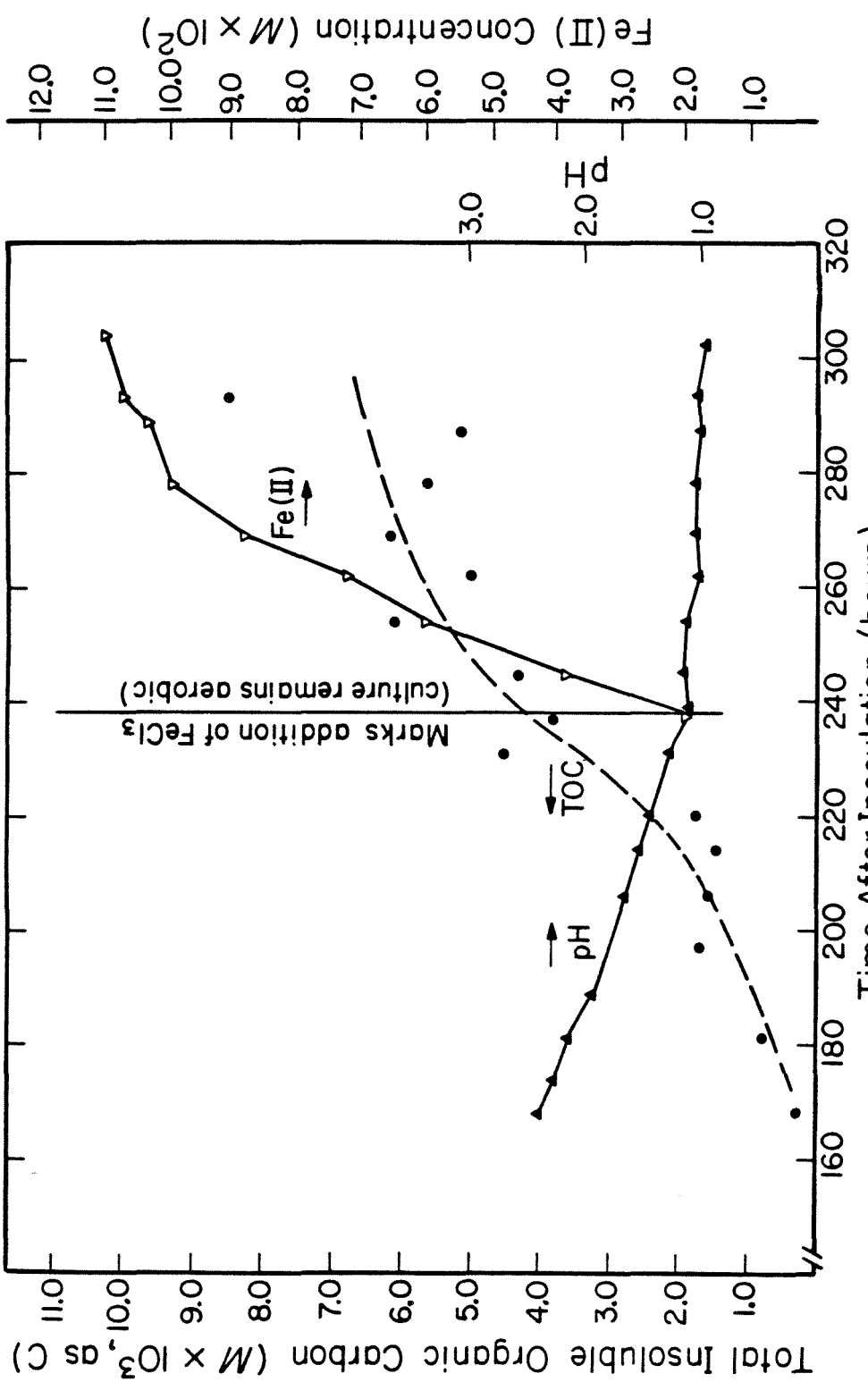

Figure A.7(b). Growth (TOC), ferrous iron, and pH as functions of time in a pure, batch culture of Thiobacillus thiooxidans (ATCC strain no. E8085).

original concentration of elemental sulfur added to the medium. Such an analysis, carried out using data from Figure A.7(a), indicates that the average change in sulfur oxidation state at the point of substrate "exhaustion" is on the order of 1 (about 4 moles of elemental sulfur are used per mole of O_2). It seems clear that sulfate and other high-oxidation-state forms of sulfur are not end products of the fermentation.

Through a similar integration procedure, it is possible to compare the moles of carbon assimilated with the moles of O_2 utilized for respiration (Y_{C/O_2}). As indicated by Table A.4, this type of analysis produces very similar results for ATCC strain nos. 19377 and E8085. There are indications that respiratory efficiency, defined as Y_{C/O_2} increases after exponential growth. Measured differences in the doubling times of these two strains can be rationalized on the basis of growth efficiency during log phase.

Low Y_{C/O_2} values indicate that oxygen consumption (and therefore sulfur oxidation) for biomass production is high. The ratio reflects the relative free-energy charges of sulfur oxidation and organic carbon synthesis. That is, growth among chemolithotrophs utilizes cellular reducing power for conversion of CO_2 to organic carbon. Reducing power is obtained at the expense of ATP generated via electron transport and oxidative phosphorylation (sulfur oxidation).

Although absolute rates of iron reduction in cultures of T. thiooxidans were comparable to those observed in cultures of B. polymyxa and B. circulans, rates normalized on the basis of TOC measurements were among the highest observed among the microorganisms screened (Table A.3).

A.1.3.3 Genus Pseudomonas.

Features of growth and iron-reduction curves corresponding to fermentations of P. aeruginosa and Pseudomonas sp. 200 (Figures A.8 and A.9, respectively) are summarized as follows:

(i) It is evident that these species grow more rapidly than other bacteria screened. The average cell-division time observed during log growth by P. aeruginosa was slightly greater than 30 minutes. Growth rates are probably related to the cell yield; as indicated in Table A.3, Pseudomonas sp. 200 is highly efficient at converting lactate carbon to biomass. Furthermore, far less oxygen is used per unit of biomass produced in experiments involving Pseudomonas sp. 200 than in the T. thiooxidans fermentations described above. Y_{O_2}/C (Table A.4) represents the molar ratio of area under the $\frac{-d[O_2]}{dt}$ versus time profile (Figure A.9(a)) divided by total insoluble organic carbon at the end of aerobic growth. It is evident that growth of Pseudomonas sp. 200 demands from 10 to 20 times less oxidant per unit carbon assimilated.

(ii) Figures A.8(a), A.8(b), and A.9(a) show clearly that optical density, oxygen utilization, and solid-phase TOC or protein are all reasonably good, highly correlated indicators of biomass and cellular activity under aerobic growth conditions. TOC and total solid-phase protein remain useful measures of biomass following high-level Fe(III) addition and establishment of anaerobic conditions.

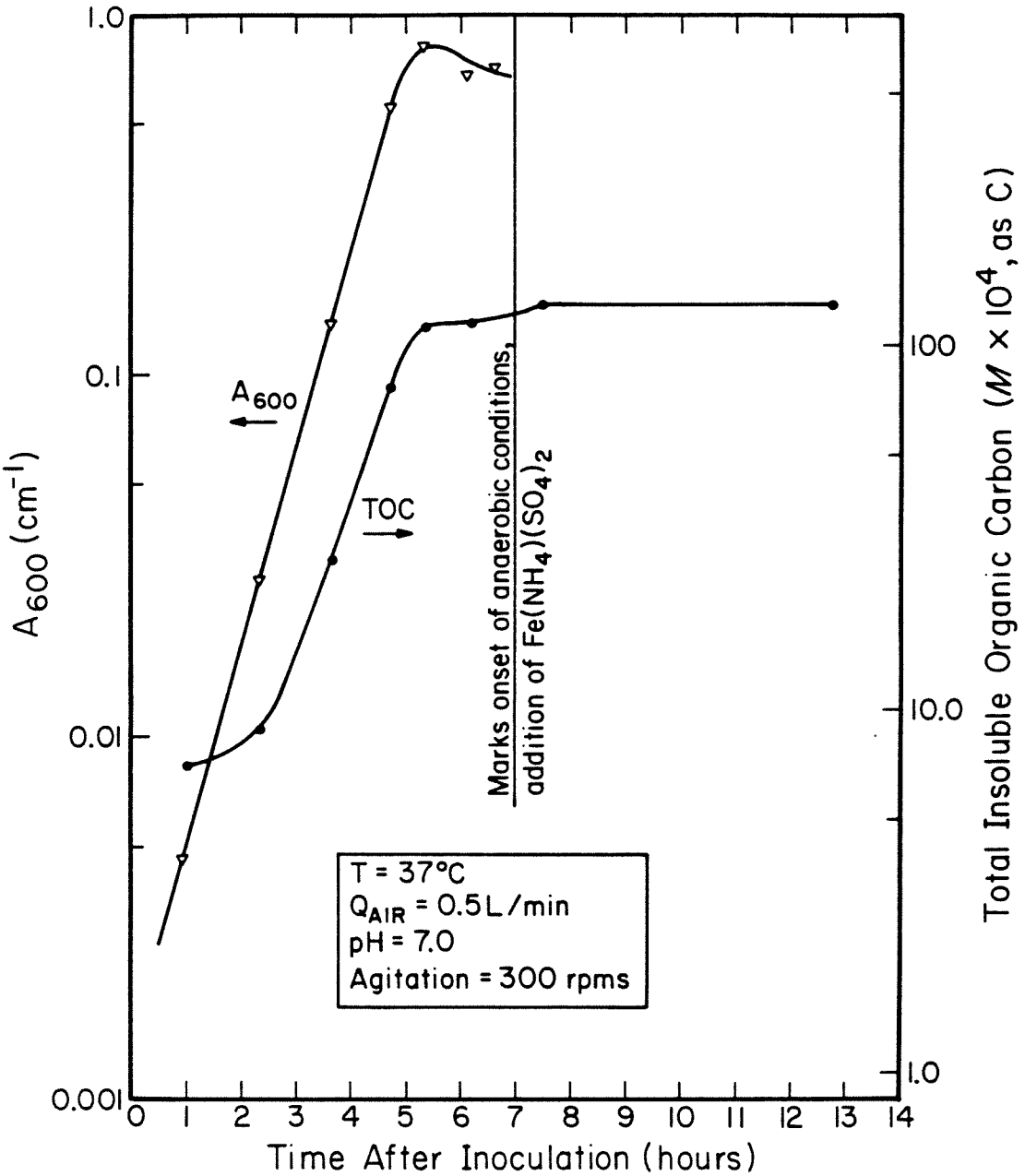

Figure A.8(a). Indicators of microbial growth as functions of time in pure, batch cultures of Pseudomonas aeruginosa.

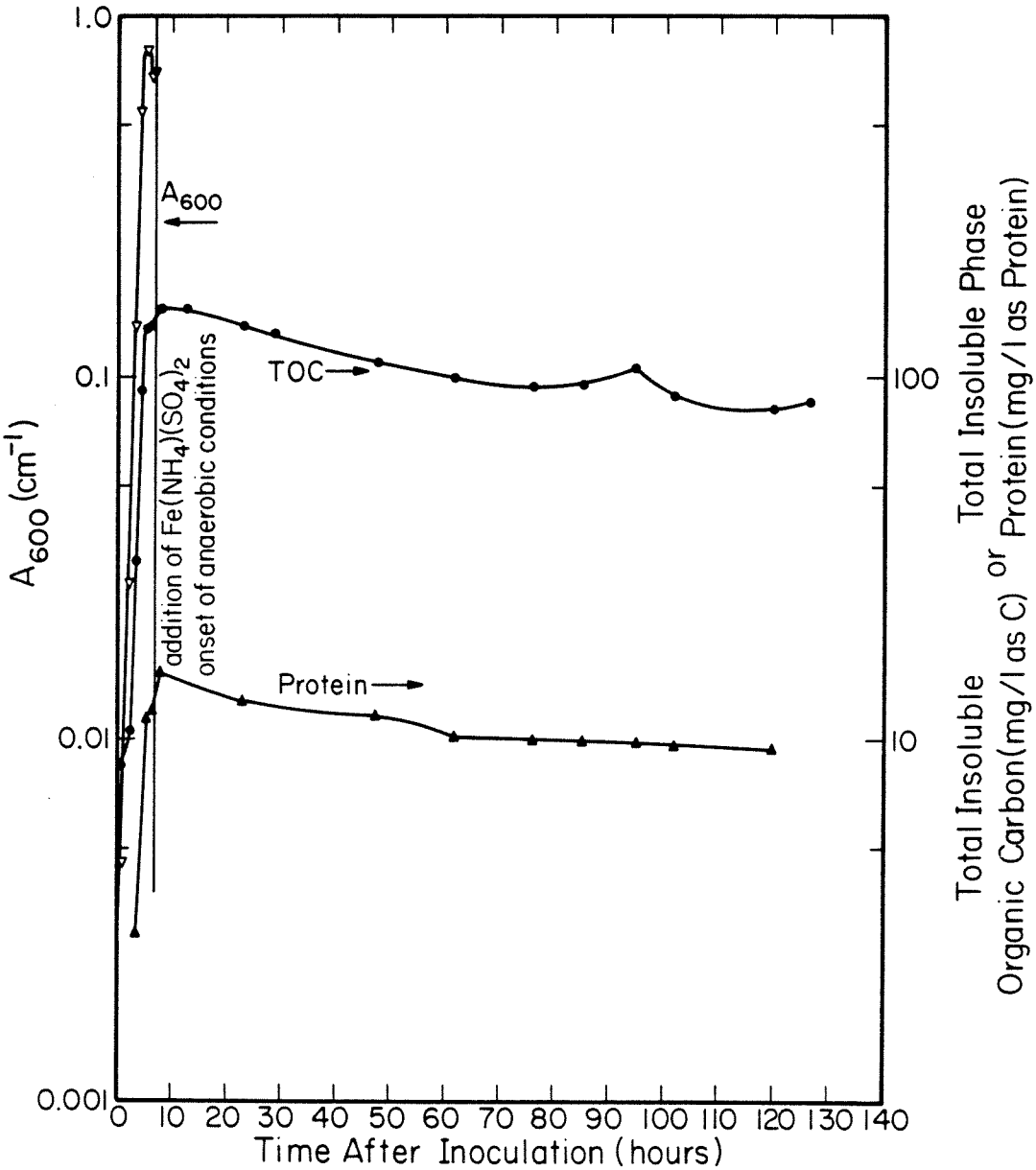

Figure A.8(b). Indicators of microbial growth as functions of time in pure, batch cultures of Pseudomonas aeruginosa.

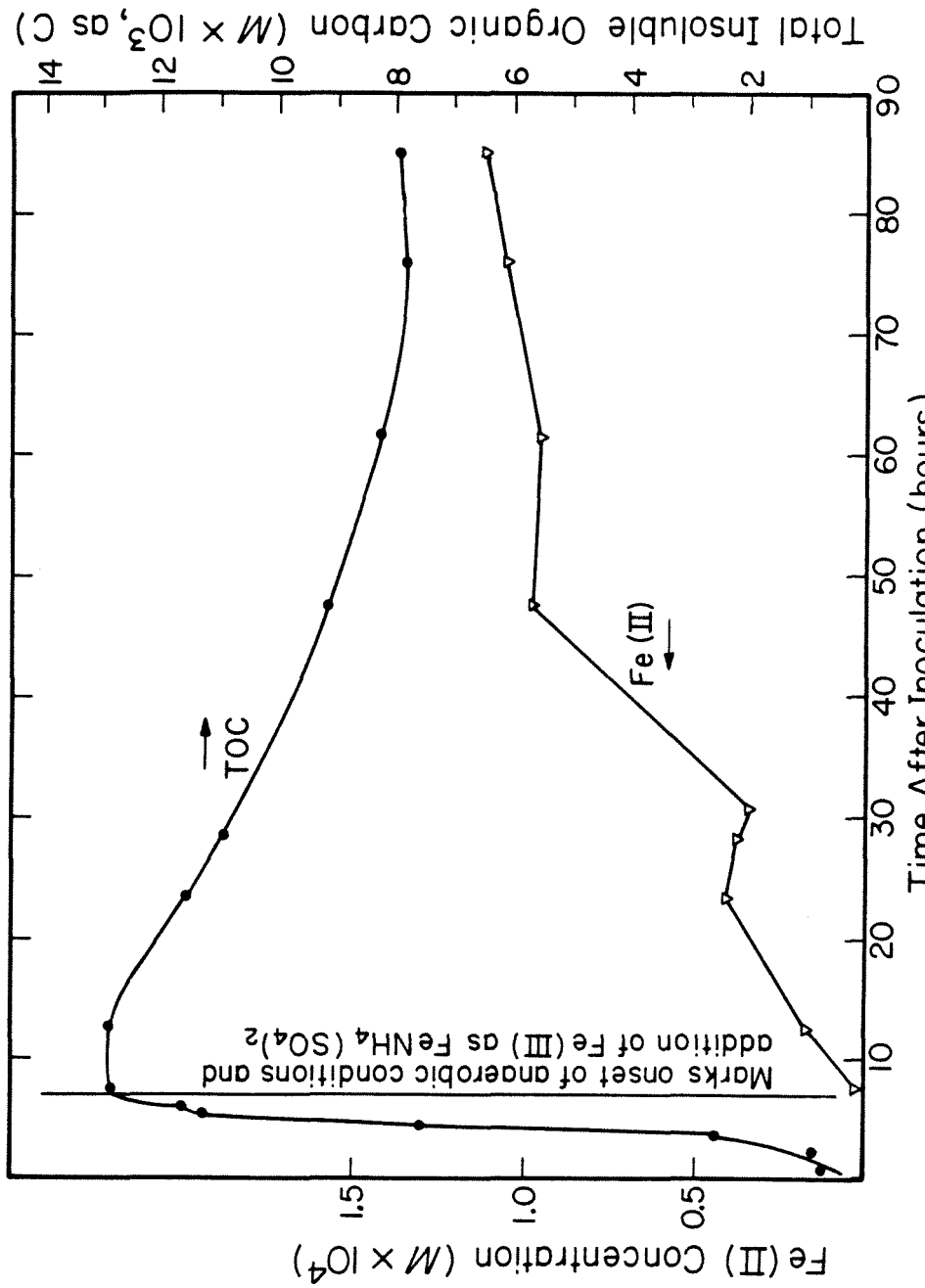

Figure A.8(c). Biomass (TOC) and ferrous iron concentration as functions of time in pure, batch cultures of Pseudomonas aeruginosa.

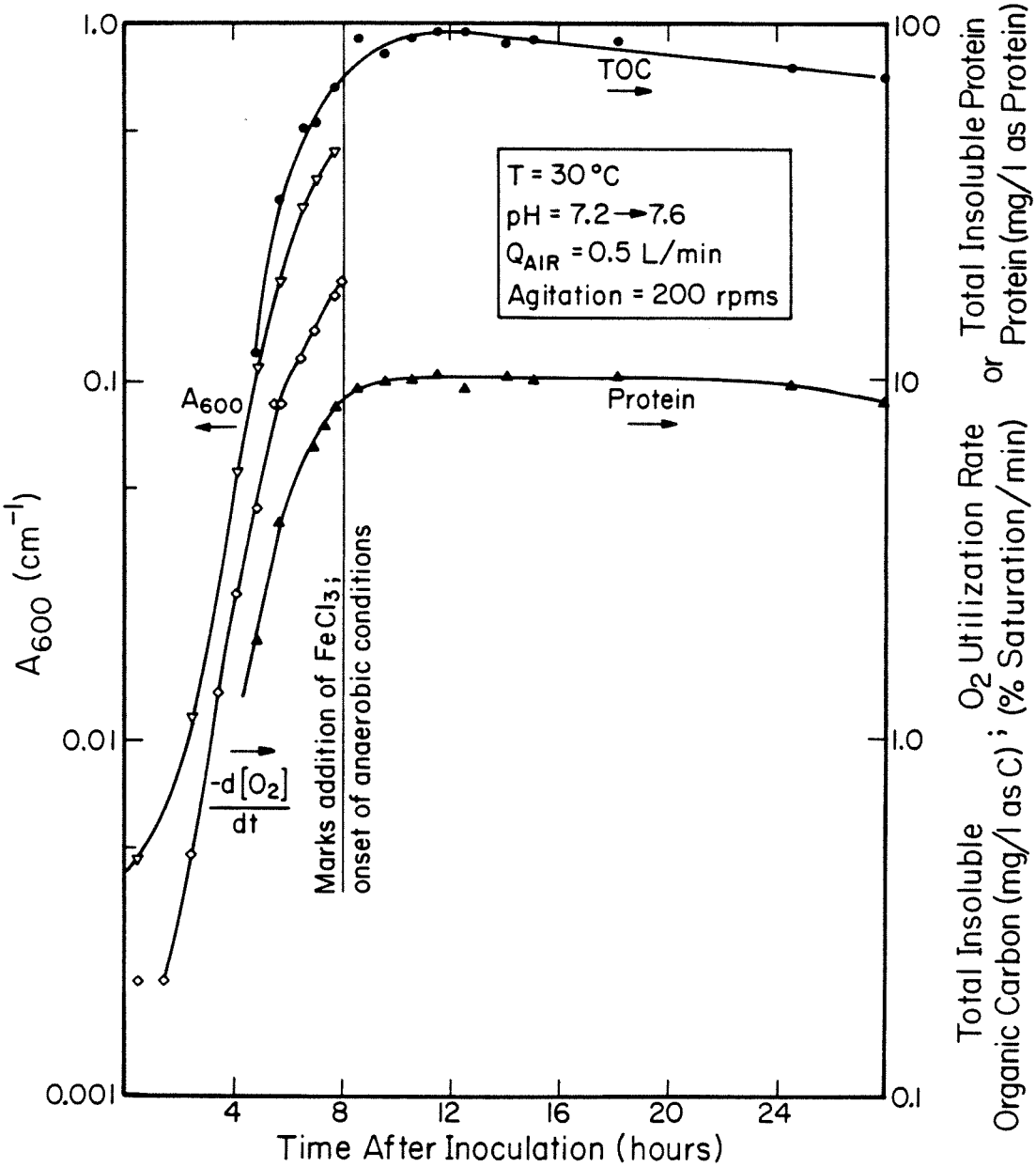

Figure A.9(a). Indicators of microbial biomass and activity as functions of time in pure, batch cultures of Pseudomonas sp. 200.

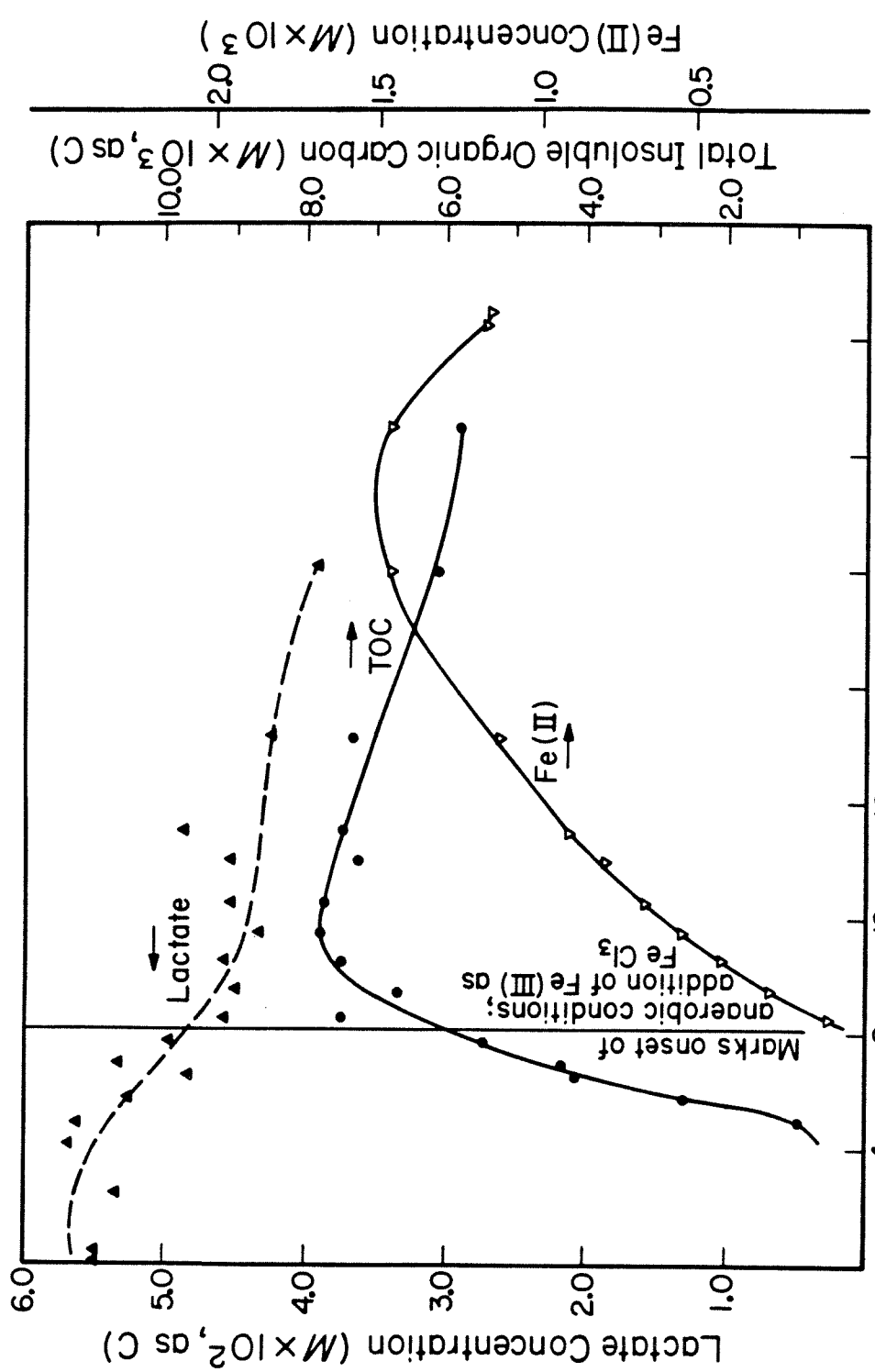

Figure A.9(b). Growth (TOC), substrate utilization, and ferrous iron concentration as functions of time in pure, batch cultures of Pseudomonas sp. 200.

(iii) Pseudomonas sp. 200 and P. aeruginosa differ significantly in their respective abilities to reduce ferric iron (Figures A.8(b) and A.9(b). P. aeruginosa is one of the least effective iron reducers investigated while the initial rate of iron reduction (Table A.3) attributable to Pseudomonas sp. 200 (immediately following iron addition and establishment of anaerobic conditions) was the highest observed among microorganisms screened. Iron-reduction rates observed under reasonably similar conditions in the two cultures differed by almost two orders of magnitude.

(iv) The ratio of protein to total insoluble organic carbon was a factor of 10 lower in the Pseudomonads than among the Bacilli screened.

A.1.4 Summary

Figure A.10 and Tables A.3 and A.4 provide a clear summary of basic screening-program results. Since the commercial relevance of extractive iron reduction will depend upon the kinetics of both bacterial growth and iron reduction, it is emphasized that only Pseudomonas sp. 200 scores well in both areas. Consequently, subsequent, more detailed investigations of iron-reduction kinetics and mechanism were confined to this species.

A.2 Preliminary Experiments Involving Pseudomonas sp. 200.

A series of preliminary experiments produced systematic investigation of the iron-reduction capabilities of Pseudomonas sp. 200. These included experiments designed to (i) establish correlations

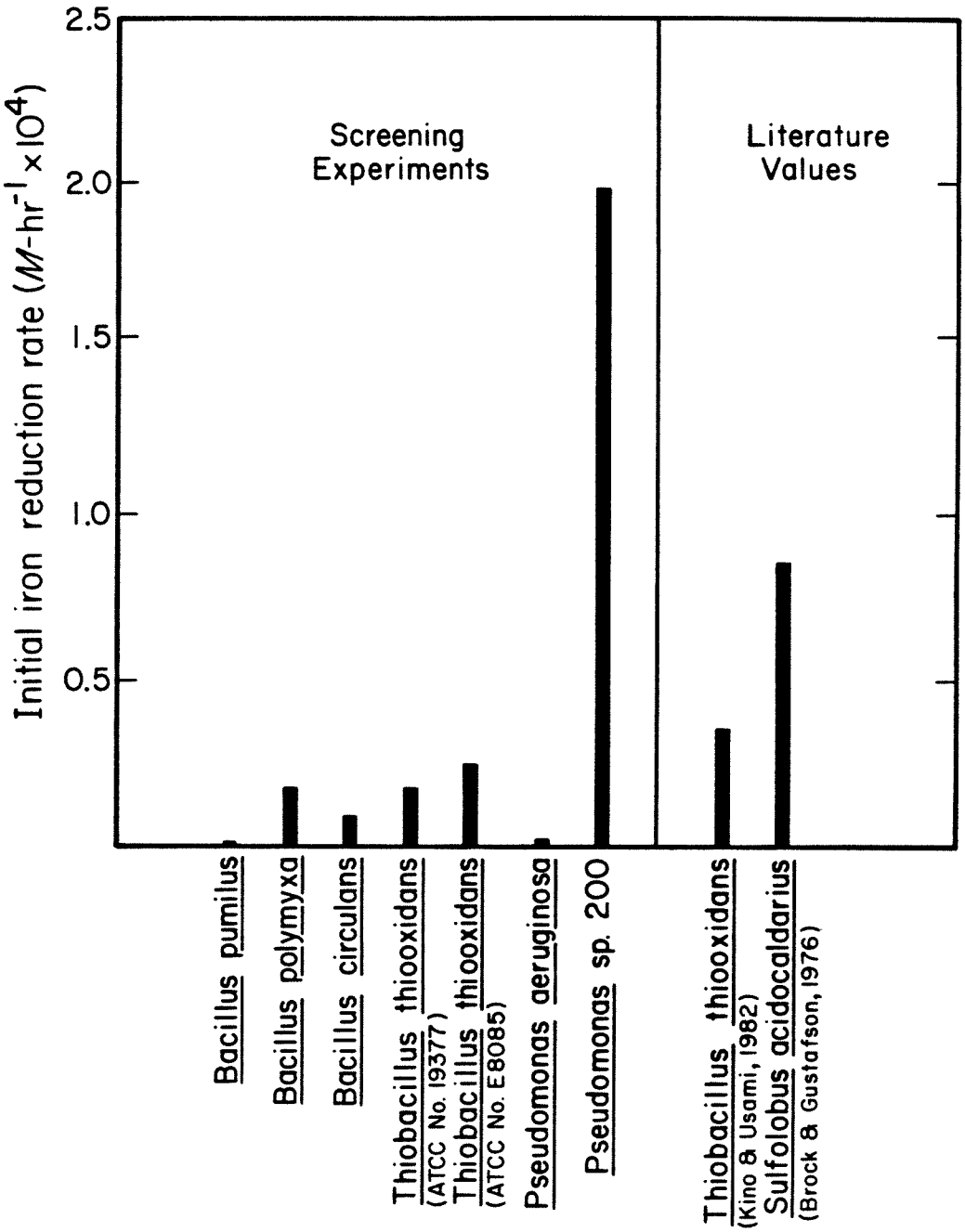

Figure A.10. Summary of initial iron-reduction rates (following establishment of anaerobic conditions and addition of high-level Fe(III)) measured in screening experiments. Iron-reduction rates extracted from the scientific literature represent the fastest encountered.

between such growth-dependent variables as optical density, cell dry weight, potential oxygen-utilization rate, and direct cell count, (ii) explore relationships between growth conditions and culture oxygen-utilization capacity, (iii) examine the dependence of iron-reduction kinetics on cell viability and protein synthesis, and (iv) determine the effect of (nutrient) Fe exhaustion on electron-transport capacity.

Growth experiments were conducted in the Biostat M reactor described previously. As described above, light attenuation was measured at = 600 nm. Cell dry weight was determined via vacuum filtration of a known culture volume (20 or 40 mls, depending on culture density) onto preweighed, 0.2 μm Gelman membrane filters. Filters were dried to constant weight and reweighed; weight difference per unit volume was cell dry weight. Cell counts were determined via serial dilution and colonization of nutrient agar plates (Difco, Bacto agar). Recorded counts represent estimates based on plate counts at three levels of dilution.

Results are summarized in Figure A.11. There is excellent qualitative agreement between cell dry weight and light attenuation as indicators of cellular growth. Logarithmic growth is apparently biphasic. The shift in rate constant observed at approximately A_{600} = 0.2 (cm^{-1}) may be due to exhaustion of a preferred nutrient source provided as yeast extract. Both the biphasic nature of logarithmic growth and the relationship between cell dry weight and light attenuation proved reproducible in subsequent experiments. Cell counts produce a very different picture than other indicators of growth but

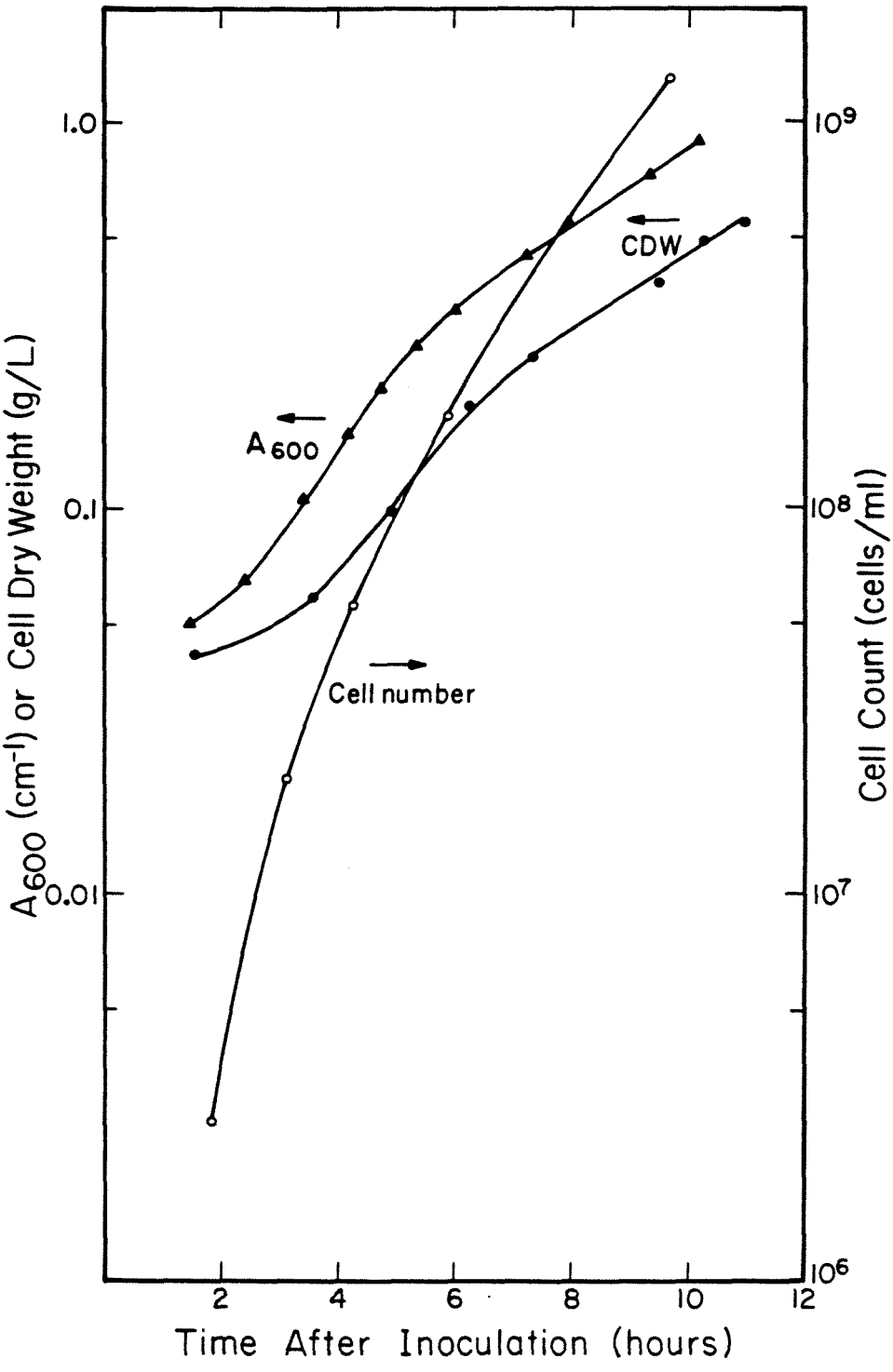

Figure A.11. Correlations among selected indicators of microbial biomass during aerobic growth of Pseudomonas sp. 200 in Westlake medium; T = 31°C.

values are considerably less reliable. The estimated concentration of cells at A_{600} = 1.0 (cm^{-1}) is 2 x 10^9/ml.

Culture oxygen-utilization capacity was estimated via continuous measurement of dissolved-oxygen concentration following interruption of airflow to the reactor at initial O_2 concentrations above those which would limit cytochrome oxidase activity. Typical results are provided in Figure A.12. Once again, excellent qualitative agreement between indicators of culture density and activity is evident, and although early-log growth is apparently somewhat faster (and late-log growth slower) than Figure A.11 results, biphasic growth is again apparent.

Additional experiments summarized in Figure A.13 indicate that culture O_2-utilization capacity is somewhat dependent upon the dissolved-oxygen concentration of the medium during cell growth. Respiratory system components may be strengthened in response to low oxygen tension (Chapter 6). Previous studies indicate that cellular respiration is limited at the dehydrogenase level (Harrison, 1976) implying that in these experiments low-O_2 or low-energy conditions lead to enhancement of the membrane dehydrogenase complement. It will be shown here, Chapter 5, that electron transport chain components of Pseudomonas sp. 200 are kinetically balanced -- that electron carriers are neither over- nor under-produced.

Finally, effects attributable to a series of cell treatments on the kinetics of dissimilative iron reduction were investigated. Treatments included chloramphenicol and kanamycin addition and heat killing. Cells were grown into late log phase ($A_{600} \cong 0.45$, see Figure A.14) in the Biostat M reactor. At that point, airflow was cut off, residual O_2 purged with high-purity nitrogen gas, and Fe(III) added as $FeCl_3 \cdot 6H_2O$ to

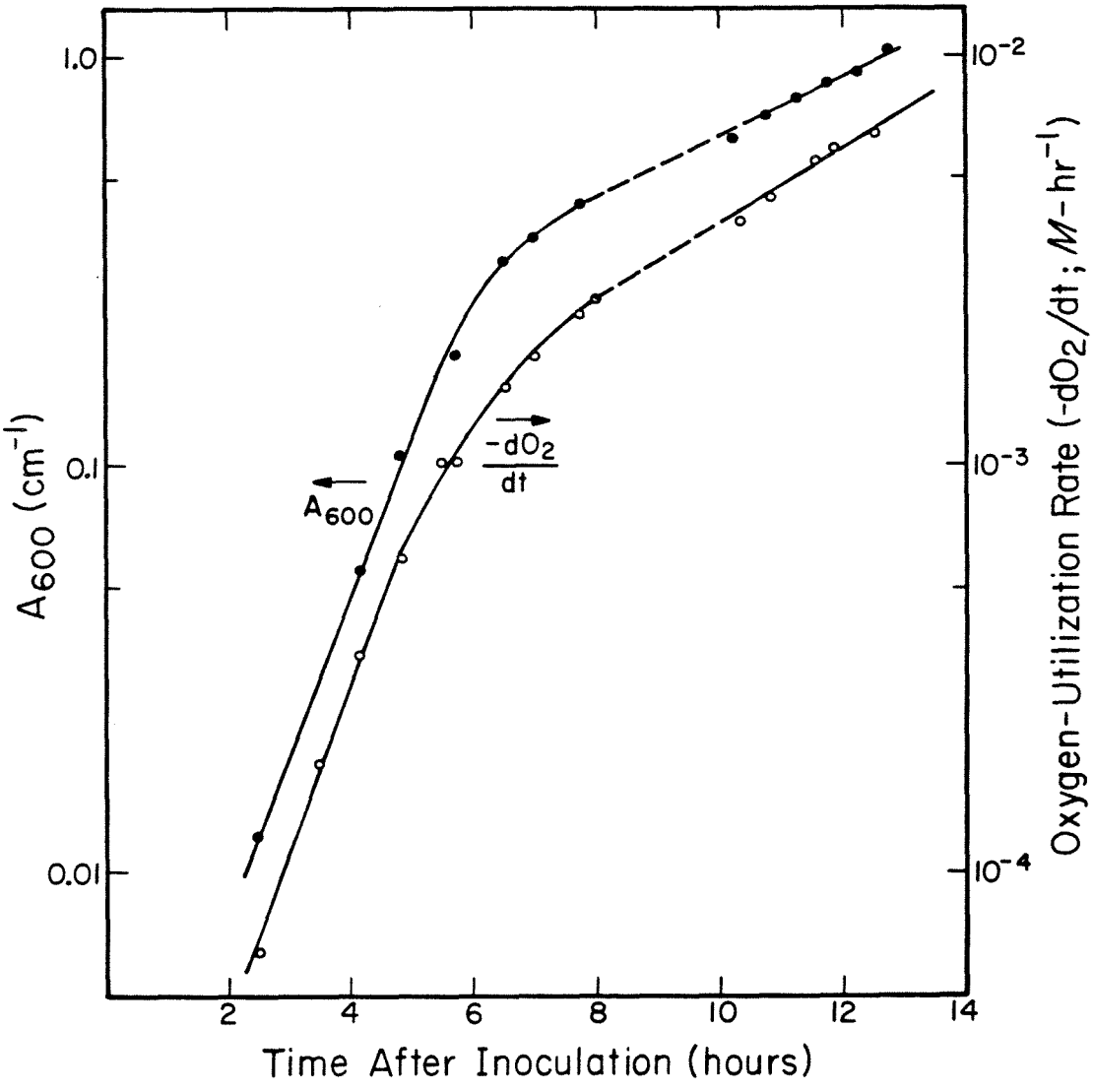

Figure A.12. Correlation between optical density and O_2-utilization capacity in batch, aerobic cultures of Pseudomonas sp. 200.

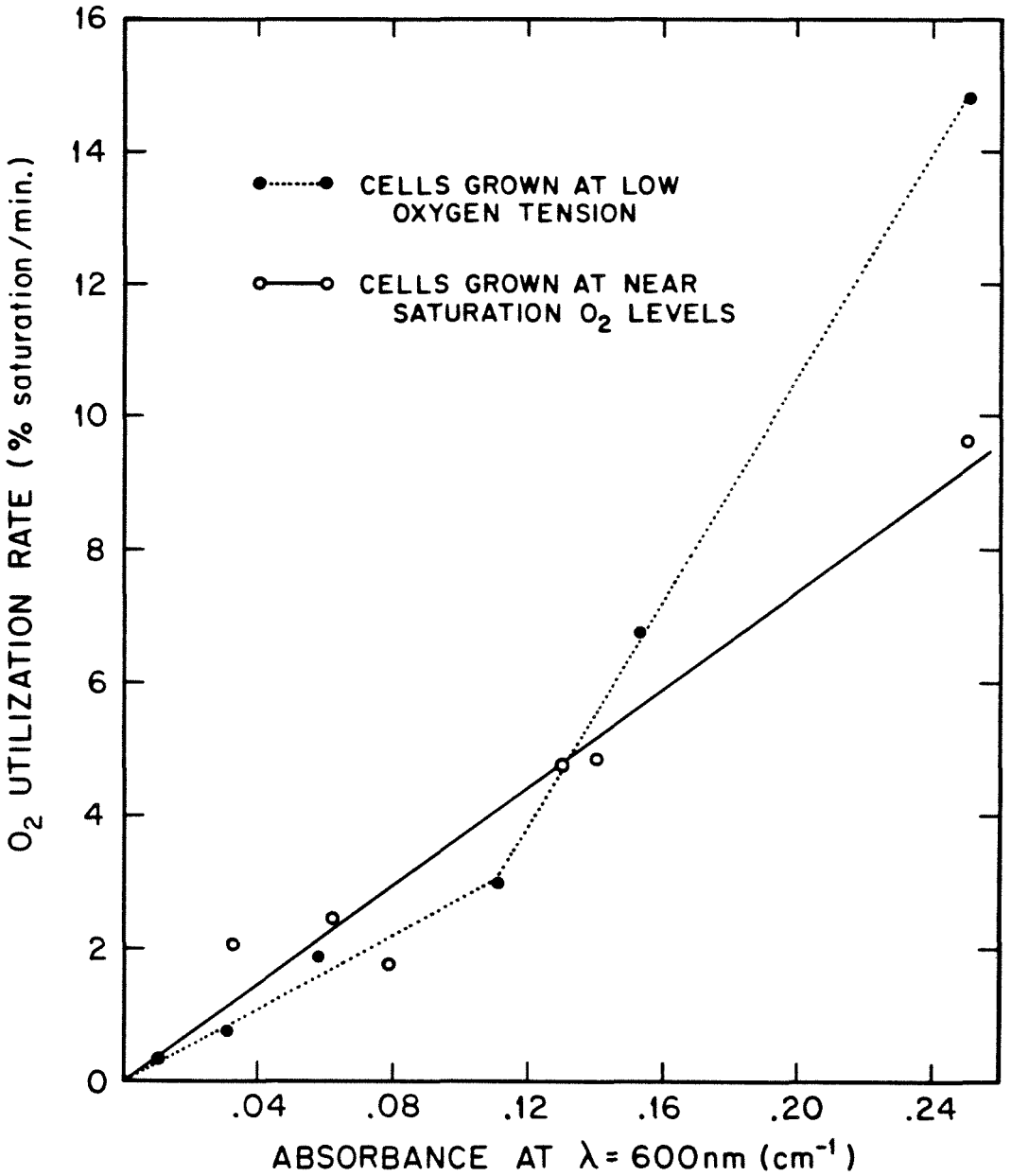

Figure A.13. Oxygen-utilization capacity in batch cultures of Pseudomonas sp. 200 as a function of culture optical density and oxygen tension during growth.

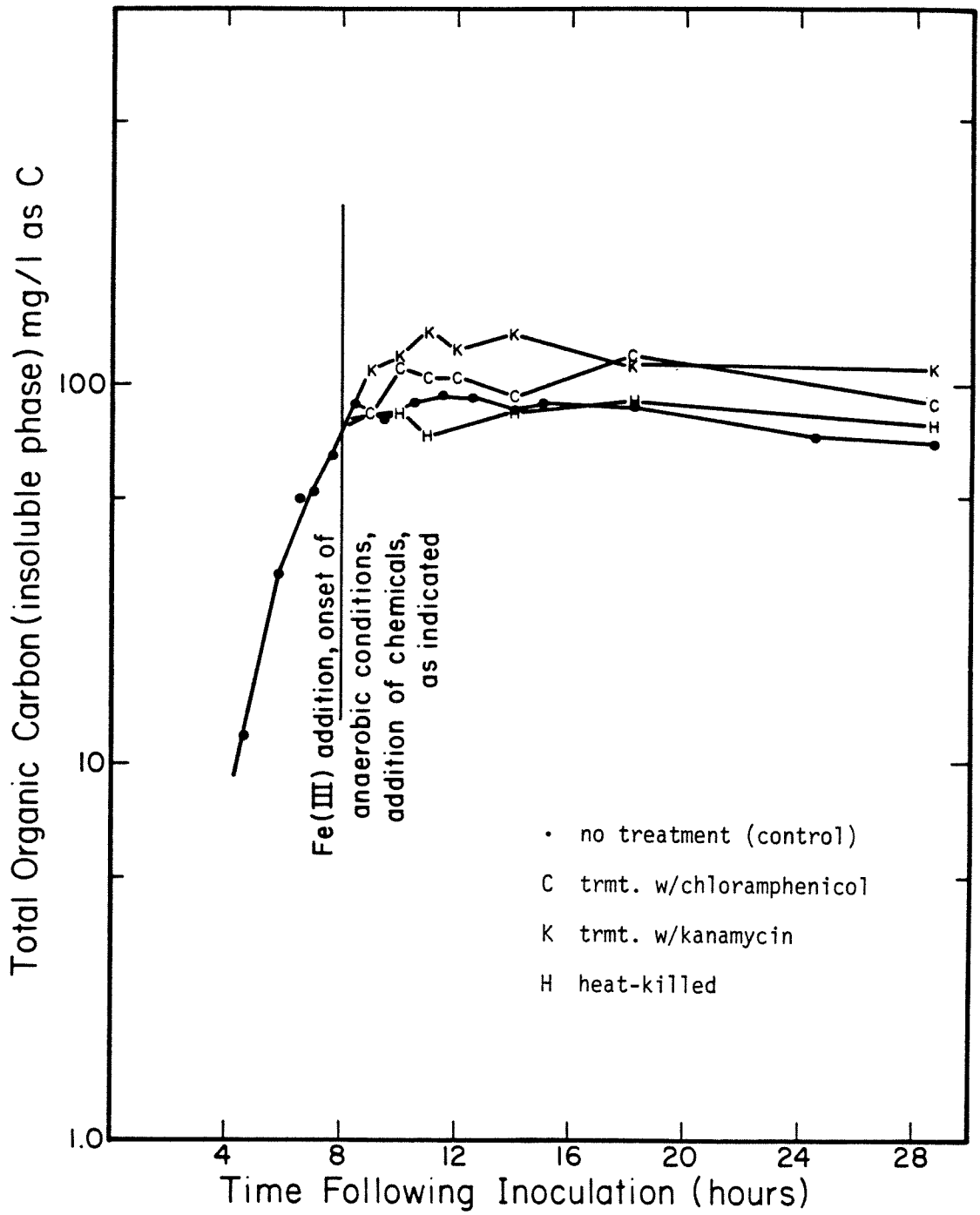

Figure A.14. Effect of physical and chemical treatments on microbial biomass in pure, batch cultures of Pseudomonas sp. 200.

a final concentration of 1.86×10^{-3} M. After pH was restored to 7.6 via addition of 2 N NaOH, three 100-ml aliquots were removed and subjected to treatments described below:

(i) heat killing -- sample was autoclaved for 10 minutes at 121°C. After treatment, no cellular locomotion was apparent.

(ii) chloramphenicol -- addition was to a final concentration of 4.6×10^{-4} M. Chloramphenicol inhibits cell growth by blocking protein synthesis -- see Chapter 5. Drug addition did not interfere with normal cell locomotion.

(iii) kanamycin -- addition was to a final concentration of 4.6×10^{-4} M. The drug inhibits cellular growth and activity by binding to ribosomes and interfering with protein synthesis (Tanaka, 1975). Drug addition resulted in eventual loss of cellular locomotion.

After aliquot removal, remaining contents of the Biostat M were maintained under anaerobic conditions as an untreated control. From Figures A.14 and A.15, it is evident that establishment of anaerobic conditions arrested net assimilation of carbon and protein production in Pseudomonas sp. 200. Treatments were essentially indistinguishable from the control in terms of total insoluble organic carbon and protein contents although heat treatment resulted in loss of an appreciable fraction of total protein from the solid phase, perhaps due to cell lysis and dispersal of cytoplasmic protein. In Figure A.16, Fe(II) concentration is plotted as a function of time for each of the treatments described above. The figure clearly shows that autoclaving eliminated dissimilative iron-reduction activity; iron reduction was essentially unaffected by treatment with chloramphenicol or kanamycin over the 20-hour course of the experiment. The short lag in iron

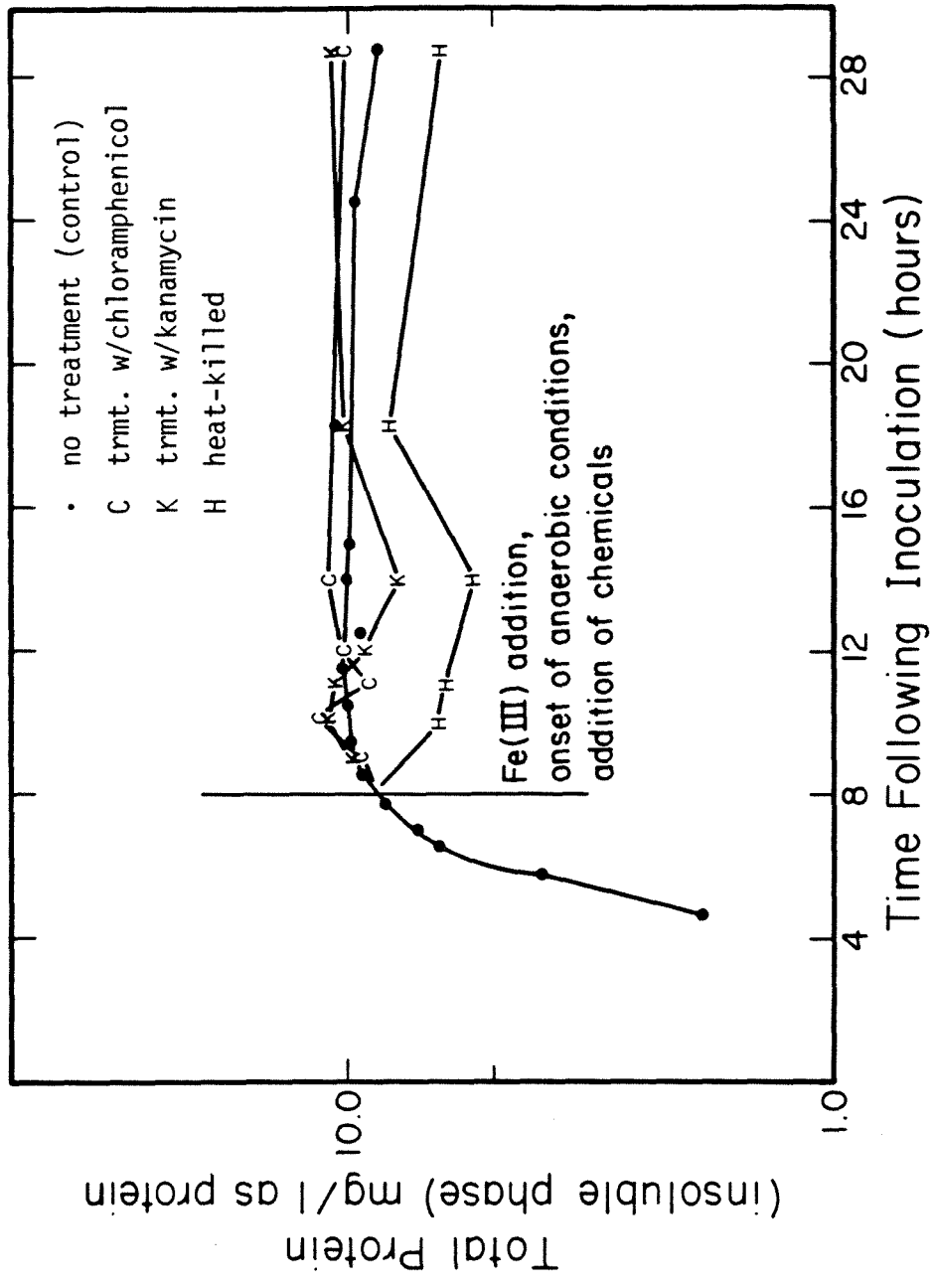

Figure A.15. Effect of physical and chemical treatments on protein content in pure, batch cultures of Pseudomonas sp. 200 grown to early stationary phase.

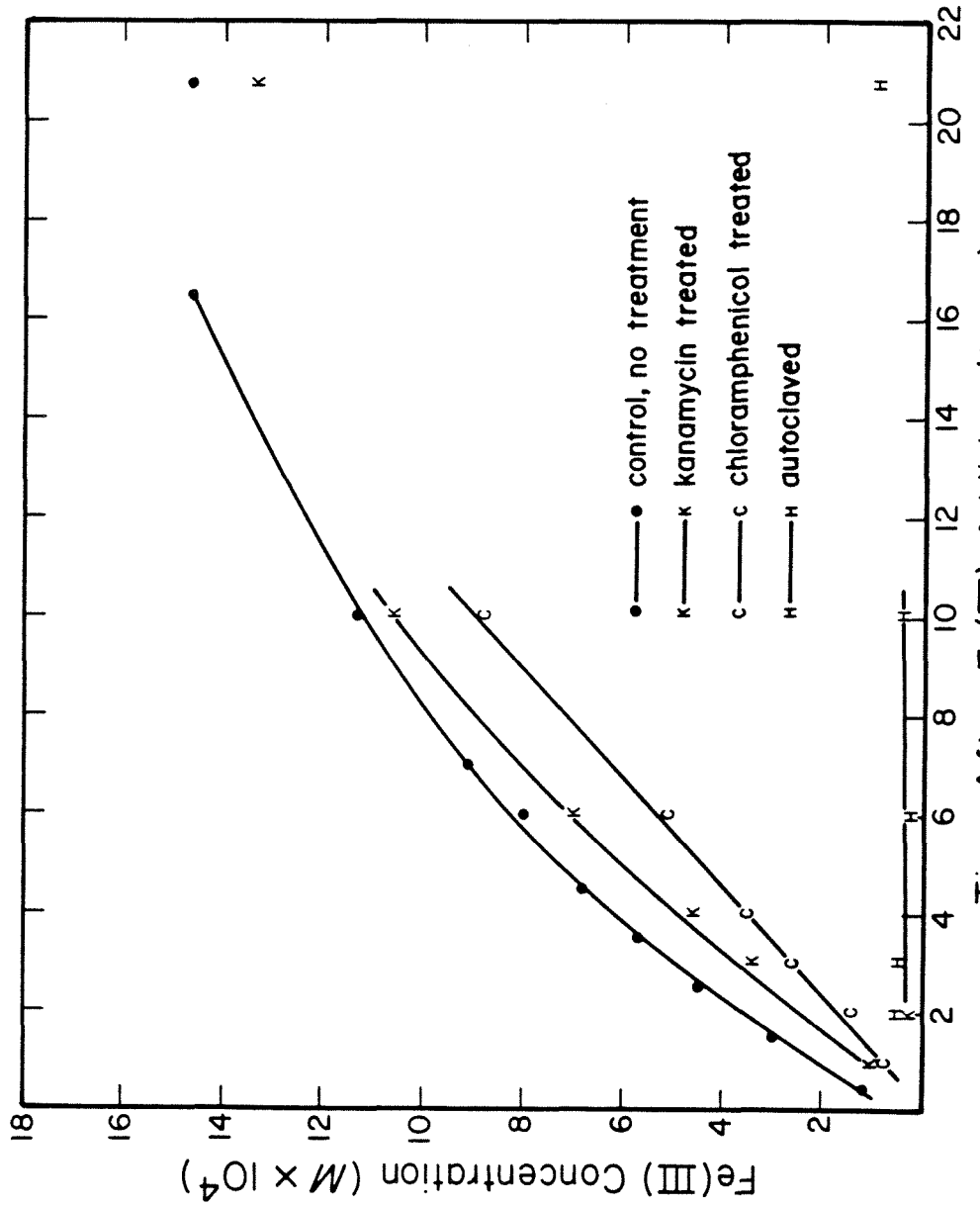

Figure A.16. Reduction of Fe(III) as a function of time in treated, anaerobic cultures of Pseudomonas sp. 200.

reduction following drug addition may have been due to reintroduction of molecular oxygen into these cultures during treatment administration.

Its effect on growth and respiration was investigated by adding 4.64 x 10^{-4} M chloramphenicol (dissolved in ethanol) to an exponentially growing culture of Pseudomonas sp. 200. As indicated in Figure A.17, O_2 utilization was affected only modestly ($\cong$ 20% loss in $\frac{-d[O_2]}{dt}$ over 30 minutes following drug addition) although growth was arrested immediately (Figure A.17). When chloramphenicol was added mid-way through an iron-reduction experiment, kinetics of the Fe(III) ----> Fe(II) transformation were unaffected (Figure A.18).

In a similar experiment, pyridine inhibition of aerobic respiration was examined. Addition of 9.0 mls of pyridine to a 1 L culture of Pseudomonas sp. 200 (A_{600} = 0.2, cm^{-1}) resulted in a loss of O_2-utilization capacity by < 10% (data not shown). Pyridine was later used as a solvent for known respiratory inhibitors in electron-transport-chain studies (Chapter 5).

In normal fermentations, iron for bacterial nutrition was provided to 7.2 x 10^{-5} M from a filter-sterilized $FeCl_3$ stock solution following heat-sterilization of other media contents. However, several experiments in which $FeCl_3$ was omitted indicated that aerobic electron-transport capacity in cultures of Pseudomonas sp. 200 is essentially constant following the exhaustion of nutrient iron from the medium. From Figure A.19 it is apparent that under normal circumstances the steady-state level of dissolved oxygen is inversely related to culture fermentation time and optical density. When $FeCl_3$ was omitted from the growth medium (Fe provided only as yeast extract component -- estimated

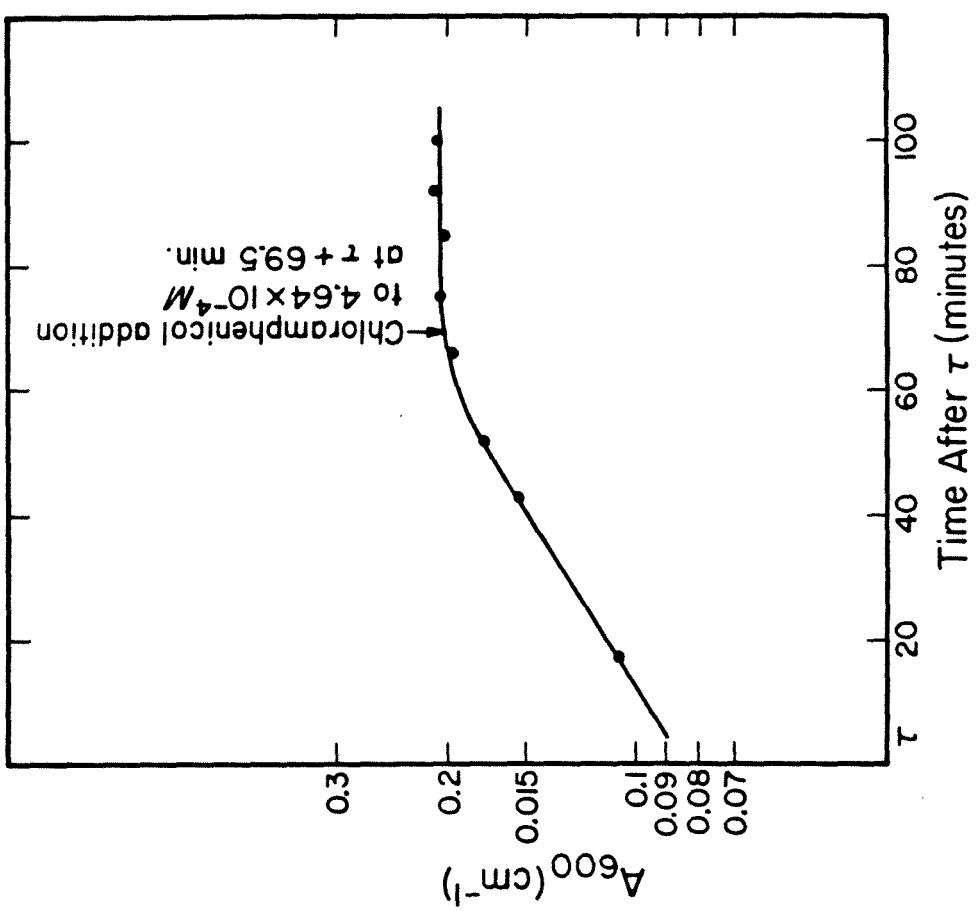

Figure A.17 Aerobic growth of Pseudomonas sp. 200 in Westlake medium as a function of time and chloramphenicol concentration (pH = 7.0, T = 31°C).

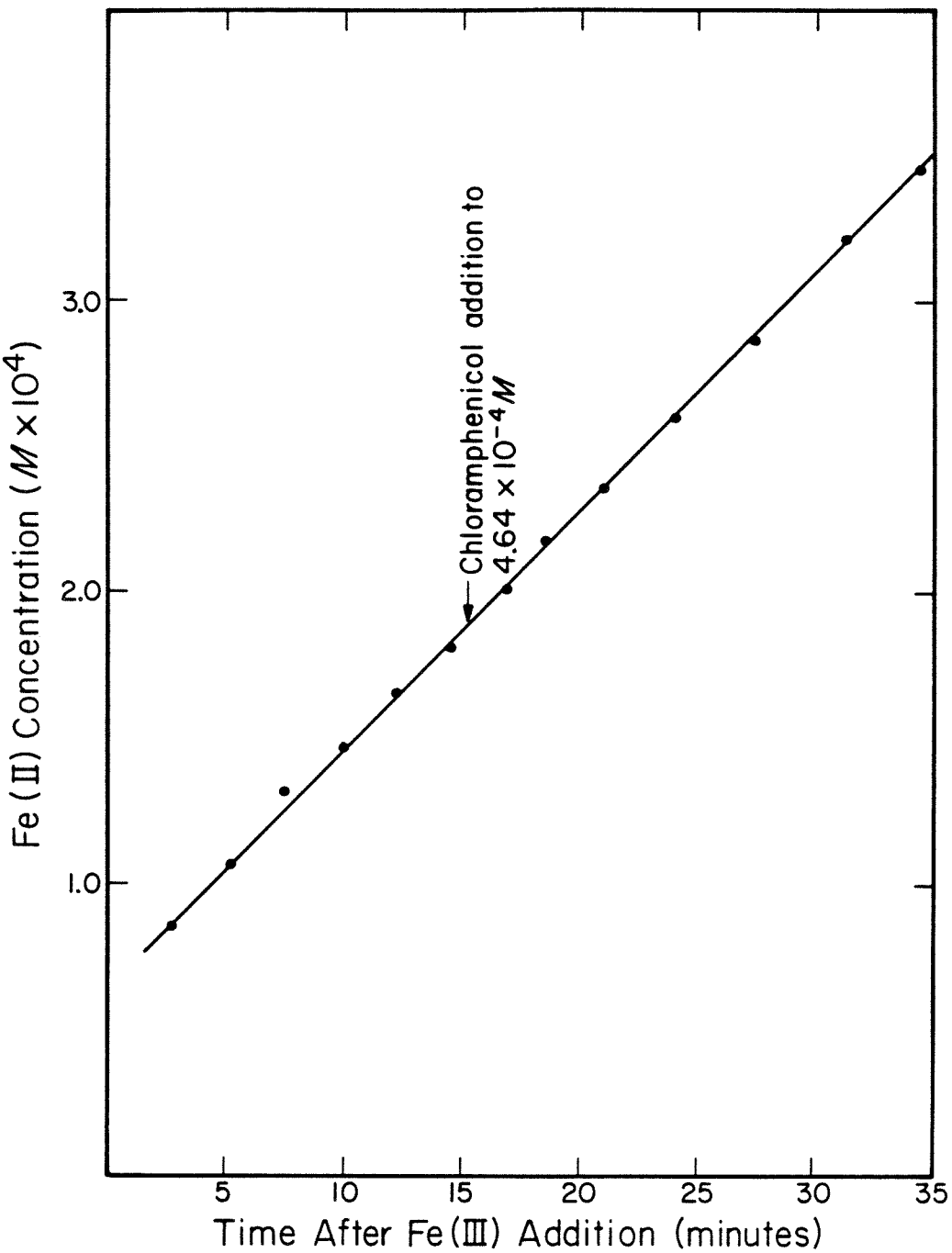

Figure A.18 Reduction of Fe(III) as a function of time (following Fe(III) addition and establishment of anaerobic conditions) and chloramphenicol concentration in a pure, batch culture of Pseudomonas sp. 200. (A_{600} = 0.2, pH 7.0, T = 31°C, Westlake medium).

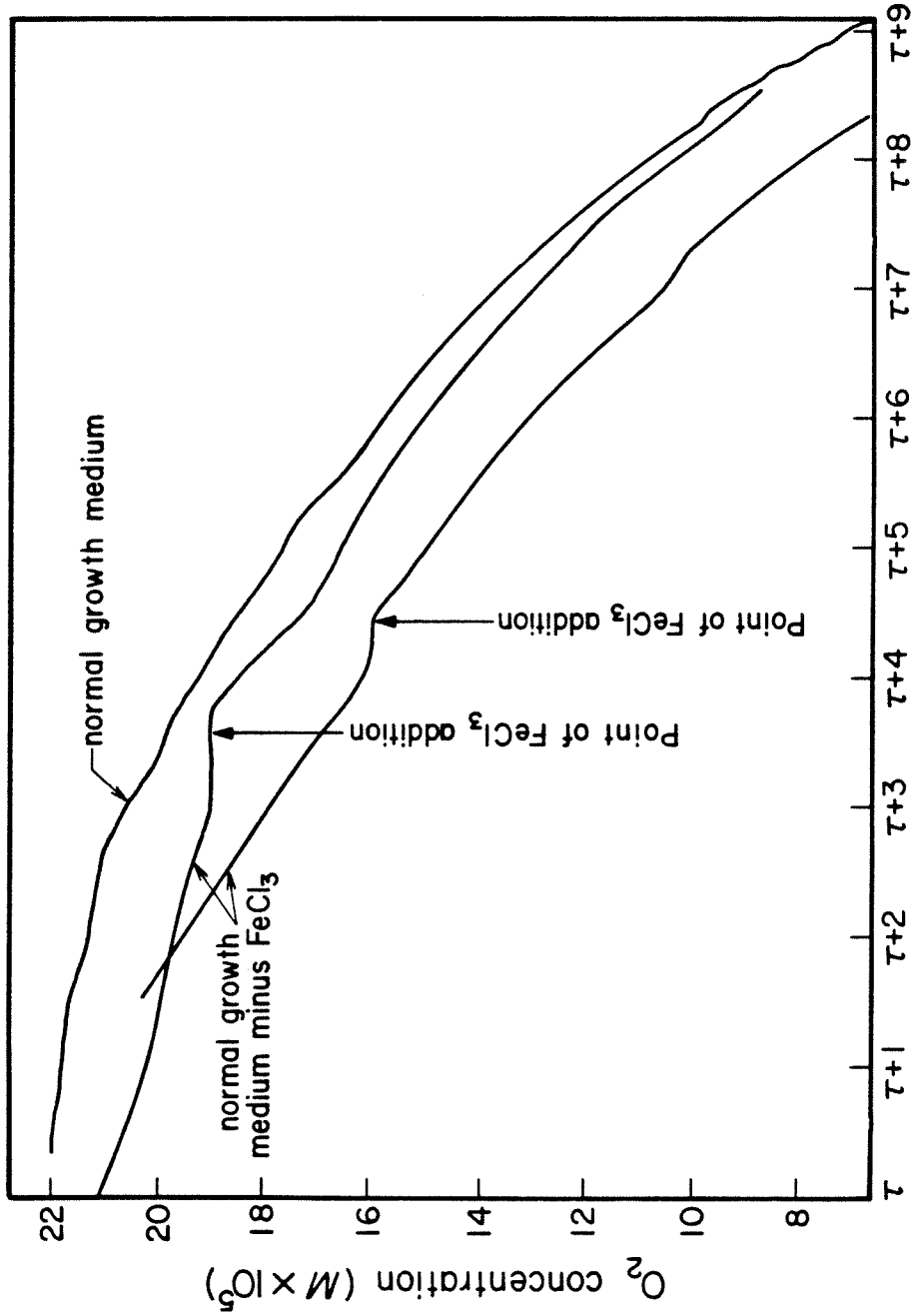

Figure A.19 Dissolved oxygen concentration as a function of time in three batch fermentations involving Pseudomonas sp. 200. All were conducted in a Biostat M lab-scale reactor; 1.5 L fermentation volume; Q_{AIR} = 0.5 L/min.; agitation rate = 250 rpms.

initial concentration in growth medium was 2.5×10^{-6} M based upon Difco analysis of yeast extract), the steady-state O_2 concentration leveled off during what is normally a period of exponential growth. Subsequent addition of 7.2×10^{-5} M Fe(III) restored the characteristic O_2 utilization pattern. The dependence of respiratory activity on continuous assimilation of iron might have been anticipated due to participation of iron-sulfur proteins and/or cytochromes in the aerobic electron-transport chain (Chapter 1).

Based upon these results, an additional experiment was undertaken to (i) assess the impact of iron exhaustion on bacterial growth (as opposed to culture aerobic electron-transfer capacity) and (ii) explore the dependence of dissimilative iron reduction (uninduced cultures) on iron assimilation. Experimental procedures were similar to those described in other growth and iron-reduction experiments. Incubations were conducted in the Biostat M reactor (Westlake media, Table 1, Chp. 3, minus $FeCl_3$). Parameters monitored throughout the fermentation included O_2 concentration, culture optical density (A_{600}, cm^{-1}) and O_2-utilization rate. Aliquots of 100 mls were periodically removed during growth -- both before and after onset of iron starvation (as indicated by the steady-state O_2 level) and purged with nitrogen gas. Following chloramphenicol addition to 2.3×10^{-4} M, Fe(III) and NTA were added to 1.86×10^{-3} M, and Fe(II) was measured as a function of time via the orthophenanthroline procedure described in Chapter 3. Results are summarized in Figure A.20.

The onset of Fe(III) deprivation was apparent in the steady-state dissolved-oxygen concentration profile about seven hours after culture inoculation, at an optical density of about $A_{600} = 0.3$ (cm^{-1}). Culture

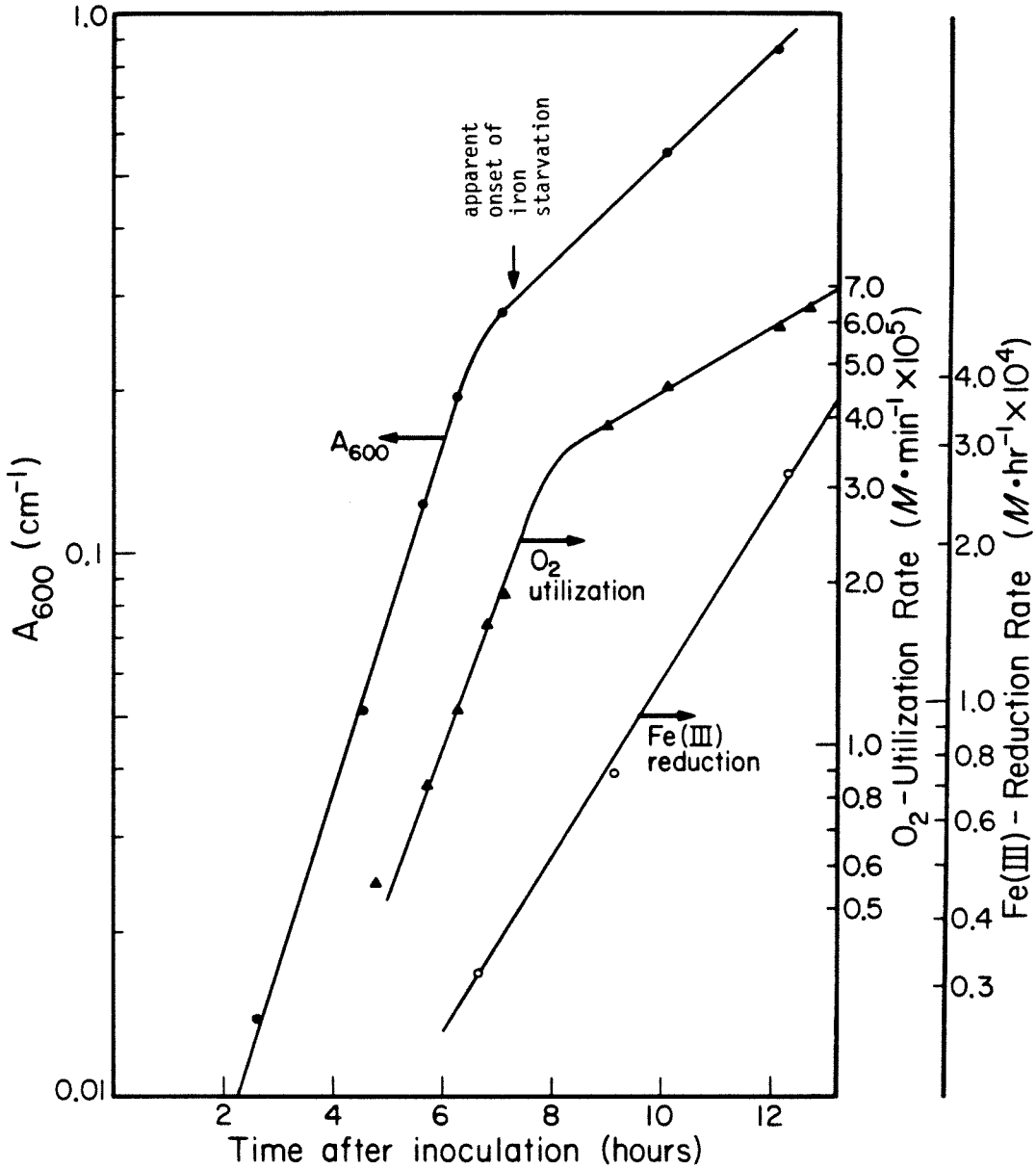

Figure A.20 Indicators of bacterial growth and electron-transport capacity during batch fermentations of Pseudomonas sp. 200 conducted under low-iron conditions.

growth characteristics were qualitatively identical to those summarized previously for Pseudomonas sp. 200 (this chapter) despite the lack of iron in the growth medium. Doubling times both before and after the log-growth discontinuity at A_{600} = 0.25 were consistent with those observed during growth in complete media. There was a similar break in the O_2-utilization curve, although (uncharacteristically) it lagged the shift in microorganism doubling time by almost an hour. However, the iron-reduction capacity of the culture showed no such discontinuity. This may have been due to alteration of the ferrireductase character as the mean cell age increased (see Chapter 5). The only effect of iron starvation which is evident from Figure A.20 is the loss of cellular O_2-utilization capacity, which becomes apparent if one normalizes oxygen-utilization rate by culture optical density. Iron reduction seems unaffected by media iron concentration during growth, although the statement should be qualified in light of the limited data base.

A.3 REFERENCES

American Public Health Association, American Water Works Association, Water Pollution Control Federation. Standard Methods for the Examination of Water and Wastewater (1981).

Brock, T. D. and Gustafson, J. Ferric iron reduction by sulfur- and iron-oxidizing bacteria. Appl. Environ. Microbiol. 32: 567-571 (1976).

Bromfield, S. M. The reduction of iron oxide by bacteria. J. Soil Sci. 5: 129-139 (1954a).

Bromfield, S. M. Reduction of ferric compounds by soil bacteria. J. Gen. Microbiol. 11: 1-6 (1954b).

Ehrlich, H. L. Geomicrobiology pp. 187-192. Marcel Dekker, New York (1981).

Hammann, R. and Ottow, J. C. G. Reductive dissolution of Fe_2O_3 by saccharolytic Clostridia and Bacillus polymyxa under anaerobic conditions. Z. Pflanzenernähr. Bodenkd. 137: 108-115 (1974).

Harrison, D. E. F. The regulation of respiration rate in growing bacteria. In: Adv. Microb. Physiol., Vol. 14, eds. A. H. Rose and D. W. Tempest (1976).

Herbert, D.; Phipps, P. J. and Strange, R. E. Chemical analysis of microbial cells. In: Methods in Microbiology, Vol. 5B, eds. J. R. Norris and D. W. Ribbons. Academic Press, New York (1971).

Kino, K. and Usami, S. Biological reduction of ferric iron by iron- and sulfur-oxidizing bacteria. Agric. Biol. Chem. 46: 803-805 (1982).

Obuekwe, C. D.; Westlake, D. W. S. and Cook, F. D. Effect of nitrate on reduction of ferric iron by a bacterium isolated from crude oil. Can. J. Microbiol. 27: 692-697 (1981).

Ottow, J. C. G. Evaluation of iron-reducing bacteria in soil and the physiological mechanism of iron reduction in Aerobacter aerogenes. Z. Allg. Mikrobiol. 8: 441-443 (1968).

Ottow, J. C. G. Selection, characterization and iron-reducing capacity of nitrate reductaseless (nit^-) mutants of iron-reducing bacteria. Z. Allg. Mikrobiol. 10: 55-62 (1970).

Silverman, M. P. and Ehrlich, H. L. Microbial formation and degradation of minerals. Advan. Appl. Microbiol. 6: 153-206.

Sung, W. and Morgan, J. J. Kinetics and product of ferrous iron oxidation in aqueous systems. Environmental Science and Technology 14: 561-568 (1980).

Tanaka, N. Aminoglycoside antibiotics. In: Antibiotics, Vol. III. Mechanism of Action of Antimicrobial and Antitumor Agents. Eds. J. W. Corcoran and F. E. Hahn. Springer-Verlag, Berlin (1975).

Troshanov, E. P. Iron- and manganese-reducing microorganisms of ore-containing lakes of the Karelian isthmus. Mikrobiol. 37: 786-791 (1968).

Troshanov, E. P. Conditions affecting the reduction of iron and manganese by bacteria in the ore-bearing lakes of the Karelian isthmus. Mikrobiol. 38: 528-535 (1969).